Enhancing drug solubility through advanced polymer extruded shellac-based matrix drug delivery systems

A thesis submitted to complete a degree of

Doctor of Philosophy

by

Guangming Yan (B. Sc)

Based on the research carried out under the supervision

Of

Dr Noel Gately, Dr Zhi Cao and Dr Declan Devine

PRISM Research Institute

Department of Mechanical and Polymer Engineering,

Technological University of the Shannon: Midlands Midwest

Athlone.

Sep 2022

Declaration

I hereby declare that this thesis submitted to the Technological University of the Shannon: Midlands Midwest for the award of Doctor of Philosophy (PhD), is a result of my work and has not in the same or altered form, been presented to this university or any other higher education institute in support for any degree other than for which I am now a candidate.

Guangming Yan

Date:

Acknowledgement

Firstly, and most importantly, I am most grateful to my supervisor Dr Noel Gately for allowing me to pursue a PhD degree. Many times, his patience and constant encouragement have steered me to the right direction. Again, I am most grateful to Dr Noel Gately for his support and help in my research work. I would also like to thank my Co-supervisors Dr Zhi Cao and Dr Declan Devine for their suggestions and most valuable input. Without their help, this project would not be finished.

Thank you to the technicians and support staff throughout the college, I very much appreciate your time and commitment to assisting us as students. Moreover, particularly Alan Murphy of CISD, for his assistance with advice and testing techniques involved with this project. His knowledge of polymer science and testing techniques was instrumental to the success of this project.

Thank you to all the staff in the Office of Research (Mark, Crevan, Lorna, Susan, Amanda, Siobhan and Maire), who were always there to take care of us. Also, I want to thank all the Postgrads for the daily conversations and advice, there are simply too many to mention individually.

This entire experience would be at most a dream if it was not for my loving family, especially my parents Jianlin Yan and Huanyu He for helping me through college, and for their love and support. I would also like to acknowledge my sister Xueli Yan and my girlfriend Li Xiong, who have provided unbelievable support during college life.

Abstract

The main objective of this study is to enhance the solubility of the model drug fenofibrate, by forming amorphous solid dispersions using a hot melt extrusion process. Hot melt extrusion offers an efficient way of increasing the solubility of a poorly soluble drug by forming amorphous solid dispersion. Shellac has potential as a pharmaceutical matrix polymer that can be used in extrusion processes, with further advantages for use in enteric drug delivery systems because of its unique pH-sensitive properties. The rheological property of a material affects the extrusion process conditions by their flow and deformation behaviour inside the barrel. However, there was a distinct lack of data on the processability of various shellac materials in the literature. Hence the initial step in this study was to explore various types of shellac and characterize their physicochemical and thermal properties along with their processability in the hot melt extrusion application. The analysis indicated that there was no chemical difference between the various shellac types compared in this study. It was found that the extrudable temperature ranges and rheological properties of different shellac types varied. SSB 55 Pharma FL had the lowest processing temperature and glass transition temperatures. Moreover, due to the shear-thinning behaviours, shellac can be extruded at lower temperatures.

Subsequently, a prototype delivery construct was produced using hot melt extrusion which was based on fenofibrate as an amorphous solid dispersion, with shellac as the polymeric component. From the analysis of the data, enhanced solubility was achieved as evidenced by an increase in the dissolution rate of the drug in dissolution media. The amorphous solid dispersion formulation improved the solubility by over 8-times relative to untreated fenofibrate. The fenofibrate-shellac binary system provides a different approach from the traditional strategies and can be considered a convenient choice for optimising the oral delivery of fenofibrate. Moreover, a shellac base drug delivery system has an innate advantage due to its pH-sensitive nature and can be potentially used as a colon target delivery system. However, this section highlighted the disadvantages of a universal screw configuration due to insufficient mixing of the kneading section. The drug content in the drug formulation is varied, resulting in the error bar in the dissolution experiment being too large. In the dissolution experiment, the dissolution profile was similar when the maximum solubility of the drug in the aqueous solution was reached.

Numerical simulation was used to understand the impact of two classical

geometrical parameters on the mixing: the influence of different screw speeds and the stagger angles of a twin-screw extruder. The mixing performance was studied based on mixing characteristic parameters such as the maximum shear rate, stretching rate, mixing index, time-averaged efficiency, and residence time distribution. Based on these studies, it was found that the best mixing performance was achieved at a screw speed of 60 rpm. In the aspect of kneading block stagger angle parameters, the increase of stagger angle can promote the mixing performance of the extruder. On the contrary, the residence time increase with the increase of the stagger angle.

Based on the simulation result, a new screw design was created and used to produce a new batch of drug formulations. The final section report, on amorphous solid dispersions of fenofibrate prepared with different types of shellac polymers and employing a hot melt extrusion process with optimized screw configuration. The predominant characteristics of the compositions were amorphous nature, reduced particle size, and improved uniformity, which resulted in an enhancement of drug dissolution and solubility. The rapid in vitro dissolution and the high degree of supersaturation demonstrated the success of these amorphous solid dispersion systems prepared by the hot melt extrusion process. The standard error of drug content, error bar in the dissolution and the SEM image confirmed the success of the newly designed screw configuration having a better mixing performance than the universal screw design.

Table of Contents

Declaration I

Acknowledgement II

Abstract III

Table of Contents i

List of Figures vii

List of Tables xiv

Nomenclatures/List of Abbreviations xvi

1 Chapter 1 Introduction 20

1.1 Aim of this study 20

1.2 The novelty of this study 20

1.3 The objectives of this study 20

1.4 Outline of the research 22

2 Chapter 2 literature review 26

2.1 Polymer-based targeted therapeutic delivery platform technology 26

2.1.1 Factors that influence drug research & development 26

2.1.2 The history of drug delivery system (DDS) 28

2.1.3 Polymer-drug delivery system 30

2.1.3.1 Introduction 30

2.1.3.2 Fundamental of a polymeric drug delivery system 32

2.2 The challenge of low solubility drugs 35

2.2.1 Poorly water-soluble drugs 35

2.2.1.1 Classification of poorly water-soluble drugs 36

2.2.1.2 Formulation strategies for solubility enhancement 37

2.2.2 Amorphous solid dispersion 40

2.2.2.1 Amorphous material *40*

2.2.2.2 Solid dispersion *42*

2.2.2.3 Preparation of solid dispersion *45*

2.3 Hot melt extrusion 52

2.3.1 The history and development of the extrusion process *52*

2.3.2 Screw design for twin screw extrusion systems (TSEs) *53*

2.3.3 Hot melt extrusion: pharmaceutical applications *55*

2.3.4 The material used in hot melt extrusion *56*

2.3.5 Modelling and simulation of the extrusion process *58*

2.3.5.1 The motivation for modelling *58*

2.3.5.2 Simulation: possibilities and limitations *59*

2.3.5.3 Advances in numerical simulation and analysis of intermeshing twin-screw extrusion processes *60*

2.3.5.4 The geometry of co-rotating extruders: conveying and kneading elements *64*

2.3.5.5 Type of mixing in hot melt extrusion *67*

2.4 Shellac material 68

2.4.1 Introduction *68*

2.4.2 Refining process *70*

2.4.2.1 Melting process *71*

2.4.2.2 Bleaching process *71*

2.4.2.3 Solvent extraction process *72*

2.4.3 Composition of shellac *72*

2.4.4 Properties of shellac *74*

2.4.5 Modification of shellac *76*

2.4.6 Application of shellac *76*

2.5 Fenofibrate 78

3 Chapter 3 Material and Method 81

3.1 Material 81

3.2 Grinding 81

3.3 Thermal properties 82

3.3.1 Differential scanning calorimetry (DSC) 83

3.3.2 Thermogravimetric Analysis (TGA) 84

3.4 Attenuated total reflectance Fourier transform infrared (ATR-FTIR) spectroscopy 87

3.5 Rheology 88

3.5.1 Oscillatory time sweeps 92

3.5.2 Oscillation amplitude sweep 92

3.5.3 Oscillation frequency analysis 92

3.5.4 Oscillation temperature sweep 92

3.6 Melt flow index (MFI) 93

3.7 Scanning electron microscopy (SEM) with an energy-dispersive X-ray spectrometry System (EDS) 94

3.8 Preparation of pH buffer solution 95

3.9 Dissolution Test 95

3.10 Drug release profile kinetics 96

3.11 High-performance liquid chromatography (HPLC) 99

3.12 Drug content analysis 100

3.13 Powder X-Ray Diffraction (PXRD) 100

3.14 Hot melt extrusion (HME) 100

3.14.1 Preparation of the physical mixture for hot melt extrusion 100

3.14.2 Hot melt extrusion process condition and formulation matrix for section 4.2 100

3.14.3 Hot melt extrusion process condition and formulation matrix for section 4.4 102

3.15 ANSYS Polyflow analysis 105
3.15.1 The simulation process outline *105*
3.15.2 Mathematical model and mesh generation *107*
3.15.2.1 Flow conditions *107*
3.15.2.2 Material constants *107*
3.15.2.3 Analysis domain mesh and moving coordinate system *109*
3.15.2.4 Boundary conditions *113*
3.15.2.5 Mixing process simulation *114*
3.15.3 Combination screw configuration *116*
3.16 Statistical analysis 118
4 Chapter 4 Result and Discussion 119
4.1 Material characteristic 119
4.1.1 Introduction *119*
4.1.2 Result and discussion *121*
4.1.2.1 IR spectrum *121*
4.1.2.2 Melt flow index analysis *125*
4.1.2.3 Rheology *127*
4.1.2.4 Differential scanning calorimetry (DSC) *133*
4.1.2.5 Thermogravimetric analysis (TGA) *136*
4.1.2.6 SEM-EDS investigation of different shellac type *139*
4.1.2.7 Dissolution *141*
4.1.3 Summary *143*
4.2 Drug formulation analysis 145
4.2.1 Introduction *145*
4.2.2 Results and Discussion *146*
4.2.2.1 Fourier-transform infrared spectroscopy (FTIR) *146*
4.2.2.2 Differential scanning calorimetry (DSC) *148*

4.2.2.3 Powder X-Ray Diffraction *150*

4.2.2.4 Dissolution study *151*

4.2.3 Summary *158*

4.3 Screw design and simulation 159

4.3.1 Introduction *159*

4.3.2 Result and discussion *160*

4.3.2.1 Screw conveying capacity *160*

4.3.2.2 Screw speed and pressure distribution *162*

4.3.2.3 Screw speed and velocity distribution *164*

4.3.2.4 Visualisation of the mixing process *167*

4.3.2.5 The influence of screw speed on the mixing properties of the screw element *170*

4.3.2.6 The influence of rotation speed on mixing properties of the kneading blocks. *172*

4.3.2.7 The influence of stagger angle on mixing properties of the kneading blocks *175*

4.3.3 Summary *178*

4.4 Optimized formulation production and characterisation based on the new screw design 180

4.4.1 Introduction *180*

4.4.2 Result and discussion *181*

4.4.2.1 Differential scanning calorimeter of new shellac material *181*

4.4.2.2 Fourier transform infrared spectroscopy (FTIR) *182*

4.4.2.3 Differential scanning calorimetry (DSC) *184*

4.4.2.4 Powder X-ray diffraction (PXRD) *187*

4.4.2.5 Dissolution study *189*

4.4.2.6 Rheology *200*

4.4.2.7 Scanning electron microscopy (SEM) *201*

4.4.3 Summary *205*

5 Chapter 5 Conclusion 207

6 Chapter 6 Recommendations for future work 213

7 Chapter 7 References 215

8 Chapter 8 Appendices i

8.1 Appendix A Technical data of various shellac materials used in this study i

8.2 Appendix B MATLAB program and output graph v

8.3 Appendix C DSC result graphs x

8.4 Appendix C Miscellaneous xi

8.5 Appendix D Publication xv

List of Figures

Figure 1-1 Outline for material characterisation research.....22

Figure 1-2 Outline for formulation prototype production.....23

Figure 1-3 Outline for screw modelling and simulation 24

Figure 1-4 Outline for optimised formulation production 25

Figure 2-1 R&D expenditure of United States, Global, and China pharmaceutical industry 2014-2023 (Frost & Sullivan, 2019). 26

Figure 2-2 R&D cost to develop new pharmaceutical compounds 2010-2020. (Deloitte, 2021). 27

Figure 2-3 Drug levels in the blood plasma (a) conventional drug dosing and (b) controlled-delivery dosing (Reddy and Rao, 2016). 31

Figure 2-4 Mechanisms of controlled polymer-based drug release systems (Saravanan and Domb, 2013).....34

Figure 2-5 The Biopharmaceutics Classification System (BCS) as defined by Amidon et al. (1995). 37

Figure 2-6 Estimated distribution of marketed and pipeline drugs by BCS classes (Ting *et al.*, 2018). 38

Figure 2-7 Schematic diagram illustrating the common strategies currently used to address low drug solubility in drug discovery and development (H. D. Williams *et al.*, 2013). 39

Figure 2-8 Schematic arrangement of molecular chains in an amorphous and semi-crystalline material (Plastics, 2017). 40

Figure 2-9 Enthalpy and volume of a different state of the drug as a function of temperature, where T_g and Tm are glass transition and melting temperature respectively; the diagram is not to scale. Reproduced from (Baghel, Cathcart and O'Reilly, 2016) ..41

Figure 2-10 Classification of solid dispersion/solution of drug molecules in a polymeric carrier matrix (Sun and Lee, 2014) 44

Figure 2-11 Methods for preparation of solid dispersion.....45

Figure 2-12 Phase Diagram of Carbon Dioxide (CO2). (a) Triple Point (-56.4ºC and 0.5MPa) (b) Critical Point (31.1ºC and 7.3MPa) (Wahl and Czernuszka, 2006). 46

Figure 2-13 Diagram of the equipment and process of conventional spray-drying (Sosnik and Seremeta, 2015). 47

Figure 2-14 Schematic of a typical electrospinning system (Sill and von Recum, 2008). 49

Figure 2-15 A typical extruder schematic (Dynisco, 2017). 50

Figure 2-16 Schematic diagram of the cross-section of a tangential twin-screw extruder shaft (Jaluria, 2003). Counter rotation: The two screws rotate in the opposite direction but at the same speed & co-rotating: the two screws rotate in the same direction and speed. 51

Figure 2-17 Schematic of a typical TSE system(Lubrizol, 2020).....51

Figure 2-18 A typical screw design of a TSEs (Angadi *et al.*, 2017). 55

Figure 2-19 Screw profile with different threads (Booy, 1978) 65

Figure 2-20 Fully wiped twin screw system 66

Figure 2-21 A simple illustration of Dispersion and distribution (Jonathan, 2015) Figure (a) shows bad dispersion and bad distribution. Figure (b) shows bad dispersion and good distribution. Figure (c) shows good dispersion. Figure (d) shows good dispersion and good distribution. 68

Figure 2-22 Photographs of examples of Shellac host trees:(A) Kusum tree, India (Schleichera oleosa); (B) Palas tree, India (Butea monosperma); (C) Ber tree, India (Zizyphus mauritiana); and (D) Raintree, Thailand & China (Samanea saman) (Osman, 2012). 70

Figure 2-23 Flow chart demonstrating the refining process for shellac (Buch *et al.*, 2009). 71

Figure 2-24 Main Components of Shellac (Irimia-Vladu *et al.*, 2013).....73

Figure 2-25 Chemical structure of shellac (Limmatvapirat *et al.*, 2007)(Wang *et al.*, 1999). 74

Figure 2-26 Proposed mechanism of polymerisation in shellac (Khairuddin, Edi Pramono, *et al.*, 2016) 76

Figure 2-27 Differential Scanning Calorimetry of fenofibrate. a) First heating run performed at 10 K/min b) Second heating run (10 K/min performed after brutal quenching of the melt (200K/min) to room temperature and after two days at room conditions. c)Second heating run performed immediately after slow cooling (10 K/min) the melt to room conditions (Di Martino, Palmieri and Martelli, 2000). 80

Figure 3-1 Mill PULVERISETTE 6 classic line ball miller 82

Figure 3-2 The various TA analysis curves (Wunderlich, 2001) 83

Figure 3-3 TA instruments DSC 2920 84

Figure 3-4 Schematic TGA curve: 1 loss of mass due to the vaporisation of volatile components; 2 pyrolysis in an inert atmosphere; 3 combustions of carbon on switching from an inert to an oxidative atmosphere; 4 residue. (Gabbott, 2008) 86

Figure 3-5 PerkinElmer Pyris 1 TGA Thermogravimetric Analyser 87

Figure 3-6 Schematic diagram of an Attenuated Total Reflectance (ATR) FTIR (PerkinElmer, 2005) 87

Figure 3-7 Perkin Elmer Spectrum One fitted with a universal ATR sampling accessory 88

Figure 3-8 The Rotational rheometer (Speyer, 1993) 90

Figure 3-9 The Cone-Plate rheometer 91

Figure 3-10 The Parallel-Plate Rheometer 91

Figure 3-11 Discovery HZ-2 hybrid Rheometer 93

Figure 3-12 (A) Ceast melt flow indexer used in this study (Left-hand side); (B) General Arrangement of Extrusion Plastometer 94

Figure 3-13 a) Bal-Tec SCD 005 sputter coater (Left-hand side); b) Tescan Mira XMU variable pressure scanning electron microscope (Right-hand side) 95

Figure 3-14 Jenway 3520 pH Meter 95

Figure 3-15 SHIMADZU UV-1280 UV Vis spectrophotometer (Left-hand side); Sotax AT7 smart dissolution system (Right-hand side) 96

Figure 3-16 Screw configuration a) initial universal configuration, b) modified configuration, a) combined with 7 kneading disks with 30˚ stagger angle; b) combined

with 10 kneading disks, with 3 @ 30˚ stagger angle, 3 @ 60˚ stagger angle and 4 @ 90˚ stagger angle..... 103

Figure 3-17 Melt extrusion conveyor device with dry compressed air-cooling line. ... 104

Figure 3-18 Flow chart for ANSYS Polyflow Time-dependent analysis 105

Figure 3-19 Flow chart for ANSYS Polyflow mixing analysis 106

Figure 3-20 Shear viscosity curve for shellac SSB 55 pharma FL and the fitting curve by the Carreau-Yasuda model. 108

Figure 3-21 Combined mesh file of a single screw element. 109

Figure 3-22 Combined mesh file of a kneading element section. 110

Figure 3-23 3D cartesian coordinate system. 111

Figure 3-24 Six sequential geometries of the screw element in one rotation. 112

Figure 3-25 Boundary condition of each analysis question. 113

Figure 3-26 A 3D model of the conveying (Left) and kneading (Right) element. 117

Figure 4-1 FTIR Spectrum of each type of shellac. 122

Figure 4-2 FTIR result of shellac AFS RTH and shellac SSB 55 Pharma FL. 123

Figure 4-3 Shellac AFS RTH and shellac SSB Pha 55 overlays at 700-750cm^{-1}. 124

Figure 4-4 Comparing shellac AFS HS 700K with Shellac SSB 55 Pha..... 125

Figure 4-5 The storage modulus of various shellac materials versus oscillation strain (%) in amplitude sweep at 90 °C (The onset points of LVR) (n=3). 129

Figure 4-6 Complex viscosity versus frequency of various shellac in frequency sweep at 70 °C (n=3). 130

Figure 4-7 The storage modulus and loss modulus versus frequency of various shellac in frequency sweep at 70 °C (n=3). 131

Figure 4-8 Viscosity versus temperature of various shellac (n=3). 132

Figure 4-9 DSC thermograms of shellac samples with thermal history removed (n=3). 135

Figure 4-10 TGA of shellac SSB 55 Pharma FL. 137

Figure 4-11 TGA of Dewaxed shellac AFS HS 700K. 137

Figure 4-12 TGA of wax containing shellac AFS RTH. 138

Figure 4-13 TGA of wax containing shellac AFS WL. 138

Figure 4-14 SEM image of four types of shellac at 200x for raw flake material, a) Shellac AFS HS 700K, b) Shellac SSB 55, c) Shellac AFS RTH, d) Shellac AFS WL. (Scale bar is at the bottom of the image)..... 140

Figure 4-15 The UV spectrum and its 1st derivative curve of four different types of shellac (n=3)..... 142

Figure 4-16 Dissolution profiles of the investigated shellac types at pH 1.2 and pH 7.4 (n=3, p<0.05)..... 143

Figure 4-17 FTIR spectra of fenofibrate (FEB) and shellac SSB 55 Pharma FL base formulation..... 147

Figure 4-18. DSC thermograms of the original fenofibrate drug (First heating cycle, n=3). 149

Figure 4-19. DSC thermograms of shellac formulation S5-S14 and the physical mixture of shellac SSB 55 Pharma FL and fenofibrate (First heating cycle, n=2). 149

Figure 4-20 PXRD spectrum of formulation S13, S14, S29, S30 and virgin fenofibrate 151

Figure 4-21 HPLC chromatograph of fenofibrate from the standard solution and extruded solid dispersions formulation (n=3). 152

Figure 4-22 Dissolution profile of drug formulation with shellac SSB 55 Pharma FL in pH 7.4 phosphate buffer solution (n=3, p<0.05)..... 154

Figure 4-23 Dissolution profile of shellac SSB 55 Pharma FL drug formulation produced with different screw speeds in pH 7.4 phosphate buffer solution (n=3, p<0.05)..... 156

Figure 4-24 Dissolution profile of Dewaxed shellac AFS HS 700K drug formulation produced with different screw speeds in pH 7.4 phosphate buffer solution (n=3, p<0.05). 156

Figure 4-25 Dissolution profile of formulation produced with a different type of shellac (n=3, p<0.05)..... 157

Figure 4-27 Natural flow rate through each combination of screws configuration at zero differential pressure..... 161

Figure 4-28 Pressure and viscosity field distributions of the screw element at various speeds. 163

Figure 4-29 Velocity field of the screw element a) Vx, b) V_y c) V_z d) V. 166

Figure 4-30 Tracking particles dispersion inside the screw element during a single rotation cycle with a screw speed of 30 RPM. 168

Figure 4-31 Segregation scale of the screw element with 30-degree stagger at screw speed 30 RPM. 169

Figure 4-32 Influence of screw speed on the a) maximum shear rate and b) maximum stretching rate (Screw element). 170

Figure 4-33 Influence of screw speed on the maximum time-average efficiency and mixing index (Screw element). 171

Figure 4-34 Influence of screw speed on the residence time distribution (Screw element). 172

Figure 4-35 Segregation scale of the kneading blocks with 30-degree stagger at screw speed 30 RPM. 173

Figure 4-36 Influence of screw speed on the a) maximum shear rate and b) maximum stretching rate (Kneading blocks). 174

Figure 4-37 Influence of screw speed on the a) maximum mixing index and b) maximum time average efficiency (Kneading blocks). 174

Figure 4-38 Influence of screw speed on the residence time distribution (Kneading blocks). 175

Figure 4-39 Influence of stagger angle on a) the maximum shear rate and b) maximum stretching rate (Kneading blocks). 176

Figure 4-40 Influence of stagger angle on the maximum mixing index and maximum time average efficiency (Kneading blocks). 177

Figure 4-41 Influence of stagger angle on the residence time distribution (Kneading blocks). 178

Figure 4-42 DSC thermograms of virgin shellac material (Red: Shellac SSB 55 Pharma FL; Blue: AFS Shellac HS 702MB) (n=2). 181

Figure 4-43 FTIR spectra of fenofibrate and formulation produced by modified screw profile based on shellac SSB 55 Pharma FL 183

Figure 4-44 T_g value of the same formulation produced with different screw configurations (n=2) 186

Figure 4-45 DSC thermograms of P1 (Produced by modified screw design, 55RPM, 15% Drug loading) Storage at room temperature. (T1=4 weeks, T2=12 weeks, T3=24 weeks, T4=32 weeks. n=2) 187

Figure 4-46 PXRD patterns of fenofibrate, shellac, and their physical mixture. 188

Figure 4-47 PXRD patterns of each formulation. 188

Figure 4-48 HPLC chromatograph of fenofibrate from the standard solution and extruded solid dispersions formulation (n=3). 190

Figure 4-49 Dissolution profile of formulation produced by newly designed screw (n=3, p<0.05). 193

Figure 4-50 Dissolution profile of formulation produced by different screw designs (n=3, p<0.05). 193

Figure 4-51 Dissolution profile of formulation produced by a different type of shellac (n=3, p<0.05). 194

Figure 4-52 Dissolution profile of formulation produced by same formulation and screw design but a different type of shellac (n=3, p<0.05). 194

Figure 4-53 Complex viscosity versus angular frequency (rad/s) curves at 90 ºC for shellac SSB 55 Pharma Fl and formulation SSB55-M-110-15 (New screw design), SSB-U-110-15 (Universal screw design) (n=3). 200

Figure 4-54 SEM image of the unprocessed shellac (Dewaxed shellac AFS HS 700K, 702MB, SSB 55, AFS HS SWALAC), drug formulation (SSB55-M-55-15, SSB55-M-110-25, SSB55-M-110-15, 700-M-110-15, 702-M-110-15, SWA-M-110-15, 702-M-55-15) and physical mixture (Physical mixture) 204

Figure 4-55 SEM Image of SSB55-M-110-15 and SSB-U-110-15 205

Figure 8-1 Full temperature range DSC result for S13 x

List of Tables

Table 2-1 Barriers to overcome for 3rd Generation DDS (Yun, Lee and Park, 2015) 30

Table 2-2 General drug release mechanisms of Polymeric based Device (Shahiwala and Misra, 2014) 33

Table 2-3 USP solubility classified according to Dahan et al. (Dahan, Wolk and Agbaria, 2014) 36

Table 2-4 Classification of amorphous solid dispersions based on the components' physical state according to Punitha et al., Singh et al.(Punitha *et al.*, 2011) (Singh, Singh Baghel and Yadav, 2011) 44

Table 2-5 Composition of sticklac, seedlac and shellac (Azouka, Huggett and Harrison, 1993) 74

Table 2-6 Physical properties of fenofibrate (PubChem, 2022a) 80

Table 3-1 Shellac material used in this section. 81

Table 3-2. Process parameter of the hot melt extrusion process 102

Table 3-3 DOE for Shellac SSB 55 Pharma FL 104

Table 3-4 Processing matrix for other shellac types 104

Table 3-5 The geometric characteristic parameters of Prism 16 twin-screw extruder in this study. 116

Table 3-6 Kneading element (Disc gap 0.4 with different stagger angle) 118

Table 3-7 Kneading blocks (Disc thickness 4mm, disc gap 1mm, stagger angle 30°) . 118

Table 3-8 Full mesh conveying element (Screw element) 118

Table 4-1 FTIR peak table of raw shellac material 121

Table 4-2 Melt flow index of different types of raw shellac material at 90˚C (n=3) 127

Table 4-3 The linear viscoelastic region (LVR) of raw shellacs at various temperatures (Onset point ± Std Err n=3). 128

Table 4-4 Glass-transition temperatures and melting temperature of different shellac grades (n=2). 135

Table 4-5 TGA of different types of Shellac (n=1) 139

Table 4-6 EDS elements analysis of four different types of shellac 141

Table 4-7 FTIR band assignment of shellac material, fenofibrate and formulation 148

Table 4-8 Uniformity of fenofibrate content of hot melt extruded solid dispersions (n=3). 153

Table 4-13 *T*g value of each shellac material used in this section (n=2). 182

Table 4-14 The band assignments of each type of shellac, fenofibrate and formulation (SSB-M-55-15). 184

Table 4-15 T_g Value of each batch of formulation (n=2). 186

Table 4-16 Drug content of the ASDs formulation as determined by HPLC (n=3). 190

Table 4-17 Statistical criteria for evaluating mathematic modelling and drug release kinetics from the shellac-based formulation (n=3). 198

Table 4-18 Mathematic modelling parameter for shellac-based formulation (n=3). 199

Nomenclatures/List of Abbreviations

ANOVA	Analysis of variance
AIC	Akaike Information Criterion
APIs	Active pharmaceutical ingredients
ASD	Amorphous solid dispersions
ASTM	American Society for Testing and Materials
ATR	Attenuated total reflection
ATR-FTIR	Attenuated total reflectance Fourier transform infrared
BC	Boundary condition
BCS	Biopharmaceutics Classification System
$CaCO_3$	Calcium Carbonate
CFD	Computational fluid dynamics
C_L	Centreline distance between two shafts
CO_2	Carbon dioxide
CVDs	Cardiovascular diseases
DDS	Drug delivery system
DOE	Design of experiment
DMA	Dynamic Mechanical Analysis
DSC	Differential Scanning Calorimetry
DTG	Differential thermogravimetry
EDS	Energy-dispersive X-ray spectrometry System
EFPIA	European Federation of Pharmaceutical Industries and Associations
FAN	Flow analysis network
FDA	Food and Drug Administration
FEM	Finite element method
FEB	Fenofibrate
FIDAP	Fluid dynamics analysis package
G'	Storages modulus
G"	Loss modulus
G*	Complex modulus
GC-MS	Gas chromatography–mass spectrometry
GI	Gastrointestinal
GIT	Gastrointestinal tract
GRAS	Generally recognized as safe

HDL-C	High-density lipoprotein cholesterol
HDPE	High-density polyethylene
HME	Hot melt extrusion
HPLC	High-performance liquid chromatography
HPMC	Hydroxypropyl methylcellulose
HPMCAS	Hypromellose acetate succinate
ICTA	International Confederation for Thermal Analysis
ICTA	International Confederation for Thermal Analysis
IR	Infrared
IVIVC	*In vitro in vivo* correlation
LDL-C	Low-density lipoprotein cholesterol
LVR	linear viscoelastic region
MFI	Melt Flow Index
MSC	Model Selection Criterion
MW	Molecular Weight
MWD	Molecular weight distribution
Na_2HPO_4	Sodium phosphate dibasic
NaH_2PO_4	Sodium phosphate monobasic
NaOH	Sodium hydroxide
NCE	New chemical element
NCE	New chemical element
P_c	Critical pressure
PhRMA	Pharmaceutical Research and Manufacturers of America
pKa	Acid dissociation constant
PLA	Polylactic acid
PVP	Polyvinylpyrrolidone
PXRD	Powder X-ray diffraction
R&D	Research and Development
R_b	Screw external radius
Rs	Screw core radius
SCF	*Supercritical Fluid*
SD	Solid dispersion
SDS	Sodium Dodecyl Sulfate
SEM	Scanning electron microscopy

TA	Thermal analysis
Tan(δ)	Loss Angle
T_c	Critical Temperature
T_d	Decomposition temperature
T_g	Glass transition temperature
TG	Thermogravimetry
TGA	Thermogravimetric Analysis
T_m	Melting temperature
TMA	Thermomechanical Analysis
TSEs	Twin screw extrusion system
USP	United States Pharmacopeia
UV	Ultraviolet
WHO	World Health Organization

Unit

°C	Temperature
cm^{-1}	Wavenumber
cm^3	Cubic centimetre
g	Gram
J	Joule
Hz	Hertz
Kg	Kilogram
M	Moore
mg	Milligram
min	Minute
mL	Millilitre
mm	Millimetres
mol	Mole
MPa	Megapascal
N	Newton
nm	Nanometre
Pa	Pascal
rad	Radian
s	Second
µm	Micrometre

Greece

E	Young's modulus
α	Root angle
β	Tip angle
$\dot{\gamma}$	Shearing rate
ε	Strain
η^*	Complex viscosity
η_0	Viscosity
σ	Shearing stress
ω	Angular frequency

Chapter 1 Introduction

1.1 Aim of this study

The overall aim of this project is to enhance the aqueous solubility and bioavailability of the model drug (Class 2 drug fenofibrate) by the formulation of a solid dispersion system employing a hot melt extrusion process.

1.2 The novelty of this study

This study will assess shellac material as a novel drug delivery platform formulation matrix to form amorphous solid dispersion through a direct hot melt extrusion process. This novel platform will increase the water solubility of a poorly soluble model drug, and because of the unique pH-sensitive properties of shellac materials, it could also be used as an enteric target drug delivery device with the benefit of enhanced drug solubility. Amorphous solid dispersion was chosen because of the amorphous nature of shellac materials, and the ability of shellac material to hold the amorphous state of the drug substance in the matrix.

1.3 The objectives of this study

The individual research objectives can be summarised as follows:

- To produce polymer-based drug formulations and evaluate their properties.
- To evaluate the stability of the drug formulations under different conditions.
- To evaluate the drug substance recrystallisation behaviour in the formulation stored at different conditions.
- To fully understand the effects that the processing conditions of hot melt extrusion (HME) have on the formulations (Screw design, Drug loading, Screw speed, Mixing method).
- To evaluate and simulate the melt extrusion screw design.
- To optimise the processing condition to produce a uniform formulation

This study was based on Dr Noel Gately's research, and further explores the pharmaceutical application of shellac materials as melt extrusion matrix material. Moreover, due to its natural, non-toxic, biodegradable, eco-friendly nature, shellac has been in consistent demand in the market, and hence its farming or cultivation has become an increasingly profitable business. It also has been permitted as a food additive by the European Union (EU) with E number E904 and has also received a GRAS (Generally Recognized as Safe) status from the U.S. FDA. Additionally, the low softening temperature of shellac material allows it to process very easily when compared with other pH-responsive polymers. Shellac has a lower processing temperature profile is very easy to clean the extrusion equipment after extrusion processing. As a result, in this project, the hot melt extrusion technique was selected as the production method to produce solid dispersions based on shellac material. Various combinations of shellac material and medicinal loadings were investigated using different characterisation techniques, which were in accordance with the literature for comparative testing. This study aims to develop a drug delivery platform device which will enhance the model poorly soluble solubility of the drug. In this initial body of work, fenofibrate was selected as the first model drug because of its low water solubility nature (Class 2), moreover, it has a low melting point (80°C) and low price.

1.4 Outline of the research

The following flow chart outlined the main point for the whole thesis and each section.

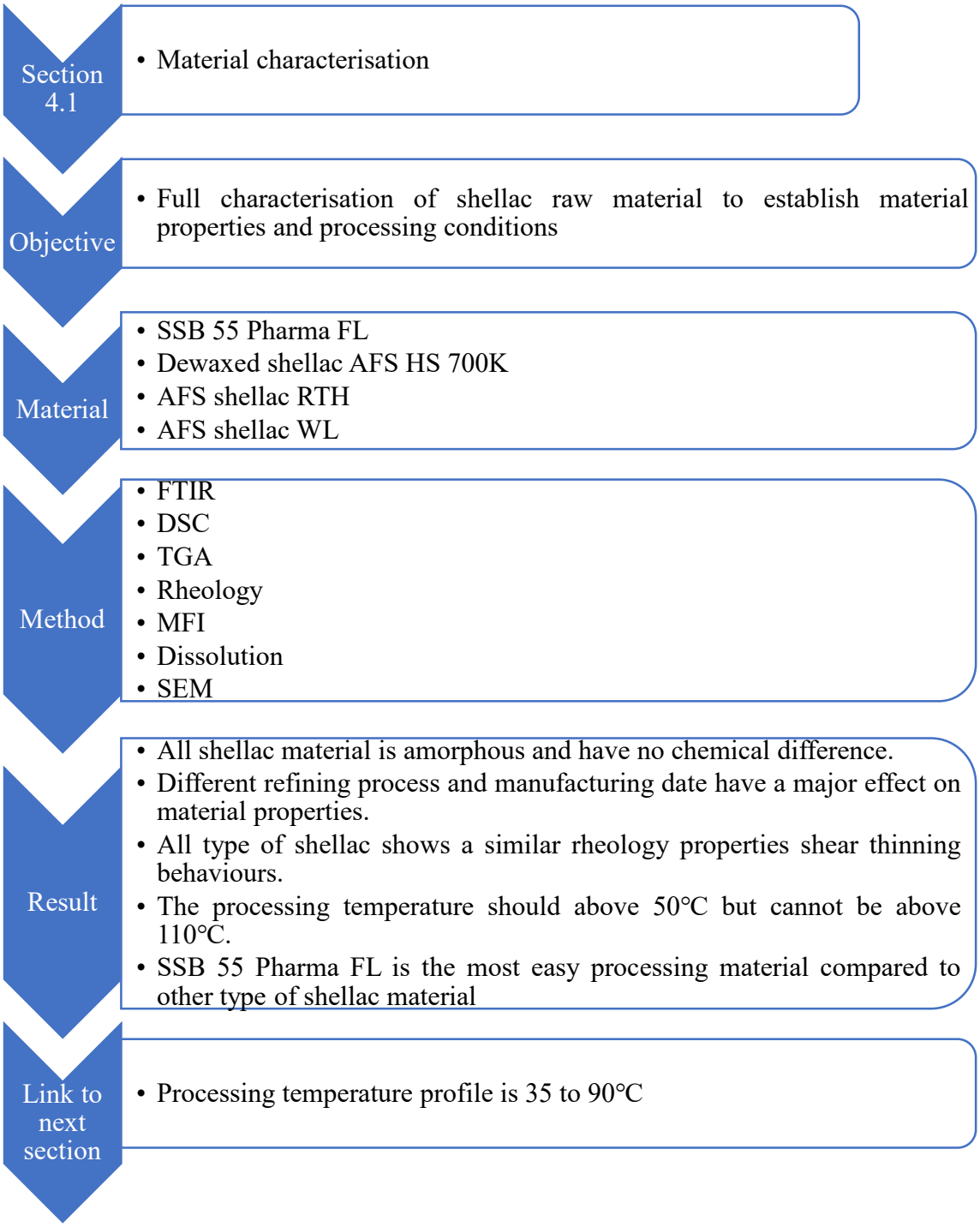

Figure 1-1 Outline for material characterisation research

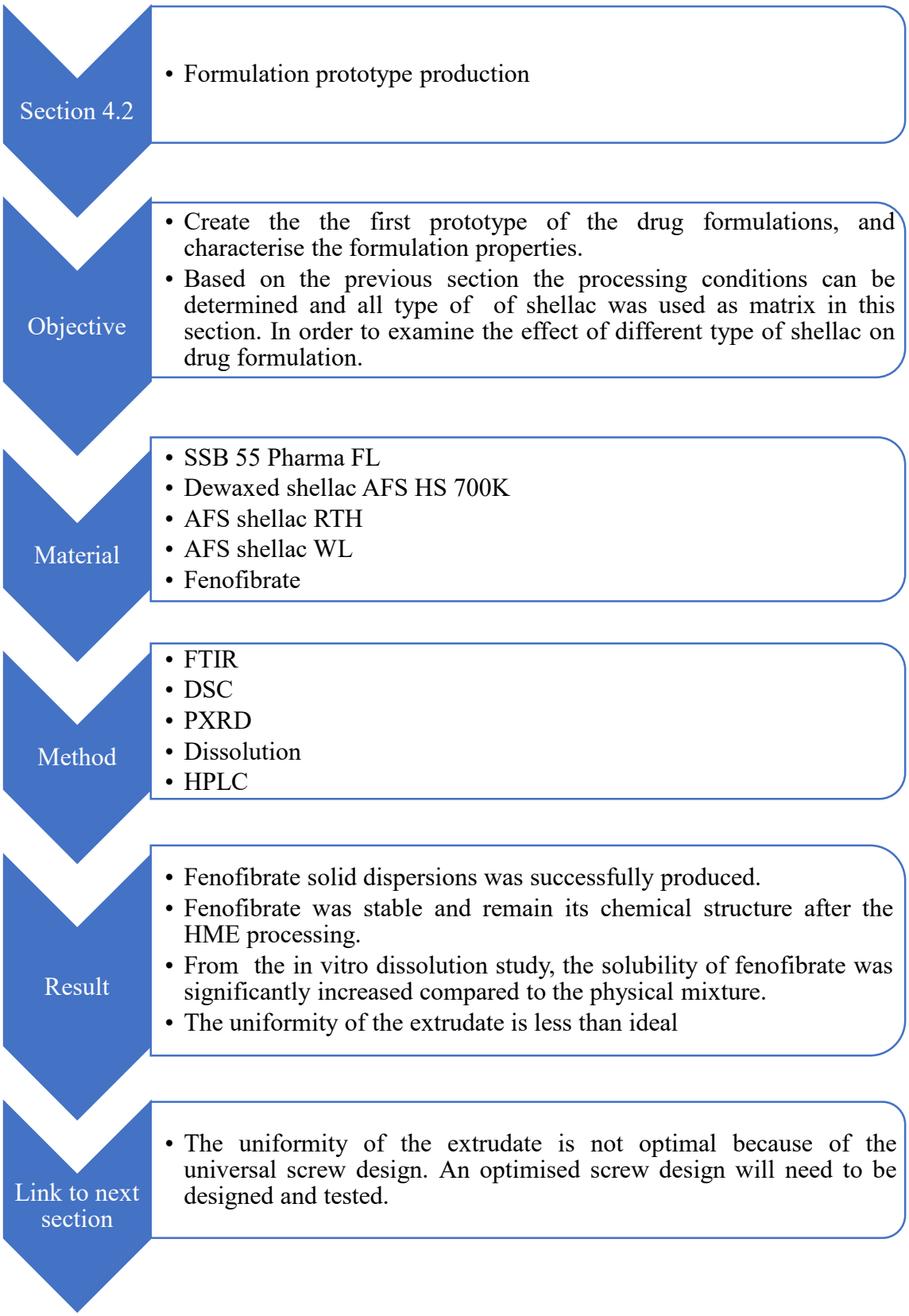

Figure 1-2 Outline for formulation prototype production

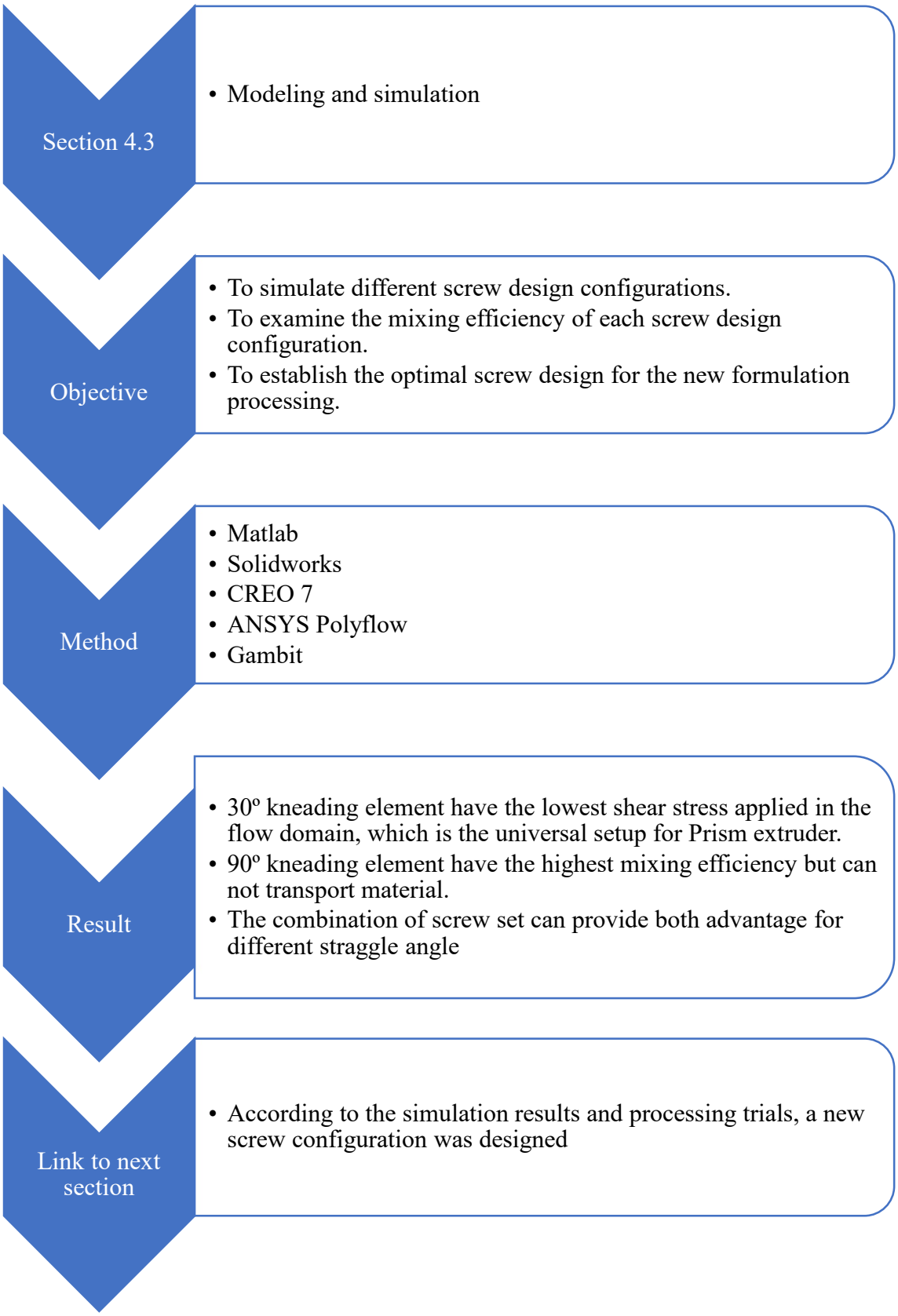

Figure 1-3 Outline for screw modelling and simulation

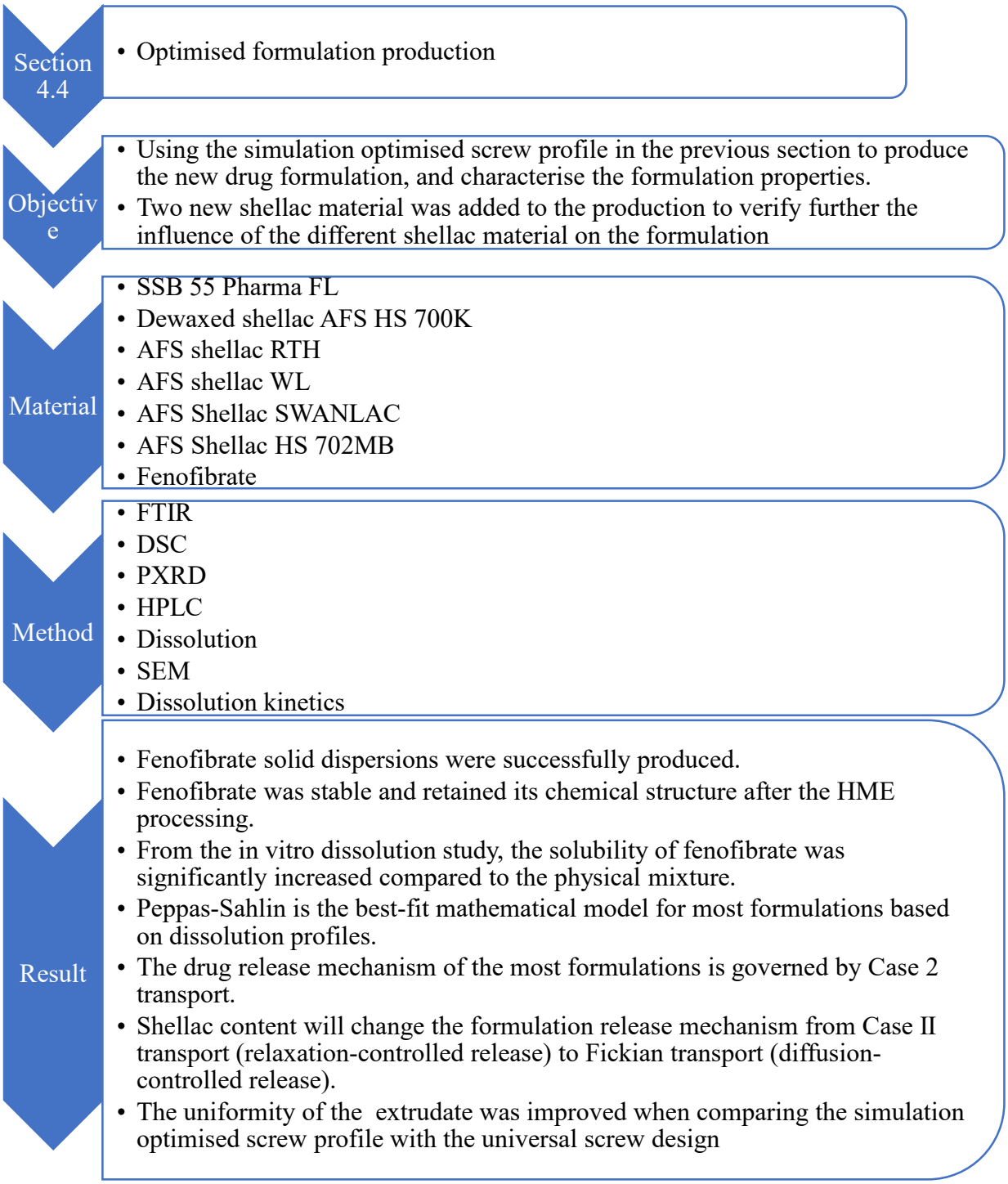

Figure 1-4 Outline for optimised formulation production

Chapter 2 literature review

2.1 Polymer-based targeted therapeutic delivery platform technology

2.1.1 Factors that influence drug research & development

Drug development is a long, complicated process. Every new drug, from development to release on the market, requires a lot of human power, and material and financial resources. According to the report by Statista (Figure 2-1), the total spending for research and development in the United States, pharmaceutical industry was over $89.6 billion a year up to 2023, and the global pharmaceutical research and development spending is over $216.8 billion, and the trend is ascension every year (Frost & Sullivan, 2019). Furthermore, the average cost to develop a new pharmaceutical compound increases every year (Figure 2-2), and the whole process may take more than 14 years (Deloitte, 2021). Due to the high cost of developing a new drug, all researchers want to maximize the research efficiency and shorten the processing time starting with its discovery and bringing the product to the market.

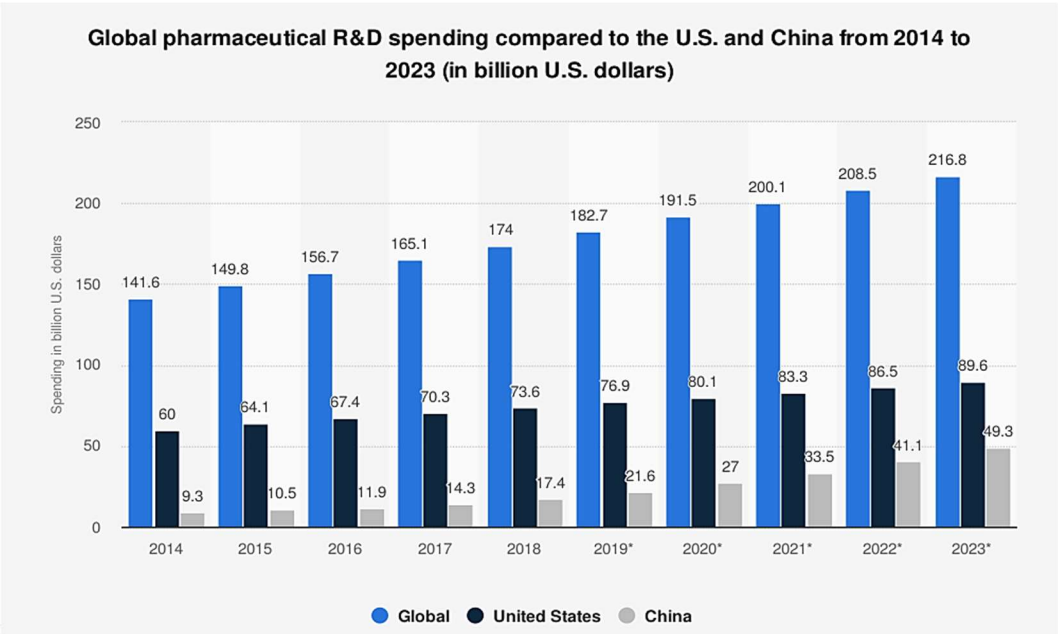

Figure 2-1 R&D expenditure of United States, Global, and China pharmaceutical industry 2014-2023 (Frost & Sullivan, 2019).

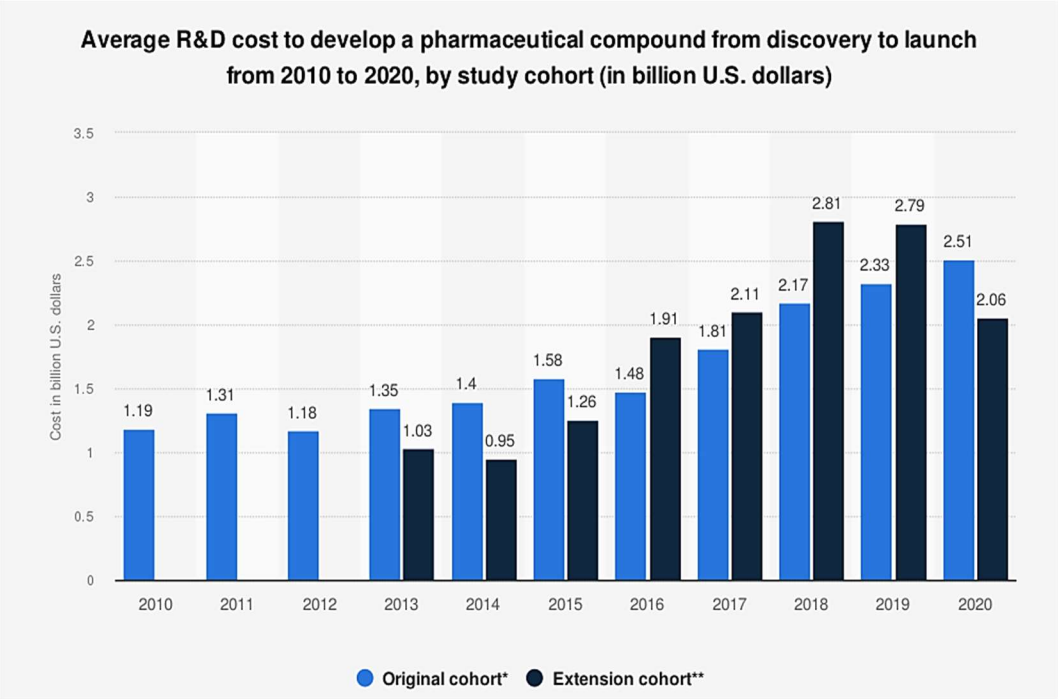

Figure 2-2 R&D cost to develop new pharmaceutical compounds 2010-2020. (Deloitte, 2021).

High-throughput screening is a new method for drug discovery; usually, the method can be divided into several stages: target/disease identification/ hit identification/discovery, hit optimisation, lead selection and further optimisation, candidate identification, and clinical trials (Hughes *et al.*, 2011). Once the target or disease is identified, there will be enough evidence to support the relationship between the target and disease, and more than ten thousand new compounds are produced and screened according to the target or disease. However, only a few of them are in line with the desired biological activity. In the next few steps, further biopharmaceutical properties would be analysed. After the high-throughput screening, the drug candidates who have the most drug-like properties, only 40% of them can make their way to Phase I clinical trial. However, the statistical data, shows nearly 90% of the compound was eliminated in the clinical trial (Gupta, Kesarla and Omri, 2013) (Lindenberg, Kopp and Dressman, 2004)(Hauss, 2013). There are many reasons for those compound failures. The critical reason is the water insoluble nature causes poor pharmacokinetics in humans, this would account for 39% of failures (Alavijeh and Palmer, 2004).

2.1.2 **The history of drug delivery system (DDS)**

Before the 1950s, the concept of drug delivery systems did not exist. All drug products were made into pill or capsule formulations. They released the loaded drug immediately when touched with liquid (Yun, Lee and Park, 2015). In 1952, Smith Klein Beecham created the first sustained release formulation, these drugs can control the drug release kinetics, and their efficacy could be up to 12h. Not until the end of the 1970s that the fundamental understanding of the controlled drug delivery system was established. "A drug delivery system (DDS) is a formulation or a device that enables the introduction of a therapeutic substance in the body and improves its efficacy and safety by controlling the rate, time, and place of release of drug in the body" (Jain, 2008). The existence of a drug delivery system is to serve drugs. In other words, in any drug delivery formulation, the most critical factor is the drug itself. Any other parts of the formulation known as carriers or excipients are used to improve the effectiveness or safety (Chaudhari and Patil, 2012).

Looking back in time, the development of a DDS can be divided into three generations. The first period (first-generation DDS) started in 1950 until the basic understanding of controlled DDS is established. During that period, the release mechanisms of the drug were investigated, such as dissolution-, diffusion-, osmosis-, and ion exchange-based mechanisms (Park, 2014). Those technologies were used to develop sustained release dosage forms, meaning those oral drug systems could release the drug slowly over a relatively extended period so that the patient can take the dosage less often. However, all the technology is still in the early stage, the 1st Generation DDS is known as the basics of controlled release drug (Liu *et al.*, 2016). Such mechanisms are also suitable for transdermal patches. Even today, there are substantial amounts of oral drug delivery systems based on the dissolution- or diffusion-controlled mechanism. The difference between these two mechanisms is, that dissolution happens due to the velocity gradient, and diffusion happens due to the concentration gradient. In addition, diffusion happens due to the random motion of molecules. Dissolution happens due to the motion of the medium. Compared with the 1st

generation DDS formulations, the 2nd generation started in 1970 and it is until 2010 that it is named as "smart delivery system", but it has been less successful because there are fewer products on the market. This situation means the 2nd generation DDS focused on much more complex delivery formulations, i.e. zero-order delivery system (Tiwari *et al.*, 2012). These systems would achieve zero-order release kinetics, maintaining a steady state for the drug concentration in the blood. Unfortunately, due to the biological barrier, there is no standard *in vitro* release test methods that can simulate *in vivo* pharmacokinetic profile. Some drug concentration *in vivo* does not maintain a steady-state value, even though the drug achieves zero-order release *in vitro* dissolution systems (Wen, Jung and Li, 2015)(Ardelean *et al.*, 2018). Moreover, the constant drug concentration is not necessary, if the concentration in the blood is above the minimum effective concentration. Overall, the 2nd generation drug delivery systems deal with drug release kinetics, nevertheless, because it cannot overcome the biological barriers, it is a limited success (Yun, Lee and Park, 2014).

The next generation of DDS (Modulated delivery systems) starts around 2010; this technology shows a much more advanced feature than the 2nd generation DDS technology to deal with both biological and physicochemical barriers (De Jong and Borm, 2008). However, many challenges need to be solved in the 3rd generation of DDS, as shown in the list following Table 2-1.

Table 2-1 Barriers to overcome for 3rd Generation DDS (Yun, Lee and Park, 2015)

Delivery technology	Formulation challenges	Biological challenges
Poor water-soluble drug delivery	• New formulation to increase drug solubility	• New formulation material non-toxic to the body • No drug precipitation in the blood
Peptide/protein/nucleic acid delivery	• Control of drug release kinetics • Control of drug loading • Control of therapeutic period	• *In vitro in vivo* correlation（IVIVC） • Long-term delivery up to a year • Non-invasive drug delivery (transdermal)
Targeted drug delivery using nanoparticles	• Control of nanoparticle size, shape, surface chemistry, functionality, and flexibility. • Modified formulation with surface modification of ligands • The active of different stimuli-sensitive delivery systems	• Controlling biodistribution through altering vascular extravasation, renal clearance, and metabolism. • Navigating the microenvironment of diseased tissues to reach target cells • Crossing endothelial barriers (e.g., blood-brain barrier) • Crossing mucosal barriers
Self-regulated drug delivery	• Signal specificity & sensitivity • Fast responsive kinetics • Ability to stop drug release	• Functional inside the body • Functional over the lifetime of drug delivery

2.1.3 **Polymer-drug delivery system**

2.1.3.1 *Introduction*

It is through novel technology approaches that, the development of drug research and discovery has accelerated. Technology, such as High-throughput screening or combinatorial chemistry, has been widely used in recent years, substantially shortening the development cycle. However, the emergence of these innovative technologies brings fresh drawbacks, newer drugs are generally more potent and have poorer solubility than traditional products (Vimalson *et al.*, 2016). Due to these limitations, scientists have to generate new DDS

systems to deliver those actives more effectively and safely which has further promoted the development of novel drug delivery systems. Ideally speaking, after the patient takes the dosage, the API should reach its appropriate concentration and remain constant. The concentration of the drug in the therapeutic window should ideally remain constant over a suitably extended period of time as shown in Figure 2-3. However, the conventional dosage formulation cannot provide an ideal pharmacokinetic profile. It has a high peak after the administration of the drug (even possibly reaching the toxic level concentration). Furthermore, conventional dosage forms can only provide a narrow therapeutic window in a limited time range, which means that the patient need to take the dosage twice or more in one day (Ummadi *et al.*, 2013). The pharmacokinetic profile can be affected by several factors, such as physicochemical barriers, biological barriers and the nature of the drug itself (Rosenblum *et al.*, 2018).

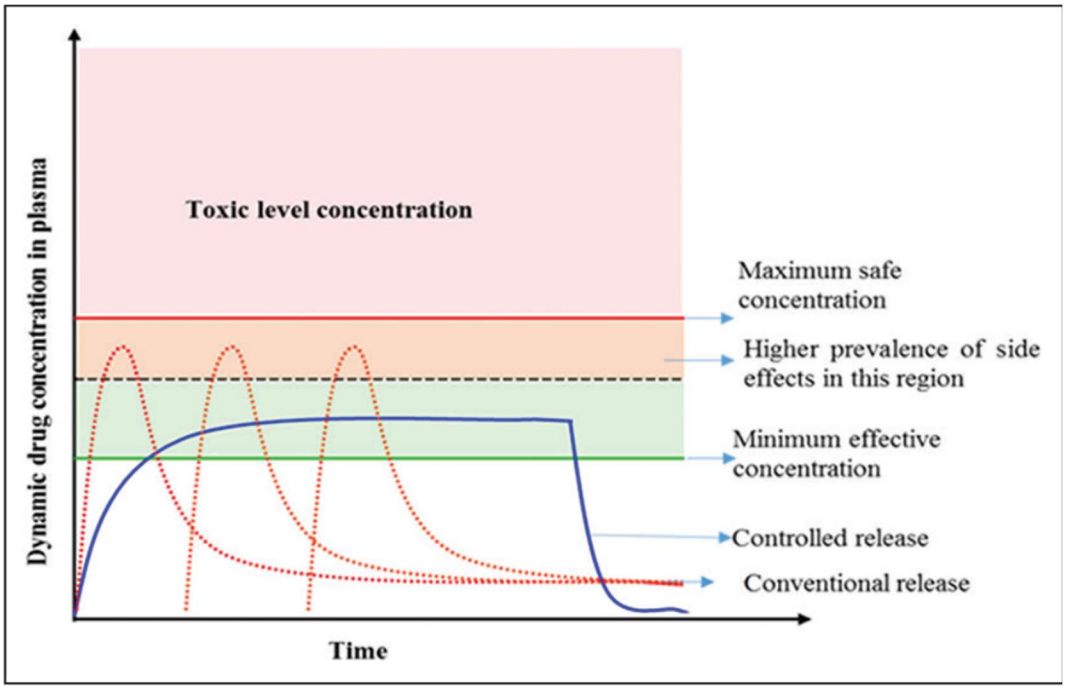

Figure 2-3 Drug levels in the blood plasma (a) conventional drug dosing and (b) controlled-delivery dosing (Reddy and Rao, 2016).

With the development of technology, increased attention and interest have focused on the new formulation of the delivery mechanism such as polymeric drug delivery systems. Novel delivery systems can provide a better pharmacological response, with these systems

frequently being used as a control-releasing system (Bhowmik, Sahu and Sahu, 2016). As mentioned in the preview chapter, after 1970, the 2nd generation drug delivery systems achieve zero-order release kinetics, and they would maintain a steady-state drug concentration in the blood as shown in Figure 2-3. Accordingly, some polymeric materials were tested as the prototype of drug delivery systems, including Vinyl polymers, natural resin, and hydrogel (Englert et al., 2018). It played a significant role in advanced drug delivery technology and provide a controlled pharmacological response over an extended time period. In recent years, the application of polymeric materials used in the pharmaceutical industry has been growing fast. Polymers have been used as drug delivery systems, medical devices, scaffolds in tissue engineering, dentistry, bone repair and many other medical fields (Sharma, Negi and Mahindroo, 2018).

2.1.3.2 *Fundamental of a polymeric drug delivery system*

Due to the different physicochemical properties of various drugs, there is a wide range of mechanisms that have been created by using polymeric materials. Moreover, the two important parameters for the release of drugs from tablet matrices are the infiltration rate of the medium into the matrix, for those drugs with reasonable aqueous solubility, and the erosion rate of the matrix system, for those drugs with poor aqueous solubility (Tahara, Yamamoto and Nishihata, 1995). Consequently, it has accelerated the development of new polymeric materials for different drug delivery mechanisms. Typically, the drug release behaviour from these systems depends on the physicochemical properties of the polymer and the physiological medium (Bedoya et al., 2020)(Thakuria et al., 2013) (Kendre, Pande and Chavan, 2014). Some possible primary factors that may affect the drug release are the environment where the drug is released, diffusion from the drug delivery device, and the chemical nature of the carriers (Lee and Yeo, 2015). Other essential factors include distribution of the drug in the polymeric device, drug solubility, drug particle size, etc. (Davis and Walker, 2017). Furthermore, some excipients also affect drug release profiles. The formulation of the DDS can be adjusted to meet the initial requirement by modifying

previously mentioned factors related to polymers, drugs and their release environment (Yun, Lee and Park, 2015). Considering the different mechanisms of drug release from the polymer, all polymeric drug delivery systems are diverse. There are several distinct types of release mechanisms which are listed in Table 2-2. As Harrison (2007) mentions, there are three main types of control mechanisms for polymeric drug delivery systems: such as temporal, distribution, and erosion systems (Harrison, 2007).

Table 2-2 General drug release mechanisms of Polymeric based Device (Shahiwala and Misra, 2014)

Type	Mechanism	Example of Polymer	Example of APIs
Covalent bonding of drug-polymer	Bond cleavage releases the drug	*N*-hydroxypropyl-L- glutamine	Norethindrone coupled with soluble polymer
Hydrophilic matrix system	Bond cleavage or shell erosion	Acrylic glycidyl ester	Progesterone
Hydrophobic matrix system	Bulk erosion and surface erosion	Polylactic acid (PLA) and glycolic acid	Norethindrone
Reservoir system	Erosion of the shell and then of the reservoir	Poly(ε-caprolactone)	Levorgestrol

Generally speaking, APIs exhibit their pharmacological action after they dissolve in the patient body's fluid physiological environment (Uhrich *et al.*, 1999). The aqueous physiological environment can be harsh to the APIs, and polymeric dosage forms can protect the drug molecules. Because of the protection, the drug release from the polymeric systems is different, besides being based on the chemistry, the dissolution mechanisms of polymeric drug delivery systems can be classified into three types, as shown in Figure 2-4 (Saravanan and Domb, 2013).

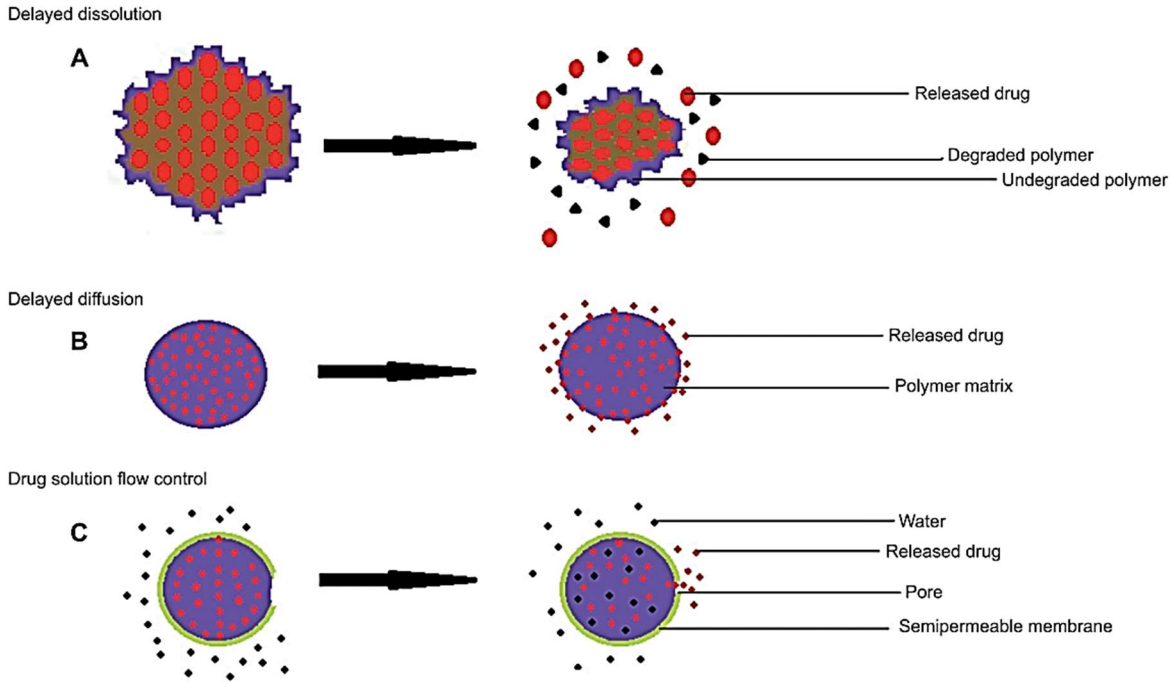

Figure 2-4 Mechanisms of controlled polymer-based drug release systems (Saravanan and Domb, 2013)

Delayed dissolution, as the name suggests, uses a polymeric drug delivery system to delay drug release by reducing the rate of drug molecules exposed to the aqueous physiological environment. Diffusion happens due to the difference in concentration gradient between the delivery device and the surrounding environment. The process starts with the intrusion of water through the polymeric shell, then the drug molecules spread out due to the random motion of molecules. Sustained release is achieved by the drug being released by passing through the voids or between the polymer chains. Delayed diffusion-controlled systems can be separated into two types, matrix systems and reservoir systems. In reservoir systems, the polymeric material plays a role in the storage device such as capsule or microcapsule (Yang and Pierstorff, 2012). In matrix systems, drugs and polymeric material are evenly dispersed together (Nokhodchi *et al.*, 2012). Drug solution flow control systems are also named osmotic controlled systems, which are systems where the penetration of solvent controls the release into the formulation. The dosage will not release the drug until absorbed water creates osmotic pressure. Furthermore, this release behaviour is known as zero-order kinetics. Swelling controlled drug delivery systems, are where the shape or dimensions of dosage remains constant during the release process. After the patient takes the

dosage, the media get into the dosage form, material swelling occurs and the drug diffuses out through the swollen polymer layer (Gupta *et al.*, 2010). The last type of mechanism is stimuli-responsive control systems, due to the specific nature of the polymeric material, the drug will only release when the dosage meets the specific stimulation and therefore, it also can be classified as a smart polymer. The stimulation can be a single signal such as a magnetic field, pH, electrical signals, ultrasonic signals, temperature, pressure or other physical or chemical stimuli which induces physical or chemical changes in the polymer, allowing the drug inside the delivery device to release (Ding *et al.*, 2016).

2.2 The challenge of low solubility drugs

2.2.1 **Poorly water-soluble drugs**

Due to the new technologies, the development of drug research and discovery has been accelerated. However, the poor aqueous solubility of a certain drug is a continuing challenge in pharmaceutical development and is becoming increasingly more prevalent among new drug candidates (Baird and Taylor, 2012). Previews reviews highlighted that an increasing number of drug candidates have been denied due to their low bioavailability. The bioavailability of a drug is determined by its solubility, and its permeability at the molecular level allows the drug to go through the gut wall. The dissolution rate and solubility of APIs in the gastric or intestinal fluid are essential factors for achieving adequate absorption. Improving APIs solubility can improve absorption and therapeutic efficiency, especially those drugs with low solubility but high permeability. Poorly soluble compounds which are dissolved in the intestines are mostly excreted through the digestive system, and only a small amount of drug is transported to the bloodstream and the target tissue (David B. Hedden and Monthira Reodacha, 2013). New advanced formulations (drug delivery systems) are required because of this trend. Without the application of special drug delivery systems, the development of clinical dosage forms for low solubility APIs are intended to be unsuccessful or take more development time, resulting in an increase in cost (Wen, Jung and Li, 2015).

The primary objective of device formulation is to achieve end-product specifications

regarding drug bioavailability, non-toxicity, uniformity, stability and handling properties (Badens *et al.*, 2017). These limitations address a major problem in drug development and discovery, as the human body can only absorb the drug which solubilizes in the gastrointestinal (GI) tract, the drug having a low solubility in the GI medium generally leads to a low dissolution rate and insufficient bioavailability, which results in low active pharmaceutical ingredient in human. The United States Pharmacopoeia (USP) classify drug compounds according to their solubility, from very soluble compounds to practically insoluble compounds, which is as shown in Table 2-3 (Dahan, Wolk and Agbaria, 2014).

Table 2-3 USP solubility classified according to Dahan et al. (Dahan, Wolk and Agbaria, 2014)

Descriptive term (solubility definition)	Parts of solvent required for one part of solute	Solubility range (mg/mL)	Solubility assigned (mg/mL)
Very soluble (vs)	<1	≥1,000	1,000
Freely soluble (fs)	From 1 to 10	100–1,000	100
Soluble (s)	From 10 to 30	33–100	33
Sparingly soluble (sps)	From 30 to 100	10–33	10
Slightly soluble (ss)	From 100 to 1,000	1–10	1
Very slightly soluble (vss)	From 1,000 to 10,000	0.1–1	0.1
Practically insoluble (pi)	≥10,000	<0.1	0.01

2.2.1.1 *Classification of poorly water-soluble drugs*

In 1995, Gordon Amidon explained the Biopharmaceutics Classification System (BCS), whereby all drugs or drug candidates have been divided into four groups (Class I, Class II, Class III, Class IVs), the system sorted out the drug by solubility, permeability and dissolution as shown in Figure 2-5 (Amidon *et al.*, 1995). Moreover, the modified BCS add two subclasses for class II, namely class IIa and IIb. The subclasses depend on the drug compounds being either a dissolution rate limited (IIa) or solubility limited (IIb). Consequently, the drug absorption of IIa drug will not be affected a lot due to the high permeability, however, for IIb class, the solubility plays a significant role in predicting the drug absorption (Butler and Dressman, 2010).

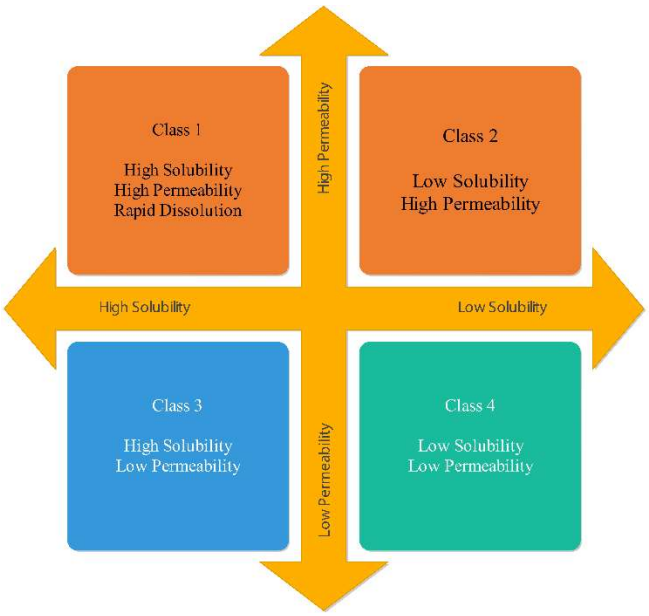

Figure 2-5 The Biopharmaceutics Classification System (BCS) as defined by Amidon et al. (1995).

2.2.1.2 *Formulation strategies for solubility enhancement*

About 40% of the drugs which have already been launched on the market have been identified as practically insoluble in water (according to USP definition <0.1mg/mL). For drug substances in development, about 90% of the drugs belong to BCS II and IV (Figure 2-6)(Ting *et al.*, 2018). The low solubility challenge of the drug may have emerged as early as in the process of drug development (Li and Zhao, 2007). Therefore, early formulation strategies are more considered during drug discovery and the process of development (Maas, Kamm and Hauck, 2007)(Kwong, Higgins and Templeton, 2011). This means when the drug substances have limited aqueous solubility in GI media, the formulation strategies need to be carried out in the initial stages (Stegemann *et al.*, 2007).

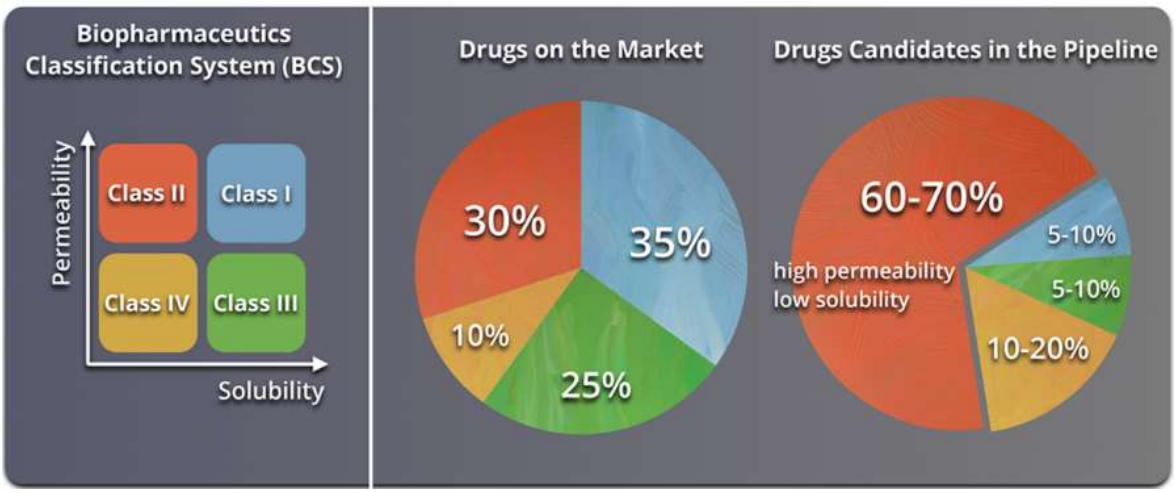

Figure 2-6 Estimated distribution of marketed and pipeline drugs by BCS classes (Ting *et al.*, 2018).

The formulation strategies to overcome the problems with low aqueous solubility can be divided into two separate ways, including chemical modification of the drug substance or physical modification (Göke *et al.*, 2018)(H. D. Williams *et al.*, 2013). In a chemical modification, there are many different ways to enhance the aqueous solubility, such as the generation of the prodrug, pH adjustment and salt formation (Limmatvapirat *et al.*, 2007; Stegemann *et al.*, 2007; Rodriguez-Aller *et al.*, 2015), surfactants (Abuzar *et al.*, 2018) (Abuzar *et al.*, 2018), co-solvent (Kendre, Pande and Chavan, 2014) and cyclodextrins (Rodriguez-Aller *et al.*, 2015), on the other hand, the physical modification includes particle size reduction (Khadka *et al.*, 2014), polymorphs, co-crystals, lipid-based systems, and amorphous solid dispersions (Vasconcelos, Sarmento and Costa, 2007; Yee, 2013; Paudel, Geppi and Van Den Mooter, 2014; Chen *et al.*, 2018; Jermain, Brough and Williams, 2018). The primary drug solubilisation strategies are summarised in Figure 2-7.

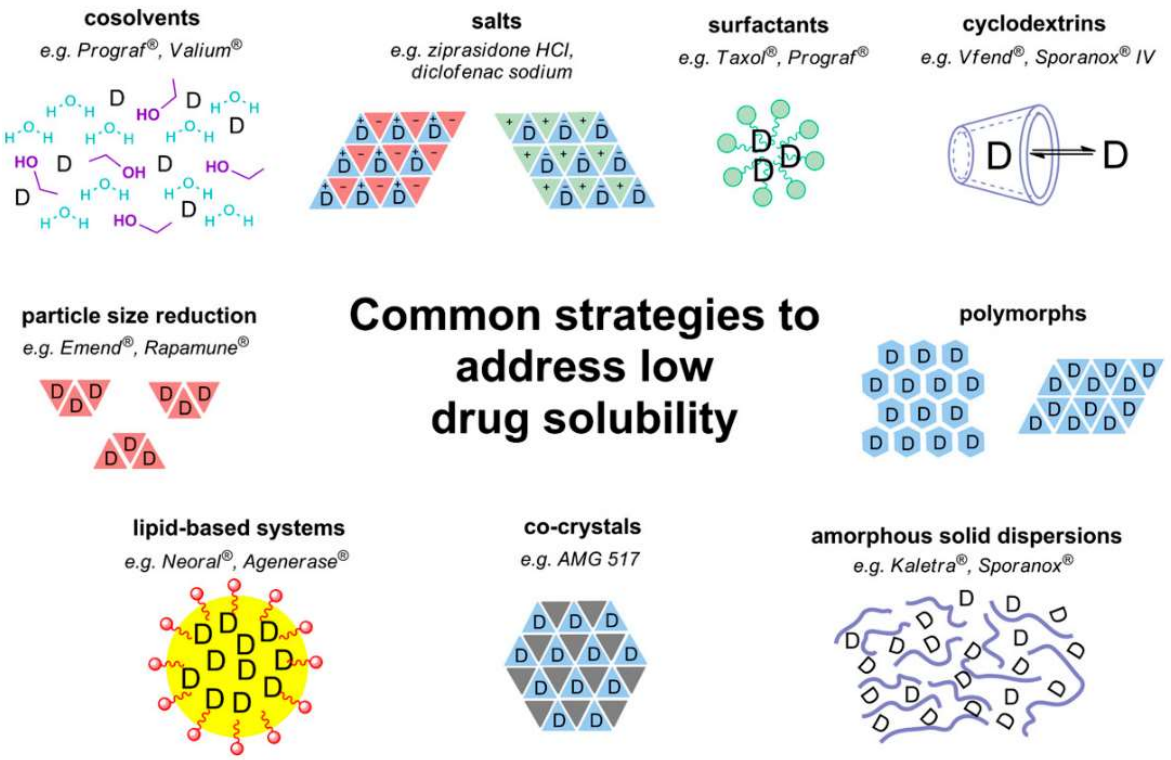

Figure 2-7 Schematic diagram illustrating the common strategies currently used to address low drug solubility in drug discovery and development (H. D. Williams *et al.*, 2013).

Of all the approaches mentioned above, particle size reduction was one of the first strategies investigated (Adeli, 2014)(Hammond *et al.*, 2007)(Wang *et al.*, 2013). Particle size reduction is achieved by the application of milling or engineered particle size control (H. D. Williams *et al.*, 2013). The mechanism of particle size reduction enhances the dissolution rate of poorly aqueous soluble drugs, which increases effective surface area (Martena *et al.*, 2014). Theoretically, the smaller the particle size is, the higher the dissolution rate will be. However, for practical purposes, reducing the particle sizes of drugs in capsules or tablets below 2-5μm is difficult, as a result, much higher particle sizes have been used during the drug discovery and development for ease of handling, formulation and manufacturing (Adeli, 2014)(Gandhi, 2016). Another approach to enhance the solubility of aqueous poorly soluble drugs is amorphous solid dispersion (Williams *et al.*, 2010). Amorphous material is the counterpart of its crystalline state. A typical crystalline structure material contains long-range ordered systems, in contrast to amorphous material which has random structure, as shown in Figure 2-8 (Bates *et al.*, 2006)(Yu, 2001). One critical property of an amorphous material is

the lack of a specific melting temperature; on the contrary, a transition temperature appears in the softening process, named glass transition temperature (Baghel, Cathcart and O'Reilly, 2016). When the poorly aqueous soluble drug is formed into an amorphous solid dispersion, it can produce a transient but highly supersaturated solution concentration (i.e., kinetic solubility), which is significantly greater than the equilibrium saturation concentration of their crystalline counterparts (Sun and Lee, 2013). The internal disordered structure of amorphous materials provides high mobility for molecules, which leads to an increase in solubility, but also reduces physical and chemical stability (Stachurski, 2011).

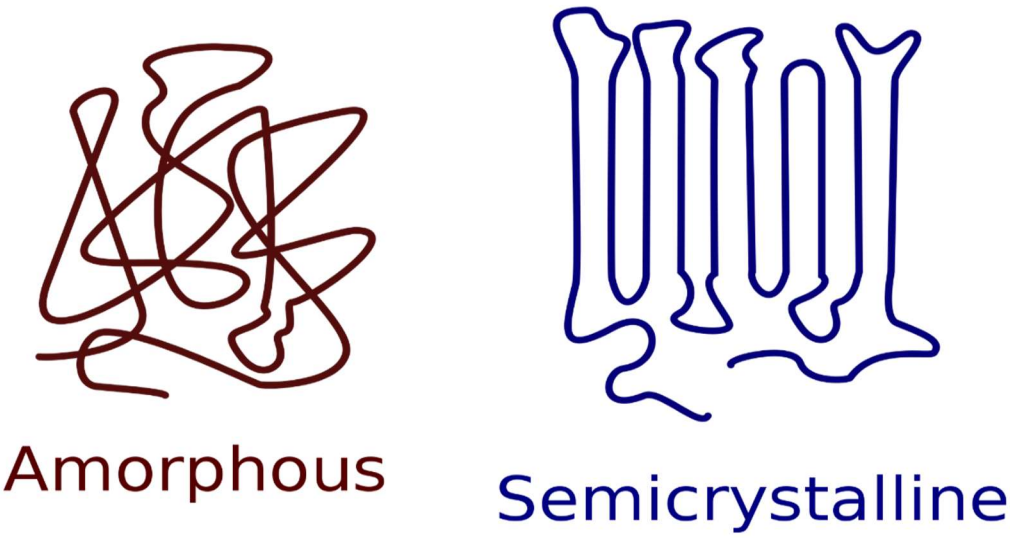

Figure 2-8 Schematic arrangement of molecular chains in an amorphous and semi-crystalline material (Plastics, 2017).

2.2.2 **Amorphous solid dispersion**

2.2.2.1 *Amorphous material*

As mentioned above, compared with crystallography, there are no such universal laws or rules that are widely known about the structure of amorphous solids; Sheng et al. also have a similar theory: "The atomic arrangements in amorphous alloys remain mysterious at present" (Sheng *et al.*, 2006). Moreover, in 1987, Cheng et al. has always thought that amorphous solids were a kind of disordered structure solids (Stachurski, 2011) (Cheng and Johnson, 1987). Amorphous materials have a higher solubility and faster dissolution

properties due to the increased area, volume and free energy. The implications and advantages of the amorphous solid dispersion, as a carrier of DDS, such as the enhanced bioavailability of poorly water-soluble drugs, will be described in the latter part of this review. Figure 2-9 shows the enthalpy change of a crystalline drug as a function of temperature. There is an apparent melting temperature for T_m that can be seen in the heating process. On the cooling cycle, assuming the cooling time is adequate, the molten drug cools slowly, resulting in the molecules having sufficient time to move from their current position to a thermodynamically stable point on the crystal lattice (Kawakami and Pikal, 2005). However, if the molten drug is cooled suddenly, then it may form into a supercooled liquid state without undergoing crystallisation. Instead, a transition zone appears in the cooling cycle, which is the glass transition process. The molecules system remains in equilibrium until the glass transition temperature T_g is reached (Graeser *et al.*, 2010), after this process, the drug enters a nonequilibrium state and converts into the glassy state of the drug (Baghel, Cathcart and O'Reilly, 2016). The amorphous materials have a significantly higher water solubility compared with their crystal form. Amorphous materials have higher free energy because there is no uniform crystal structure between the molecules, increasing the solubility of the drug. However, the increase in molecule movement can promote physical changes in crystal polymorphs. Furthermore, this can affect product stability (Ting *et al.*, 2018).

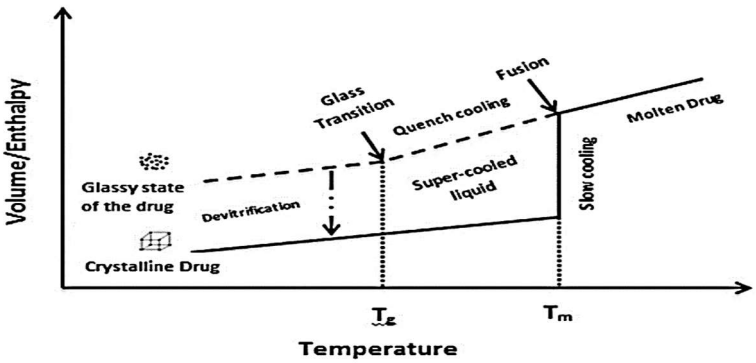

Figure 2-9 Enthalpy and volume of a different state of the drug as a function of temperature, where T_g and Tm are glass transition and melting temperature respectively; the diagram is not to scale. Reproduced from (Baghel, Cathcart and O'Reilly, 2016)

2.2.2.2 *Solid dispersion*

Solid dispersion technology is considered one of the most successful strategies for improving the dissolution and absorption of poorly water-soluble APIs (Beneš *et al.*, 2017). The first solid dispersion (SD) was introduced by Sekiguchi and Obi in 1961 (Sekiguchi and Obi, 1961). Chiou and Riegelman have defined solid dispersion (SD) as "The dispersion of one or more active ingredients in an inert excipient or a matrix, where the active ingredients could exist in finely crystalline, solubilised, or amorphous states" (Chiou and Riegelman, 1971)(Adeli, 2014). Simply speaking, solid dispersion is a kind of solid composite material that consists of at least two components. In the modern pharmaceutical industry, solid dispersions are now a broad concept which acts by dispersing drugs into polymeric carriers through different preparation processes (melting (fusion), solvent or melting-solvent method) to produce a drug-polymer mixture (Singh, Singh Baghel and Yadav, 2011)(Tran *et al.*, 2019). In this mixture, the carrier can be either crystalline or amorphous materials. Moreover, the drug state can be a molecular dispersion, amorphous clusters or micro drug crystal scattered in the matrix. The preparation method or the properties of the carrier-API composition generally affects the type of solid dispersion formed and thus subsequent behaviour of the solid dispersion. That is increasing the dissolution rate of poorly water-soluble drugs or decreasing the drug release rate of highly water-soluble drugs (Vasconcelos, Sarmento and Costa, 2007)(Beneš *et al.*, 2017).

The common preparation methods for solid dispersions include hot melt extrusion (melting method) and spray drying (solvent methods) (Davis and Walker, 2017). Compared with other formulation strategies, such as particle size reduction, salt form, and co-crystal of self-emulsifying drug delivery systems for solubility or absorption enhancement, solid dispersions have more benefits in some respects (Cutler *et al.*, 2006; Majerik *et al.*, 2007) (Yoshihashi *et al.*, 2006). Compared with chemical approaches, the salt formation can only be used for weakly acidic or basic drugs and not for neutral drugs where solid dispersions are easier to produce and more applicable. Furthermore, compared with another physical

formulation strategy, solid dispersions are more acceptable by the patients than solubilisation products since solid dispersion comes as a solid dosage form instead of liquid suspensions as solubilisation products (van der Merwe *et al.*, 2020). Normally, for practical purposes, significantly higher particle sizes are used in the particle size reduction technology formed by milling or micronisation (Craig, 2002) (Pouton, 2006). Instead, solid dispersions are more efficient than the above particle size reduction technology, generally speaking, it can provide a particle size of around 2-5 μm (Karavas *et al.*, 2006)(Craig, 2002). This range of particle size generally can significantly improve the drug solubility or drug release in the colon. Moreover, it can enhance bioavailability (Rasenack and Müller, 2004). However, the solid drug with such a low particle size has poor mechanical properties, specifically the compressive properties, and high adhesion and such small particle are difficult to process (Muhrer *et al.*, 2006) (Punitha *et al.*, 2011).

Depending on the different physical states of the drug and polymer, a solid dispersion can be classified into six different types as shown in Table 2-4 (Punitha *et al.*, 2011)(Singh, Singh Baghel and Yadav, 2011). The physicochemical properties of the drug or polymer as well as the preparation method or any interactions between the components have a significant effect on the physical state of solid dispersion, therefore, governing the type of solid dispersion and its properties (Singh, Singh Baghel and Yadav, 2011)(Leuner and Dressman, 2000)(Serajuddin, 1999). Normally, there are three different physical states of the element, including crystalline, amorphous, and molecularly dispersed. Based on the physical state classification theory, crystalline glass suspensions, amorphous glass suspensions and solid glass solutions are the most common types of amorphous solid dispersion as shown in Figure 2-10 (Punitha *et al.*, 2011)(Shingel *et al.*, 2017)(Sun and Lee, 2014). According to this classification, extruded shellac would correspond to glass suspension.

Table 2-4 Classification of amorphous solid dispersions based on the components' physical state according to Punitha et al., Singh et al.(Punitha *et al.*, 2011) (Singh, Singh Baghel and Yadav, 2011)

	Solid dispersion type	Matrix *	Drug **	No. Phases
I	Eutectics	C	C	2
II	Amorphous precipitations in a crystalline matrix	C	A	2
III	Continuous solid solutions	C	M	1
	Discontinuous solid solutions	C	M	2
	Substitutional solid solutions	C	M	1 or 2
	Interstitial solid solutions	C	M	2
IV	Glass suspensions	A	C	2
V	Glass suspensions	A	A	2
VI	Glass solution	A	M	1

*A: Matrix in an amorphous state, C: Matrix in the crystalline state.

**A: Drug dispersed as amorphous clusters in the matrix, C: Drug dispersed as a crystalline particle in the matrix, M: Drug molecularly dispersed throughout the matrix.

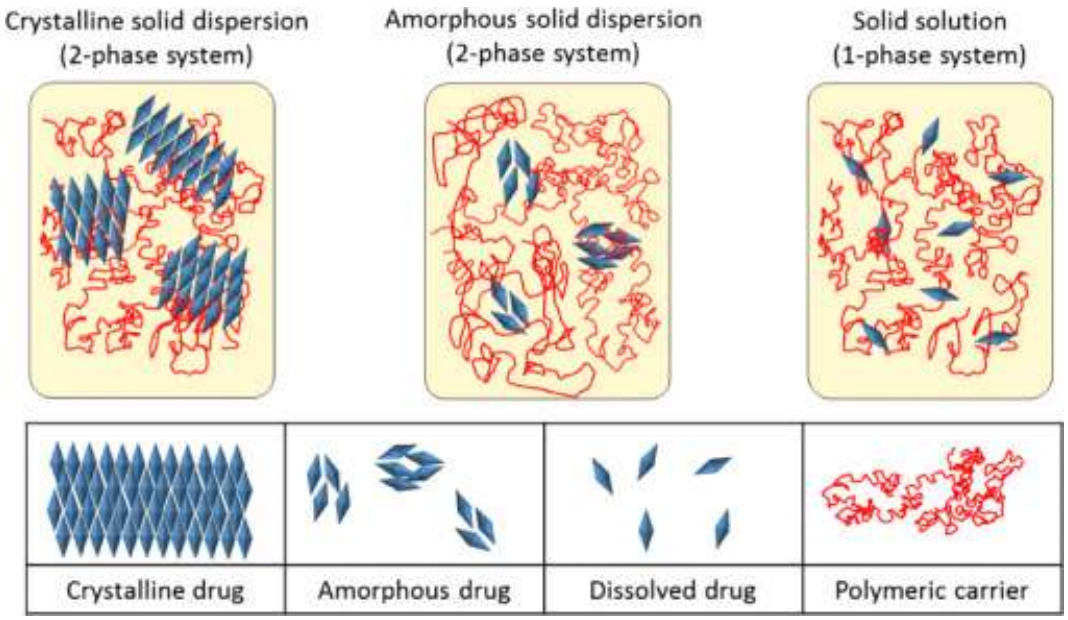

Figure 2-10 Classification of solid dispersion/solution of drug molecules in a polymeric carrier matrix (Sun and Lee, 2014)

2.2.2.3 *Preparation of solid dispersion*

With technological developments, solid dispersions can be prepared by several methods. These include Supercritical Fluid, Spray Freeze Drying, Solvent evaporation, Fusion method, High-speed electro-spinning technology, and Hot Melt Extrusion (HME), as shown in Figure 2-11.

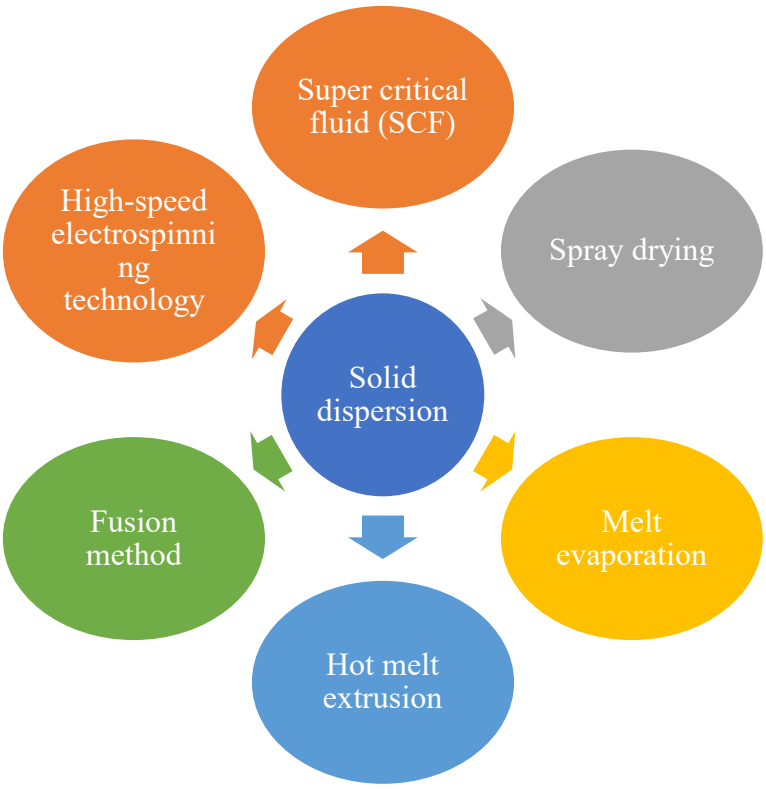

Figure 2-11 Methods for preparation of solid dispersion.

Supercritical Fluid (SCF)

While a fluid whose temperature and pressure are simultaneously above its critical point (T_c, P_c), the fluid exists as a single liquid phase having some advantageous properties of both a liquid and a gas (Eckert, Knutson and Debenedetti, 1996). As a result, becoming a supercritical fluid (SCF). The general fluid used as SCF is Carbon dioxide (CO_2) (Critical Point T_c=31.1ºC and P_c=7.3MPa) Figure 2-12 (Wahl and Czernuszka, 2006)(Kompella and Koushik, 2001), just because it is chemically inert, non-toxic, inexpensive and easy to achieve its critical condition (Vasconcelos, Sarmento and Costa, 2007)(Majerik *et al.*, 2007).

The SCF can provide a new alternative for formula coprecipitates which may be smaller in particle size, so that they could have better flowability and thus improve the solubility (H. D. Williams *et al.*, 2013)(Djuris *et al.*, 2019).

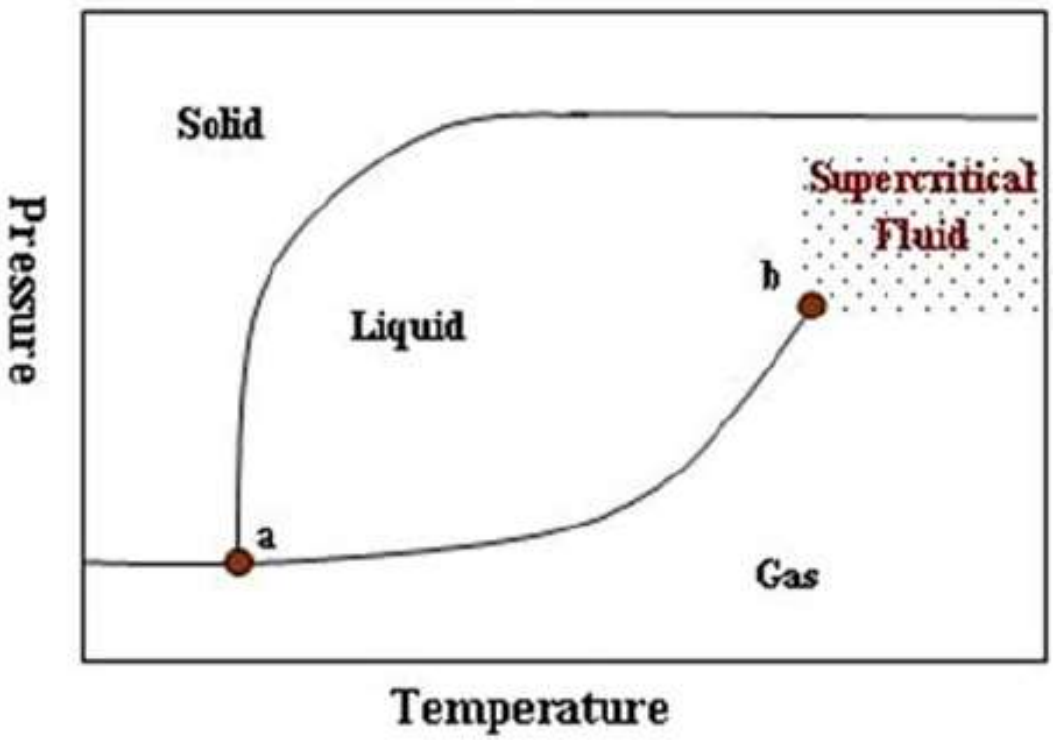

Figure 2-12 Phase Diagram of Carbon Dioxide (CO2). (a) Triple Point (-56.4ºC and 0.5MPa) (b) Critical Point (31.1ºC and 7.3MPa) (Wahl and Czernuszka, 2006).

Normally, the SCFs process consists of the following steps: (1) Put the drug and suitable matrix into the autoclave. (2) Loading the supercritical carbon dioxide at the precise critical temperature and pressure, causes the carriers to swell. (3) Mechanical stir by paddle in the autoclave. (4) Rapid decompression of the autoclave through a computer-controlled orifice to obtain the required particle size. Even though SCF has many benefits in manufacturing solid dispersion because most of the solubility of the drug in CO_2 is incredibly low and the value decreases with the increasing polarity the application of this technology is limited (Tran and Park, 2021). When compared with using organic solvents supercritical fluid has lower effectiveness (Punitha *et al.*, 2011)(Sapkale *et al.*, 2010)(Kulkarni, 2013).

Spray Drying

The Spray drying technology has been widely used to prepare the amorphous solid dispersion. It is a single-step continuous drying technology, that transforms liquid solution or suspensions into fine powder or particles by rapidly atomizing the solution and drying it with hot gas (Paudel *et al.*, 2013)(Williams, Watts and Miller, 2016). In this method, all the drugs or matrices are dissolved in a suitable solvent, and then the solvent is evaporated by the spray drying method. The schematic diagram for spray dry equipment and process is depicted in Figure 2-13 (Sosnik and Seremeta, 2015), including (1) Atomization, in this step, the atomiser produces a spray of small droplets having a uniform size. (2) Droplets Drying, all the small droplets are dispersed in the drying chamber with the drying gas. (3) Formation of dry particles, the droplets are rapidly solidified into microparticles in the drying gas. (4) Separation and collection of the dry product, the dry particles are transferred into the collector chamber by the cyclone (Paudel *et al.*, 2013)(Cal and Sollohub, 2010)(Schafroth *et al.*, 2012)(Umemoto *et al.*, 2020).

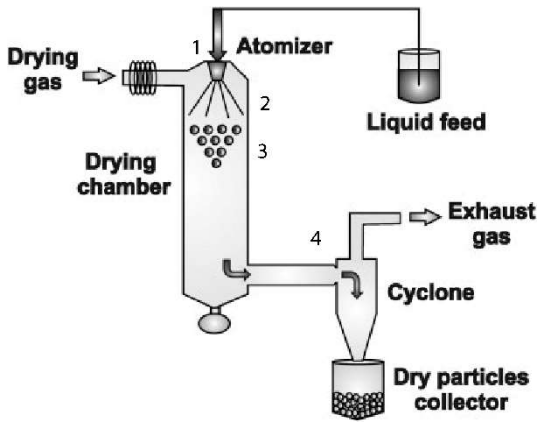

Figure 2-13 Diagram of the equipment and process of conventional spray-drying (Sosnik and Seremeta, 2015).

Melt evaporation

In this method, the drug first is dissolved in a suitable minimum amount of liquid solvent then mixing the solution directly into the molten carriers such as polyethylene glycol. After that, an evaporation processes is required to remove all solvent and obtain a clear dispersion product. The solid dispersion requires further drying until any weight loss is

eliminated. The different solvents used in this method may affect the polymeric form of the drug in solid dispersion. However, the disadvantage is clear, from a practical standpoint, this method can only handle a low therapeutic dose. Moreover, this method is not applicable to heat sensitive material, and because of the unique procedure of the method, this method has the advantages of both the melting and solvent methods (Hu, Lou and Hageman, 2018).

Fusion method

As mentioned above, the first solid dispersion (SD) was introduced by Sekiguchi and Obi in 1961 (Sekiguchi and Obi, 1961)(Chiou and Riegelman, 1971). They prepared the first solid dispersion of sulfathiazole and urea with this technology. In their study, all the components were mixed with stirring until melted completely by the use of an electric furnace. The resulting molten mixture was poured onto a plate and solidified, then the solid mixture crushed down and passed through a sieve (Sekiguchi, Obi and Ueda, 1964). Unfortunately, the high processing temperature may affect the drug matrix properties (Van Drooge et al., 2006).

High-speed electrospinning technology

Electrospinning has been described in the literature since the 1930s (Anton, 1938), also named as electrostatic spinning. This process utilises a high voltage source to apply high direct current to a polymer solution or melt to produce a polymer jet through a nozzle which is known as a Taylor cone. As the jet travels in the air, it accelerates toward a collector of opposite polarity to produce nanofibers. The resulting electrospinning polymeric fibres with diameters in the range of 100nm-500nm (Yu, 2001)(Sill and von Recum, 2008)(Ignatious *et al.*, 2010)(Yu *et al.*, 2018). Using the electrospinning technology produce nanoparticulate drug-embedded nanofibers. Therefore, it can enhance the dissolution rate of drugs with a poor water solubility (Ignatious *et al.*, 2010). A typical electrospinning system includes a capillary with the Taylor Cone to produce a jet; a high voltage DC supply with positive or negative polarity, which injects charge into the liquid, and the rotating and translation ground

collector (Figure 2-14).

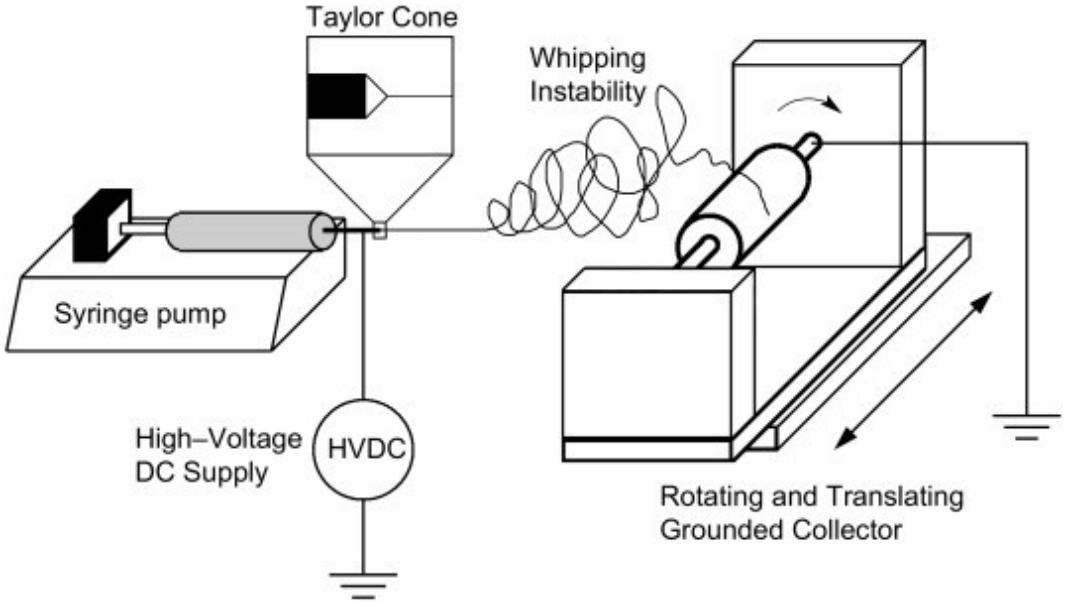

Figure 2-14 Schematic of a typical electrospinning system (Sill and von Recum, 2008).

Hot Melt Extrusion (HME)

The extruder consists of a rotating screw or a set of screws inside a heated barrel and is a very mature manufacturing method. In 1795, to produce a seamless pipe Joseph Bramah made a manual piston extruder, which is regarded as the first extruder in the world (Wuxi Weite Machinery Co., 2017). However, during the first 50 years of the 19th century, the extruder was only used to produce lead pipes, macaroni and other food processing, and in the brick and ceramic industry. In 1935 the German machinery manufacturer Paul Troester produced an extruder for thermoplastics. After four years, they made considerable progress, a modern single screw extruder was developed (Patil, Tiwari and Repka, 2016). Usually, an extruder consists of six parts including transmission, feeding device, barrel, screw and die as shown in Figure 2-15.

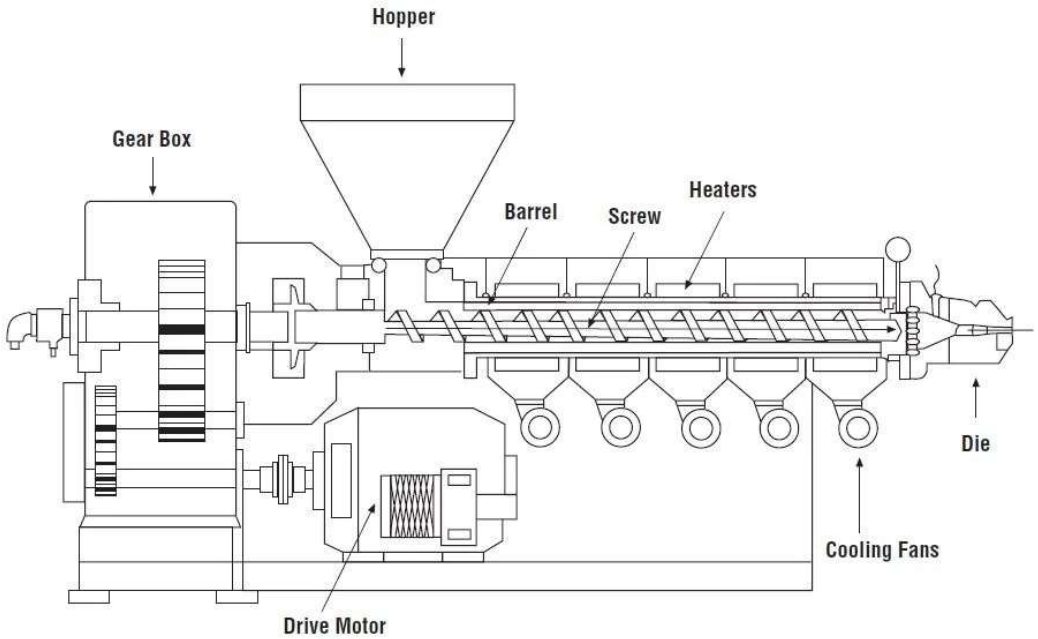

Figure 2-15 A typical extruder schematic (Dynisco, 2017).

A transmission is a motor with a gearbox; it is the power source, feeding device feeds the material to the barrel. The screw sitting inside the barrel is the most important part of the extruder. They produced a very high-pressure mix, melted and drive the material through a die. The screw drives the material to the nose and dies to form a unique shape. A schematic diagram of the extruder is shown in Figure 2-15 (Brazel and Rosen, 2012).

There are many twin-screw extruders commercially available. The one to use depends on the end-use application (Wagner, Mount and Giles, 2014). Different models have two parallel screw shafts that either rotate in the same direction (called co-rotating) or rotate in opposite directions (called counter-rotating), with varying distances between the screw shafts (Figure 2-16). If the centre line distance between the shafts is less than the screw diameter, the screws are called intermeshing, while screws with a distance between the shafts equal to the screw diameter are non-intermeshing (Kolter, Karl and Gryczke, 2012)(Jaluria, 2003).

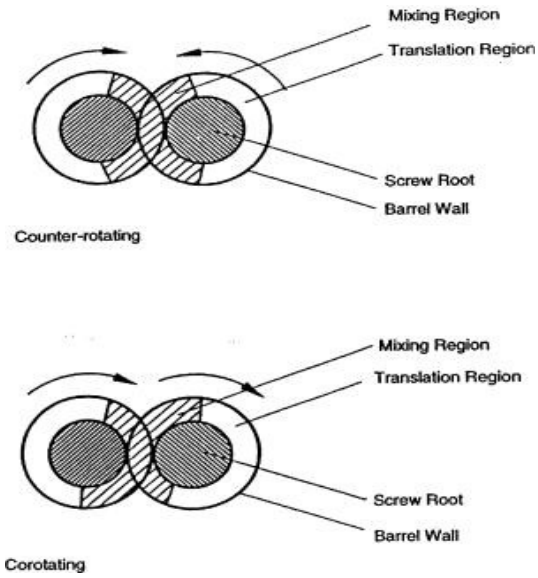

Figure 2-16 Schematic diagram of the cross-section of a tangential twin-screw extruder shaft (Jaluria, 2003). Counter rotation: The two screws rotate in the opposite direction but at the same speed & co-rotating: the two screws rotate in the same direction and speed.

The final product of the HME technique enhances the solubility of poorly water-soluble drugs because the drug is homogeneously dispersed in polymer carriers and forms an amorphous solid dispersion (Luo *et al.*, 2013)(Sathigari *et al.*, 2012)(X. Liu *et al.*, 2012). Moreover, the resulting extrudate can then be further processed into normal formulation (Tablet, capsule) as shown in Figure 2-17 (Lubrizol, 2020)(Baghel, Cathcart and O'Reilly, 2016).

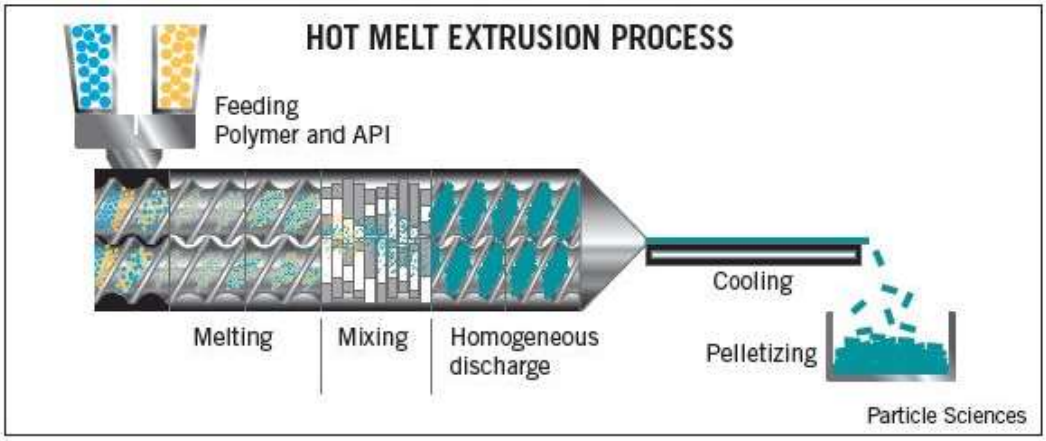

Figure 2-17 Schematic of a typical TSE system(Lubrizol, 2020)

Nowadays, when compared with other preparation methods, HME has a considerable

number of benefits. Therefore, it has increased interest in the pharmaceutical industry to produce solid dispersions (Hywel D. Williams *et al.*, 2013). These advantages include; (1) HME is an efficient and solvent-free process, compared with other processing techniques, it requires fewer steps. (2) HME processing can handle remarkably high or incredibly low drug loading dosage. (3) HME processing can convert the crystalline drug into an amorphous form, or the high shear rate can ground the API into very small particles. (4) The intermediates can be easily further processed into the desired shape. Unfortunately, the HME is limited because of its inability to process heat-sensitive or high melting point drugs (Shah *et al.*, 2013)(Madan and Madan, 2012)(Srirangam *et al.*, 2008).

2.3 Hot melt extrusion

2.3.1 **The history and development of the extrusion process**

In the modern plastic industry, Hot melt extrusion is one of the most widely applied processing techniques. The first application of metal screws can be traced back to the 16th century used in mechanical applications (Usher, 1954). In the 1935s, Paul Troester in Germany built the first machine used for thermoplastic materials (Tadmor and Klein, 1970)(Rauwendaal, 2014). The first twin-screw extruder used for polymer processing was built by Roberto Colombo (co-rotating) and Carlo Pasquetti (counter-rotating). Around this time, H. Heidrich developed electrical heating systems to replace the steam-heating units (White, Potente and Berghaus, 2003). Around the 1950s, scientists began to do theoretical research on extrusion technology, which greatly promoted the development of extrusion technology. Thus, after more than ten years of efforts by many scientists, a quantitative description of the extrusion process from the feed hopper to the die was generated (Carley and McKelvey, 2005; Rauwendaal, 2014). After that, twin screw extrusion has become more popular in industrial applications because it offers several advantages over single screw extrusion. For example, compared to single screw extrusion because twin-screw extruder has two screw mesh with each other. Therefore, it is easier to feed material, has higher kneading or dispersing capacity, has a lower propensity to overheat, has higher process

productivity and flexibility, and has better control of process parameters.

The first recorded application for melt extrusion used in the pharmaceutical industry was in 1971 (Frazza and Schmitt, 1971). Since then, the hot melt extrusion process shows significant potential as a continuous pharmaceutical process (Singhal, Lohar and Arora, 2011). Nowadays, large numbers of research groups demonstrated that the extrusion process is a significant viable technique for the production of pharmaceutical drug delivery formulation, the formulation can include granules, pellets, sustained-release tablets (Shergill *et al.*, 2016), transdermal and transmucosal drug delivery systems and implants (Srirangam *et al.*, 2008)(Chokshi and Zia, 2004)(Gupta, Kesarla and Omri, 2013)(Patil, Tiwari and Repka, 2016)(Crowley, Zhang, *et al.*, 2007). Compared with other processing methods, melt extrusion technology has its advance. Hot melt extrusion is a solvent-free process. It achieves solid molecular dispersions by a melt blending process, the intense mixing and agitation imposed by the rotating screw cause disaggregation of suspended particles in the molten polymer resulting in a more uniform dispersion and the process is continuous and efficient. As a result, the API is dispersed and dissolved into a polymeric matrix. It is an excellent alternative to other conventionally available techniques such as roll spinning and spray drying.

Compared to the typical plastics extruder, several requirements must meet regulatory for a pharmaceutical-grade extruder. The metallurgy of the contact surfaces must not be reactive, additive or absorptive with the product. Furthermore, the equipment is ready for the cleaning and validation requirements associated with a pharmaceutical environment. Otherwise, the operation of the extruder for pharmaceutical products is virtually identical to a polymer extrusion process (Crowley, Kumar Battu, *et al.*, 2007).

2.3.2 **Screw design for twin screw extrusion systems (TSEs)**

For a typical TSEs system, the extrusion process is performed similarly. Firstly, materials were fed into the extruder barrel and conveying happens. After passing through a

series of pressurised and mixing regions, the materials will be melted and miniaturisation via mixing elements and conveyed via flighted elements. The flighted elements discharge the melt through a die or other device to form various shapes for other downstream processes. During any twin-screw extrusion process, the rotating screws contained within the barrel are the key to the system (Todd, 1998). No matter co-rotating or counter-rotating, inter-meshing or non-intermeshing, the basic concept of the screw is the same, which is made of these continuous, longitudinal, small-mass mixing devices as shown in Figure 2-18. There are many inherent characteristics of the twin-screw extruder which include:

- Sanitary, the design of the extruder can guarantee that the material is continuously conveying, mixing and melting inside the metallic barrel to avoid stagnation.
- Continuous, the process runs stably and reproducibly, it can run uninterrupted until finished production.
- A small mass, due to its unique design, between the screw shapes and the barrel walls a localized bounded domain of a mass of material is contained, this design helps the accurate distribution of small formulation constituents.
- Longitudinal, the length of the process section consisting of barrels and screws can be extended until some boundary condition finally limits the systems. For example, heat transfer inside the barrels, shaft torque, vent velocity, minimum dwell time, or any other limitations.
- Screw interaction, because the two screws come together and mesh with each other, the flow patterns in the "apex region" can enhance the distributive and dispersive mixing during the process; transmit power through two-shaft, with the benefit of modern technology, the shaft transmit high torque to the materials, even though the barrel is long enough to reach the limitation boundary (Singhal, Lohar and Arora, 2011; Ghebre-Sellassie *et al.*, 2018).

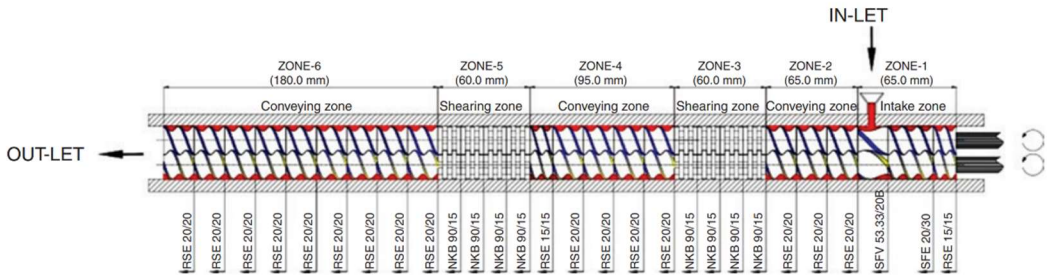

Figure 2-18 A typical screw design of a TSEs (Angadi *et al.*, 2017).

The screw design of TSEs is complex. It can be a single shaft design which can transfer significant higher torque, or the screw consisting of different screw elements on the shaft that can handle lower torque, but much more adjustable to different configurations and designs based on real-world conditions. Furthermore, mathematical predictive modelling of material behaviour in twin-screw extrusion is quite complicated because of the complexity of screw design, as well as the non-Newton fluid nature of most polymer materials that are processed. To meet some particular requirements of the screw design, most commercial extruders have a modular design, providing a choice of screws or interchangeable sections which alter the configuration of the feed, transition, and metering zones (Whelan and Goff, 1988).

2.3.3 **Hot melt extrusion: pharmaceutical applications**

As mentioned above, the extrusion process started in the food and rubber plastic industry in the 19th century, today the future for twin-screw extrusion has found its place in the array of pharmaceutical manufacturing operations, and it will eventually dominate the pharmaceutical manufacturing landscape for new drug entities. Nowadays, the melt extrusion process has been used for different purposes in the pharmaceutical industry, such as

1) Improving the solubility and dissolution rate of the drug by forming solid dispersion or solid solution,

2) Modifying or controlling the release of the drug,

3) Masking the bitter taste of an APIs (Patil, Tiwari and Repka, 2016).

2.3.4 **The material used in hot melt extrusion**

Theoretically, a solid dispersion is a complex mixture of drug substances and function excipients. For the HME process, the excipient used in the formulation was to deal with the process challenges, such as plasticiser, glidant, lubricant, antioxidants, surfactants, etc. (Ghebre-Sellassie *et al.*, 2018). Compared with the oral dosage form, functional excipients give melt-extruded pharmaceuticals some unique properties (Chokshi and Zia, 2004)(Crowley, Kumar Battu, *et al.*, 2007). Furthermore, all the materials must meet the same level of purity and safety as those used in conventional dosage forms. Fortunately, most of the substances used in HME pharmaceuticals applications have been used to produce the traditional solid dosage forms such as tablets, pellets and other oral dosage forms (Agrawal *et al.*, 2022). However, the materials must exhibit some thermal, physical, and chemical stability during the processing, even though the transitional time during the process is short. The shorter residence time may become an exception for some materials. The properties of an API usually limit its potential formulation and preparation options. Compared with other conventional pharmaceutical technologies, melt extrusion is a relatively new technology in the pharmaceutical industry, and it has many advantages. For example, the melt extrusion process does not require any solvent, which avoids any potential drug degradation caused by hydrolysis after adding certain solvents such as aqueous or hydroalcoholic solvents (Stanković, Frijlink and Hinrichs, 2015)(Tiwari, Patil and Repka, 2016). Also, the application of continuous processing technology makes it possible to directly cut the extruded rod to make tablets, which eliminates any potential tabletting problems that occur in conventional compressed dosage forms (Gohel and Jogani, 2005). The melt extrusion process is a thermal process. As a result, the polymer must present thermoplastic characteristics, and the physicochemical properties of the drug should be characterized before processing. The polymer material used in the process depends on its miscibility, polymer stability and some specific function of the final dosage form. In general, large

quantities of drugs can be dissolved in the polymer with a high solubilisation capacity. Moreover, high solubilisation capacity requires some fundamental prerequisites such as lipophilicity, hydrogen bonding acceptors or donors and the amide groups (Forster, Hempenstall and Rades, 2001). Furthermore, the solubility parameter could be another important parameter to determine the API and polymers are compatible or not (Forster *et al.*, 2001)(Patterson *et al.*, 2008). Many researchers had reported many different polymers used in the melt extrusion process. Such as polyvinylpyrrolidone (PVP) and its derivative (Febriyenti, Rahmi and Halim, 2019), polyethylene glycols (Belyatskaya *et al.*, 2019), HPMCAS (Solanki *et al.*, 2019), Kollidon® VA 64 (Szafraniec-Szczęsny *et al.*, 2021a), Soluplus® (Gajda *et al.*, 2018), poly (lactide) (PLA) (Stanković, Frijlink and Hinrichs, 2015), hydroxypropyl methylcellulose (HPMC)(Yang *et al.*, 2019), Eudragit® E PO (Yang *et al.*, 2019).

Overall, the pharmaceutical compounds used in the traditional processing systems are also compatible with the hot melt extruded forms. The main feature is their thermal stability during the process, however, due to the short residence time, not all thermolabile compounds are excluded. The use of additives such as plasticisers, and functional excipients can help the formulation achieve different purposes such as lower the processing temperatures or modifying the drug release profile (Kulkarni, 2013)(Chokshi and Zia, 2004)(Stanković, Frijlink and Hinrichs, 2015).

Nowadays, the hot melt extrusion process becomes an efficient way to manufacture drug delivery systems. This technology can be conducted in the broad scope of different dosage forms, resulting in both semi-solid and solid preparations. The properties of the polymer or the use of additives can modify the physical state of the drug substance in the formulation. They could be a crystalline form for sustained release application or create an amorphous solid dispersion form to improve the dissolution of poorly water-soluble drugs. However, the drawback of this technology is often related to the high energy input mainly caused by shear forces and temperature. Therefore, the processing condition or screw

configuration becomes significant (Breitenbach and Gmbh, 2002). The resulting extrudate often requires further downstream processes such as finish, shape and analysing of the extrudate, which causes the process to be non-continuous. So, increased research working in this field to create many novel and exciting aspects of this technology such as nanoparticles released systems, continues downstream process.

2.3.5 **Modelling and simulation of the extrusion process**

The finite element method (FEM) is a popular method for numerically solving differential equations arising in engineering and mathematical modelling. ANSYS software is a general-purpose finite element computer program for the solution of engineering analyses. Its capabilities problem solving for a vast range of engineering problems such as static analysis, elastic, plastic, thermal stress, stress stiffened, large deflections, et al. Analyses can be made in one, two, or three dimensions, including axisymmetric and harmonic element options. ANSYS also contains a complete graphics package and extensive pre and postprocessing capabilities (Kohnke, 1982). Ansys Polyflow is a finite element computational fluid dynamics (CFD) program package in ANSYS, designed primarily for simulating applications where viscous and viscoelastic flows play a significant role. The flows can be isothermal or non-isothermal, two- or three-dimensional, steady-state or time-dependent. Ansys Polyflow is used primarily to solve flow problems in polymer and rubber processing, food rheology, glass-work furnaces, and many other rheological applications. This program can perform several complex calculations such as multi-domain simulations, coextrusion of several fluids, three-dimensional extrusion and time-dependent calculation of free surfaces (ANSYS, 2021)(Pepliński and Mozer, 2011).

2.3.5.1 *The motivation for modelling*

There are many reasons for modelling screws (Kohlgrüber, 2007a):

- Screw design
- To increase process understanding

- To simulate individual effects or conduct qualitative studies
- To calculate inaccessible or difficult-to-access process values
- To simulate system-critical process conditions
- Scale-up/scale-down (generally with characteristics)
- To save on testing costs
- For training purposes (offline)
- For process monitoring and control (online).

Typically, modelling is utilized to help with screw design. It also makes a significant contribution to improving process comprehension. The end goal in this scenario is to create a "glass extruder," which has all properties visible from the outside. To get a feel for the machine's behaviour, system operators can initially mimic all operating situations "offline". System-critical process circumstances won't cause financial losses if the process is improperly controlled. (Chen *et al.*, 2017).

2.3.5.2 *Simulation: possibilities and limitations*

Due to the limitations of different dimensional models, the possibilities and limitations of the different models can be outlined as below:

- Possibilities
  - They provide data on the process's values (pressure, melt temperature, power, among others)
  - 3D models provide detailed information about the screw cross-section. 1D models provide information about changes in process values as the screw geometry changes (predominantly the melting process)
  - They make it possible to define process conditions quickly.
  - It is possible to quickly determine the effects of changing screw configuration (or geometry), process values, and materials.

- Limitations
  - Processes that are not appropriate can be ignored right away (trial planning)
  - The quality of the input values has a significant impact on the simulation's quality.
  - There is currently no 3D model for an entire screw setup.
  - In the design process, process simulation will never be able to replace engineering expertise.
  - Simulating specific material systems is limited.
  - Real-world processes are frequently far more complicated.

As a result, while not all process steps can be modelled, simulation allows us to gain a better understanding of the processes at hand. However, experience, as always, is required for the interpretation and organisation of the results (Kohlgrüber, 2007b).

2.3.5.3 *Advances in numerical simulation and analysis of intermeshing twin-screw extrusion processes*

Co-rotation twin-screw extruders play a particularly important role in polymer processing in modern processing technology. Over the years, great progress has been made in the design and manufacture of co-rotating twin-screw extruders. However, due to the complexity of the flow path shape and material movement inside the extruder barrel, the knowledge and understanding of the extrusion process and extrusion mechanism is still at a very early stage (Hyvärinen, Jabeen and Kärki, 2020). Nevertheless, with the rapid increase in computing performance of PC machines, Computational fluid dynamics (CFD) simulation techniques are becoming increasingly widely used to analyse the mass and heat transfer of fluid flows, especially, in the field of polymer processing. To explore the solid conveying mechanism, melting mechanism, melt conveying mechanism and mixing mechanism of the twin-screw extrusion process, a combination of mathematical simulation and experimental analysis has been used to describe the twin-screw extrusion process by mathematical and physical models. The development of modern computer technology has provided a powerful

and advantageous tool which aims to use the numerical simulation method to study the extrusion process. Firstly, it is necessary to establish a specific physical model as well as a corresponding mathematical model to express the relationship between several variables in the extrusion process, which are simulated by a computer. With the advancement of science and technology and the improvement of theoretical basis, numerical simulation techniques in polymer processing have changed considerably in the last few decades.

The study of twin-screw extrusion mechanisms began in the 1960s, and in 1964, Erdmenger (1964) showed that there was a spiral "∞" flow in the meshed, co-rotating twin-screw extrusion flow channel (Erdmenger, 1964). In 1969, Flumerfelt et al. discussed the flow of isothermal power-law fluids in parallel plates in detail (Flumerfelt *et al.*, 1969). In the 1970s, a lot of research work was completed on the melt transfer zone in twin-screw extruders. In 1974, Tadmor (Tadmor, Lipshitz and Lavie, 1974) proposed a mathematical model of the dynamic operation of an extruder. In the late 1970s, Tadmor and Gogos (Tadmor and Gogos, 2006) established a parallel plate model based on the principle of dynamic pressurization. Newtonian fluid was taken as an example to deduce the velocity distribution, shear stress distribution and flow calculation formula when the melt was in laminar flow. The flat plate model is a typical one-dimensional model, which is the basis for the theory of single and twin-screw extrusion melt transport. When a one-dimensional model is used to analyse the twin-screw extrusion process, the effect of screw curvature on flow is not considered. When the one-dimensional model analyses the extrusion process, a lot of simplifications are made on the extrusion process, so its simulation accuracy can only meet the requirements to a certain extent. With further in-depth study and research, a two-dimensional numerical model was introduced. In 1976, Janssen et al (Janssen, JJ and JM, 1976) used a two-dimensional model to study the pressure build-up during the process and output of a twin-screw extruder. Werner (Werner, 1978) presented the mathematical model and experimental results of the screw element and the kneading disc element. In the early 1980s, Denson et al. use finite element method (FEM) to analyse the flow of Newtonian

fluid in the flow channels of screw elements with different geometries and discussed the effect of the distribution of axial pressure on fluid flow inside the barrel. However, this study did not consider the influence of the meshing zone (Denson and Hwang, 1980). Later, Booy discussed the isothermal flow of Newtonian fluid in two different kinds of flow regimes, namely filled with liquid and partly fulfilled flow regimes. In this study, the author established the equations of drag flow, pressure flow and leakage flow in the meshing area (Booy, 1980). In 1987, Szydlowski et al. proposed a new physical model of melt transport and applied the fluid lubrication approximation theory and flow analysis network (FAN) method to solve the two-dimensional isothermal flow field of a Newtonian fluid in a rectangular groove. The two-dimensional model is to analyse the flow in the section perpendicular to the cross-section of the channel, or the flow in the section perpendicular to the axis, however, the effect of screw curvature on the flow was ignored (Szydlowski and White, 1987). As a result, the model cannot fully and truly reflect the flow of materials in the twin-screw extruder. In the last 30 years, with the development of computer technology and the emergence of large-scale finite element analysis software, it has become possible to establish a three-dimensional flow field analysis model based on one-dimensional and two-dimensional numerical calculations. Based on the model, a lot of research has been performed on its mixing performance and mechanism. The established 3D physical model is much closer to the actual working state, and the calculation results are more accurate. Steller have reported the exact solution for the isothermal flow of a power law fluid in a rectangular channel including both longitudinal and transverse velocity components (Steller, 1990). Yang and Mana Zloczower-emulated the three-dimensional flow in the kneading disc element using the fluid dynamics analysis package-FIDAP, obtained the distribution of velocity, pressure and shear stress, and discussed the influence of extruder design variables and process conditions on the flow characteristics (Yang and Manas-Zloczower, 1992). White and Chen performed simulations of non-isothermal flow in screw and kneading disc elements (White and Chen, 1994). Goffart and Wal ignored the influence of the screw flight

in the meshing area on the flow direction and analysed the three-dimensional flow in the meshing and non-meshing areas of the threaded element and the kneading disc element. In this study the pressure field, velocity field and temperature field of the Newtonian fluid were solved (Goffart *et al.*, 1996; Van Der Wal *et al.*, 1996). Bravo et al carried out a three-dimensional isothermal numerical simulation of a meshing co-rotating twin-screw extruder under the quasi-static assumption and analysed the influence of the structure of the elements in the kneading disc and the boundary conditions of the inlet and outlet on the pressure and velocity distribution (Bravo, Hrymak and Wright, 2000). Takeshi Ishikawa et al used FEM technology to establish a non-Newtonian and non-isothermal three-dimensional model of the kneading disc element and the conventional screw element in the meshing co-rotating twin-screw extruder, obtained distribution of pressure, velocity and temperature in the flow field. Additionally, the study compared and verified the simulation results with experimental data. Yoshinaga et al. simulated the flow of the three-head kneading disc element area by FEM method and using marker tracking method to analyse the performance in distributive mixing for three different types of kneading blocks in terms of the residence time distribution and the nearest distance between markers at various periods of time (Yoshinaga *et al.*, 2000).

In terms of analysis software, simulation content and visualization of simulation results, numerical simulation software has evolved from ANSYS at the end of the 1990s to FLUENT, POLYFLOW and FIDAP software (Engelman, 1983; ANSYS, 2022a, 2022b). Simulation content has evolved from simple field quantities such as velocity, pressure and viscosity to quantitative indicators such as residence time distribution, distribution mixing index and separation ratio. Visualization of simulation results has evolved from static clouds, contour plots, velocity vectors, and visualization of results. The visualization of the simulation results has evolved from static cloud maps, contour maps and velocity vector maps to the current 3D dynamic particle motion simulation animation. By using a variety of existing professional analysis software, the flow field can be quantitatively analysed from macroscopic to microscopic based on a reasonable simplification of the actual production

situation, accurate construction of geometric structure models and reasonable set of boundary conditions, and the introduction of statistical parameters(Malik, Kalyon and Golba, 2014; Lewandowski and Wilczyński, 2022)(Hyvärinen, Jabeen and Kärki, 2020)(Nakayama *et al.*, 2018).

2.3.5.4 *The geometry of co-rotating extruders: conveying and kneading elements*

The geometry of closely intermeshing co-rotating twin-screw extruders is distinguished in practice by the fact that adjacent screw elements are identical in geometry, are symmetrical, and rotate at the same speed. Geometries in which the two shafts rotate at different speeds and which have different numbers of threads have not achieved practical significance (Booy, 1978).

As shown in Figure 2-19, a screw profile with different threads can be divided into two times symmetrical parts. A screw profile is composed of three parts within this symmetrical area: tip, flank, and root. The tip comprises an arc its diameter equals the external diameter of the screw profile, and the centre point is the centre of the shaft. One edge of each tip borders the adjacent flank. For screws that wipe the inside of the barrel, the flanks each comprise an arc its radius equals the centreline distance. The flanks merge tangentially into the root area. The diameter of the root area corresponds to the diameter of the screw core, and its centre is the centre of the shaft. The tip cleans the root of the opposite screw and vice versa. The corner of the profile between the tip and the flank cleans the opposite flank. These types of screw profiles are named as fully wiped twin-screw profiles.

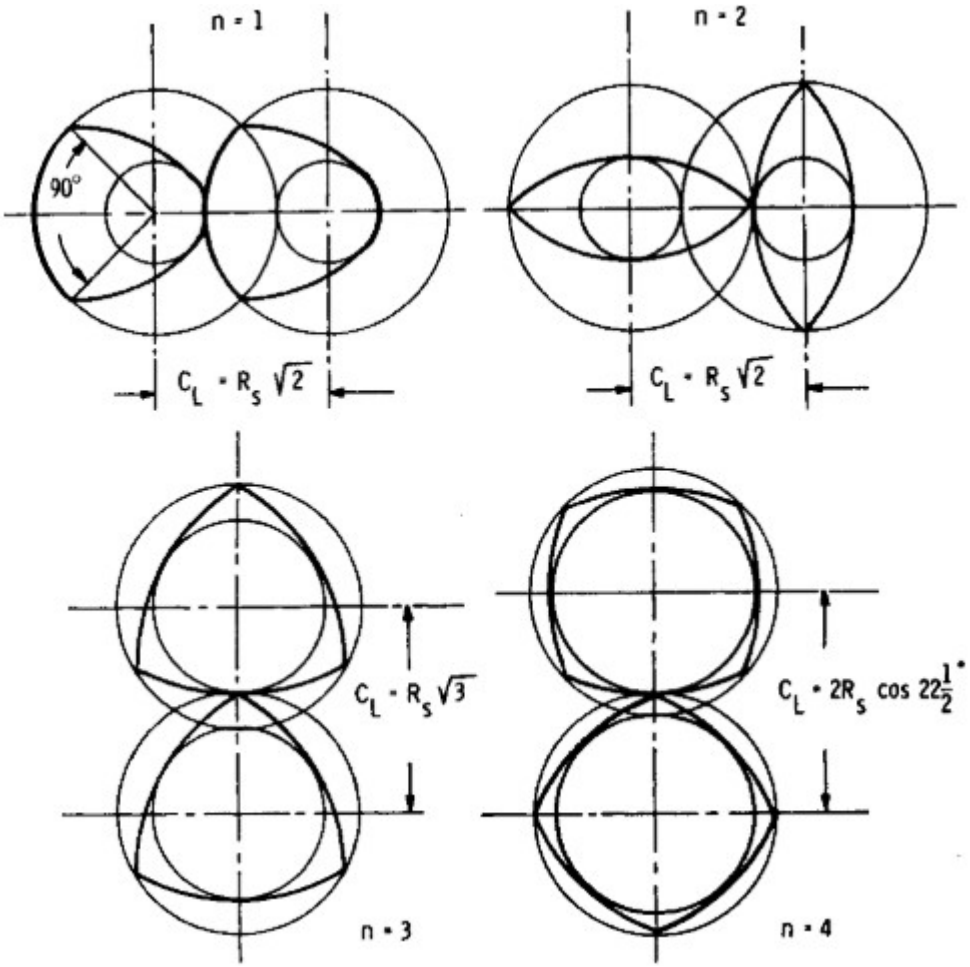

Figure 2-19 Screw profile with different threads (Booy, 1978)

The screw profile equation for each arc has already been extensively studied by many researchers. In 1978, Booy published an article to describe the geometry of fully wiped twin screw system (Booy, 1978) as shown in Figure 2-20.

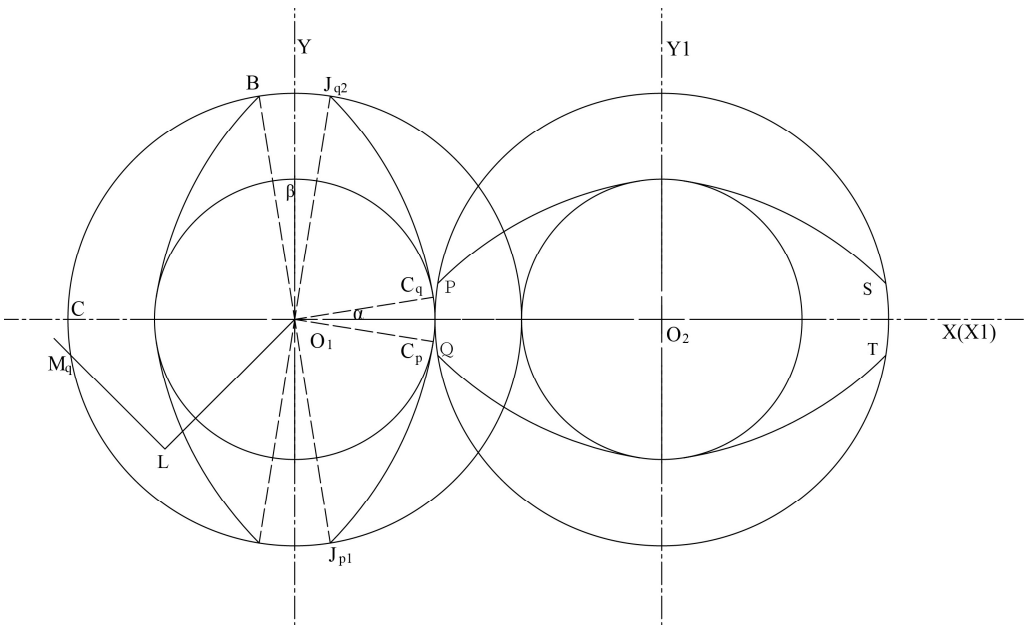

Figure 2-20 Fully wiped twin screw system

Because the screw profile is symmetrical, therefore for two flight profiles, one equation for arc C_qJ_{q2} is enough to represent the other three arcs.

For arc C_pC_q

$$x^2 + y^2 = R_b^2 \qquad 2\text{-}1$$

For arc C_qJ_{q2}

$$(x - x_q)^2 + (y - y_q)^2 = C_L^2 \qquad 2\text{-}2$$

$$\begin{cases} x_q = -R_s \cos(\alpha/2) \\ y_q = -R_s \sin(\alpha/2) \end{cases} \qquad 2\text{-}3$$

For arc $J_{q2}B$:

$$x^2 + y^2 = R_s^2 \qquad 2\text{-}4$$

Note: R_b is screw external radius

R_s is screw core radius

C_L is the centreline distance between two shafts

α is root angle

β is tip angle

Equation 2-1, 2-2, 2-3 is the Cartesian coordinate equation of the C_p-B segment of the screw profile curve, and the equations of the other segments can be obtained in the same

way. The equation 2-1, 2-2, 2-3 can be expressed in polar coordinates as follow:

$$\rho(\theta)\begin{cases} R_b & \begin{cases} -\frac{\alpha}{2} \le \theta \le \frac{\alpha}{2} \\ \pi - \frac{\alpha}{2} \le \theta \le \pi + \frac{\alpha}{2} \end{cases} \\ -R_s \cos\left(\theta - \frac{\alpha}{2}\right) + \sqrt{C_L^2 - R_s^2 sin^2\left(\theta - \frac{\alpha}{2}\right)} & \begin{cases} \frac{\alpha}{2} \le \theta \le \frac{\pi}{2} - \frac{\beta}{2} \\ \frac{\pi}{2} + \frac{\beta}{2} \le \theta \le \pi - \frac{\alpha}{2} \\ \pi + \frac{\alpha}{2} \le \theta \le \frac{3\pi}{2} - \frac{\beta}{2} \\ \frac{3\alpha}{2} \le \theta \le 2\pi - \frac{\alpha}{2} \end{cases} \\ R_s & \begin{cases} \frac{\pi}{2} - \frac{\beta}{2} \le \theta \le \frac{\pi}{2} + \frac{\beta}{2} \\ \frac{3\pi}{2} - \frac{\beta}{2} \le \theta \le \frac{3\pi}{2} + \frac{\beta}{2} \end{cases} \end{cases} \qquad 2\text{-}5$$

2.3.5.5 *Type of mixing in hot melt extrusion*

In polymer hot melt extrusion, the material is normally present as pellets or powders. Ideally, additives/APIs need to be in the form of very fine particles to distribute satisfactorily and fine particles tend naturally to agglomerate. Consequently, optimum mixing of the particles into melted polymer requires finite forces sufficient to separate the individual particles and wet them within the melted liquid polymer. To accomplish this, the particles must be further mixed to achieve a uniform concentration throughout the polymer. These two steps are described as 'Dispersive Mixing 'and 'Distributive Mixing', as shown in Figure 2-21.

Distributive mixing: An operation that increases the randomness of the spatial distribution of the minor constituent within the major base with no changes in the size of the minor particle (Gale, 2009).

Dispersive mixing: An operation that reduces an agglomerate size of the minor constituent to its ultimate particle size (Shenoy, 1999).

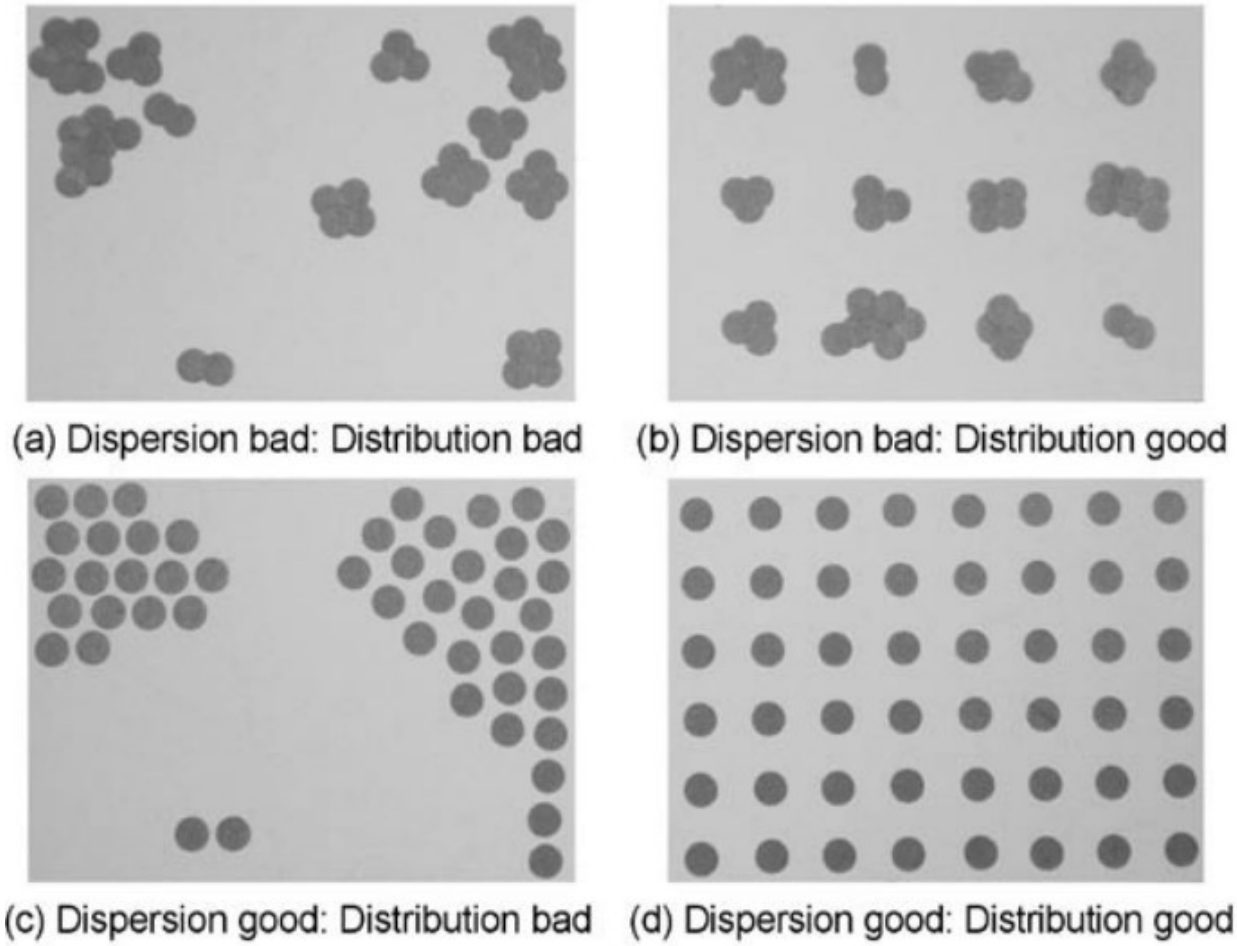

Figure 2-21 A simple illustration of Dispersion and distribution (Jonathan, 2015) Figure (a) shows bad dispersion and bad distribution. Figure (b) shows bad dispersion and good distribution. Figure (c) shows good dispersion. Figure (d) shows good dispersion and good distribution.

2.4 Shellac material

2.4.1 **Introduction**

Shellac also known as lac, gommelaque and lacca is a purified form of a natural polymeric resin produced by the female insect, Laccifer lacca, which is mostly cultivated in host trees in India, Thailand and the South area of China (Farag and Leopold, 2011) (Chauhan *et al.*, 1973). The term ‘‘lac’’ comes from the Sanskrit word ‘‘lakh,’’ meaning a thousand, to signify the immense number of insects and larvae that make the lac tree their abode. Ancient Asian cultures found many functions for shellac and its constituents in textiles, ornaments, and cosmetics (Das and Jacob, 2011).

The lac insect lives on several specific trees and bushes, the so-called lac hosts. Even though more than 300 different host trees are surviving, only a few of them are used for large-scale cultivation (Gullan and Kondo, 2007). The Kerria Lacca (Kerr) Lindiger (Coccideae) are parasitic insects on certain trees in India, which are considered the most important species because they have the highest lac productivity. Other insects like the Kushmi strain are related to the Kusum tree (Figure 2-22A) (Schleichera oleosa), whereas insects of the Rangeeni strain (Bysakhi) habituate on the Palas (Butea monosperma) and Ber (Zizyphus mauritiana) trees (Figure 2-22B, C). In Thailand, the major species is Laccifer Chinensis (Madihassan), habituating on the Raintree (Figure 2-22D) (Samanea saman). Furthermore, in China, there is a slightly different species, Kerria yunnanensis, related to Colona floribunda, Dalbergia balansae Prain or Raintree (Osman, 2012)(Buch *et al.*, 2009).

As mentioned above, shellac is a natural resin produced by the female insect. These insects, which only have six months of life, consume the tree sap while secreting lac through their pores (Das and Jacob, 2011)(Rowe, Sheskey and Quinn, 2009). There are two generations of lac insects in one year. After the adult insect gives birth to the young insect, the stick lac is collected by scraping the resin of twigs or cutting down the lac bearing twigs (Farag, 2010).

As the refining processes progress, the Lac can be distinguished into three kinds, such as sticklac, seedlac, and shellac; however, there is one more kind of lac not as commonly known, called lump lac, all better distinguished as follows (Charles Hatchett, 1804).

1. Sticklac, is the substance or comb in its natural state, incrusting small branches or twigs.
2. Seedlac is purified sticklac, which has been separated from the twigs and reduced into a small fragment.
3. Lump lac is formed from seedlac, liquefied by fire, and formed into cakes.
4. Shellac, according to Charles Hatchett (1804), is prepared from the cells, liquefied,

strained, and formed into thin transparent laminae.

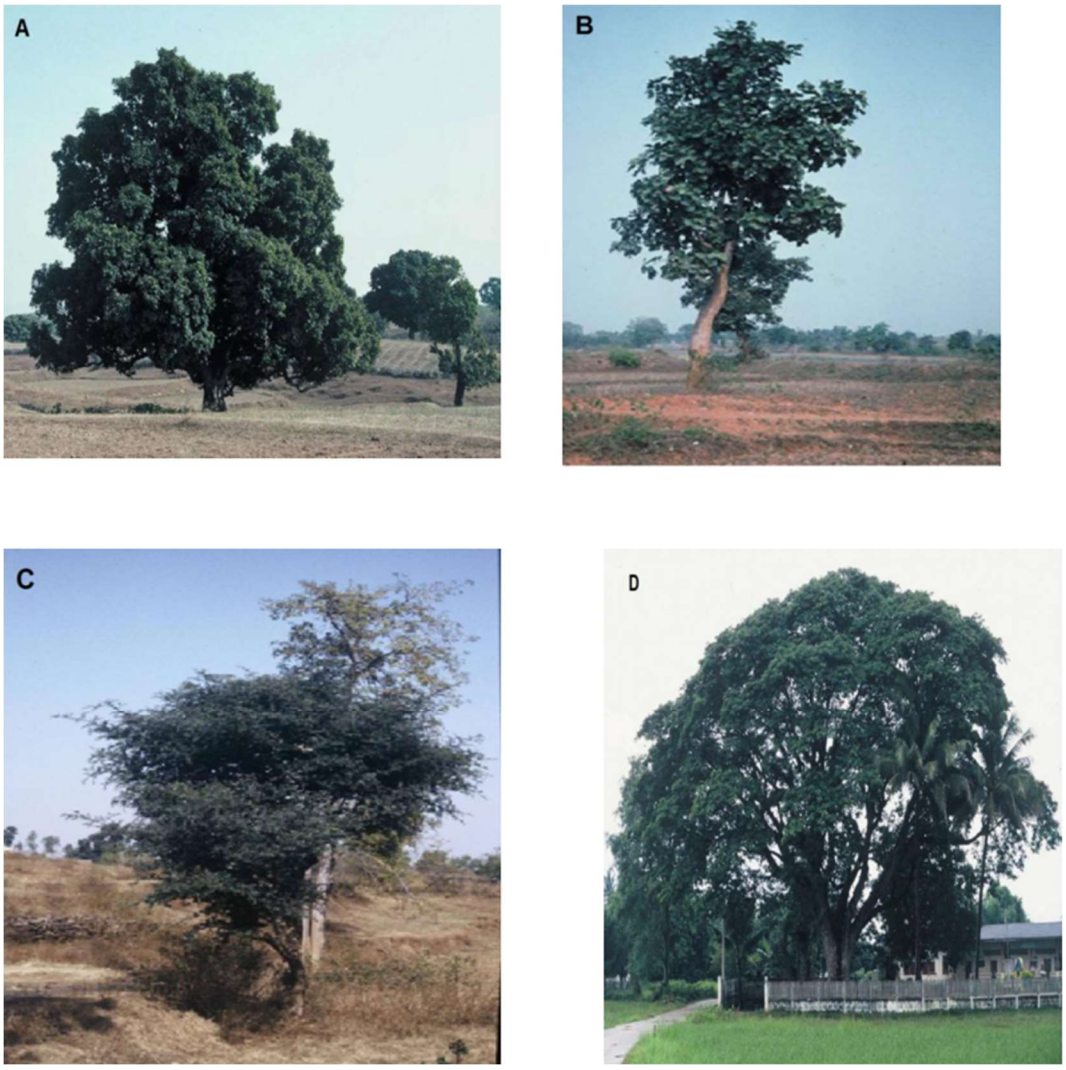

Figure 2-22 Photographs of examples of Shellac host trees:(A) Kusum tree, India (Schleichera oleosa); (B) Palas tree, India (Butea monosperma); (C) Ber tree, India (Zizyphus mauritiana); and (D) Raintree, Thailand & China (Samanea saman) (Osman, 2012).

2.4.2 **Refining process**

The collected stick lac required further processing and washing with water to remove any existing twigs or insect residue, water-soluble colouring agent laccaic acid. The resulting product is called seedlac, and there are three different processes used for refining seed lac to the final product shellac (Shown in Figure 2-23). The chemical compositions, properties, and release characteristics are depending on the different seedlac, as well as the process used for refining (Penning, 1996).

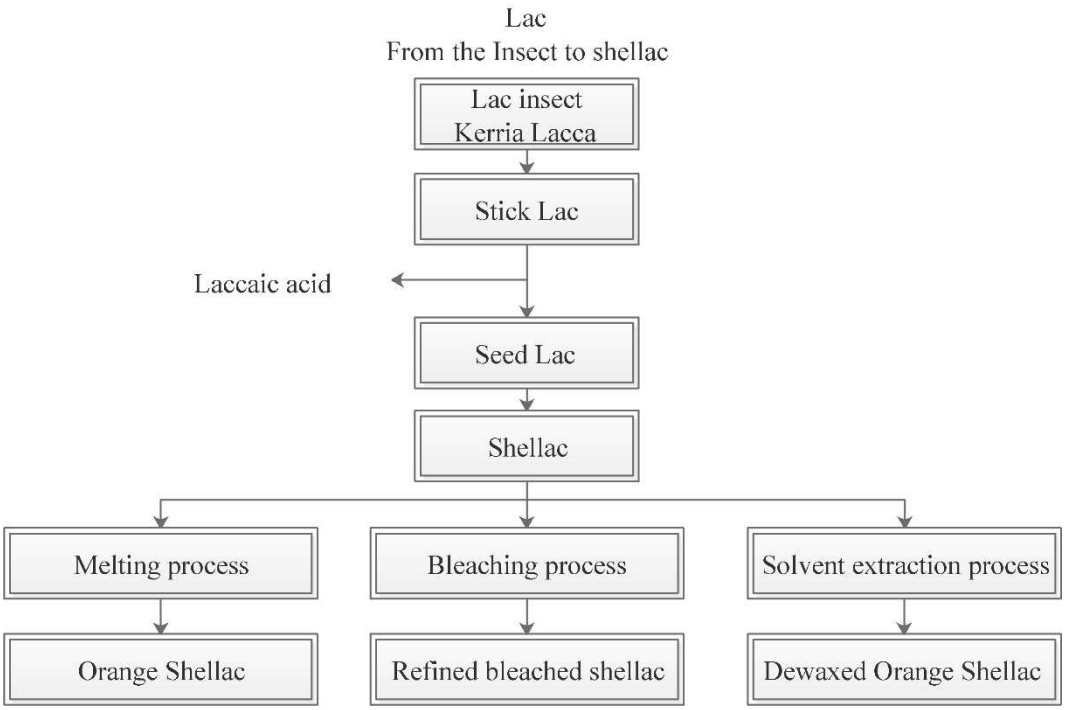

Figure 2-23 Flow chart demonstrating the refining process for shellac (Buch *et al.*, 2009).

2.4.2.1 *Melting process*

The melting process is a traditional process of refining seedlac. In this process, the seedlac melting down in steam-heated hydraulic presses are in line with the filter, and the pure molten lac is pressed out and cast into a thin film on a roller band. After the film cooling, it is crushed down to small flakes. In this method, the shellac wax cannot be removed, and the colour of the shellac depends on the seedlac used in the process (Azouka, Huggett and Harrison, 1993) (Farag, 2010) (Osman, 2012).

2.4.2.2 *Bleaching process*

In this method, the seedlac firstly is dissolved in an aqueous alkaline solution, and then add the sodium hypochlorite to destroy and removes the colouring materials in the lac, which is mainly due to the water-insoluble erythrolaccin. Finally, it is followed by the addition of sulphuric acid to precipitate the shellac. Although the bleaching process product has lots of benefits for many technical applications, the addition of chlorine and change in molecular structure can lead to cross-linking and polymerisation. This batch of shellac is used for the coating of citrus fruits and apples as well as for confectionery and pharmaceutical glazes

(Osman, 2012)(Farag, 2010)(Azouka, Huggett and Harrison, 1993)(Pearnchob, Siepmann and Bodmeier, 2003a)(Khorram, Ramezanian and Hosseini, 2017)(Soradech *et al.*, 2017).

2.4.2.3 *Solvent extraction process*

The solvent extraction process is a very gentle process for refining shellac. The first step of this process is to dissolve seedlac in ethanol, and then filter the insoluble wax and impurities. The light-coloured grades of shellac are achieved by the addition of activated carbon. After the further filtration step and the removal of ethanol, the resin is drawn to a thin film. The films are required to break into flakes after cooling. In this refining process, the shellac molecular structure was not affected. The properties of the final product depend on the type of seedlac and the processing parameters (Farag, 2010)(Rowe, Sheskey and Quinn, 2009)(Buch *et al.*, 2009).

2.4.3 **Composition of shellac**

As mentioned above, shellac is the refined form of seedlac; it is a complex mixture of aliphatic and alicyclic acid (Jalaric Acid and Shellolic Acid), which is illustrated in Figure 2-24 (Chauhan *et al.*, 1973). Shellac is made up of resin (70-80%), wax (6-7%), colouring matter (4-8%), and other materials (15-25%) such as debris and moisture. Different types of shellac have similar compositions, but different amounts as illustrated in Table 2-5. Chemical structures of the main components of shellac reported in other papers were listed in Figure 2-25 (Wang *et al.*, 1999)(Singh, Mhaskar and Dev, 1978)(M. S. Wadia, R. G. Khurana, 1969). The resin has two fractions: a soft fraction is made up of single esters of a sesquiterpenoid acid and a hydroxy fatty acid, and a substantial fraction in which the aforementioned single esters are polymerised by ester linkages (Al-Gousous, Penning and Langguth, 2015)(Wang *et al.*, 1999). This ester structure has been confirmed and further specified by a modern analytical methods such as liquid and gas chromatography (Chauhan *et al.*, 1973)(Cunningham, Furneaux and Hillman, 1976) or combined pyrolysis and mass spectrometry (Wang *et al.*, 1999)(Chiavari *et al.*, 1995)(Chiavari, Fabbri and Prati, 2002).

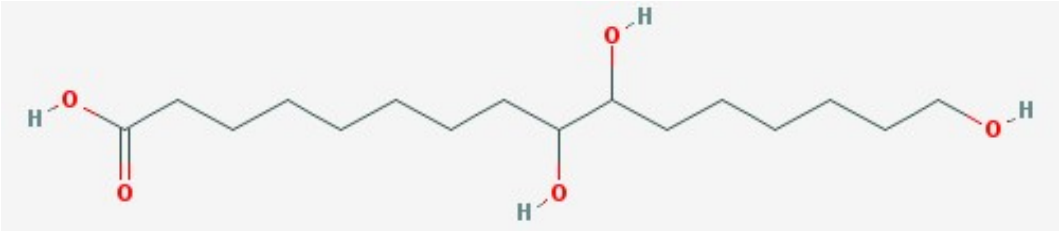

Aleuritic Acid (PubChem, 2005)

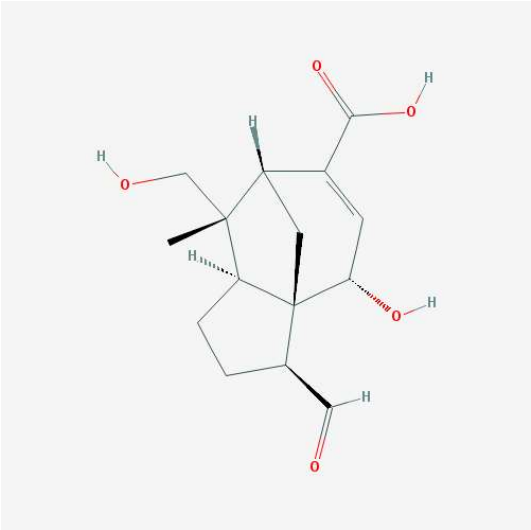

Jalaric Acid (PubChem, 2007)

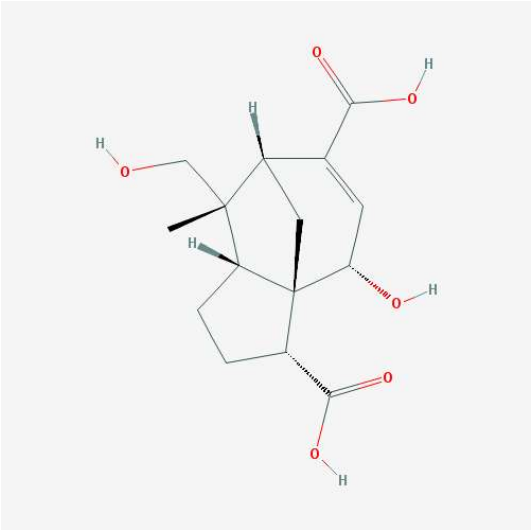

Shellolic Acid (PubChem, 2015)

Figure 2-24 Main Components of Shellac (Irimia-Vladu *et al.*, 2013)

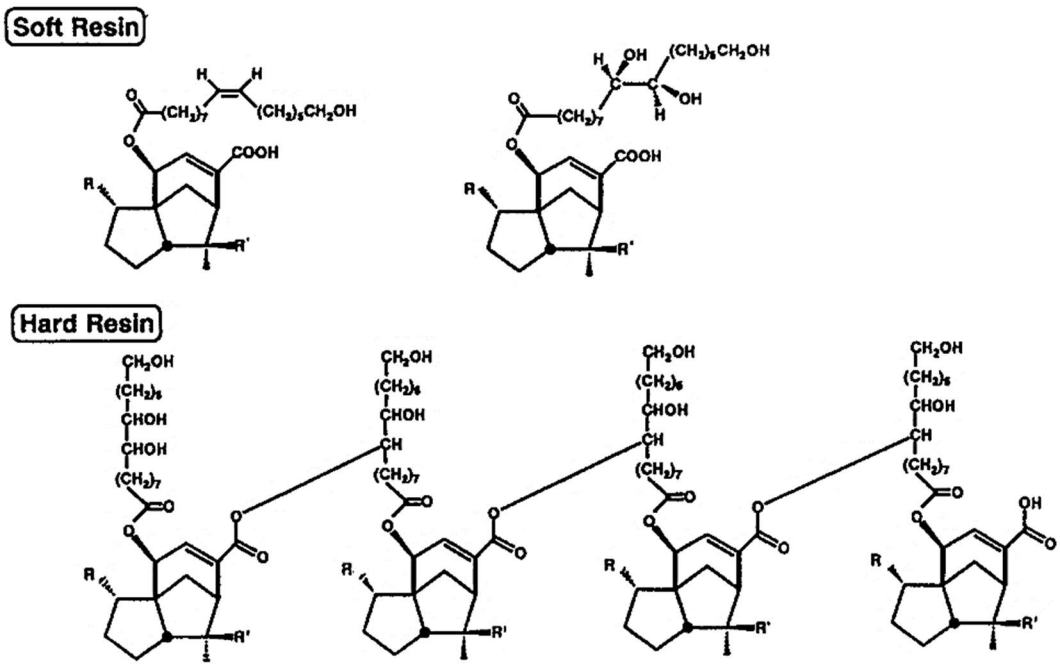

Figure 2-25 Chemical structure of shellac (Limmatvapirat *et al.*, 2007)(Wang *et al.*, 1999).

Table 2-5 Composition of sticklac, seedlac and shellac (Azouka, Huggett and Harrison, 1993)

Percentage composition	Sticklac	Seedlac	Shellac
Resin	68.0	88.5	90.0
Wax	6.0	4.5	4.0
Colouring matter	10.0	2.5	0.5
Gluten	5.5	2.0	2.8
Impurities	6.5	-	-
Loss(moisture)	4.0	2.5	1.8

2.4.4 **Properties of shellac**

Shellac is a brittle and hard amorphous solid. Except for the bleaching shellac and dewaxed shellac, its colour is affected by the lac wax and the lac dyes, which can range from semi-transparent light yellow to opaque dark red. The colour of the material is usually characterized by the Gardener or Lovibond scale (Mishra, 1983). When heating or melting the material, a characteristic fragrance can be smelled (Buchbauer *et al.*, 1993). This is

because the major component of shellac, aleuritic acid is used as the starting material for the synthesis of fragrance (Mishra, 1983)(Mathur and Bhattacharyya, 1963). Shellac has a particularly good ability to form a film, and its film provides high gloss, low permeability for water vapour and gases and good dielectric behaviour (Goswami, 1985)(Hagenmaier and Shaw, 1991).

In 1981, the shellac export council listed some 50 properties of shellac, and they claimed that shellac was not toxic and physiologically harmless and thus listed by the Food and Drug Administration (FDA) as GRAS (generally recognized as safe) (Labuschagne, Naicker and Kalombo, 2016).

As a rigid material, shellac can be softened readily by dry heat. Moreover, like other amorphous resins, shellac has no sharp softening or melting point. Instead, a glass transition temperature appears in the thermal analysis curve. In the glass transition process, the shellac transforms from the solid to the liquid, but the change of state is not uniformly continuous. The glass transition temperature depended on the shellac type and varied between 30 to 50°C for the acid form (Buch *et al.*, 2009). In the America pharmacopoeias, the council characterise shellac material only by their acid value (United States Pharmacopeial Convention., 2006). The Ph. USA allows a range of acid value between 68-76. The acid value of dewaxed orange shellac types is about 71-79. Whereas the acid value of bleaching shellac can be considerably higher, in addition, the acid of aged shellac may be significantly lower (Farag and Leopold, 2009).

After long-term storage shellac would undergo ageing because most of the acid contain more than one hydroxyl group and some more than one carboxyl group, it is believed that the ageing is a result of self-esterification of the shellac (Figure 2-26). As a result, the solubility of the shellac decreases, the acid value decreases and glass transition increases (Farag and Leopold, 2009)(Nath Goswami *et al.*, 2009).

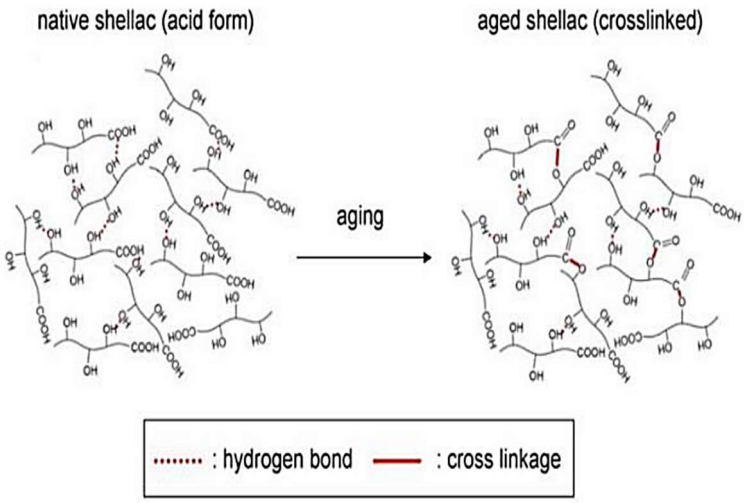

Figure 2-26 Proposed mechanism of polymerisation in shellac (Khairuddin, Edi Pramono, *et al.*, 2016)

2.4.5 **Modification of shellac**

Increased modifications were found to change the properties of the shellac, to achieve long-term storage and higher solubility (Limmatvapirat *et al.*, 2005)(Limmatvapirat *et al.*, 2004), such as salt forms and partially hydrolysed (Limmatvapirat, Panchapornpon, *et al.*, 2008). However, it turned out that partially hydrolysed shellac was less stable (Limmatvapirat *et al.*, 2004).

2.4.6 **Application of shellac**

Typical use of shellac can be tracked into ancient times, and it is a multipurpose resin that has been applied to many different applications. It is the best know as a binding material in music records (Cornell *et al.*, 2007) and as an ingredient in colours and lacquers where it has been used as a protective layer on artistic objects (Chiavari, Fabbri and Prati, 2002) (Chiavari *et al.*, 1995). Although, shellac was soon substituted by synthetic polymers because of its brittleness. To expand its application field, various type of shellac were developed, and some additives or surfactant were employed in the modification of the lac properties (Wang *et al.*, 2006).

Because of the non-toxic and physiologically harmless properties. Shellac is widely used in the food industry (Krause and Müller, 2001). Additionally, shellac has been used in the pharmaceutical industry, being used for moisture protection and glossing due to its low

permeability of water. The existence of carboxyl groups, which means that shellac can be used as an enteric coating film former in pharmaceuticals. Nonetheless, the use of an enteric coating of pharmaceutical products has been dramatically declined in recent years because of its stability issues associated with the self-esterification and polymerisation (Cole, Hogan and Holton, 1995)(Limmatvapirat *et al.*, 2007)(Penning, 1996). Nevertheless, researchers are investigating the possibility to use shellac as a matrix polymer (Limmatvapirat, Limmatvapirat, *et al.*, 2008)(Pearnchob, Siepmann and Bodmeier, 2003b).

In 1930, Milton S. Wruble created the first shellac application for enteric coating in the world, and he made a statement that the ammoniacal solution of shellac was proved to be far more effective as an enteric coating than alcoholic (Osman, 2012). Moreover, nowadays the pharmaceutical market is of special commercial interest, shellac has a high potential as a coating material for moisture protection and taste masking (Thombare *et al.*, 2022). Another important application is as a coating material in the food industry. Moreover, the production volume on food industry is much higher than the previous (Soradech *et al.*, 2017). Shellac coating for food application is commonly applied from ethanolic solution. This is because the ethanolic solvent can be removed by drying (Farag, 2010).

With the development of technology, researchers produced a different formulation of shellac in order to replace the organic shellac coating systems, for example, aqueous shellac dispersions were prepared by high-pressure homogenisation (Krause and Müller, 2001). However, as all those formulations contain shellac, which undergoes ageing, resulted in the drug release profile, not in line with the desired needs. Hence its use in pharmaceutical applications declined (Penning, 1996)(Karsa *et al.*, 1996).

From its chemical structure, because of the existence of carboxyl group, shellac exhibits the attributes of a weak acid with a pKa of about 6, being dissolvable in water with a pH > 7. Under acidic conditions (pH< 7), the protonation of shellac hinders its dissolubility (Yuan *et al.*, 2021). Which means it can remain nearly undissloved in the low pH solution such as

gastric fluid (Buch *et al.*, 2009). It requires high pH for dissolution, usually above pH 7.2 (Limmatvapirat *et al.*, 2007). Due to its high dissolution pH, nearly insoluble in the gastric fluid and low solubility in the intestinal fluid, shellac is suitable for enteric coating especially colon target drug delivery (Ravi, Siddaramaiah and Pramod Kumar, 2008)(Ravi, Pramod Kumar and Siddaramaiah, 2008).

2.5 Fenofibrate

Cardiovascular diseases (CVDs) still rank as the number one cause of death globally and are responsible for 17.5 million or 31% of all global deaths per year according to the World Health Organization (WHO) (Benjamin *et al.*, 2018). Since dyslipidaemias are recognized as a primary major risk factor for CVDs, aggressive lipid modulation has a positive and profound impact on the prevention and treatment of CVDs. Over the past three decades, statin therapy aimed at lowering low-density lipoprotein cholesterol (LDL-C) has become the cornerstone of reducing CVDs. The high effectiveness of statins for lowering LDL-C levels and the benefit of this approach have been demonstrated by many studies(Hua Linga, Luomab and Hillemanc, 2013)(Tziomalos and Athyros, 2006). Fenofibrate is categorized as a BCS class II drug because it is poorly aqueous soluble (0.8 μg/ml) but has high permeability (>90%) through a lipid membrane (Jamzad and Fassihi, 2006)(Buch *et al.*, 2010). Therefore, administrating fenofibrate with foods can increase drug absorption (Hua Linga, Luomab and Hillemanc, 2013). The nano-crystallised (Tricor®) formulation and the solid dispersion with PEG (Fenoglide®) have been used to increase the bioavailability of fenofibrate (Law *et al.*, 2003)(Shegokar and Müller, 2010). Consequently, the fenofibrate content per tablet can be reduced from 100 mg of the conventional fenofibrate tablets to 67 mg or less in fenofibrate nano crystallised and solid dispersion formulations (Guichard and Levy-Prades Sauron, 1993)(Vogt, Kunath and Dressman, 2008).

Polymorphic forms of one drug substance could have different chemical and physical properties, including melting point, chemical reactivity, apparent solubility, dissolution rate, optical and mechanical properties, vapor pressure and density (Shi, Shao and Sheng, 2018).

The amorphous fenofibrate does not spontaneously crystallise because it has high configuration entropy and high molecular mobility is required for crystallisation (Zhou *et al.*, 2002). Consequently, it has a low probability of molecular insertion to form nuclei for the nucleation. However, the amorphous fenofibrate crystallises immediately after being triggered by scratching its surface or seeding by using its crystal (Amstad, Spaepen and Weitz, 2015)(Yang, 2013). Three fenofibrate polymorphs have been reported in PubChem Database (PubChem, 2022b). The stable form I (with a melting point at 80°C) is the standard polymorph used as API in commercial tablets and capsule formulations. Form I can be obtained by a slow solvent evaporation method (Watterson *et al.*, 2014). The metastable form II, initially reported by Di Martino and co-workers in 2001, is produced by the recrystallisation of amorphous fenofibrate from the melt (Di Martino, Palmieri and Martelli, 2000). This metastable polymorph has a melting point of 74°C. It immediately converts to the stable form I via melt recrystallisation during heating and melting again at 80°C (Górniak *et al.*, 2011)(Heinz *et al.*, 2009) Figure 2-27. The melting point and Powder X-ray diffraction (PXRD) data were reported by Di Martino and co-workers. Later, Heinz et al. reported the Raman spectrum of fenofibrate polymorph II. However, the literature on fenofibrate form II is rather confusing, as there is inconsistency in its characteristic data among various sources. Barlendiran and colleagues revealed the single-crystal structure of FF form II as a monoclinic crystal with no supporting information on its melting point and spectroscopic data (Balendiran *et al.*, 2012)(Balendiran *et al.*, 2012). It is unclear whether the fenofibrate form IIs reported by the literature groups are the same polymorphs. To avoid the confusion that arises from these findings, the FF form II from Di Martino et al. and Heinz et al. will be addressed as fenofibrate form IIa in this study and the one from Barlendiran will be addressed as form IIb (Heinz *et al.*, 2009)(Balendiran *et al.*, 2012). The summary of the physical properties of fenofibrate is reported in Table 2-6.

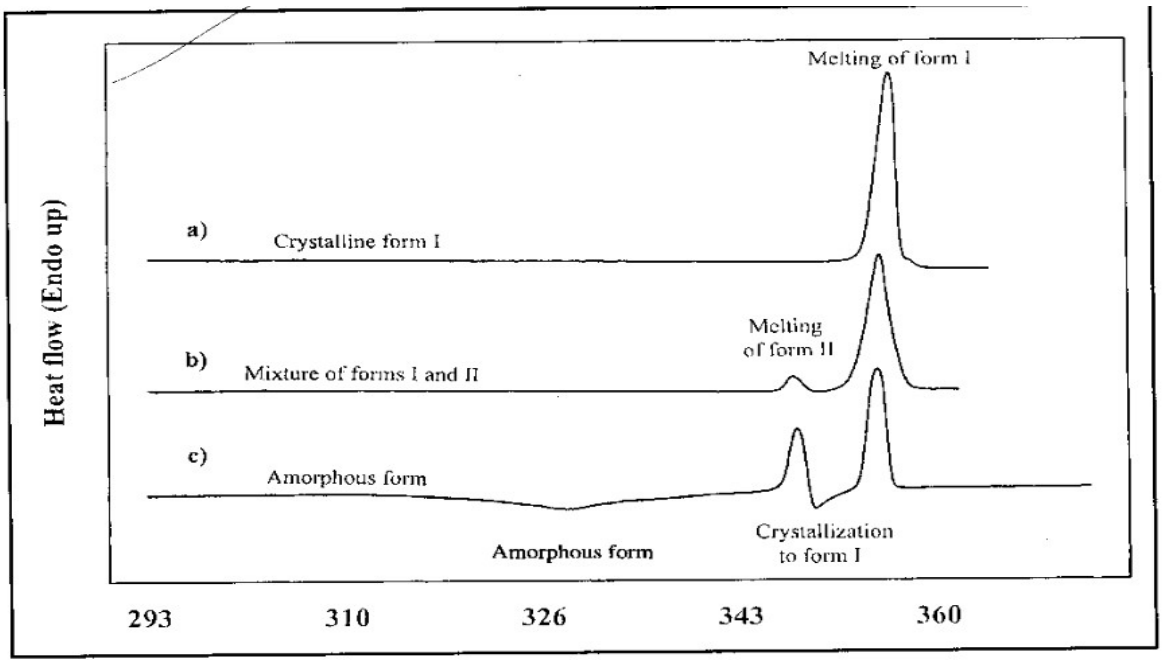

Figure 2-27 Differential Scanning Calorimetry of fenofibrate. a) First heating run performed at 10 K/min b) Second heating run (10 K/min performed after brutal quenching of the melt (200K/min) to room temperature and after two days at room conditions. c)Second heating run performed immediately after slow cooling (10 K/min) the melt to room conditions (Di Martino, Palmieri and Martelli, 2000).

Table 2-6 Physical properties of fenofibrate (PubChem, 2022a).

Properties	Fenofibrate
Molecular weight	360.8g/mol
Formulation	$C_{20}H_{21}ClO_4$
pKa	-4.9
Solubility	0.42µg/ml
Log P	5.2
Permeability	>90%
Density	1.29g/cm^3
Glass transition	-20°C
Configuration entropy (ΔS)	76.6J/mol*K
Mobility required for crystallisation (1/τ)	72.3s^{-1}

Chapter 3 Material and Method

3.1 Material

All the shellac materials used in this study are shown in Table 3-1. Dewaxed Shellac AFS HS 700K, Dewaxed Shellac AF·S HS 702MB, AFS HS SWANLAC, AFS Shellac WL, and AFS Shellac RTH were purchased from A.F. Suter (Witham, United Kingdom). Shellac SSB 55 Pharma FL was purchased from SSB (Stroever Schellack, Bremen, Germany). Fenofibrate (Class 2) was purchased from Tokyo Chemical Industry UK Ltd. Sodium phosphate monobasic dihydrate and Di-sodium hydrogen phosphate extra pure were purchased from Sigma Aldrich Ireland Ltd. Sodium Dodecyl Sulfate (SDS) was purchased from Fisher Scientific (Ireland), Acetonitrile 200 was purchased from LENNOX (Ireland). Phosphoric acid and sodium hydroxide were purchased from Sigma Aldrich.

Table 3-1 Shellac material used in this section.

Batch name	Type	Seedlac	Refining process	Manufacture date
Dewaxed Shellac AFS HS 700K	Dewaxed shellac	Kushmi	Solvent extraction	03/03/2019
SSB 55 Pharma FL	Dewaxed shellac	Kushmi	Solvent extraction	10/2020
AFS Shellac WL	Wax containing shellac	Kushmi	Melting process	05/01/2019
AFS Shellac RTH	Wax containing shellac	Kushmi	Melting process	20/02/2018
Dewaxed Shellac AFS HS 702MB	Dewaxed shellac	Bysakhi	Solvent extraction	20/05/2020
AFS Shellac HS SWANLAC	Dewaxed Bleached Shellac	Kushmi	Bleaching Process	14/08/2020

3.2 Grinding

Ground shellac was prepared by milling shellac flakes in a Planetary Mono (Figure 3-1) and sieving through a 500-μm mesh sieve. During the grinding process, a short operation time of 30s is required to prevent material from melting in the steel bottle. All materials were cooled in liquid nitrogen before using a ball miller. Ground shellac was used for the melt flow rate test, the determination of thermal properties including glass transition temperatures

(T_g) or decomposition temperature T_d, Fourier Transform Infra-Red (FT-IR) spectroscopy, rheometer properties and extrusion process.

Figure 3-1 Mill PULVERISETTE 6 classic line ball miller

3.3 Thermal properties

Thermal analysis (TA) is a group of techniques for measuring the physical and chemical properties of the sample related to temperature. In all those methods, the sample is under a programmed temperature subjected to cooling, heating or isothermal. TA includes a lot of technology such as differential scanning calorimetry (DSC), differential thermal analysis (DTA), thermogravimetry (TG), thermomechanical analysis (TMA) and dynamic mechanical analysis (DMA) (Wunderlich, 2001). The various TA analysis curves are shown below in Figure 3-2.

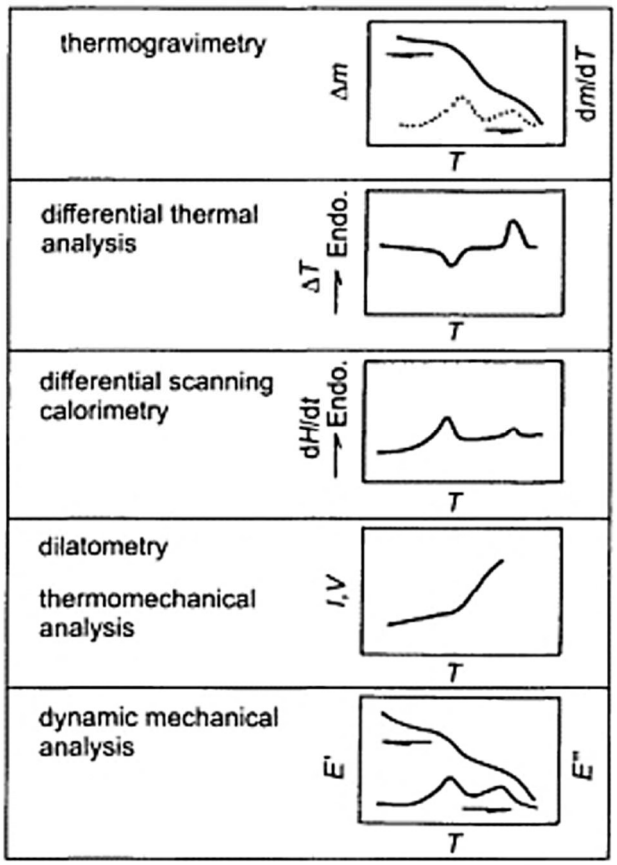

Figure 3-2 The various TA analysis curves (Wunderlich, 2001)

Normally measurement is performed in an inert atmosphere and depending on the test method the gas can be Nitrogen, Argon, Helium or an oxidative atmosphere (Air, Oxygen). Even though the tests are being carried out and the atmosphere can be switched during the test if required. Each subsequent method below will describe which inert atmosphere was used in this study.

3.3.1 **Differential scanning calorimetry (DSC)**

Differential Scanning Calorimetry (DSC) measured the heat flow rate of the sample during heating, cooling down or at a constant temperature, and it is a fundamental tool in thermal analysis. A TA instrument DSC 2920 was used throughout the work (Figure 3-3). Samples of between 4 and 6 mg were weighed out using a Sartorius scale having a resolution of 1×10^{-5}g. Samples were then placed in non-perforated aluminium pans which were crimped before testing, with an empty crimped aluminium pan being used as the reference

cell. Volatiles were removed from the purging head with nitrogen at a rate of 30 ml/min. Calibration of the instrument was performed using indium as standard. Tests were performed applying a temperature ramp from -30 to 120°C at 10°C/min. An isothermal step of 1 min at 120 °C was introduced to remove excessive water. The T_g and Tm were determined from the second heating run by the TA Universal Analysis 2000 software version 4.5A.

Figure 3-3 TA instruments DSC 2920

3.3.2 **Thermogravimetric Analysis (TGA)**

Thermogravimetric analysis is a kind of TA experimental technology which measures the sample weight as a function of temperature in a programmed scanning mode. Compared with the DSC technique the heating scanning not only includes melting, glass transition, and crystallisation but also has desorption, absorption, sublimation, vaporisation, oxidation, reduction and decomposition. This technique is a widely used testing method in modern polymer characterisation. It is used to characterise the decomposition and the thermal stability of the material.

In 1903, Nenst and Riesenfeld used a quartz torsional balance to study the weight loss of spar, opal and alunite at elevated temperatures (Komarewsky, Rideal and Frankenburg, 1953). Later in 1905 Brill continuous weighing $CaCO_3$ to 1200 °C, recorded the first weightlessness curve. In 1915, Honda Kotaro studied the weight loss process with heating and named the instrument thermo-balance (Chen and McKeever, 1997). Until 1977 the International Confederation for Thermal Analysis (ICTA) officially named this technology "thermogravimetry", referred to as "TG" (Brown, 1988).

In general, with the sample heating, it often begins to lose weight. This loss of mass can result from vaporisation or a chemical reaction in which gaseous products are formed and evolved from the sample. In addition, if the atmosphere is not inert, the sample may even have a chemical reaction with the gas. Therefore, the mass of the sample may increase if there is an oxidation reaction happened in the sample (Liming Lu, 2009).

In TGA, the recorded data is the mass of the sample as a function of temperature or time. This data provides information on the properties of the sample and its composition. If any chemical reactions are occurring within the sample in the current atmosphere, the TGA curve will become a stepwise fashion. The temperature, as the step progresses can become the result of the thermal stability of that atmosphere. A typical TGA curve is shown in Figure 3-4. The composition of the sample can be determined by analysis of the temperature and the height of the independent mass steps.

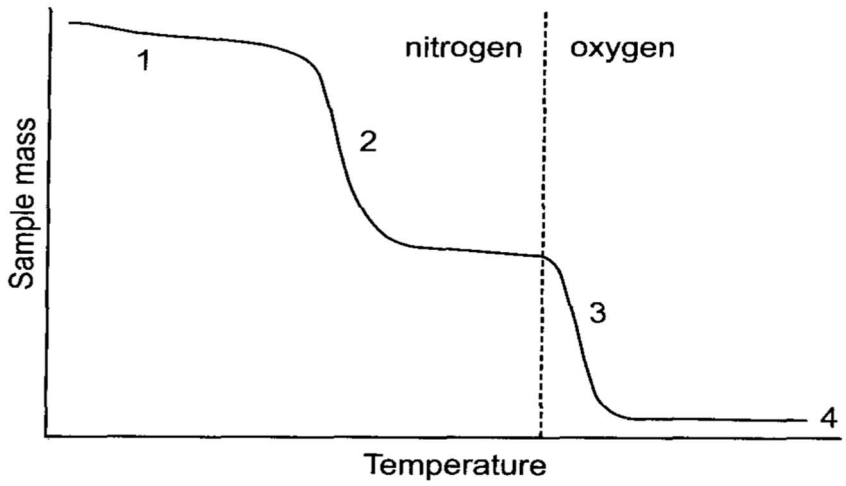

Figure 3-4 Schematic TGA curve: 1 loss of mass due to the vaporisation of volatile components; 2 pyrolysis in an inert atmosphere; 3 combustions of carbon on switching from an inert to an oxidative atmosphere; 4 residue. (Gabbott, 2008)

With the temperature increasing, the volatile components will release at a lower temperature. The loss rate of this kind of component depends on the gas pressure, with the increase in the gas pressure, the rate of losing weight increases. The analysis of the pyrolysis in an inert atmosphere can determine the water content of the material and in some cases, can even determine the kind of material.

Normally, the TGA testing gives a first derivative of the TGA curve named as Differential thermogravimetry (DTG) curve. In the TGA curve, the step loss is shown as peaks in the DTG curve. The DTG curve corresponds to the rate of mass change as a function of temperature. The peak point is the maximum mass losing rate occurring in the sample (Gabbott, 2008).

TGA was performed to evaluate the degradation temperature of different types of shellac. Tests were conducted using a Perkin Elmer Pyris 1 TGA Thermogravimetric Analyzer (Figure 3-5) under a nitrogen atmosphere. The tests were run from 30 to 600°C, at a heating rate of 10°Cmin^{-1}. Samples weighing between 2 and 4 mg were used for the measurement.

Figure 3-5 PerkinElmer Pyris 1 TGA Thermogravimetric Analyser

3.4 Attenuated total reflectance Fourier transform infrared (ATR-FTIR) spectroscopy

ATR-FTIR is a chemical analytical technique that measures the infrared intensity versus the wavenumber of light named Infrared (IR) spectroscopy. A typical schematic diagram of an ATR-FTIR is illustrated in Figure 3-6. FTIR spectroscopy was employed to investigate the presence of molecules in the material where the peak positions in an infrared spectrum correlate with the molecular structure.

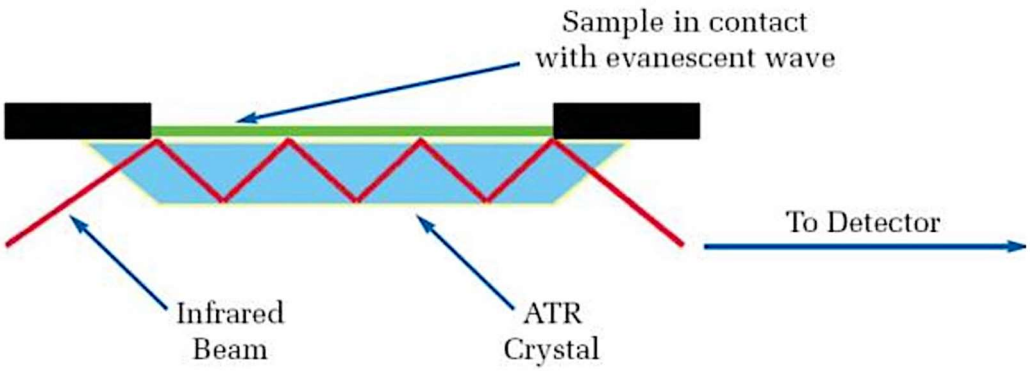

Figure 3-6 Schematic diagram of an Attenuated Total Reflectance (ATR) FTIR (PerkinElmer, 2005)

ATR-FTIR was conducted on a Perkin Elmer Spectrum One (Figure 3-7) fitted with a universal ATR sampling accessory. All data were recorded at room temperature, in the spectral range of 4000-650cm^{-1}, utilizing 16 scans per sample cycle and a fixed universal

compression force of 70N. In chapter 4.1, to have better visual comparison and indications of functional group intensities between spectra, all the spectra were baseline corrected to 0 and normalised at one intensity in absorbance mode, at the characteristic C-H stretching bands shared by all samples at 2934-2920 cm^{-1}. The spectra can only be used for the comparison. Subsequent analysis was conducted using OMNIC Spectrum software version 9.2.86.

Figure 3-7 Perkin Elmer Spectrum One fitted with a universal ATR sampling accessory

3.5 Rheology

"Rheology" is the science that studies the flow and deformation of materials, its name was invented by Professor Bingham of Lafayette College, Easton, PA, on the advice of a colleague, the Professor of Classics. Rheology in polymer material is to study the polymer liquid, which mainly refers to the polymer melt, or polymer solution, to characterise their linear and non-linear viscoelastic behaviour while flowing, and the relationship between this behaviour and material structure and other physical, and chemical properties (Osswald and

Rudolph, 2015).

Flow and deformation belong to the concept of two categories, flow is the material properties of the liquid, and deformation is the solid (crystal) material properties. Liquid flow, showing viscous behaviour, causes permanent deformation where the deformation is unable to be restored and dissipated as energy. Consequently, when the solid deformation shows elastic behaviour, the applied force will cause elastic deformation which can be recovered when the force is removed. Furthermore, the deformation can store energy, when it recovers, and the stored energy will be released too. This means the material has a flexible memory effect (Dealy and Wissbrun, 1990).

Normally, the fluid flow follows Newton's law of motion the shearing stress of the material is proportional to the shear rate ($\sigma = \eta_0 \dot{\gamma}$), and the flow process is always time-dependent, which means the flow of the material can only be observed after a period of time. The general solid deformation follows Hooke's law - the stress of the material is proportional to the deformation (strain) ($\sigma = E\varepsilon$), and the stress, strain response is referring to the instantaneous response.

Newtonian fluid and Hooke's law are two kinds of ideal modes for a material, their properties are simplified, but the actual materials often show far more complex mechanical properties. Asphalt, clay, rubber, oil, plasma, chemical raw materials, crust, especially all kinds of polymer materials and products that can flow or deform, can be sticky or flexible. These materials will occur viscous loss when deformation happens, and when they flow, the flexible memory effect would exist. For these kinds of materials, Newton's law of motion or Hooke's elasticity law cannot fully describe the complex mechanical response. As a result, Rheology is a term to describe those responses and properties and is widely used in polymer characterisation. Generally, it can be divided into two main parts, such as:

- High molecular material structure rheology
- Polymer materials processing rheology

Rheometers

The measurement of the rheological properties and the evaluation of fluid models require specific devices that can be named rheometers. These devices can be used for several objectives; the principal objective is to measure the viscosity of the material at a range of shear rates (Barnes, Hutton and Walters, 1989). In addition, it measures viscosity as a function of temperature, frequency, and amplitude. What is more, the rheometer is used to understand the complex behaviour of the polymer in the large and relatively unexplored field of nonlinear viscoelasticity.

Rotational rheometer

This type of rheometer relies on rotational motion to achieve a simple shearing flow. The instrument schematic diagram is shown in below Figure 3-8. The head of the instrument is a high-sensitivity force sensor; it can measure the force or shear force. In the current application, the rotational rheometer has many different types, but the Cone-Plate and Parallel-Plate rheometer are most commonly used.

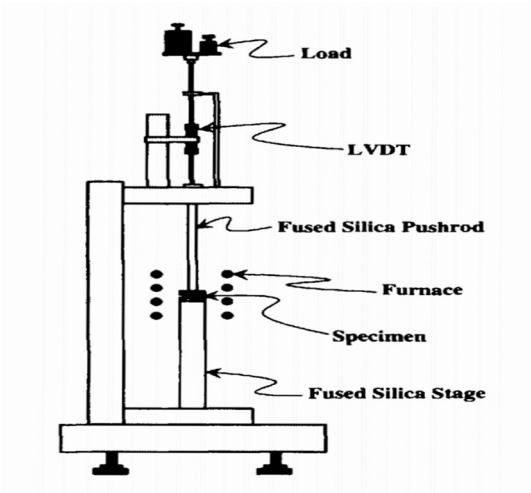

Figure 3-8 The Rotational rheometer (Speyer, 1993)

The cone-plate rheometer is used to measure the viscosity along with the primary and

the secondary normal stress coefficient functions as a function of shear rate and temperature. The schematic diagram is shown in Figure 3-9.

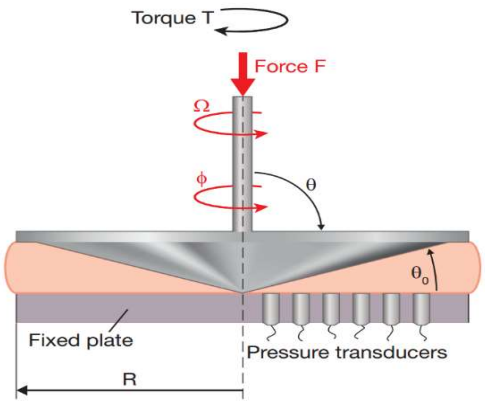

Figure 3-9 The Cone-Plate rheometer

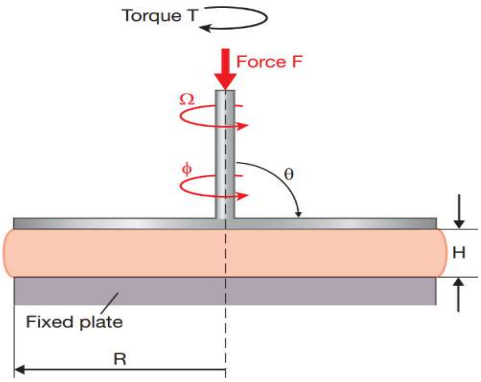

Figure 3-10 The Parallel-Plate Rheometer

The geometry of a parallel-plate rheometer is as shown in Figure 3-10, which consists of two parallel plates, and it is similar to the cone plate, in that the lower plate is fixed, but the upper one can support the rotational and shear force. However, it cannot generate a uniform shearing flow (Larson, 1999).

Comparing the parallel-plate rheometer and the Cone-plate rheometer, both have a wide range of applications, but a parallel-plate rheometer has some advantages compared to a cone-plate rheometer. For example, the shear rate of the parallel plate rheometer can be changed, and it can test within a range of shear rates, in contrast to the cone-plate rheometer with a constant shear rate. Furthermore, the thermal expansion would have more effect on the cone-plate system (Dealy *et al.*, 2013). In order to find the processability of the shellac material, the rheology of shellac needs to be tested. Moreover, when doing the screw design simulation, the rheology data of shellac is the material data which necessary in the material properties section.

Melt rheological experiments were conducted in an oscillatory mode, on a rotational rheometer (TA Discovery HR-2 hybrid Rheometer) equipped with a parallel plate (25 mm diameter) as shown in Figure 3-11. All samples were measured at various temperatures (70°C, 80°C,90°C) with a 1000μm gap distance.

3.5.1 **Oscillatory time sweeps**

The first set of rheology tests performed were oscillatory time sweeps. This test directly provides the necessary information about material changes as a function of time. This study was characterized at 90°C and with a constant angular frequency of 1Hz and 1 % strain.

3.5.2 **Oscillation amplitude sweep**

When the applied strain is higher than the linear viscoelastic region, the material structure would be destroyed, and its response would be non-linear. In addition, the storage modulus would begin to decrease (Menard, 2008). As a result, determining the linear viscoelastic region of an unknown material would be the second necessary step in rheology analysis (Kaboorani and Blanchet, 2014). This study was performed with a strain range of 0.01% to 100% at an angular frequency of 1 Hz in the oscillation model.

3.5.3 **Oscillation frequency analysis**

Frequency analysis was used to find out how material reacts with shear rate. This study was performed with a constant strain of 1% which was identified by the amplitude sweep and the angular frequency performed with a range of 0.1 to 100 Hz.

3.5.4 **Oscillation temperature sweep**

The samples were heated from 65 to 110°C with a heating ramp rate of 3°C/min at a frequency of 1Hz with a strain value of 1%.

Figure 3-11 Discovery HZ-2 hybrid Rheometer

3.6 Melt flow index (MFI)

MFI was used to identify how well the material flowed (Viscosity) under heat and pressure while additionally providing an indirect measure of the molecular weight. In this study, the Melt Flow Index values of different shellac materials were assessed using a fixed weight of 1.2Kg with a CEAST Melt Flow Quick Indexer under ASTM D1238-10 (Figure 3-12). The molten material flowed through an orifice of 2.16mm in diameter for a duration of 10 mins and the values were reported in g/10min. All the samples were tested at 90℃.

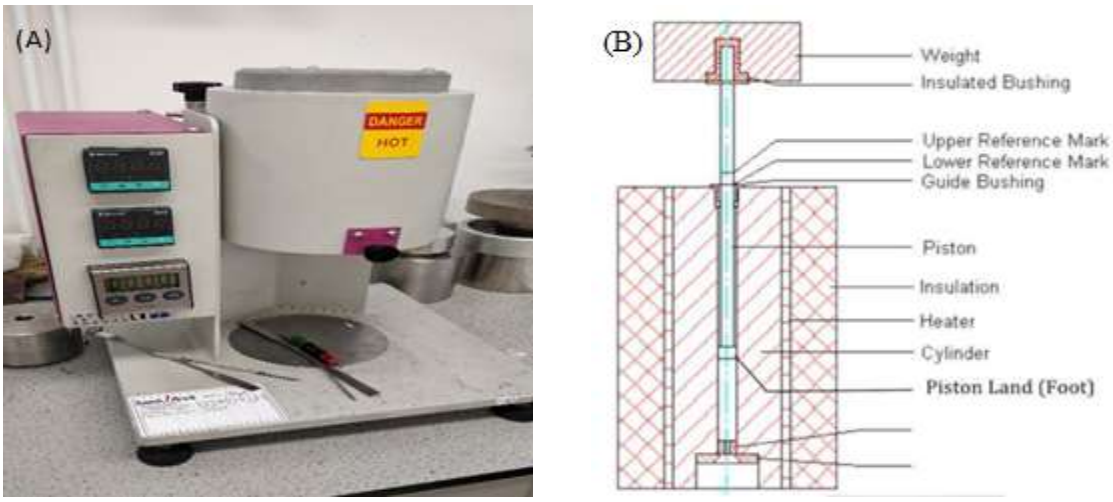

Figure 3-12 (A) Ceast melt flow indexer used in this study (Left-hand side); (B) General Arrangement of Extrusion Plastometer

3.7 Scanning electron microscopy (SEM) with an energy-dispersive X-ray spectrometry System (EDS)

Scanning electron microscopy (SEM) was performed on a Tescan Mira XMU variable pressure SEM (Figure 3-13b) with a magnification of 10kx. This instrument allowed the examination of surface morphology and overall elemental uniformity through the distribution of shellac. The shellac materials tested are non-conducting by nature. Therefore, samples required a coating before testing to increase the electrical conductivity of the sample. Sample preparation involved placing samples onto an aluminium stub using double-sided conductive carbon tape. Subsequently, the sample was placed in a Bal-Tec SCD 005 sputter coater (Figure 3-13a) for 110 sec at 0.1mBar vacuum to apply a 10-30nm layer of gold on the surface. The quantitative investigation of the surface of the shellac was performed with an EDS system.

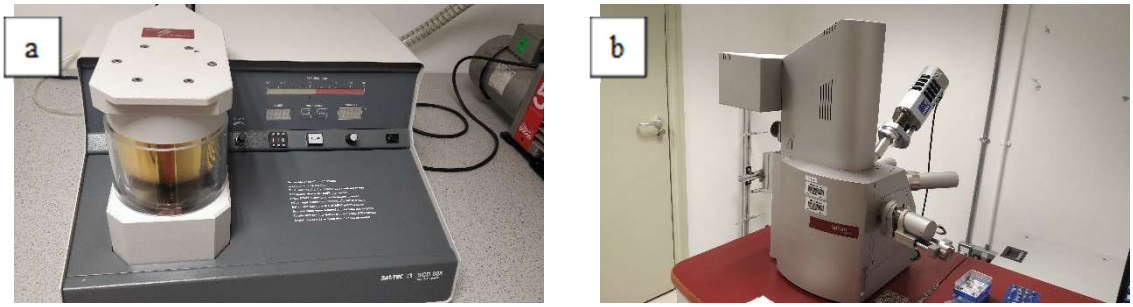

Figure 3-13 a) Bal-Tec SCD 005 sputter coater (Left-hand side); b) Tescan Mira XMU variable pressure scanning electron microscope (Right-hand side)

3.8 Preparation of pH buffer solution

Due to the pH-sensitive properties of the shellac material, it would not dissolve until pH>7.2. Moreover, luminal pH in the proximal small bowel ranges from 5.5 to 7.0 and gradually rises to 6.5–7.5 in the distal ileum. As a result, sodium phosphate monobasic (NaH_2PO_4), Sodium phosphate dibasic (Na_2HPO_4) were used to prepare the pH 7.4 buffer solution for in vitro dissolution testing to simulate the environment of the colon. 0.2M sodium hydroxide (NaOH) was used to adjust the pH value. The pH of the solution was confirmed using a Jenway 3520 pH meter (Figure 3-14).

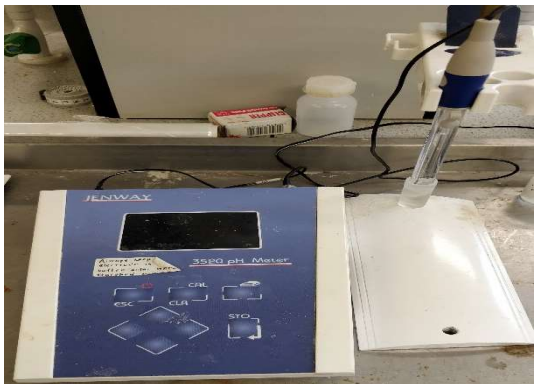

Figure 3-14 Jenway 3520 pH Meter

3.9 Dissolution Test

Dissolution testing was carried out using a Sotax AT7 smart dissolution system from Carl Stuart Ltd, displayed in (Figure 3-15b). Tests were carried out using the Paddle method (USP XXV). The dissolution media used in these tests consisted of manually prepared phosphate buffer solutions (pH 7.4). All tests were carried out at 37°C ± 0.5°C. The stir rate was set to 100 rpm with 900 ml of dissolution media used per vessel. The wavelength and

absorption of 100% shellac concentration were determined using a SHIMADZU UV-1280 UV Vis spectrophotometer (Figure 3-15a, Japan). In the case of extruded samples, test specimens of constant size and surface area were produced by cutting the extrudate strands manually to give granules of length 1 cm and accurately weighed using Sartorius scales having a resolution of 1 x 10^{-5}g. Samples were manually taken every 15 minutes, filtered with the glass microfiber filters (1.2µm), and recorded spectrophotometrically at 221nm using a SHIMADZU UV-1280 UV Vis spectrophotometer (Japan), before being returned to the dissolution vessel. The dissolution profiles were observed from a plot of time versus absorbance. Analysis was carried out in triplicate and the standard error of the mean was calculated.

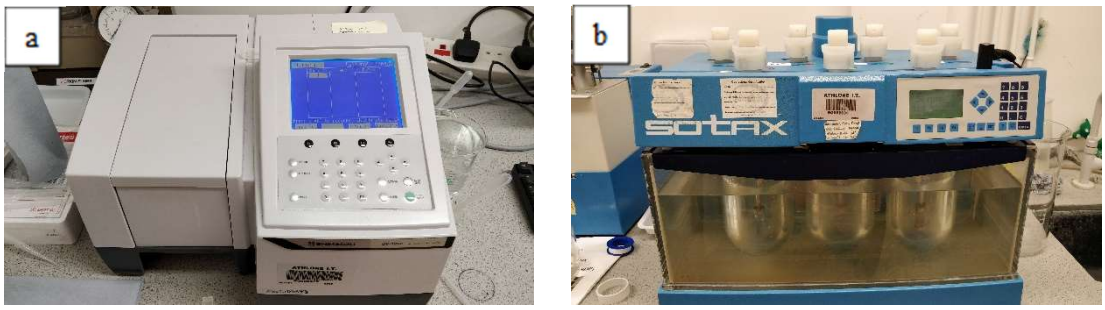

Figure 3-15 SHIMADZU UV-1280 UV Vis spectrophotometer (Left-hand side); Sotax AT7 smart dissolution system (Right-hand side)

3.10 Drug release profile kinetics

The drug release profile kinetics were analysed by fitting the experimental data to five mathematical models including zero-order, first-order, Higuchi, Hixson-Crowell Korsmeyer-Peppas, and using DDsolver (Zhang *et al.*, 2010) with the internal build-in equations, given by equation

Zero Order

$$F = F_0 + k_0 \cdot t \qquad 3\text{-}1$$

where F represents the amount of active agent released during the time t, F_0 is the initial concentration of active released (generally, F_0= 0), and k_0 is the zero-order constant. For zero-order kinetics, the release of an active agent is only a function of time, and the process

takes place at a constant rate independent of active agent concentration.

First-order

$$\log F = logF_0 + \frac{k_1 \cdot t}{2.303} \qquad 3\text{-}2$$

where F is the amount of active agent released on time t, F_0 is the initial amount of drug dissolved, and k_1 is the first-order constant.

This model has been used to describe the absorption and/or elimination of a variety of therapeutic agents. However, it is difficult to define first-order kinetics using a basic theory. In this sense, first-order release kinetics states that change in concentration with respect to change in time is dependent only on the concentration

Higuchi

$$F = k_H \cdot t^{0.5} \qquad 3\text{-}3$$

where k_H is the release constant of Higuchi. This equation is the simplified Higuchi model, which relates the concentration of the active agent to the square root of time, representing a linear function. Some assumptions need to be followed with the use of the Higuchi model

(1) The matrix contains an initial drug concentration much higher than the solubility of the drug.

(2) The diffusion is unidirectional because the edge effects are negligible.

(3) The thickness of the dosage form is much larger than the size of the drug molecules

(4) The swelling or dissolution of the matrix is negligible.

(5) The diffusivity of the drug is constant.

(6) Perfect sink conditions are attained in the release environment.

Korsmeyer-Peppas

$$F = k_{KP} \cdot t^n \qquad 3\text{-}4$$

where F is the amount of drug released, k_{KP} is the constant of incorporation of structural modifications and geometrical characteristics of the system (also considered the release velocity constant), and n is the exponent of release (related to the drug release mechanism) in the function of time t. This model was developed specifically for the release of a drug molecule from a polymeric matrix, such as a hydrogel.

Hixson-Crowell

$$\sqrt[3]{F_0} = \sqrt[3]{F_i} + k_{HC} \cdot t \qquad 3\text{-}5$$

where F_0 is the initial amount of the drug in the system; F_i is the amount remaining in the system on time t; and k_{HC} is the constant of incorporation, which relates to surface and volume. This equation applies to dosage forms such as tablets, in which the dissolution happens in planes parallel to the surface of the dosage form; this surface decreases proportionally over time and the geometrical form maintains constant.

When this model is used, it is assumed that the drug release is limited by dissolution velocity and not by diffusion, which can occur through the polymeric matrix. Thus, the Hixson–Crowell equation applies to pharmaceutical dosage forms such as tablets, considering that dissolution occurs in planes parallel to the surface of the active agent if the tablet dimensions decrease proportionally, but with the maintenance of the geometrical characteristics.

Peppas–Sahlin model

$$F = k_1 \cdot t^m + k_2 \cdot t^{2m} \qquad 3\text{-}6$$

Where k_1 is the constant related to the Fiskian kinetics; k_2 is the constant related to Case-II relaxation kinetics; m is the diffusional exponent for a device of any geometric shape which inhibits controlled release (Zhang *et al.*, 2014). This release kinetics model is a consequence of the indication that it is possible to calculate the approximate two contribution mechanisms (diffusional and relaxational) in an anomalous drug release process.

The mechanism of drug release from polymer-based matrices is complex and not completely understood. Some systems may be classified as either pure diffusion or erosion controlled, while most systems exhibit a combination of these mechanisms. In 2008, Sanganwar reported the dissolution profile of the fenofibrate-silica formulation showed a good fit into Korsmeyer–Peppas equation in a neutral medium (Sanganwar and Gupta, 2008). Higuchi model is applicable if diffusion through water-filled matrix pores substantially controls drug release. A good match to the Korsmeyer-Peppas equation suggested that the drug release processes were a combination of erosion and diffusion (Korsmeyer *et al.*, 1983). In the case of Fickian release (diffusional controlled release), the 'm' has the limiting value of 0.45 for release from cylinders. Case II transport or relaxation-controlled release, the exponent 'm' is 0.89 for the release from cylinders. The anomalous transport of the drug occurred when the n values between the limiting values of Fickian and Case II transport. The non-Fickian kinetics corresponds to coupled diffusion/polymer relaxation. Occasionally, values of m > 0.89 for release from cylinders have been observed, which has been regarded as Super Case II kinetics (Peppas and Sahlin, 1989).

3.11 High-performance liquid chromatography (HPLC)

The chemical purity of fenofibrate in the extruded doses was determined using HPLC. Analysis was carried out based on the USP standard method using a system consisting of a Waters Alliance e2695 separations module combined with a Waters 2487 dual λ absorbance detector. An employed Thermo Scientific ODS Hypersil (150 mm x 4.6 mm; 5µm) column was maintained at 35°C. The mobile phase was a solution of water acidified with phosphoric acid to a pH of 2.5 in HPLC grade acetonitrile (Romil) 30:70. A flow rate of 1.2 mL/min was maintained during the procedure, the detector was set at 286 nm, and the sample injection volume was 10µL. A filtered solution of acetonitrile and acidified water 50:50 was used to wash the needle between injections. Before testing, samples were diluted in the mobile phase to inhibit the precipitation of the drug and filtered using 0.20 mm syringe filters.

3.12 Drug content analysis

The drug content of fenofibrate in the extruded doses was determined using HPLC. Three different formulation samples were randomly taken from the extrudate samples storage bag, were accurately weighed and completely dissolved in a known volume of methanol. And diluted 10 times with the mobile phase. Before HPLC testing, solutions were filtered using 0.20 mm syringe filters.

3.13 Powder X-Ray Diffraction (PXRD)

PXRD studies were performed for fenofibrate and extrudates formulation using the XCalibur S Single Crystal X-Ray Diffractometer (Galway, Ireland). The diffraction measurements were performed under the following conditions: Enhanced Mo source (3 kW), 40 kV voltage, and 40 mA current. The 2θ scanning range was 4–36°, with a step width of 0.02°/S at a scanning speed of 2°/min. Samples placed on a sample holder were gently compressed with a clean metal bar and diffractograms were collected at room temperature (20–25°C).

3.14 Hot melt extrusion (HME)

3.14.1 **Preparation of the physical mixture for hot melt extrusion**

The shellac materials and model drug (fenofibrate) were weighed according to the designed formulation and then put into a sealed HDPE (High-density polyethylene) box. Due to static interactions between metal and the drug powder which causes the drug powder to adhere to its surface, a glass rod was utilised for premixing. Dispersion of the components could be visually assessed due to differences in colours of the individual components. The formulation mixed by the rotational mixer was set at a speed of 1500RPM, with a short period of the 30s to prevent melting of the formulation inside the HDPE box. The mixing time was 2 min in total.

3.14.2 **Hot melt extrusion process condition and formulation matrix for section 4.2**

The prepared physical mixtures were extruded by a bench-top Prism™ twin-screw co-

rotating extruder with 16 mm diameter screws and a 25:1 length to diameter ratio, equipped with a Thermo standard screw configuration consisting of 1 mixing zones (universal screw design 7 kneading discs assembly with 30º stagger angle). Physical mixtures were manually starve feeding into the extruder hopper. The temperature profile from the feeding zone to die was 35 °C / 50 °C / 90 °C /90 °C / 90 °C for the processing of the binary amorphous dispersions. Different process screw speeds (55RPM and 110RPM) were selected for checking the feasibility of the extrusion process. The resulting extrudates were allowed to cool by a high-pressure airline built in a conveyor belt device. As shown in Table 3-2. There are four different FEB drug loading from 0%-20% and blends with four different shellac materials with two different screw speeds were prepared for analysis.

Table 3-2. Process parameter of the hot melt extrusion process

Run no	Sample no	%Drug Loading	Shellac Type	Screw Speed (RPM)
1	S1	0	SSB 55 Pharma FL	55
2	S2	0	SSB 55 Pharma FL	110
3	S5	5	SSB 55 Pharma FL	55
4	S6	5	SSB 55 Pharma FL	110
5	S9	10	SSB 55 Pharma FL	55
6	S10	10	SSB 55 Pharma FL	110
7	S13	20	SSB 55 Pharma FL	55
8	S14	20	SSB 55 Pharma FL	110
9	S17	0	Dewaxed AFS shellac HS 700K	55
10	S18	0	Dewaxed AFS shellac HS 700K	110
11	S21	5	Dewaxed AFS shellac HS 700K	55
12	S22	5	Dewaxed AFS shellac HS 700K	110
13	S25	10	Dewaxed AFS shellac HS 700K	55
14	S26	10	Dewaxed AFS shellac HS 700K	110
15	S29	20	Dewaxed AFS shellac HS 700K	55
16	S30	20	Dewaxed AFS shellac HS 700K	110
17	S33	0	AFS shellac RTH	55
18	S34	0	AFS shellac RTH	110
19	S37	5	AFS shellac RTH	55
20	S38	5	AFS shellac RTH	110
21	S41	10	AFS shellac RTH	55
22	S42	10	AFS shellac RTH	110
23	S45	20	AFS shellac RTH	55
24	S46	20	AFS shellac RTH	110
25	S49	0	AFS shellac WL	55
26	S50	0	AFS shellac WL	110
27	S53	5	AFS shellac WL	55
28	S54	5	AFS shellac WL	110
29	S57	10	AFS shellac WL	55
30	S58	10	AFS shellac WL	110
31	S61	20	AFS shellac WL	55
32	S62	20	AFS shellac WL	110

3.14.3 **Hot melt extrusion process condition and formulation matrix for section 4.4**

The prepared physical mixtures were extruded using a Prism co-rotating extruder with

two different screw setups. The modified screw configuration consists of 1 combined mixing zones, as shown in Figure 3-16b. The modified screw design consists of 10 kneading discs assembly with different stagger angles, which would provide much more shear stress and increase the residence time for the melt. The universal screw design consists of 7 kneading discs assembly with only a 30º stagger angle. Physical mixtures were manually starve-fed directly to the extruder feeding zone. The temperature profile from the feeding zone to die was 35 °C / 50 °C / 90 °C /90 °C / 90 °C for the processing of the binary amorphous dispersions. The resulting extrudates were allowed to cool using a dry compressed airline transport device as shown in Figure 3-17. In order to minimize the material usage and eliminate the impact of human factors in the extrusion process and disrupt the processing order, a factorial design was used with half fraction experiment batches. The four factors were screw design, screw speed, drug loading and mixing method. The DoE preparation by Minitab 20.3 (Design of experiment) of 2 different fenofibrate drug loadings of 15% & 25% and blends with shellac SSB 55 Pharma FL was outlined in Table 3-3. Also, two different screw speeds (55 RPM and 110 RPM) were used for this analysis. he formulations and processing matrix for the other forms of shellac material are shown in Table 3-4.

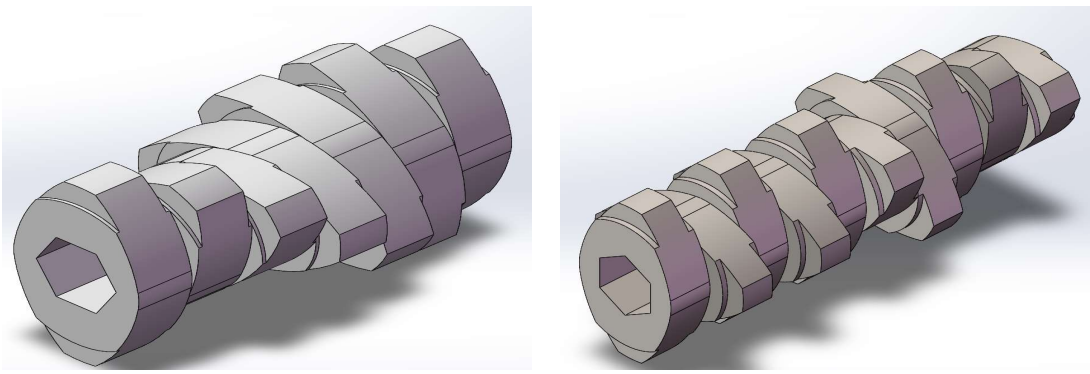

a b

Figure 3-16 Screw configuration a) initial universal configuration, b) modified configuration, a) combined with 7 kneading disks with 30˚ stagger angle; b) combined with 10 kneading disks, with 3 @ 30˚ stagger angle, 3

@ 60˚ stagger angle and 4 @ 90˚ stagger angle.

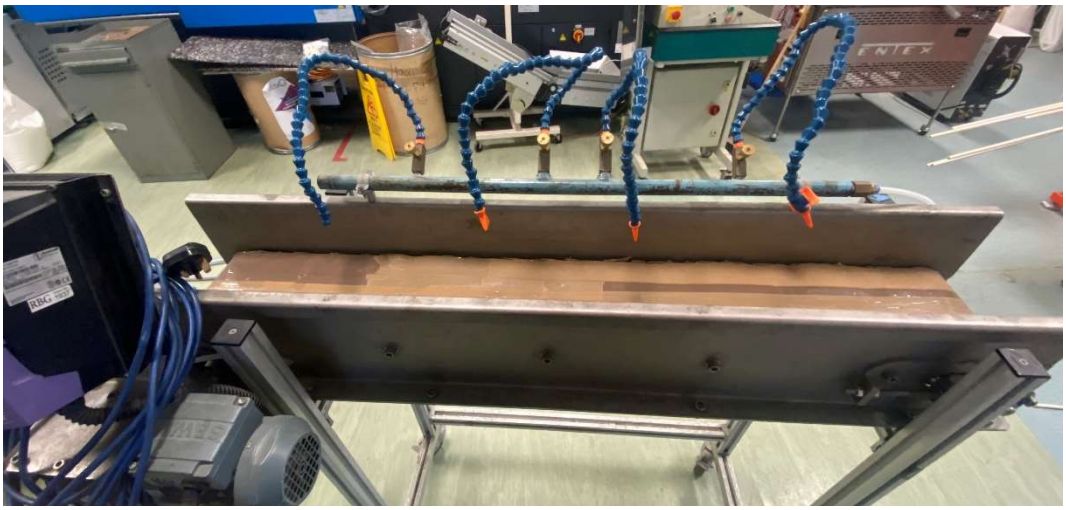

Figure 3-17 Melt extrusion conveyor device with dry compressed air-cooling line.

Table 3-3 DOE for Shellac SSB 55 Pharma FL

Batch No	Batch Name	Run Order	Center Pt	Blocks	Screw Speed (RPM)	Drug loading (%)	Screw Design
P1	SSB-M-55-15	1	1	1	55	15	Modified screw
P2	SSB-M-110-25	6	1	1	110	25	Modified screw
P3	SSB-M-55-25	7	1	1	55	25	Modified screw
P4	SSB-M-110-15	8	1	1	110	15	Modified screw
P8	SSB-U-110-25	2	1	1	110	25	Universal screw
P9	SSB-U-55-15	3	1	1	55	15	Universal screw
P10	SSB-U-110-15	4	1	1	110	15	Universal screw
P11	SSB-U-55-25	5	1	1	55	25	Universal screw
P15	Physical Mixture	0				25	No processing

Table 3-4 Processing matrix for other shellac types

Batch No	Batch Name	Run order	Shellac type	Drug loading	Screw speed
P6	702-M-110-15	9	AFS shellac HS 702MB	15%	110RPM
P12	702-M-55-15	10	AFS shellac HS 702MB	15%	55RPM
P13	702-M-110-25	11	AFS shellac HS 702MB	25%	110RPM
P14	702-M-55-25	12	AFS shellac HS 702MB	25%	55RPM
P5	700-M-110-15	9	Shellac AFS HS 700K	15%	110RPM
P7	SWA-M-110-15	11	Shellac AFS HS SWANLAC	15%	110RPM

3.15 ANSYS Polyflow analysis

3.15.1 **The simulation process outline**

The simulation process can be broken done into several steps, as shown in below Figure 3-18 and Figure 3-19

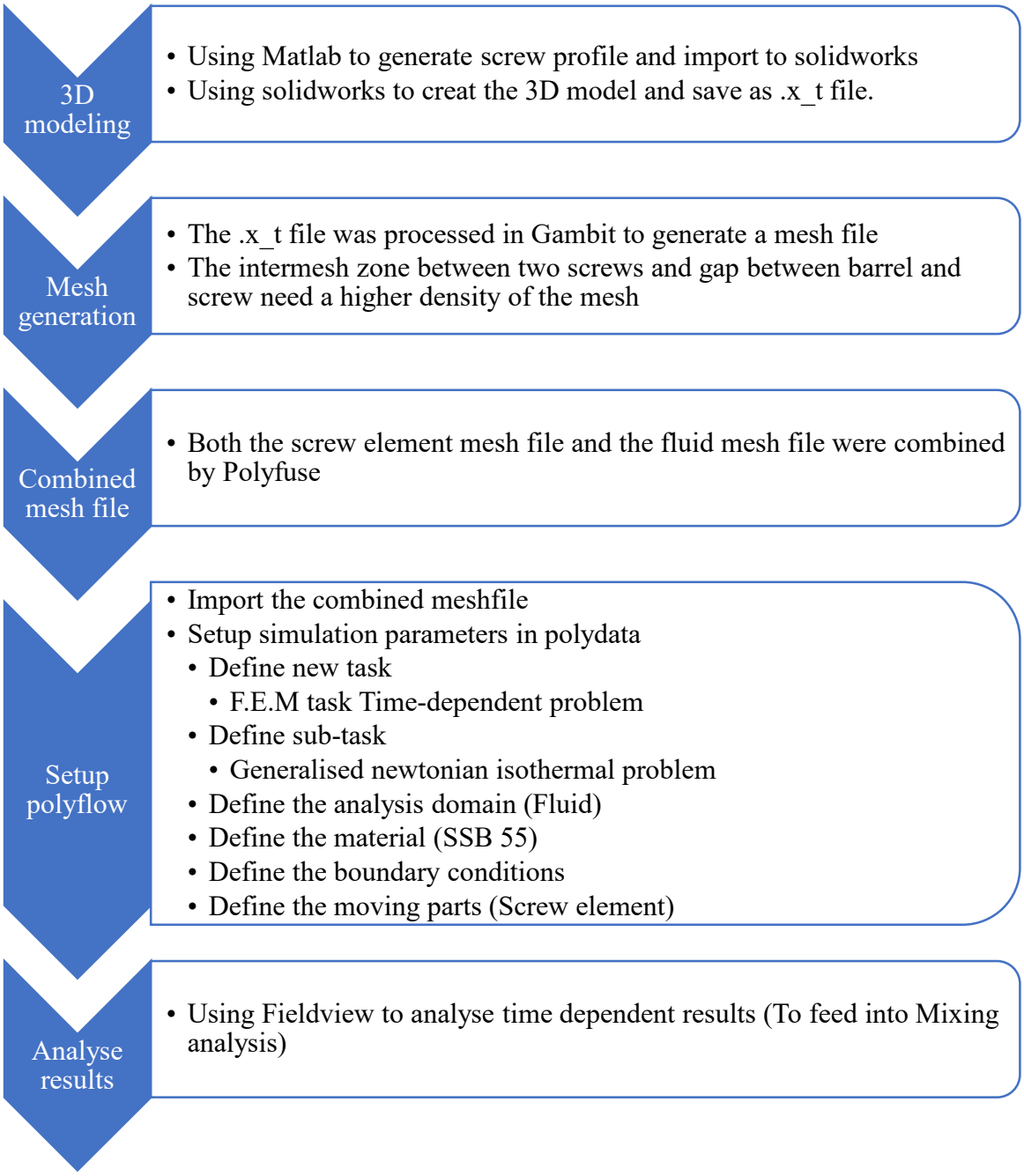

Figure 3-18 Flow chart for ANSYS Polyflow Time-dependent analysis

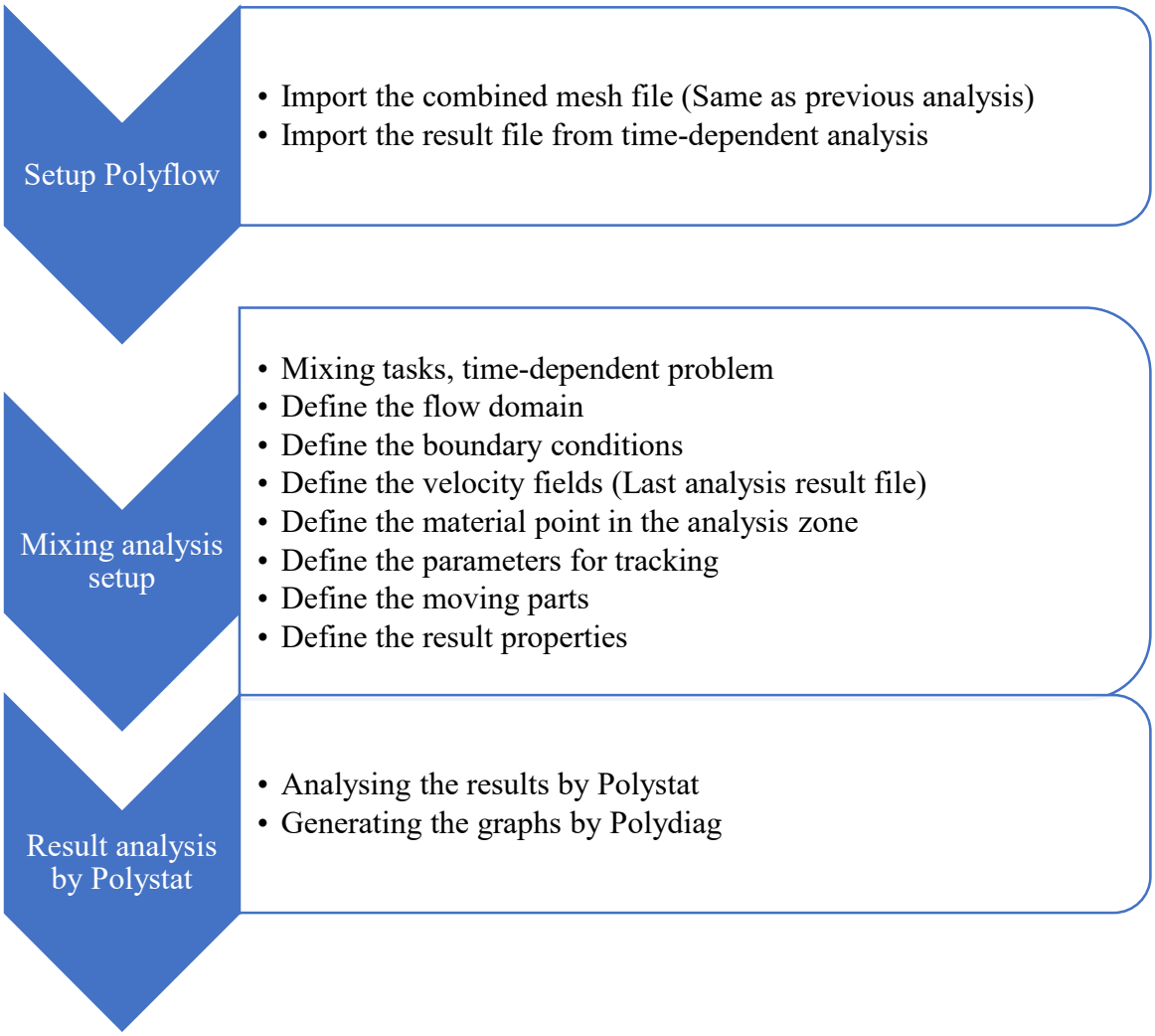

Figure 3-19 Flow chart for ANSYS Polyflow mixing analysis

3.15.2 **Mathematical model and mesh generation**

3.15.2.1 *Flow conditions*

The following assumptions as flow conditions were used in the simulations:

(1) The flow channel is filled with the polymer melt.

(2) The fluid is incompressible and pure viscous non-Newtonian.

(3) The flow is isothermal and steady.

(4) The inertia and gravitational forces are negligible because of the high viscosity fluid.

(5) The Reynolds number is small, and the flow is laminar

(6) There is no slip on the flow channel wall

3.15.2.2 *Material constants*

The material data simulated in this study was generated by TA Discover 2 Rheometer, SSB 55 Pharma FL was chosen as the model fluid in the simulation causing the better processing ability found in the previous section. The shear viscosity curve for the material is shown below in Figure 3-20. Carreau-Yasuda Law model was used as the constitutive model of pure viscous non-Newtonian fluid which described as

$$\eta = \eta_\infty + (\eta_0 - \eta_\infty)[1 + (\lambda\dot{\gamma})^\alpha]^{\frac{n-1}{\alpha}} \qquad 3\text{-}7$$

Where η_0 is zero-shear-rate viscosity

η_∞ is infinite-shear-rate viscosity

λ is natural time (that is, inverse of the shear rate at which the fluid changes from Newtonian to power-law behaviour)

α is an index that controls the transition from the Newtonian plateau to the power-law region

n is a power-law index

From section 4.1 and section 4.2, shellac SSB 55 has better processability and faster

drug release profile. As a result, in the simulation fluid material part, the values of the fluid material data constants were taken from the experimental data of the shear viscosity curve for a shellac material (SSB 55 Pharma FL). The experimental data and the fitting curve by the Carreau-Yasuda model are shown in Figure 3-20. The values of η_0, η_∞, λ, α, n are 34620.1, 586.2, 0.00377, 0.2654, and 0.03432 respectively.

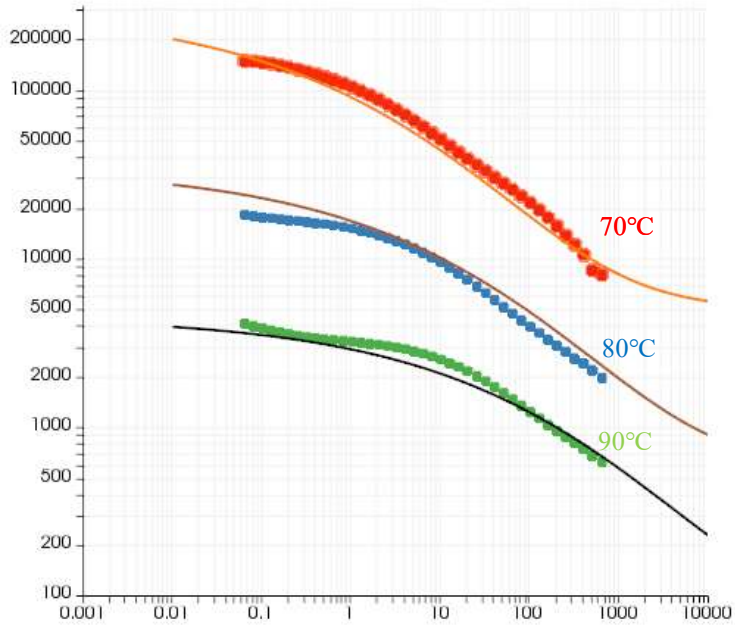

Figure 3-20 Shear viscosity curve for shellac SSB 55 pharma FL and the fitting curve by the Carreau-Yasuda model.

3.15.2.3 *Analysis domain mesh and moving coordinate system*

For the screw element, the analysis domain can be reduced to a single pitch because of the steady condition and the system's periodic nature of the screw rotation. This would help to reduce the computing time and the usage of the PC resource. The solid screw part with 9097 quadrilateral elements and 2386 nodes. The fluid domain with 61440 quadrilateral elements and 68935 nodes in the screw pitch includes the flow channel between the screw and barrel, and the intermesh area between the screw, as shown in Figure 3-21.

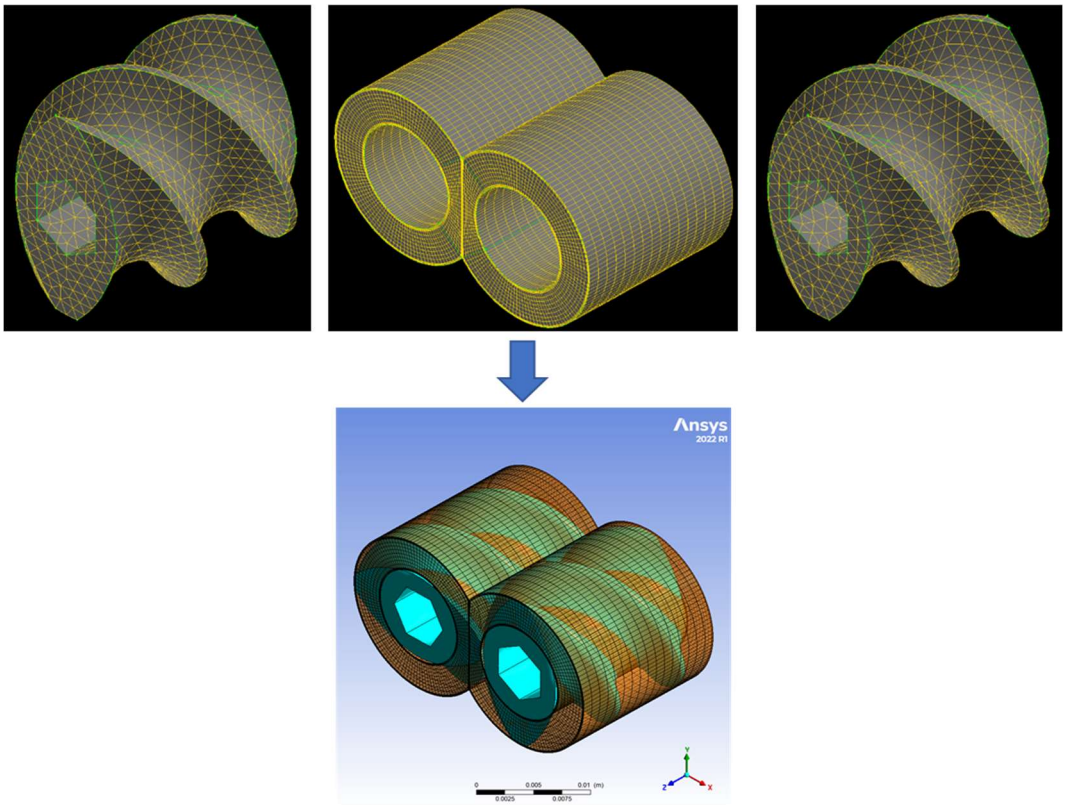

Figure 3-21 Combined mesh file of a single screw element.

For the kneading section, the kneading element part with 41254 quadrilateral elements and 9531 nodes. In the fluid domain with 349440 quadrilateral elements and 373060 nodes, the analysis domains include the whole kneading blocks. The 3D model of these domains is shown in Figure 3-22.

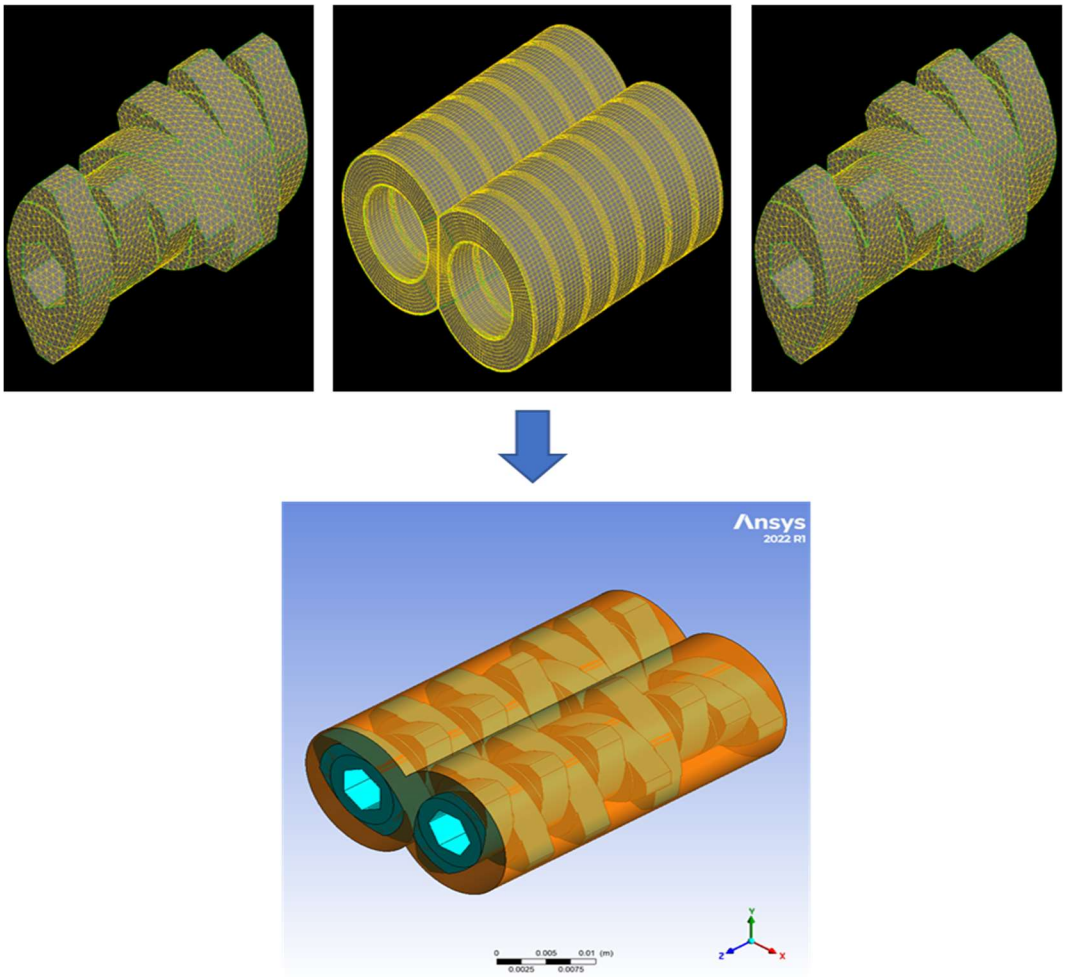

Figure 3-22 Combined mesh file of a kneading element section.

To facilitate mesh division and make the analysis concise and clear, the Cartesian coordinate system is selected here, as shown in Figure 3-23. The coordinate origin is the midpoint of the connecting line between the centres of the two screws and at the inlet section. The positive direction of the axis is right, the positive direction of the Y-axis is up, and the positive direction of the Z-axis is determined by the right-hand rule along with the extrusion direction (Lewandowski and Wilczyński, 2022).

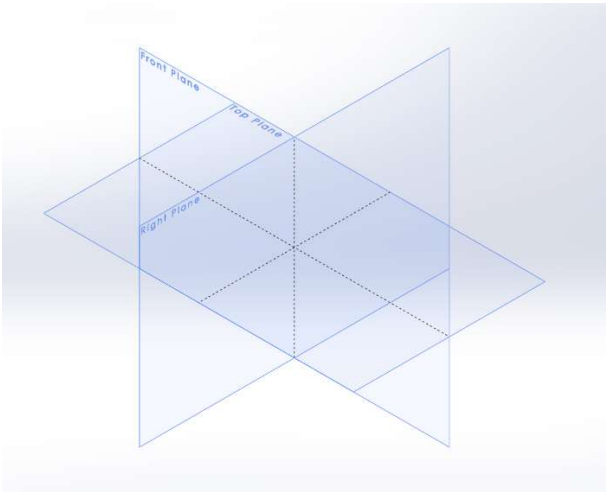

Figure 3-23 3D cartesian coordinate system.

The regeneration of the finite element mesh can be a tedious and time-consuming process. In this work, an automatic mesh generator was developed to overcome the problems associated with multiple regenerations. Due to the steady condition and the system's periodic nature of the screw rotation. There were 30 sequential geometries specified to represent half of the complete cycle of rotation for a geometry of screw element, according to Figure 3-24 (only 6 images out of 30 are listed). Variable α represents the angle between the left rotor tip and the y-axis for the first disc. Increments of 6˚ for each time step were taken, corresponding to a time interval of 0.01667 seconds for a rotation speed of 60 rpm.

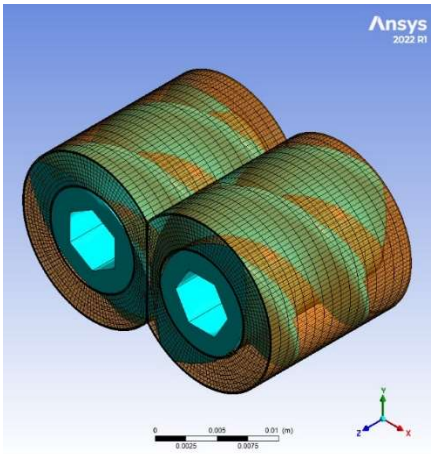

α=30 °

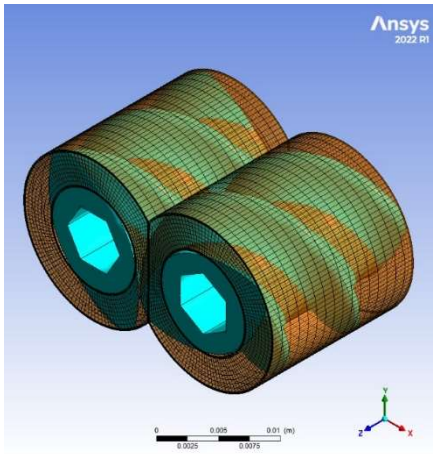

α=60 °

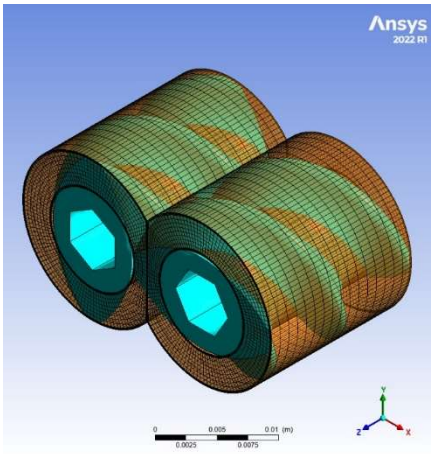

α=90 °

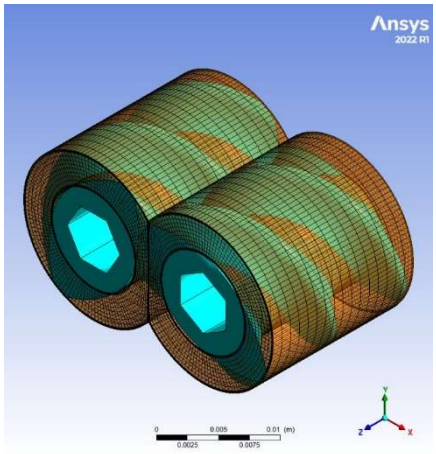

α=120 °

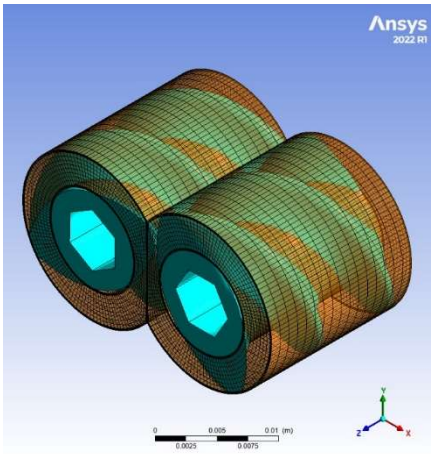

α=150 °

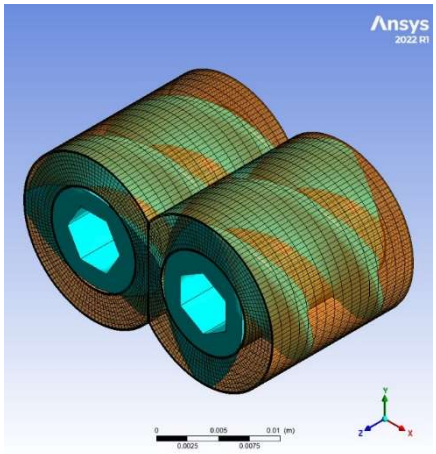

α=180 °

Figure 3-24 Six sequential geometries of the screw element in one rotation.

3.15.2.4 *Boundary conditions*

The computation scheme is depicted in Figure 3-25. Three subdomains are distinguished, for the flowing material (Subdomain 1) and for the screws (Subdomain 2, Subdomain 3).

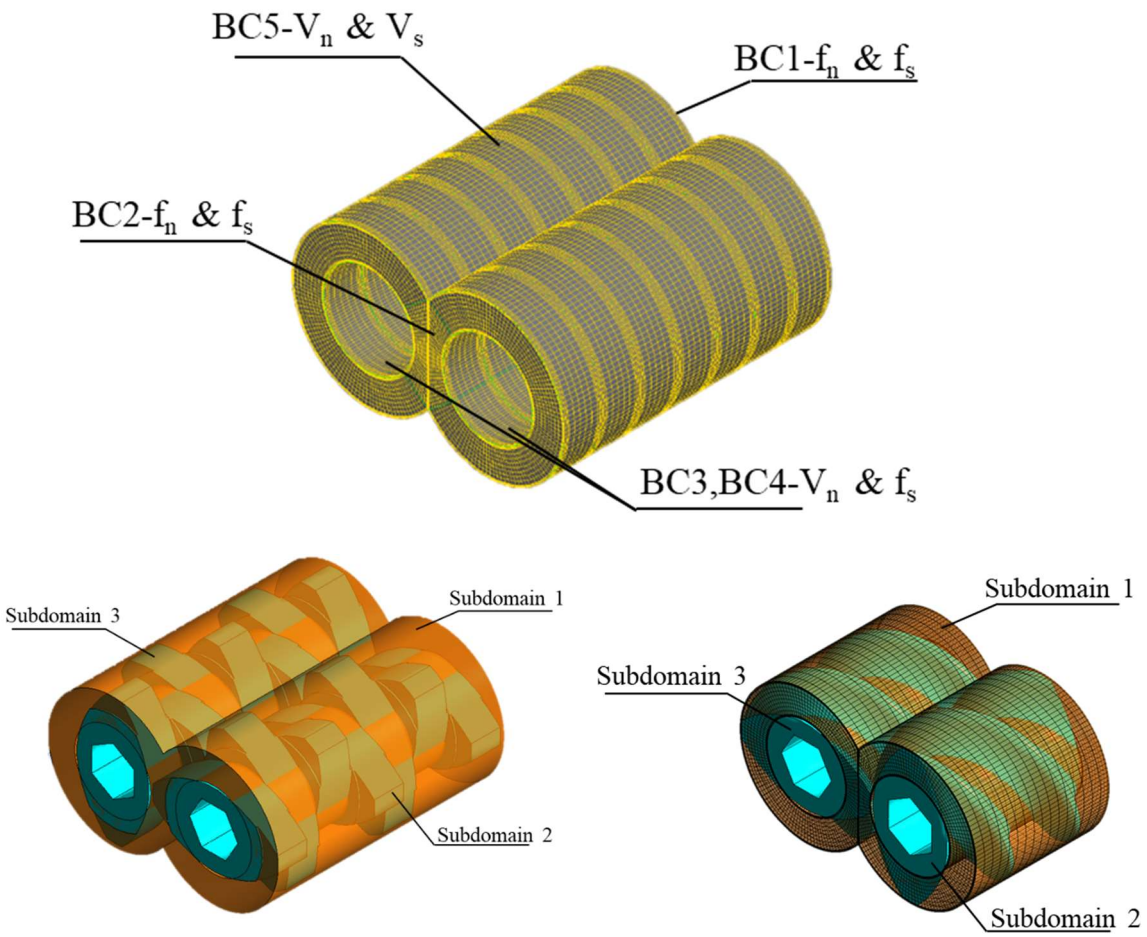

Figure 3-25 Boundary condition of each analysis question.

The following flow boundary conditions were applied to define the process:

− At the inlet to the flow domain: boundary BC1-f_n & f_s, normal forces and tangential velocities are imposed (f_n and v_s) = (0, 0), the flow rate (Q_{in}) = (Q) is imposed,

− At the outlet of the flow domain: boundary BC2-f_n & f_s, normal forces and tangential velocities are imposed (f_n and v_s) = (0, 0), which means that the flow rate (Q_{out}) = (Q) is imposed,

− On the barrel wall: boundary BC5, zero wall velocity, vanishing normal and tangential velocities are imposed (v_n and v_s) = (0, 0), which means that the velocity vanishes at the barrel wall.

− On the screw contact domain: boundary BC3 and BC4, slip boundary condition, Normal velocity and tangential force imposed (v_n and f_s) = (0, 0), which means that there is no material can through this wall and material is not subject to tangential forces.

The boundary conditions, BC1 and BC2 are free to flow, i.e., normal forces and tangential velocities (f_n and v_s) = (0, 0), implying that pressure may be developed over the screws. Since the pressure at the screw element end is not known, the pressure gradient is computed relative to the zero pressure at the element exit. Negative pressures which may result from simulations do not mean negative pressures in the extrusion process (Lewandowski and Wilczyński, 2022).

3.15.2.5 *Mixing process simulation*

The flow field inside the screw and kneading element were simulated by POLYFLOW. After the flow field was computed, a mixing task was executed by using the mixing module program to calculate the trajectories of 2000 material points which were located initially at the entrance of melt conveying in the analysis domain. Then, the mixing characteristic parameters inside the flow domain were analysed using POLYSTAT statistical module to evaluate the local value of the mixing characteristic parameters respectively.

There are many ways of characterizing mixing that has been proposed over the years, with no one method being able to quantify all aspects of mixing for every process. Given a motion $x = \chi(\mathrm{X}, \mathrm{t})$, where initially $x = \chi(\mathrm{X}, 0)$ for an infinitesimal material line segment $dx = F \cdot dX$ located at position x at time t where the deformation tensor is $F = \nabla\chi$, the length of stretch of material line is defined as $\lambda = |dx| \,/\, |dX|$. Then the local efficiency of mixing e_λ is then defined as (Ansys, 2022)

$$e_\lambda = \frac{\dot{\lambda}/\lambda}{(\boldsymbol{D}:\boldsymbol{D})^{1/2}} = \frac{D\ln\lambda/Dt}{(\boldsymbol{D}:\boldsymbol{D})^{1/2}} \qquad 3\text{-}8$$

Where the rate of strain tensor $\boldsymbol{D}$ is the symmetric part of the velocity gradient tensor. This efficiency quantitatively characterizes the stretching rate during mixing and can be thought of as the fraction of the energy dissipated locally that is used to stretch fluid elements. The time-averaged efficiency is defined as (Xu *et al.*, 2014)

$$\langle e_\lambda \rangle = \frac{1}{t}\int_0^t e_\lambda dt \qquad 3\text{-}9$$

For 3D flows, define an infinitesimal surface "dA" with a normal direction $\widehat{N}$. With time, this surface deforms, at time t, this surface is noted "da", with a new normal direction $\hat{n}$. The area stretch S is the ratio of the deformed surface "da" at time t, over the initial surface "dA", $S = S(X, \widehat{N}, t) = da/dA$, then (Fan *et al.*, 2019)

$$e_s(X, \widehat{N}, t) = \frac{\dot{S}/S}{\boldsymbol{D}} \qquad 3\text{-}10$$

$$\langle e_S \rangle (X, \widehat{N}, t) = \frac{1}{t}\int_0^t e_S(X, \widehat{N}, t) dt \qquad 3\text{-}11$$

In polymer blending, a minor component is generally present as droplets (or filaments) in a continuous phase called the matrix. Mixing is the process to deform those drops in the flow field. The deformation of drops is enhanced by the viscous stress τ caused by the flow field and reduced by the interfacial stress σ/R (σ= interfacial tension, R= local radius of the drop) (Ansys, 2015).

When the viscous stress τ is not excessive and competes with the interfacial stress, the drops are extended and finally break up into smaller droplets. This kind of mixing is called "dispersive mixing". In conclusion, to evaluate the mixing capabilities of an extruder, it is important to calculate the viscous stress: if its value is too low, no breakup will occur. Every piece of material will undergo viscous stress, high enough to break up drops. Another key point is that extensional flow is much more efficient to break up droplets than shear flow: to estimate the fraction of the matter going through extension, the mixing index was calculated,

defined as follows (Fan *et al.*, 2019):

$$Mixing\ index = \frac{\dot{\gamma}}{\dot{\gamma}+\omega} \qquad 3\text{-}12$$

where $\dot{\gamma}$ the equivalent shear rate, ω is the magnitude of the vorticity vector. The mixing index can range from 0 to 1. At 0, the flow is locally a plug flow; at 0.5, the flow is locally a pure shear flow; while at 1, the flow is locally a pure extensional flow (Cheng and Manas-Zloczower, 1997).

3.15.3 **Combination screw configuration**

The geometric characteristic parameters of the Prism 16 twin-screw extruder in this study are listed in below Table 3-5. The number of flights is 2, barrel inner diameter is 16 mm, clearance between barrel and screw is 0.2 mm, and assembly centreline distance is 12.5 mm. The full mesh co-rotating twin screw extruder profile was generated by MATLAB (As shown in Appendix B). All the data points were then imported to Solidworks 2022 to generate the profile arcs. The 3D model of the kneading and conveying element created are shown below in Figure 3-26.

Table 3-5 The geometric characteristic parameters of Prism 16 twin-screw extruder in this study.

Barrel bore diameter	16 mm
Screw outside diameter	15.6 mm
Pitch	8 mm
Screw root diameter	9 mm
Centreline distance of screw	12.5 mm
Clearance between screw	0.2 mm
Clearance between screw barrel	0.2 mm

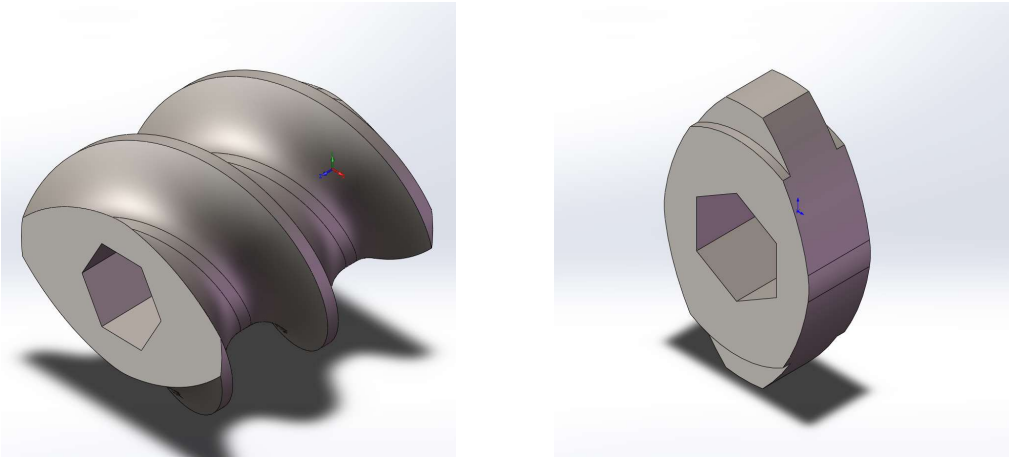

Figure 3-26 A 3D model of the conveying (Left) and kneading (Right) element.

As the calculation and simulation involve a variety of screw elements of Prism 16 extruder, to facilitate the study and comparison of the different combinations, the screw elements are numbered as follows according to their characteristics.

KB/30/ 7 /28/30

- Screw speed
- Kneading block length
- Number of kneading discs
- Straggle angle/forward angle
- Kneading Block

CE/2/ 8/ 16/ 30

- Screw Speed
- Length of conveying element
- Pitch of conveying element
- Number of flights
- Conveying element

According to this numbering system, the simulation matrix can be classified into distinct groups shown in Table 3-6, Table 3-7, and Table 3-8.

Table 3-6 Kneading element (Disc gap 0.4 with different stagger angle)

Number	Stagger angle (°)	Length of kneading block (mm)	Screw speed (RPM)
KB/30/7/28/30	30	28	30
KB/60/7/28/30	60	28	30
KB/90/7/28/30	90	28	30

Table 3-7 Kneading blocks (Disc thickness 4mm, disc gap 1mm, stagger angle 30°)

Number	Stagger angle (°)	Length of kneading block (mm)	Screw speed (RPM)
KB/30/7/28/30	30	28	30
KB/30/7/28/60	30	28	60
KB/30/7/28/90	30	28	90
KB/30/7/28/120	30	28	120

Table 3-8 Full mesh conveying element (Screw element)

Number	Length of Conveying element (mm)	Screw speed (RPM)
CE/2/8/16/30	16	30
CE/2/8/16/60	16	60
CE/2/8/16/90	16	90
CE/2/8/16/120	16	120

3.16 Statistical analysis

A statistical analysis of the melt flow index, differential scanning calorimetry, drug content, and dissolution profile data was performed. Following assessment of normality of distribution and homogeneity of variance, treatments were compared using a one-way ANOVA with a Tukey's Honesty Significant Difference Post hoc test to determine differences between individual dissolution profiles. Differences were considered significant when $p<0.05$. To perform this analysis, the IBM SPSS statistics version 23 software was used. Moreover, except DSC result all other graphs were produced by Origin Lab Pro Version 2022b.

Chapter 4 Result and Discussion

4.1 Material characteristic

4.1.1 **Introduction**

Shellac is the refined form of the natural resin LAC produced by the female insect, Kerria Lacca. India, Thailand and southwest China are the main production areas of LAC (Chauhan *et al.*, 1973; Das and Jacob, 2011). Shellac is a complex mixture consisting of aliphatic and alicyclic acid components. Different types of insect species and host trees determine the composition of shellac material. However, there are no chemical differences between various shellac materials, only the content of each component is different (Wang *et al.*, 1999). In various pharmacopoeias, shellac is classified by its refining process as well as its chemical properties and acid values. Besides the acid value, the shellac quality can be characterised by its glass transition temperature, pK_a value and intrinsic dissolution rate (Buch *et al.*, 2009; Farag and Leopold, 2009). In the pharmaceutical industry, shellac was employed as an enteric coating material due to its pH-sensitive properties (Panchapornpon *et al.*, 2011; Alzahrani, Bedir and Al-Hayani, 2013; Arnautov, Korhov and Faitelson, 2013; Soradech, Limatvapirat and Luangtana-anan, 2013). Pearnchob stated that shellac could provide the same water resistance and taste masking with a lower coating level. Additionally, Pearnchob et al. (2003) and Sontaya et al. (2008) investigated the feasibility of extended-release shellac-matrix tablets prepared by either compression of powder or wet granules methods (Pearnchob, Siepmann and Bodmeier, 2003a; Limmatvapirat, Limmatvapirat, *et al.*, 2008). In 2017, Gately et al. investigated the targeted delivery of probiotics prepared by melt extrusion technology (Gately and Kennedy, 2017). Over the last two decades, hot melt extrusion has been inducted into the pharmaceutical industry. It has long been known that twin-screw extrusion can increase the solubility of drugs by the formation of a solid dispersion (Tran, Lee and Tran, 2021). The processability of the material is appreciably affected by the way the polymer reacts with flow and deformation (Aho *et al.*, 2015). When determining the extrusion parameters before processing, polymers with high viscosity,

always require higher melt temperature profiles and higher shear rates in the barrel. Furthermore, discharge pressure and more power consumption are often required. This would help to reduce the number of trials needed to find the desired conditions for extrusion (Maru *et al.*, 2011; H. Liu *et al.*, 2012; Gupta *et al.*, 2015; Bochmann *et al.*, 2017).

This section will explore four different types of shellac and investigate their physicochemical properties and processability with the subsequent view to using shellac material as a matrix polymer for enteric targeted drug delivery systems.

4.1.2 **Result and discussion**

4.1.2.1 *IR spectrum*

4.1.2.1.1 ***Investigating the effect of different shellac on FTIR spectrum***

The characteristic peaks of Shellac resin scanned by FTIR are depicted in Table 4-1. The table is meant as a reference tool when discussing and reviewing spectra obtained for this study.

Table 4-1 FTIR peak table of raw shellac material

Molecular motion	IR peak	cm^{-1} possible (in) Functional group	
O-H stretch	3416	3700-3200	hydroxyl
C-H stretch	2930	2940-2860	alkanes
C-H stretch	2857	2960-2940	alkanes
C=O stretch	1710-11	1780-1710	carboxylic acid
C=O stretch (fresh shellac)	1636	1700-1680	sat. aldehyde (ester)
C=C stretch	1636	1680-1630	alkenes
CH_2 bend	1462	1470-1350	alkanes
CH_3 bend	1374	1390-1365	alkanes
C-O stretch	1247	1250-970	alkanes-from ester
C-O stretch	1147	1250-970	alkanes-from acid
C-O stretch	1002	1250-970	alkanes-from alcohols
C-H stretch/CH_2	943	995-880	alkenes
CH_2 rocking chain	722	740-710	wax

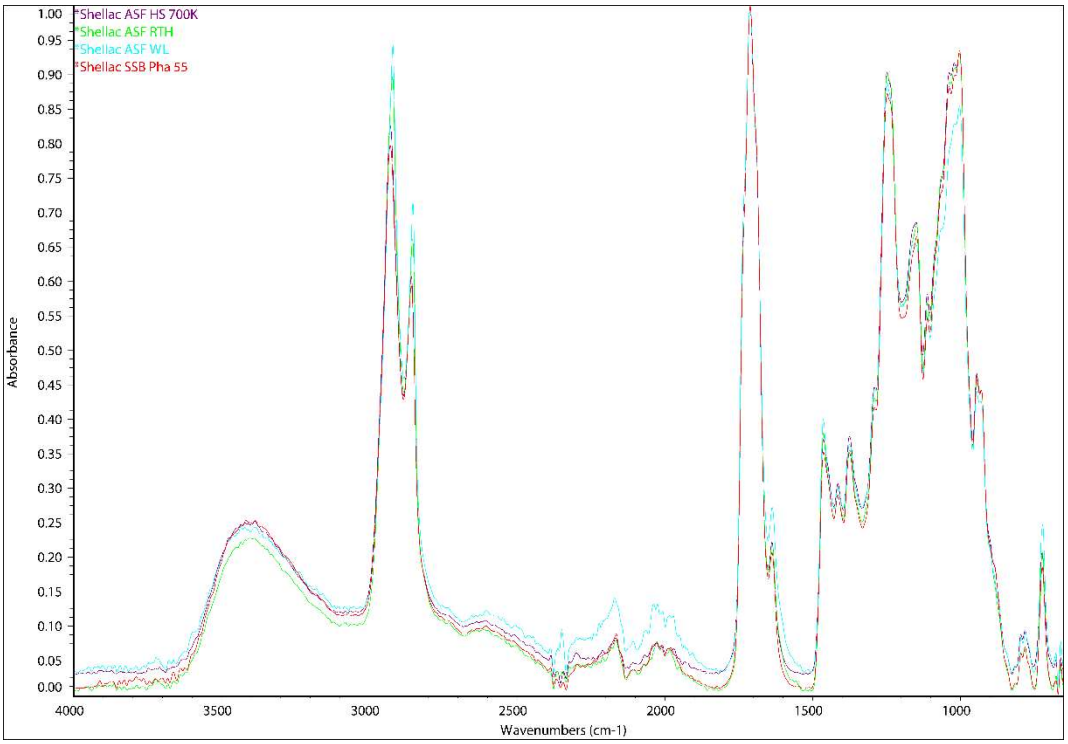

Figure 4-1 FTIR Spectrum of each type of shellac.

In Figure 4-1, characteristic peaks associated with Shellac were observed in the FTIR spectrum of the different shellac base materials. The characteristic peaks observed were a broad band in the range of 3700–3200cm^{-1} with a maximum at 3416 cm^{-1} which is attributed to the -OH vibrations from acidic and hydroxyl functional groups, as well as a strong absorption band at 2928-2920cm^{-1} and 2587cm^{-1}, which represents –CH stretching (Khairuddin, E. Pramono, *et al.*, 2016). The carbonyl band from the acid formation is visible at 1710cm^{-1} with a slight shoulder at 1636cm^{-1}, corresponding to the C=O band of an ester. As a result of all the manner of bending vibrations within the molecule, the right-hand side of the diagram (from about 1500 to 650cm^{-1}) usually contains a complicated series of absorptions. This region is called the fingerprint region. In the fingerprint region, the main absorption bands are at 1462cm^{-1} (CH_2 bend), 1374cm^{-1} (CH_3 bend), 1246cm^{-1} (C-O) stretch from ester), 1148cm^{-1} (C-O stretch from acid), a broad band between 1010 and 1000cm^{-1} (C-O stretch from alcohol), 943cm^{-1} (C-H stretch/CH_2 from alkenes) and a weak peak visible at 720cm^{-1}, which may represent CH_2 rocking in the shellac wax. Moreover,

there are two peaks around 2000-2300cm^{-1} in shellac AFS WL that could attribute to carbon dioxide in the environment. The FTIR result shows that the received shellac is a mixture containing ester, acid and hydroxyl groups which refer to the resin part of the composition, along with some trace quantities of wax even in dewaxed shellac. Moreover, all the similarly characteristic peaks observed show that there is little or no chemical difference between various shellac types, the only difference being the concentration of each basic constituent molecule. As a result, it is not possible to identify each sample by its FTIR spectrum (Gately, 2011).

4.1.2.1.2 ***Comparing shellac SSB 55 with shellac AFS RTH***

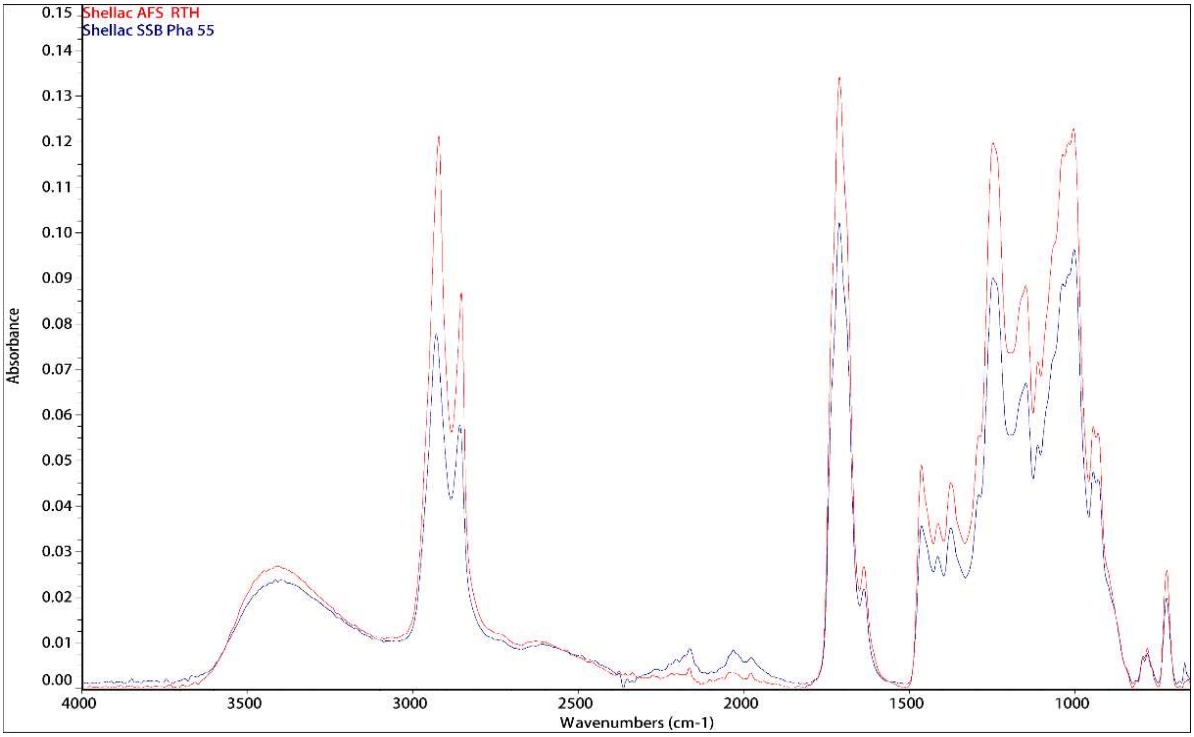

Figure 4-2 FTIR result of shellac AFS RTH and shellac SSB 55 Pharma FL.

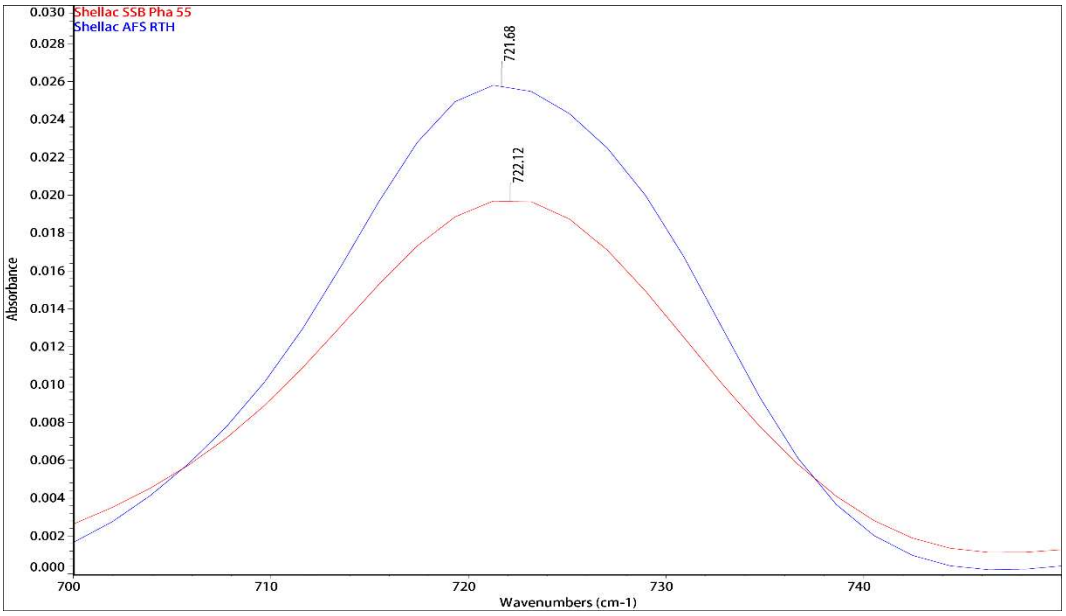

Figure 4-3 Shellac AFS RTH and shellac SSB Pha 55 overlays at 700-750cm^{-1}.

As shown in Figure 4-2, SSB 55 pharma FL and AFS RTH have similar chemical structure. However, SSB Pha 55 was produced by solvent extraction method, it is a decolourised shellac, and it is light yellow colour. AFS RTH is produced from light coloured seedlac by melting process; the colour is brown. Additionally, SSB Pha 55 is dewaxed shellac, and RTH is classified as a wax containing shellac. From the spectra Figure 4-2, the characteristic peaks for both shellacs are remarkably similar with the peak intensity being the only difference between the two spectra. In Figure 4-3, Shellac wax shows a characteristic doublet peak at 720-730cm^{-1}, the intensity differences of both samples are attributed to AFS RTH having a significantly higher wax content which is approximately 4-6%, thus having a higher absorbance value (Derry, 2012; Khairuddin, Edi Pramono, *et al.*, 2016). Even though SSB Pha 55 is dewaxed shellac, it is shown that although most of the wax has been removed, there are some traces of wax detectable in the sample.

4.1.2.1.3 ***Comparing shellac AFS HS 700K with shellac SSB Pha 55***

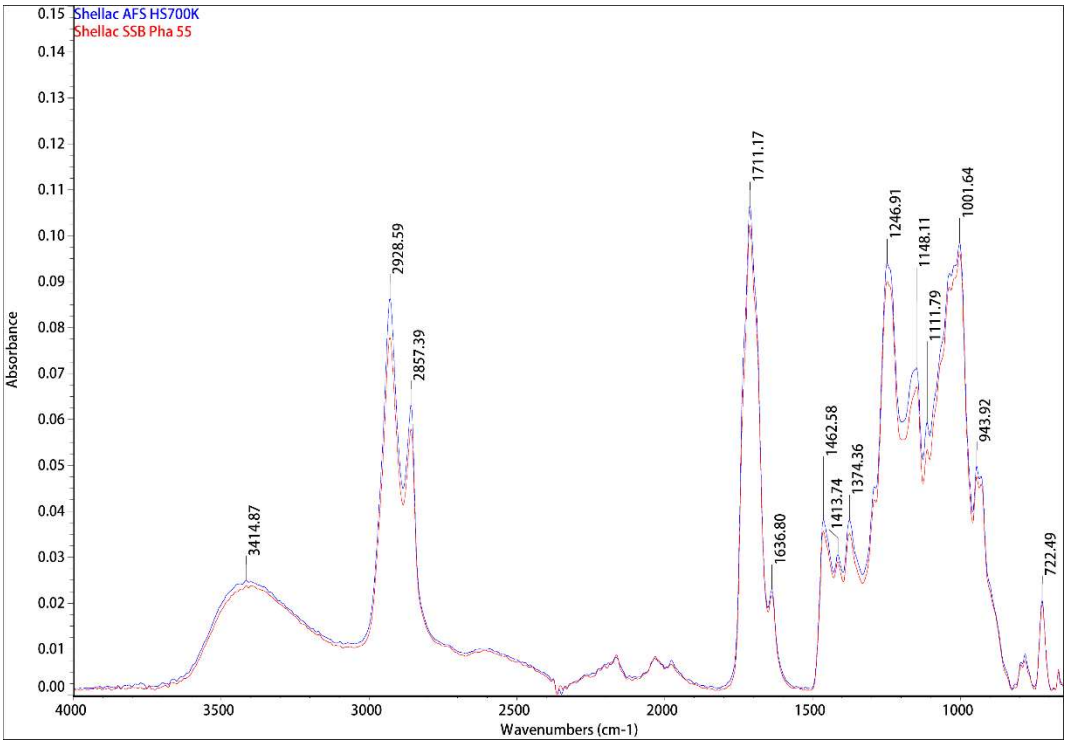

Figure 4-4 Comparing shellac AFS HS 700K with Shellac SSB 55 Pha.

As shown in Figure 4-4, AFS HS 700K and SSB 55, are both dewaxed, decolourised shellac, but the production date of SSB 55 Pha is earlier than AFS HS 700K. From previous work, all the shellac materials have little or no chemical difference, and the samples gave almost identical spectra. Even though there is some peak intensity variation, the higher intensity bands belong to AFS HS 700K and it is highly unlikely to be able to identify each shellac type by FTIR spectrum.

4.1.2.2 *Melt flow index analysis*

MFI can determine the quality of a polymer, relate its flow properties to its application and measure the viscosity of the polymer in a molten state. Because the shear stresses used in most fabricating processes are much higher than the applied shear stresses or resultant shear rates in the test, the data obtained from this test does not necessarily correlate with the processability of the polymer. However, the results obtained do provide a useful indication of the relative ease with which different samples will flow when they are fabricated. Generally, a low molecular weight material is much easier to flow than a high molecular

weight material (Cao *et al.*, 2016). Thus, high MFI values indicate easier melt flow so the polymer or polymer blend which has a relatively high MFI is most often chosen as the raw material when the fabrication process involves high rates of shear (e.g., HME).

In this section, as can be seen in Table 4-2, each type of shellac has quite different MFI values. Shellac SSB 55 has the highest MFI value with 11.88g/10min compared to other shellac variations. Shellac AFS RTH also have a high MFI value of 9.45g/10min. Nevertheless, Shellac AFS WL has the lowest MFI value (3.00g/10min), meaning that under these test conditions, Shellac WL had the highest resistance to flow. From the FTIR result, little chemical difference between various shellac was shown, with the only difference being the variations in base ingredient contents mainly due to the different seedlac and refining processes (Buch *et al.*, 2009). According to the material certificate of analysis (CoA) document (Appendix A), the Shellac RTH and WL are refined by the same refining process but originate from different seedlac materials, most likely contributing to the different flow viscosities. Moreover, Shellac AFS HS 700K and SSB 55 are refined from the same seedlac (Kushmi seedlac) and refining processes but different companies and manufacturing dates, giving rise to the MFI value of HS 700K being approximately half of that of SSB 55 MFI value. Shellac WL has the highest wax content. The phase change of the shellac material was not completed, the presence of non-melting wax perhaps restricts the flow of the material (Rudra Murthy and Gumtapure, 2020). MFI values can significantly affect the process applications the composite material may subsequently be used in and are taken into consideration as part of this study. For example, if injection moulding is selected as the processing technique used to produce a tablet, it may require higher back pressure to fill the material into the mould.

Table 4-2 Melt flow index of different types of raw shellac material at 90˚C (n=3).

Name	MFI value (g/10 min)	Std Err
AFS Shellac WL	2.98	0.001
Dewaxed Shellac AFS HS 700K	5.61	0.002
AFS Shellac RTH	9.45	0.001
SSB 55 Pharma FL	11.88	0.007

4.1.2.3 *Rheology*

Recently, the pharmaceutical industry has demonstrated great interest in the HME process (Tran, Lee and Tran, 2021)(Simões, Pinto and Simões, 2019). In this study, shellac was processed by HME technology to produce samples with good drug dispersion. Therefore, a good understanding of rheological properties is particularly important as it not only investigates the flow and deformation properties of a material in specific settings and conditions but also yields insight into the underlying molecular structure of the polymers by comparing their viscoelastic properties (D'Este, Alini and Eglin, 2012). Additionally, rheological analysis of shellac materials aids in the determination of the conditions of shellac processing (Gupta, Solanki and Serajuddin, 2016). In this study, steady-state parallel plate rheometry was performed on all four shellac samples. The rheological behaviour of a polymer material may be affected by many factors (Kalyon and Aktaş, 2014).

The first set of rheology tests performed were oscillatory time sweeps. This test directly provides the necessary information about material changes as a function of time. Before any subsequent rheological testing, it is important to identify that the material properties do not change during the test period at the constant test temperature, 90 °C in the case of this study. The oscillatory time sweep on shellac material shows that the material's storage modulus (G') remained at a steady value which indicates that the material's structure was not altered during the 900 s testing period at 90 °C.

When the polymer material is under a critical stain, its rheological properties remain at a steady-state value. That range is called the linear viscoelastic region (LVR) (Liptak, 2003)(Kaboorani and Blanchet, 2014). A strain sweep was used to determine the material's linear viscoelastic region (LVR). Figure 4-5 overlays the results of the amplitude sweep of each shellac material at 90 °C. Additionally, Table 4-3 illustrates the LVR of shellac materials at different temperatures. The test procedure could not be completed when the analysis was running at 60 °C, or even lower temperature, as the material was too viscous to flow, which exceeded the test range of the machine. Except for AFS Shellac RTH, all other types of shellac had a narrow LVR at low temperatures.

At a lower temperature, AFS Shellac RTH had a higher LVR range compared to the other three types of shellac, which is likely due to the existence of wax in the AFS Shellac RTH, acting as a plasticiser when it is not in a molten state (Douroumis, 2012). However, when the temperature increased to 80 °C, shellac SSB 55 Pharma had a wider LVR range, almost twice that of Dewaxed Shellac AFS HS 700K and AFS Shellac WL.

Table 4-3 The linear viscoelastic region (LVR) of raw shellacs at various temperatures (Onset point ± Std Err n=3).

Sample \ Temperature	60 °C (%)	70 °C (%)	80 °C (%)	90 °C (%)
AFS Shellac WL	N/A	0.2 ± 0.01	30.8 ± 0.8	78.9 ± 0.4
Dewaxed Shellac AFS HS 700K	N/A	0.1 ± 0.01	33.7 ± 0.6	82.6 ± 1.0
Shellac SSB 55 Pharma FL	N/A	0.1 ± 0.004	64.2 ± 1.6	85.5 ± 1.0
AFS Shellac RTH	N/A	15.3 ± 0.3	51.0 ± 0.2	68.4 ± 0.8

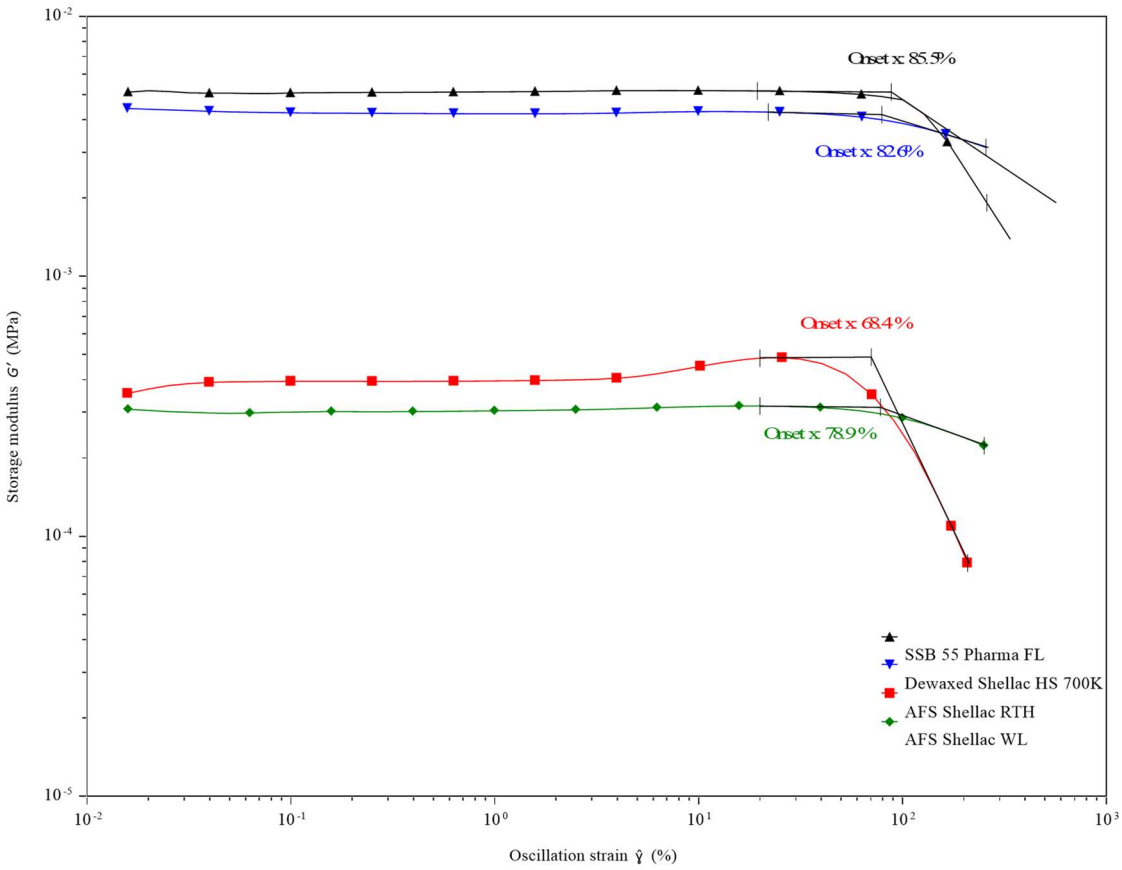

Figure 4-5 The storage modulus of various shellac materials versus oscillation strain (%) in amplitude sweep at 90 °C (The onset points of LVR) (n=3).

During melt extrusion, the materials undergo vigorous mixing under pressure and shear rate, which accelerates the dissolution of one component into the other in a drug/polymer mixed system. Therefore, it is necessary to ascertain the effect angular frequency would have on the viscosity of mixtures at a defined temperature (Solanki, Gupta and Serajuddin, 2018). As a result, oscillation frequency analysis is required to find out the effects of angular frequency on complex viscosities for each shellac at 70 °C. As shown in Figure 4-6, the viscosity was first determined at the given temperature at the angular frequency of 0.1 Hz, which was then increased gradually up to 100 Hz. As shown in Figure 4-6, the viscosity of shellac material in this study was found to follow a shear-thinning behaviour typical of many polymer responses. In all cases, with the increase in shear rate (indicative of processing speed) the viscosity of shellac decreased (Maru *et al.*, 2011). Moreover, AFS Shellac WL alone had the highest melt viscosity of all shellac types tested, which indicates the existence of wax,

directly affecting the viscosity of the shellac at a lower temperature. This result correlates well with results obtained using MFI analysis where AFS shellac WL has the lowest flow value. Furthermore, in all cases, there was a much sharper decrease in viscosity with the increase in angular frequency. The profound drop in viscosity for AFS Shellac WL may be attributed to the larger amount of wax initially present in the shellac (The actual wax content was analysed by the manufacturer see appendix section). The viscosity reduction in Dewaxed Shellac HS 700K is much higher than Shellac SSB 55 Pharma FL, which may be because of the different processing parameters used by different supplier companies and the earlier manufacture date.

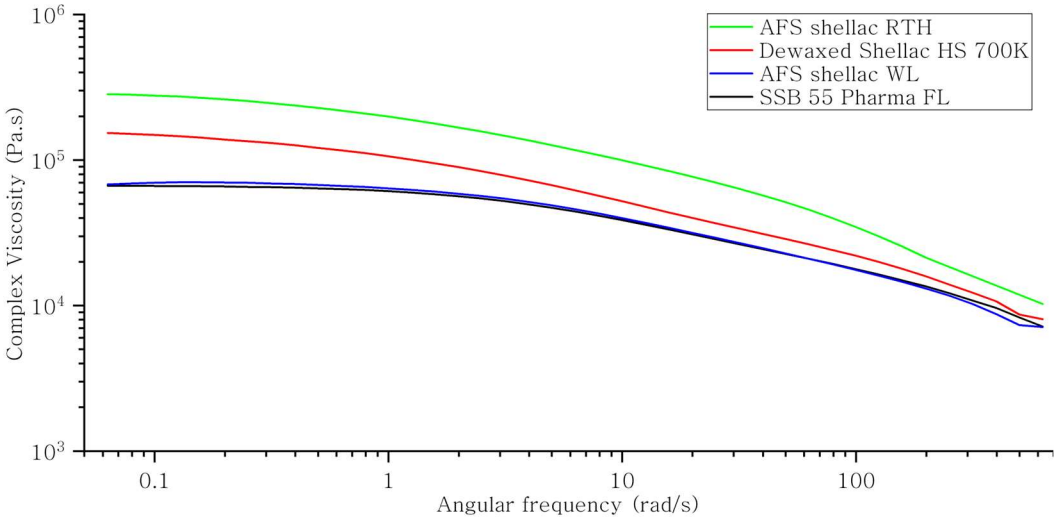

Figure 4-6 Complex viscosity versus frequency of various shellac in frequency sweep at 70 °C (n=3).

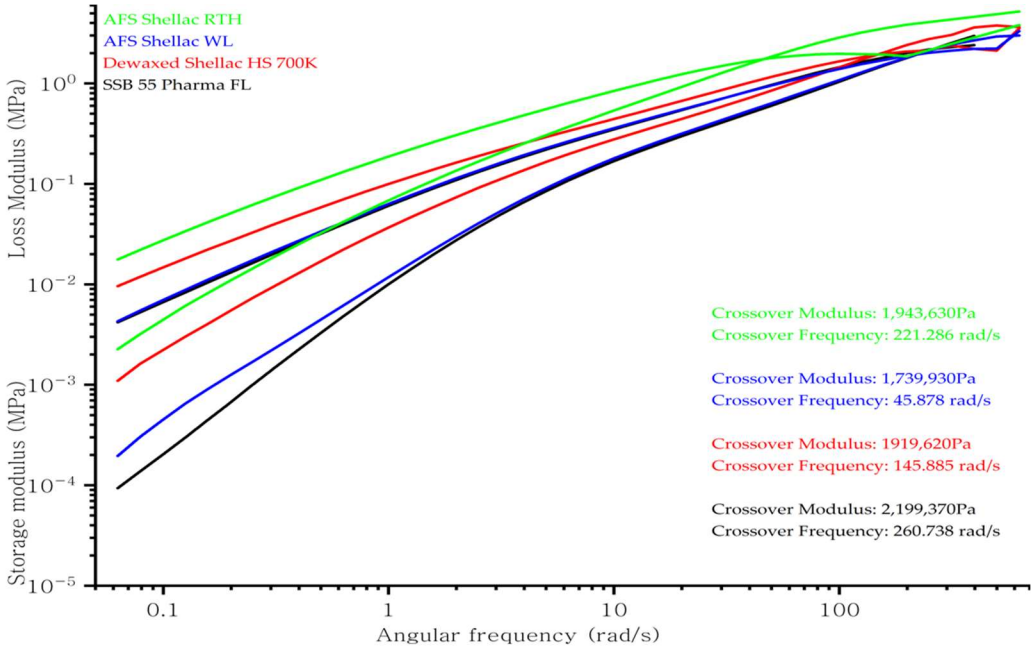

Figure 4-7 The storage modulus and loss modulus versus frequency of various shellac in frequency sweep at 70 °C (n=3).

Figure 4-7 illustrates the storage and loss modulus of the shellac in frequency sweep analysis at 70 °C. Typically, the molecular weight (MW) and the molecular weight distribution (MWD) of the material would affect the crossover point of the modulus in frequency sweep analysis. When the polymer has a higher MW, the crossover point will move to a lower frequency compared to a lower Mw. Alternatively, when the polymer has a narrower MWD, the crossover point would shift to higher modulus values (Coelho *et al.*, 2012). The result indicates that AFS Shellac WL may have a lower MW compared to other shellac materials assessed. Moreover, shellac SSB 55 Pharma FL may have the narrowest MWD (Aho *et al.*, 2015).

When using hot melt extrusion technology to process the polymer, the materials undergo a programmed temperature profile. As a result, it is necessary to determine what effect temperature has on the viscosity of mixtures across a range. Temperature ramp analysis investigates how increasing thermal energy affects the material's viscosity and the materials melt strength (Gupta *et al.*, 2014; Monteyne *et al.*, 2016). The results of the temperature ramp of four types of shellac at a constant strain and frequency are shown in

Figure 4-8. The viscosity was first determined at the given strain at the temperature of 65 °C, which was then increased gradually up to 110 °C with a heating rate of 3 °C/min. Figure 4-8 illustrates that all the shellac materials were sloped almost identically as a function of temperature at an angular frequency of 1 Hz. With the temperature increasing the viscosity of shellac decreases. Moreover, the AFS Shellac WL alone had the highest melt viscosity when compared to all other shellacs, which suggests that the wax affects the viscosity of the shellac. Additionally, in all cases, there was a much sharper decrease in viscosity with an increase in temperature. The profound drop in viscosity for AFS Shellac WL may be attributed to the larger amount of wax initially present in the shellac, as shown in Figure 4-9, the two melting peaks by DSC around 78˚C for both wax-containing shellacs, With these waxes melting gradually when the temperature increased, This experiment provided evidence that the viscosity of shellac SSB 55 pharma FL altered the least as the temperature changed.

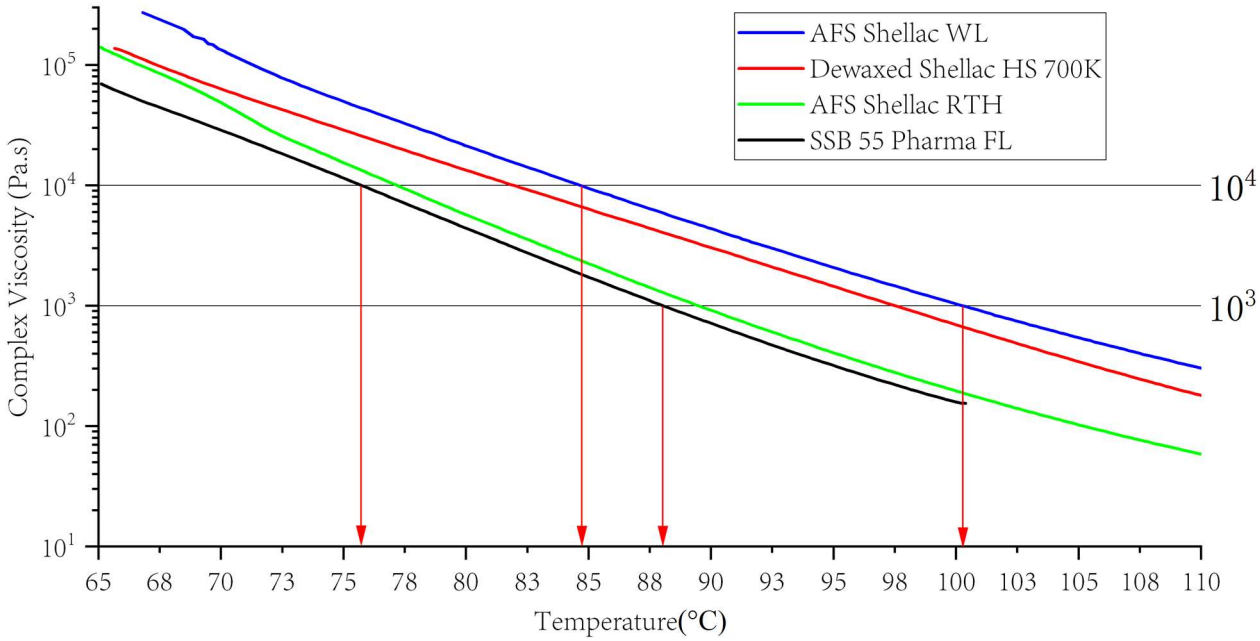

Figure 4-8 Viscosity versus temperature of various shellac (n=3).

From an earlier report by other researchers, the extrudable viscosity range for a polymer material was reported to be 1000 to 10,000 Pa*s (Gupta *et al.*, 2014). This range is determined by one simple rule: the viscosity of the polymer should be low enough for the

drug to dissolve in it and high enough for the extrusion process to occur. For AFS Shellac WL, Dewaxed Shellac AFS HS 700K, AFS Shellac RTH and shellac SSB 55 Pharma FL, the temperatures corresponding to the viscosity of 1000 to 10,000 Pa s were 85 to 100 °C, 82 to 97 °C, 77 to 89 °C and 75 to 87 °C, respectively; therefore, the extrudable temperature range for distinct types of shellac was different (Meena *et al.*, 2014). However, due to the existence of shear-thinning behaviours, each shellac material may be extruded at lower temperatures.

4.1.2.4 *Differential scanning calorimetry (DSC)*

Glass transition temperature (T_g) is one of the fundamental properties of the shellac material, it is essential in material processing and design, especially for the amorphous polymer (Austen Angell and Sivarajan, 2017). The glass transition is also known as the glass-liquid transition and it is the reversible process in an amorphous material, or semicrystalline material from the vitreous state into a rubbery state with increasing temperature, which means the polymer molecules start to become flexible (Baghel, Cathcart and O'Reilly, 2016). The heat capacity of the various shellac resins changes during the glass transition process and DSC is one useful method to determine the glass transition temperature. However, the transition does not occur at a specific temperature for a short time but over a temperature range as shown in Figure 4-9. The determination of glass transition temperature is mostly related to glasses or polymeric substances, in this study, the temperature in the middle of the sloped region is taken as T_g.

As mentioned above, differential scanning calorimetry can record data on the overall heat flow as a function of temperature (Duflot, Kitaeva and Duflot, 2015). The study of the thermal behaviour of shellac was carried out using DSC analysis. In matrix-assisted laser desorption/ionization (MALDI) measurements, shellac consists mostly of monomeric and oligomeric compounds, however, the glass transition still can be observed. While below its T_g value, shellac is a hard, brittle amorphous substance and above its T_g value shellac becomes soft and flowable thermoplastic (Buch *et al.*, 2009). As it can be seen in Table 4-4,

as well as Figure 4-9, all T_g values are in a range between 41°C and 52°C. All shellac grades showed relatively similar thermal behaviour, having a single glass transition temperature. The onset in the step of glass transition is perceptible. SSB 55 Pharma FL, based on Kushmi seedlac, has the lowest T_g (41.62°C). The T_g of Shellac AFS HS 700K, refined by the bleaching process and based on Kushmi seedlac, is at 44.75°C noticeably higher than SSB 55. Moreover, Buch et al. (2009) have confined that generally bleached shellac grades have the higher T_g than those of unbleached shellac grades (Buch *et al.*, 2009). Shellac RTH, refined by a melting process, based on an Indian seedlac has the T_g (46.48°C). Shellac AFS WL, based on light-coloured seedlac, as expected, yielded the highest T_g (48.44°C). This result corresponds well to the MFI test which is WL has the lowest MFI value. With the higher T_g value, shellac WL are harder to flow. Nonetheless, the two wax-containing shellac batches have a noticeable small melting peak around 76°C to 78°C. This melting peak may result in the shellac wax melting temperature, the existence of wax would cause a larger viscosity drop in rheology analysis. Similar findings were reported by Zheng et al. in 2011 where the wax was reported to have a melting of approx. 76/78°C (Zheng *et al.*, 2011).

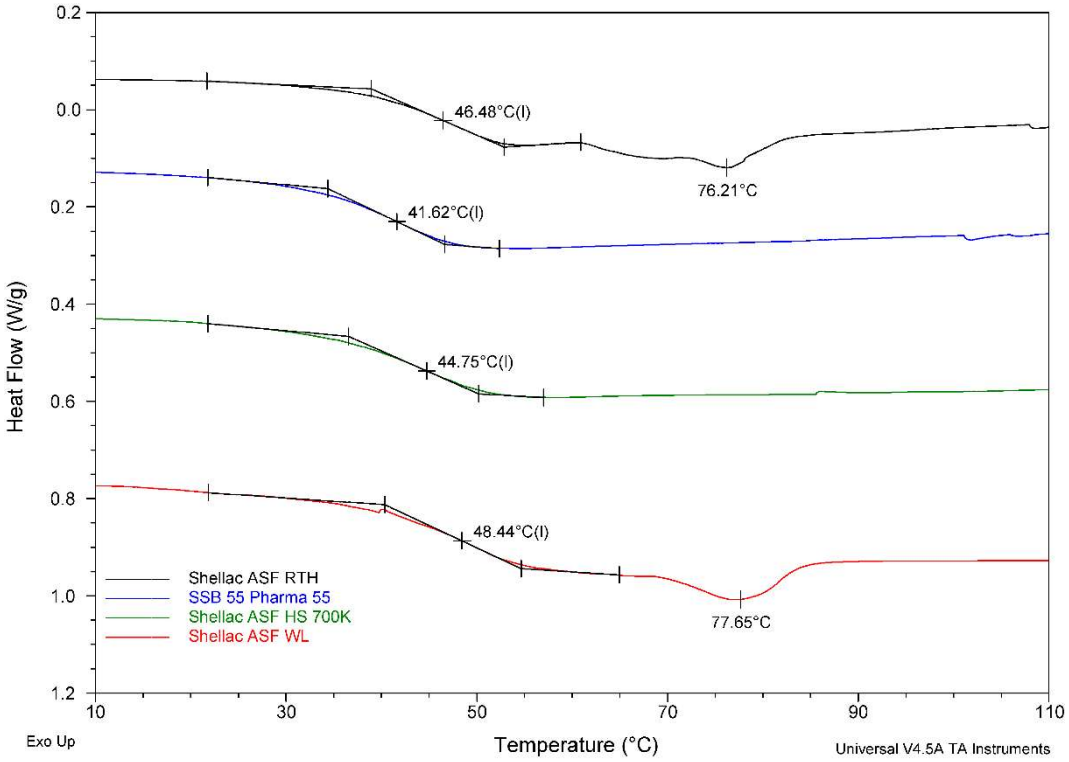

Figure 4-9 DSC thermograms of shellac samples with thermal history removed (n=3).

Table 4-4 Glass-transition temperatures and melting temperature of different shellac grades (n=2).

Material	T_g (°C) ± Std Err	T_m (°C) ± Std Err
SSB Pha 55	41.7±0.1	-
AFS Dewaxed HS 700K	44.6±0.1	-
AFS Shellac RTH	46.4±0.1	76.21±0.3
AFS shellac WL	48.2±0.2	77.65±0.2

The shellac materials investigated in this study are chosen as the matrix carrier for drug delivery systems. For this special application purpose, the selection of polymer systems with glass transition temperatures well above storage and release temperatures is advantageous, as glassy matrices often offer improved stability over rubbery matrices of similar composition (Hancock and Zografi, 1997). The samples in this work fulfil this design criterion and this is particularly important taking into consideration that interactions between the drug and polymer can have a plasticising effect and lower the T_g of such samples

(Maurice, 2015).

4.1.2.5 *Thermogravimetric analysis (TGA)*

In principle, all organic materials can be degraded by increasing temperature. Thermal Gravimetric Analysis (TGA) is a suitable technique for examining the thermal sensitivity of a polymer and the shellac materials were chosen as the matrix base in the DDS (Drug Delivery System) as well as the system being produced by HME. The material remains at an elevated temperature during the process. Given this, at the extrusion temperature, which is usually around, it must be stable or nondegradable. TGA is not designed for detailed information about cross-linking of the polymer chains or their possible inter-reactions, it provides at least an indication of the behaviour of the material that takes place upon heating. Therefore, the mass changes correspond to the increasing temperature (Kolter, Karl and Gryczke, 2012). The thermo-gravimetric analysis was carried out to determine the onset of the degradation temperature of the matrix material, shellac (Illustrated in Figure 4-10, Figure 4-11, Figure 4-12 and Figure 4-13). All the figures illustrate a similar degradation behaviour due to the same chemical structure of all shellac types, also confined by FTIR in section 4.1.3.1.

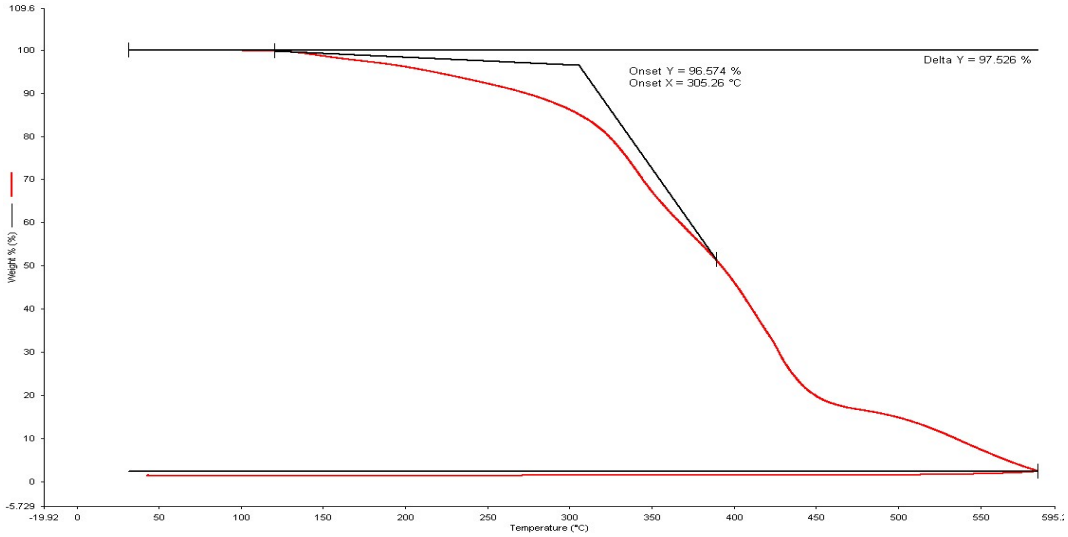

Figure 4-10 TGA of shellac SSB 55 Pharma FL.

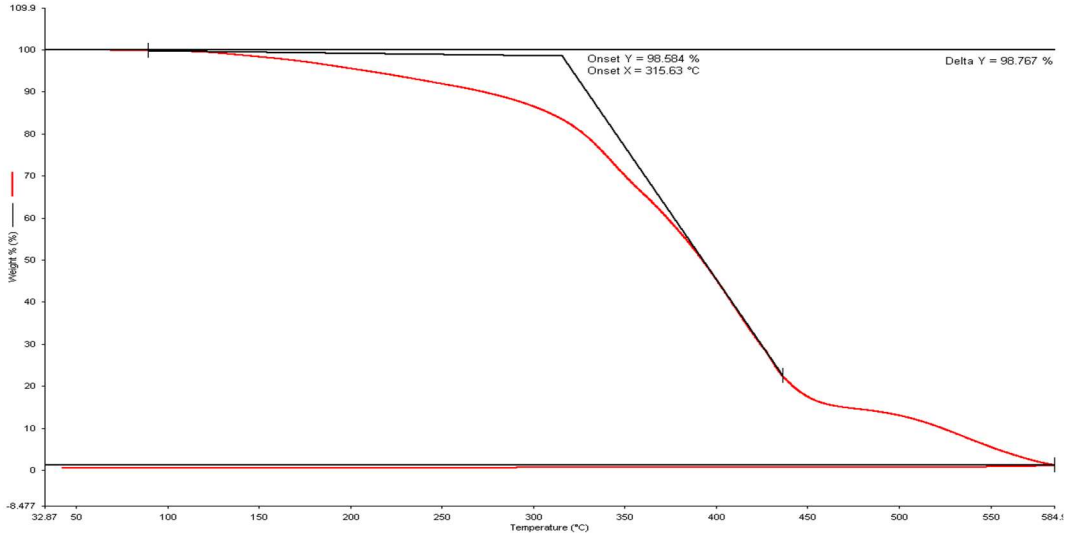

Figure 4-11 TGA of Dewaxed shellac AFS HS 700K.

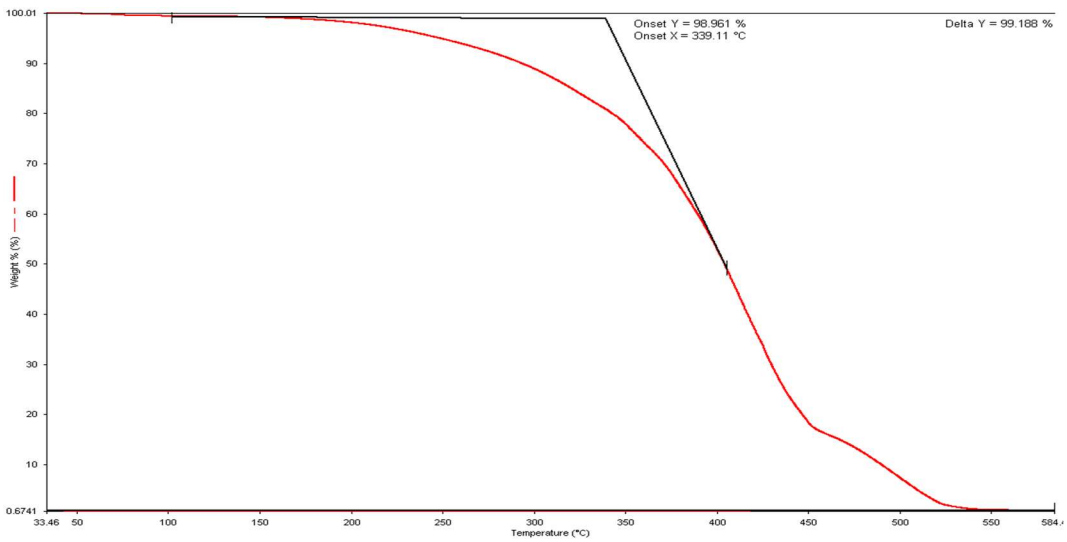

Figure 4-12 TGA of wax containing shellac AFS RTH.

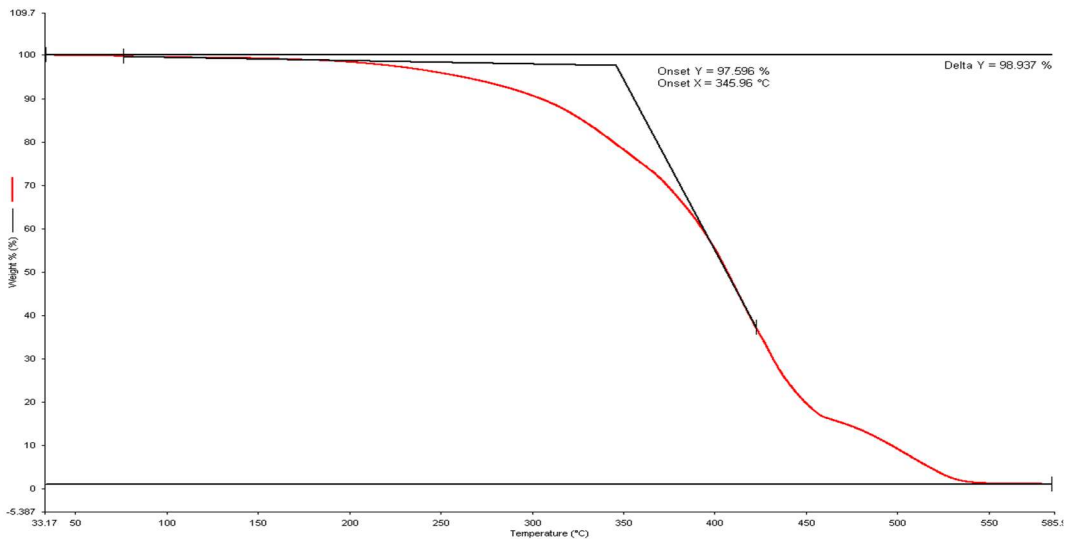

Figure 4-13 TGA of wax containing shellac AFS WL.

As seen in Table 4-5, the onset of the degradation temperature of SSB 55 has the lowest value starting at 305.26℃ as well as AFS HS 700K, RTH, WL giving 315.63 ℃, 339.11 ℃, 345.96℃ degradation temperatures respectively. Moreover, the percentage of the non-degradable material in shellac was also determined by the TGA test. On completion of each test, residual mass confirms the non-degradable material of shellac SSB 55, in which 97.526 wt.% had degraded, Shellac AFS HS 700K, in which 98.767 wt.% had degraded, Shellac AFS RTH, 99.188 wt.% and Shellac AFS WL, in which 98.937 wt.% had degraded. From

these results, it can be concluded that the wax containing Shellac AFS WL displayed better thermal stability than the others. This phenomenon may be explained by the existence of the wax within the shellac, which wax has a higher melting temperature and could improve the overall thermal stability of shellac material (Rudra Murthy and Gumtapure, 2020). Moreover, from the residual mass, it can be assumed that shellac material degraded completely.

Table 4-5 TGA of different types of Shellac (n=1)

Material	Degradation temperature (T_d°C)	The residue (%)
SSB 55	305.26	97.526
AFS HS 700K	315.63	98.767
AFS RTH	339.11	99.188
AFS WL	345.96	98.937

4.1.2.6 *SEM-EDS investigation of different shellac type*

In this study four samples of virgin shellac material were analysed to identify their surface morphology and structure; the structural characteristics of the material play a significant role in determining its properties (Srilalitha and Prasad, 2015)(Klonos *et al.*, 2018). Figure 4-14a-d shows the SEM images (in raw flake form) of the distinct types of shellac. All the SEM images of the shellac showed relatively uniform membrane surface and good homogeneity of polymer resin. Figure 4-14a and b are dewaxed sample material showing smooth surfaces, while the presence of white spots of different dimensions on the examined surface areas can contribute to dust grains occasionally deposited on the surface during the drying. Figure 4-14 c and d are wax-containing shellac materials; their surface morphology shows rough surface and micropore structure. This may be the result of different refining processes. These two shellacs are refined by a melting process, the elevated temperature may boil the shellac, causing a micropore structure due to the air bubbles (Walker and Steele, 1923).

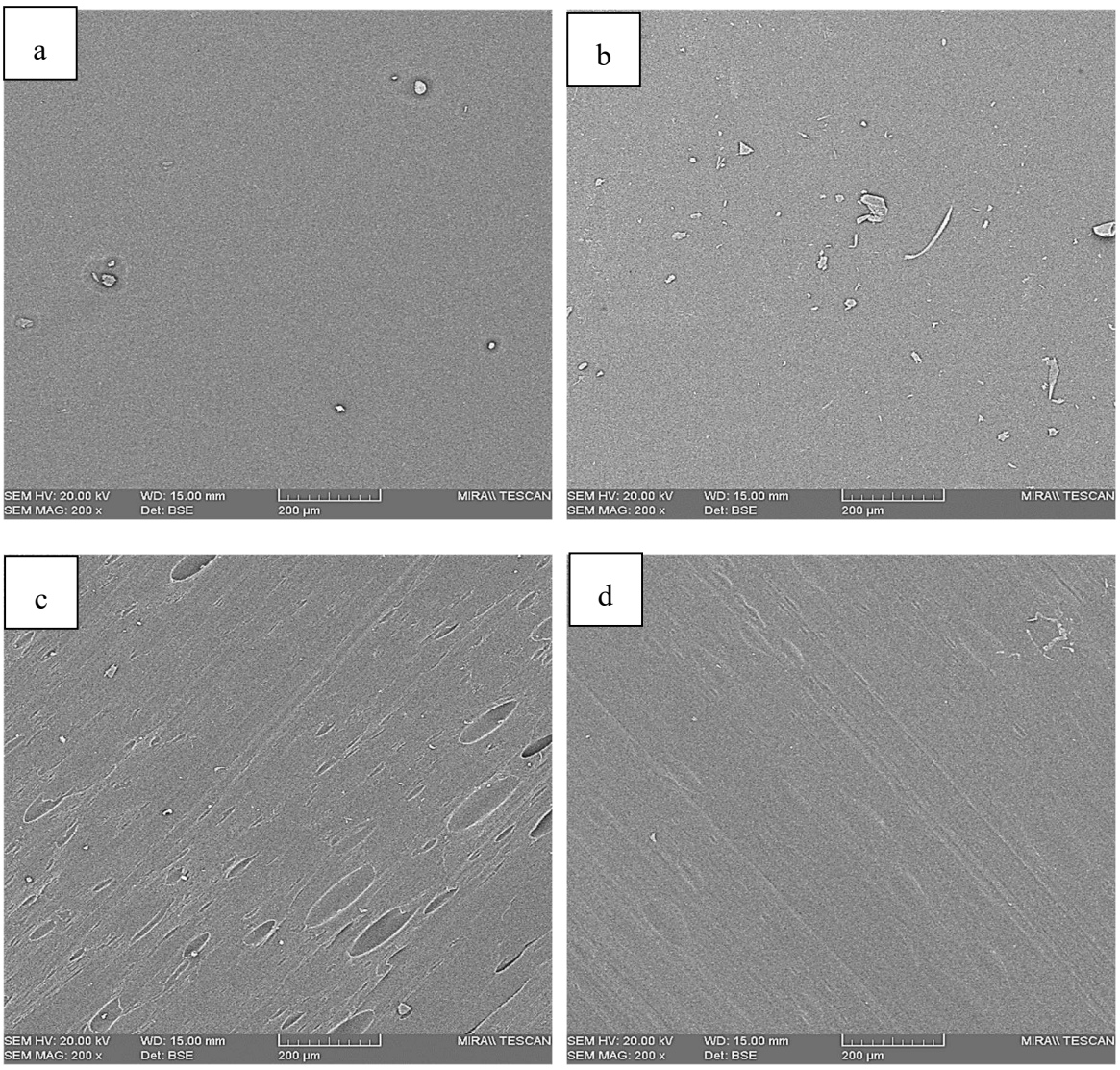

Figure 4-14 SEM image of four types of shellac at 200x for raw flake material, a) Shellac AFS HS 700K, b) Shellac SSB 55, c) Shellac AFS RTH, d) Shellac AFS WL. (Scale bar is at the bottom of the image)

EDS analysis performed on the surfaces of each type of shellac confirmed the expected elemental compositions. From the previous literature review and IR result, there is little to no chemical difference, all shellac types were expected to contain the same elements (Table 4-6). Gold (Au) detected in all types of shellac was due to the gold coating and all results were recalculated excluding the Au element. Moreover, from its chemical structure, C and O should be the only elements contained in the shellac (H is not detectable by EDS analysis). The EDS element analysis has confined this. Only carbon and oxygen were detected in the result.

Table 4-6 EDS elements analysis of four different types of shellac

Spectrum	C	O	Total
Shellac AFS HS 700K	77.69	22.31	100
AFS RTH	77.64	22.36	100
SSB 55	77.02	22.98	100
AFS WL	77.77	22.23	100

4.1.2.7 *Dissolution*

To use a spectrophotometer to record the shellac dissolution profile, the wavelength and absorption of 100% shellac concentrations were determined first. As shown in Figure 4-15, all types of shellac showed similar spectrum curves, again reinforcing that there is little to no chemical difference between each material which is further confirmed by FTIR and TGA results. The minute differences between shellac types were caused by different amounts of their various constituent ingredients and not by their bulk structure. All materials had a maximum UV absorption at 221 nm independent of shellac type. The standard calibration line of each shellac type was determined depending on the investigated batch. In this study, the investigation was focused on the raw material without any drug loading; spectrophotometric detection was a suitable method for recording the dissolution profiles. From previous literature reviews, shellac is a weak acid. The dissolution profiles were expected to be pH dependent. Furthermore, because the nature of shellac is the same, the pH dependence was applicable for all samples. With increasing pH value, the dissolution rate and the amount of dissolved shellac increased (Farag and Leopold, 2009).

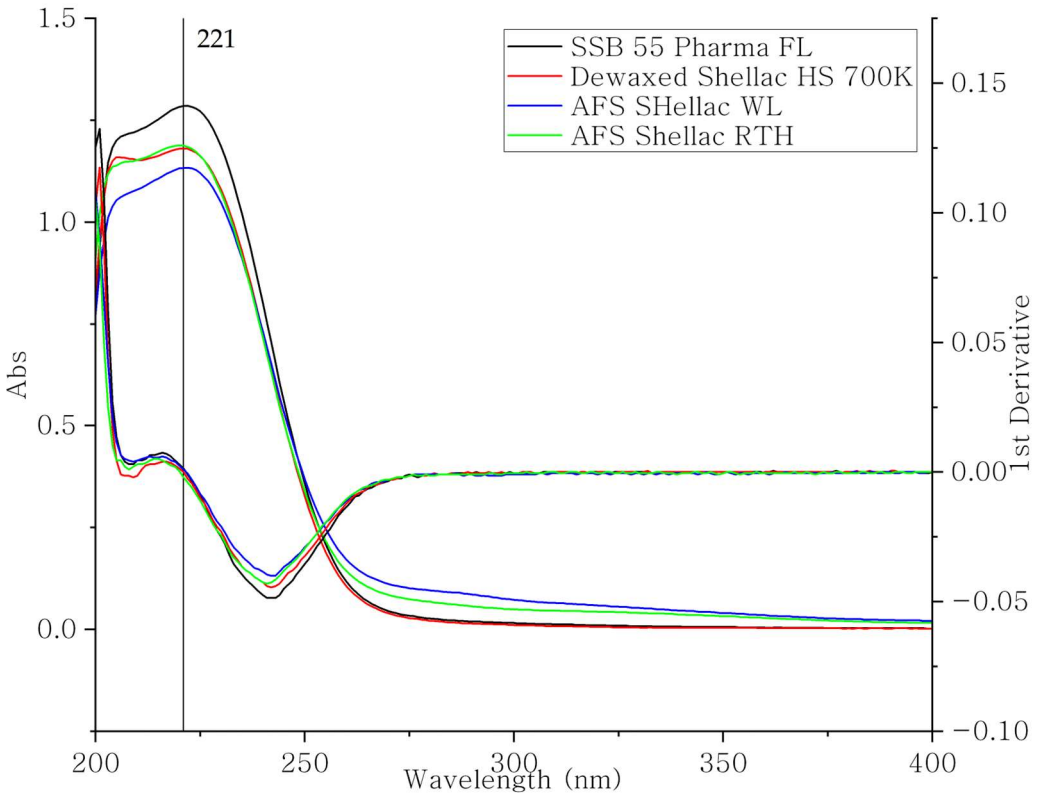

Figure 4-15 The UV spectrum and its 1st derivative curve of four different types of shellac (n=3).

The recorded dissolution profiles of shellac in different pH media shown in Figure 4-16. All types of shellac illustrated similar dissolution behaviours. At pH 1.2 no dissolution occurred. When the media changed to pH 7.4 PBS, the dissolution rate and the amount of dissolved shellac increased. From the dissolution curve, shellac SSB 55 Pharma FL had the highest dissolution rate compared to the others, which was expected, because of its lower T_g and acid value (Farag and Leopold, 2009; Yan *et al.*, 2021) . Moreover, as the dissolution process progressed, the dissolution rate decreased. Compared to the two wax-containing shellac types, dewaxed shellac had a higher dissolution rate, which is attributed to the wax being hydrophobic and slowing down dissolution in the solution (Phaechamud and Choncheewa, 2016). At pH 7.4, shellac SSB 55 Pharma Fl showed complete dissolution after 3.5 h, and Dewaxed Shellac HS 700K completely dissolved after 5.5 h. AFS Shellac RTH had the longest dissolution time, being completely dissolved after 9.5 h. However, at pH 7.4, all shellac materials dissolved completely.

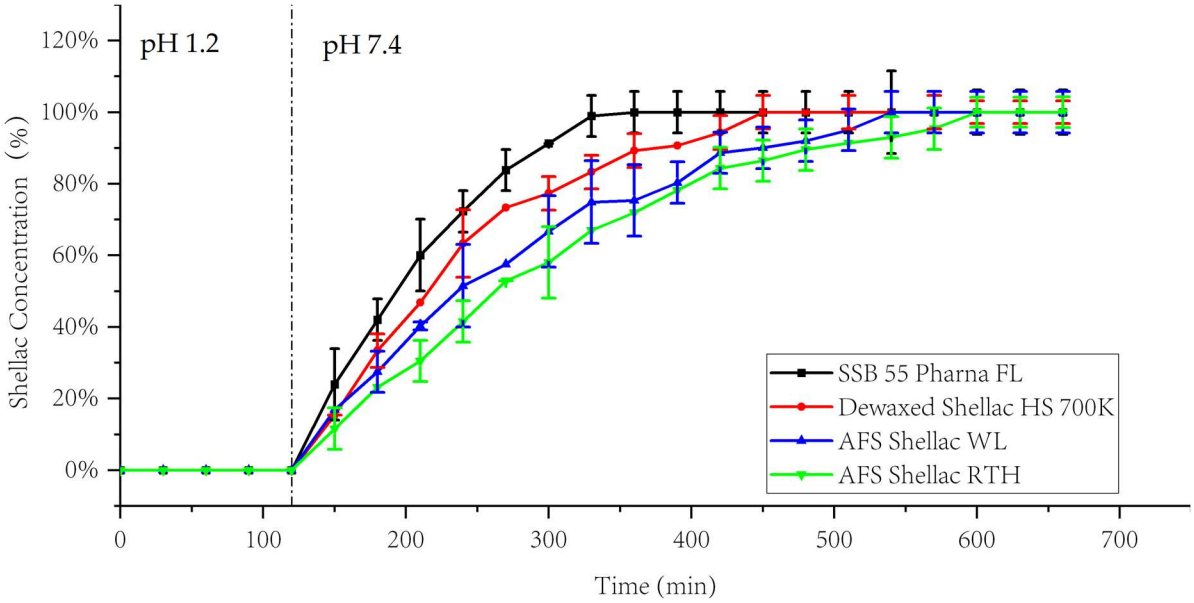

Figure 4-16 Dissolution profiles of the investigated shellac types at pH 1.2 and pH 7.4 (n=3, $p<0.05$).

4.1.3 **Summary**

This section explores the various types of shellac and investigates their physicochemical properties and processability as a potential matrix for enteric-targeted drug delivery systems. Physical, thermal, and rheological analysis of the shellac materials was conducted to support its application in hot melt extrusion as a potential drug delivery platform. All shellac materials were amorphous and had no difference in chemical structure by FTIR. From the DSC result, the glass transition temperature of the material was determined to be in the range of 41 °C and 49 °C. This means the temperature profile for the processing must be below 40 °C at the feeding zone and rise above the T_g of the material, along the extruder barrel to the die. Otherwise, the material would melt in the first conveying area, which is undesirable. Moreover, from the rheology analysis, all shellac materials exhibited shear thinning behaviour, which indicates that the processing temperature could be reduced at a higher screw speed. Additionally, compared to the other shellac materials, shellac SSB 55 Pharma has the lowest processing temperature, which indicates the highest processability. This study provides necessary data to determine the process conditions for the hot-melt extrusion process involving shellac material. The content of wax and ageing has a significant effect on the physical properties of shellac. However, the ageing behaviour of

shellac is based on the self-esterification of one compound of the natural resin: aleuritic acid. This difference can be observed by Gas chromatography-mass spectrometry technology. Consequently, in future studies, it is recommended to use GC-MS or HPLC/MS technology to identify the chemical content difference between the various types of shellac.

From this section, based on the physical and rheology analysis result, SSB 55 Pharma FL was the easiest processing material and has a faster dissolution rate compared to other shellac materials. However, dewaxed shellac AFS HS 700K also could be used as matrix material in the solid dispersion processing.

4.2 Drug formulation analysis

4.2.1 **Introduction**

Every year about 17.9 million people die from cardiovascular diseases (CVDs), it is the number one cause of death globally (Dinesen *et al.*, 2019). CVDs are a collective term for a series of diseases related to the heart and blood vessels which include coronary heart disease, cerebrovascular disease, rheumatic heart disease and other conditions. With the help of modern medical technology, scientists identified important risk factors for CVDs such as elevated low-density lipoprotein cholesterol (LDL-C) and reduced high-density lipoprotein cholesterol (HDL-C)(Hixson *et al.*, 2017)(Colin *et al.*, 2013). To manage dyslipidaemia, fenofibrate (FEB) has been widely used clinically (Liu *et al.*, 2014). It can reduce total cholesterol, LDL-C, apolipoprotein B, total triglycerides and triglyceride-rich lipoprotein(Chapman, 2003). However, it is a lipophilic compound which is practically insoluble in water but has high permeability (>90%) through a lipid membrane (Jamzad and Fassihi, 2006). As a result, FEB was classified as a class II (high permeability/low solubility) drug based on the biopharmaceutical classification system (BCS).

Poor solubility of a drug can result in poor absorption in the body even if it has high permeability. Because based on the drug absorption process, dissolution will be inhibited while the solubility limit is reached (Macheras, Karalis and Valsami, 2013) (Lachowicz *et al.*, 2016). ASDs could be processed either by a melting method or by a solvent method (Vilhelmsen, Eliasen and Schæfer, 2005)(Pokharkar *et al.*, 2006). Recently, more new techniques have been applied in the HME process to produce the drug's solid dispersion products. This is simply because compared with other processes, it is a continuous, economical, scalable and solvent-free process (Repka *et al.*, 2018).

Shellac is a purified form of a natural polymeric resin produced by the female insect, Laccifer lacca (Farag and Leopold, 2011)(Chauhan *et al.*, 1973). Shellac cannot dissolve in water because of the existence of a carboxyl group, the pKa value of shellac sits between 5.6-6.6. However, it can dissolve at higher pH values, usually above pH 7.2 (Limmatvapirat

et al., 2007). Moreover, because of these pH-sensitive properties, shellac is insoluble in the gastric fluid and low solubility in the intestinal fluid, renders it suitable for enteric delivery, especially colon target drug delivery (Ravi, Siddaramaiah and Pramod Kumar, 2008)(Ravi, Pramod Kumar and Siddaramaiah, 2008), but a novel application for pharma grade shellac for the preparation of monolithic matrices using hot melt extrusion was reported. (Gately and Kennedy, 2017).

In this section, amorphous solid dispersions were produced by the hot melt extrusion process. Fenofibrate was used as a model drug to study the possibility of shellac as the polymeric carrier and to enhance its solubility and dissolution in comparison to pure drugs. The physicochemical characterisation was performed by powder X-ray diffraction (PXRD), and differential scanning calorimetry (DSC). Stability tests, conducted for eight weeks, evaluated the maintenance of the amorphous form by considering DSC data. To investigate the effects of screw speed on the drug formulations, two process screw speeds were used in the production of samples.

4.2.2 **Results and Discussion**

4.2.2.1 *Fourier-transform infrared spectroscopy (FTIR)*

The FTIR spectra of the fenofibrate, Shellac SSB 55 Pharma FL and drug formulations are presented in Table 4-7 and Figure 4-17. The observed broader band shapes and less well-resolved peaks in the FTIR spectra of the fenofibrate solid dispersion formulation suggest the presence of amorphous fenofibrate (Heinz *et al.*, 2009). The fenofibrate FTIR spectra showed characteristic peaks at 1725cm^{-1} (indicating a C=O stretching of the ester group), 2985 and 2938cm^{-1} (represented the benzene ring; aromatic stretching), 1648 cm^{-1} (C=O of the ketone group), 1595cm^{-1} (lactone carbonyl functional group), 1505cm^{-1} (C----O stretching), 926cm^{-1} (C-C-H in-plane deformation), 853 and 765 and 1385cm^{-1} (C-O of ether group). Also, the presence of CH_2Cl group is indicated by a peak at 1285cm^{-1} (Gunasekaran, Renuga Devi and Sakthivel, 2008). Therefore, the FT-IR spectra confirm the purity of the fenofibrate. The sharp bands present at 1176, 1146, 1093, 1011, 974 and 924

cm^{-1} are suggested as C-H in-plane deformations. The sharp peaks observed at 851, 822, 762 and 740cm^{-1} in the FTIR spectrum is assigned to C-H out of plane deformation of fenofibrate.

FTIR spectra of the drug excipients mixture showed no interaction with the fenofibrate and prominent peaks of fenofibrate was not affected. There was neither shift nor disappearance of characteristic peaks suggesting that there is no interaction between fenofibrate and other excipients or no degradation in drug molecule. Hence, the drug and excipients compatibility were established. The model drug can be extruded with shellac material without changing the chemical structure of the fenofibrate.

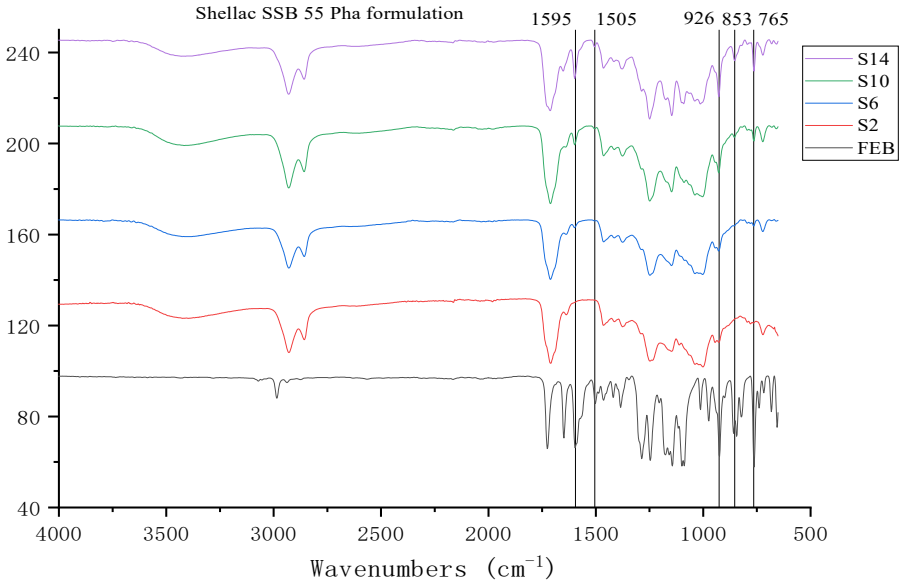

Figure 4-17 FTIR spectra of fenofibrate (FEB) and shellac SSB 55 Pharma FL base formulation

Table 4-7 FTIR band assignment of shellac material, fenofibrate and formulation

FTIR band assignment				
SSB 55	700K	Fenofibrate	Drug formulation	
3380.63	3418.22		3414.86	O-H stretching
		2985.14		benzene ring
2928.81	2928.32		2929.96	CH Stretching
2857.03	2856.71		2857.76	C–H stretching
1709.80	1709.98	1725.54	1711.91	C=O stretching
1637.00	1634.27	1648.88	1655.96	C=O stretching
		1596.31	1598.32	C=O stretching
		1502.57	1506.06	C----O stretching
1464.14	1464.44	1463.89	1465.33	C----O stretching
1413.69	1415.57	1419.07	1416.17	CH3 deformation
1374.86	1373.10	1384.45	1375.7	CH3 deformation
		1286.09	1286.88	CH2Cl stretching
1246.49	1247.32	1246.5	1249.71	C-O stretching
		1175.88	1172.91	C-C-H in plane deformation
1145.81	1148.29	1143.89	1146.23	O-H in plane deformation
		1115.94	1101.42	C-C-H in plane deformation
1110.89	1111.14	1098.95	1089.83	C-C-H in plane deformation
		1088.34	1066.43	C-C-H in plane deformation
1000.71	1002.15	1012.87	1014.02	C-C-H in plane deformation
944.32	944.00	974.3	927.41	C-C-H in plane deformation
		858.59	853.62	C-O stretching
779.61	780.26	763.26	763.61	C-H out of plane deformation
721.87	722.68		721.97	C-H out of plane deformation
		682.59	680.26	C=C bending
		655.53	661.47	O-H out of plane deformation

4.2.2.2 *Differential scanning calorimetry (DSC)*

In the thermal analysis (Figure 4-18), fenofibrate showed a sharp endotherm peak at 82.65 ± 0.27°C corresponding to its melting point with an associated enthalpy of 105.57±0.68J/g in the first heating cycle. There is no recrystallisation behaviour occurring during the cooling cycle in all raw fenofibrate samples, therefore, in the second heating cycle, the melting peak was absent. Moreover, a single Tg value for fenofibrate was found at -19.9°C. All the DSC data from the previous work in section 4.1, confirmed the amorphous nature of raw shellac material. In the second heating cycle, a transition was observed at the

40-50°C range, which corresponds to the Tg of the pure shellac polymer.

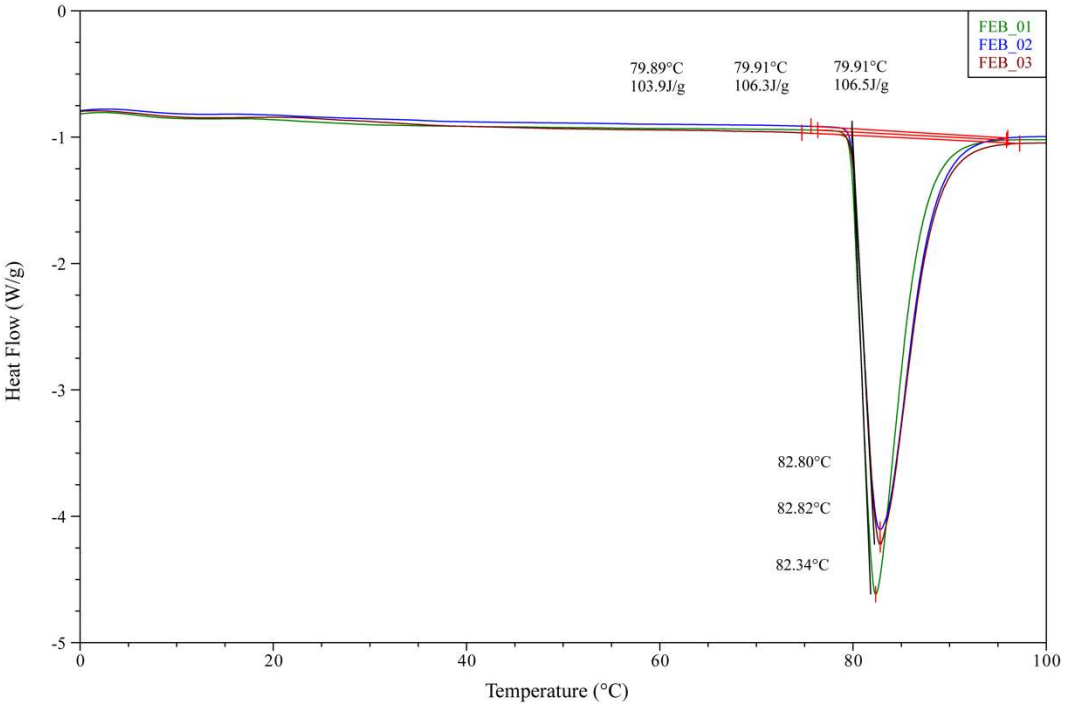

Figure 4-18. DSC thermograms of the original fenofibrate drug (First heating cycle, n=3).

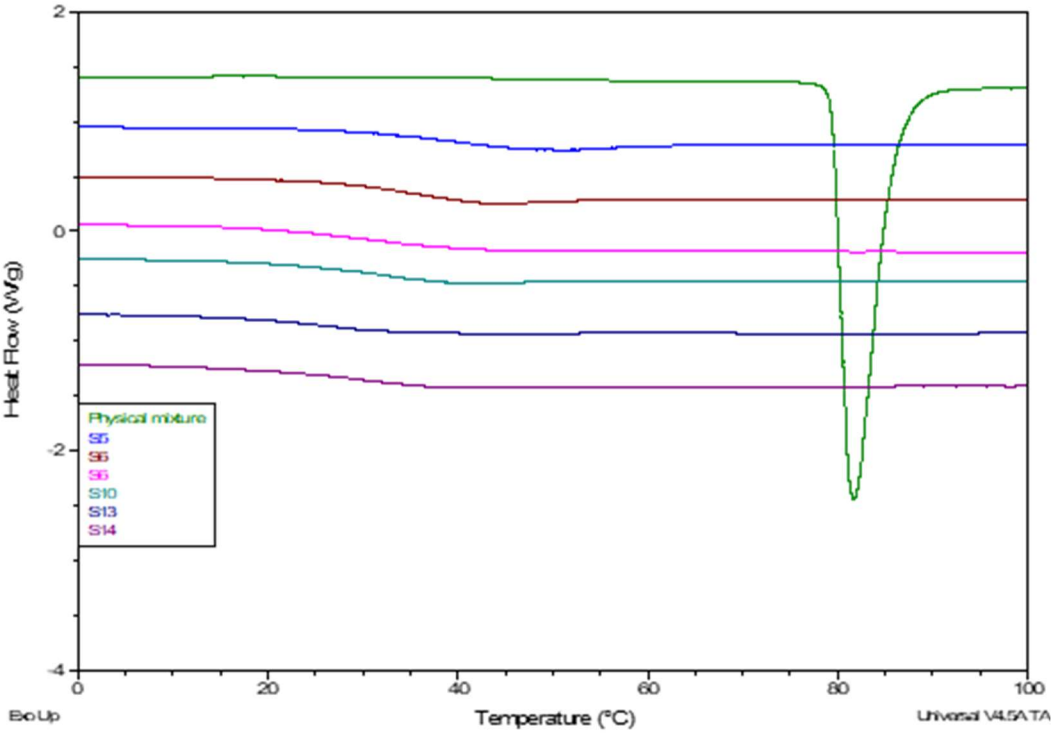

Figure 4-19. DSC thermograms of shellac formulation S5-S14 and the physical mixture of shellac SSB 55 Pharma FL and fenofibrate (First heating cycle, n=2).

The full temperature range DSC analysis showed only one single for the formulation (Data shown in Appendix C). Moreover, the thermogram of the formulation physical mixture based on shellac SSB 55 (20% drug loading) exhibited a sharp endotherm with a single melting point of around 82 °C as shown in Figure 4-19, which has a similar enthalpy compared to pure fenofibrate. While all the formulations with different drug loads from 5% to 20% showed no signs of crystallinity, indicating the successful formation of ASDs. Also, throughout each thermal curve, only one single T_g for all the drug formulations confirmed the molecular level dispersions of the drug in the polymer (Szafraniec-Szczęsny *et al.*, 2021b). Given that the drug and polymer have different T_g values, their resulting ASDs had different T_g values from the pure drug and polymer. According to the Gordon-Taylor equation, the resultant T_g depends on the T_g of individual components (Kallakunta *et al.*, 2020). The formulation T_g was dependent on drug load concentration, and a higher drug load resulted in a lower overall T_g because the drug's T_g was much lower (−19.9 °C) than that of the polymer (40–50 °C). This may be the reason T_g was lowered with increased drug plasticising effect.

4.2.2.3 *Powder X-Ray Diffraction*

In PXRD analysis (Figure 4-20), the crystalline molecule fenofibrate showed characteristic peaks at 14.34°,16.11°,16.57°, 19.09°, 20.73°, 22.11°, 24.57°, and 26.07°. Except for formulation S29, most of the prepared ASDs tested exhibited no characteristic peaks of fenofibrate, indicating the amorphous nature of ASDs. These results further support the DSC results and infer that the API-polymers were miscible at molecular levels. The reason for this amorphous nature may also be attributed to the amorphous nature of the polymer which prevents drug-drug interactions leading to recrystallisation. S29 was prepared with Dewaxed shellac AFS HS 700K using a low screw speed, there are some fenofibrate crystal characteristic peaks were found in the spectrum graph, which means a small amount of crystal structure detected in the formulation which cannot be detected by the DSC method. However, this small amount of fenofibrate crystals showed to become

amorphous when the processing screw speed increases because the higher screw speed would generate more shear and heat to the resulting extrudate, allowing it to form a completely amorphous and uniform formulation (Venkatesh *et al.*, 2021).

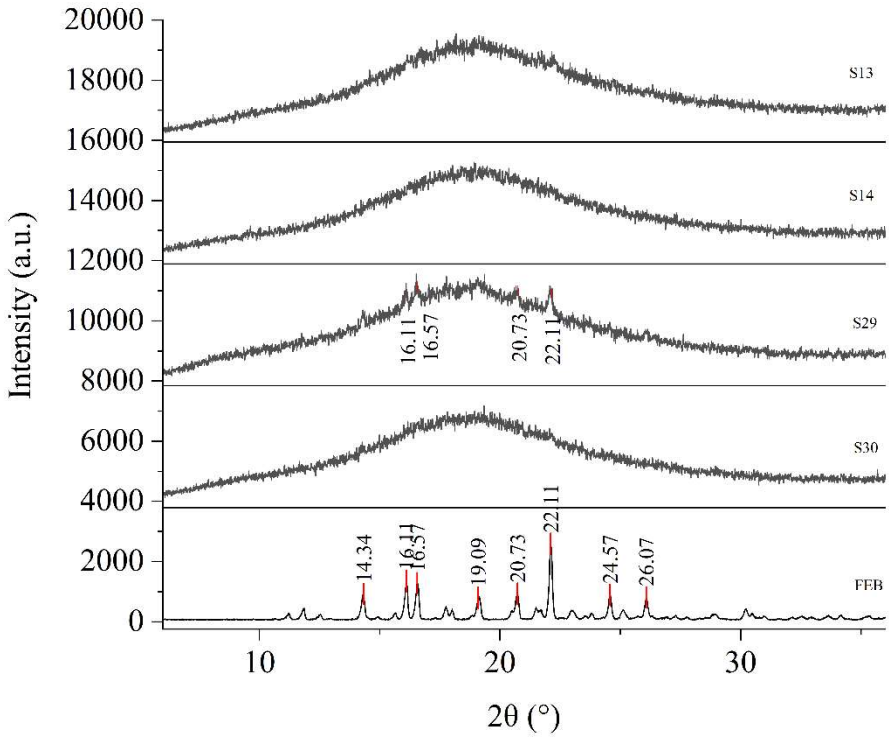

Figure 4-20 PXRD spectrum of formulation S13, S14, S29, S30 and virgin fenofibrate

4.2.2.4 *Dissolution study*

During the manufacture of amorphous solid dispersions using hot melt extrusion, the high shear forces and temperatures applied to the drug formulation system results in the drug being susceptible to degradation. Therefore, it is important to determine the effect of the extrusion step on the distribution and stability of the drug. The content of fenofibrate and its chemical purity was evaluated by HPLC before assessing the solubility of the dispersions. The fenofibrate chromatographs obtained from the extruded solid dispersions showed a single peak with a retention time equal to the standard solutions at 6.059 ± 0.04 min (As shown in Figure 4-21). The results corroborate the chemical integrity of the active ingredient after the thermal and mechanical treatment applied during processing (Pezzoli *et al.*, 2019).

The concentration of fenofibrate in the different drug formulations were quantified to evaluate the drug uniformity of content of the extrudates. The results are presented in Table 4-8 and these values obtained for the real content of fenofibrate were used for the calculation of the dissolution studies. The actual drug content is off from the designed drug content, this could be because of the melt processing, some of the drugs are not fully entering the processing section, they have adhered to the barrel wall. Moreover, the wearing of the screw profile is another reason. The self-wiping screw cannot fully mesh with each other.

From the material datasheet, fenofibrate is a lipophilic compound with a pKa of -4.9 and no ionizable group, this means the solubility of fenofibrate was not influenced by changes in medium pH (Jamzad and Fassihi, 2006). Due to the pH-sensitive properties of the carrier material shellac, the formulation is only dissolved in media with a pH above 7.2. Therefore, the dissolution behaviour of fenofibrate was evaluated in an alkaline (pH7.4) medium to simulate the environment in the colon.

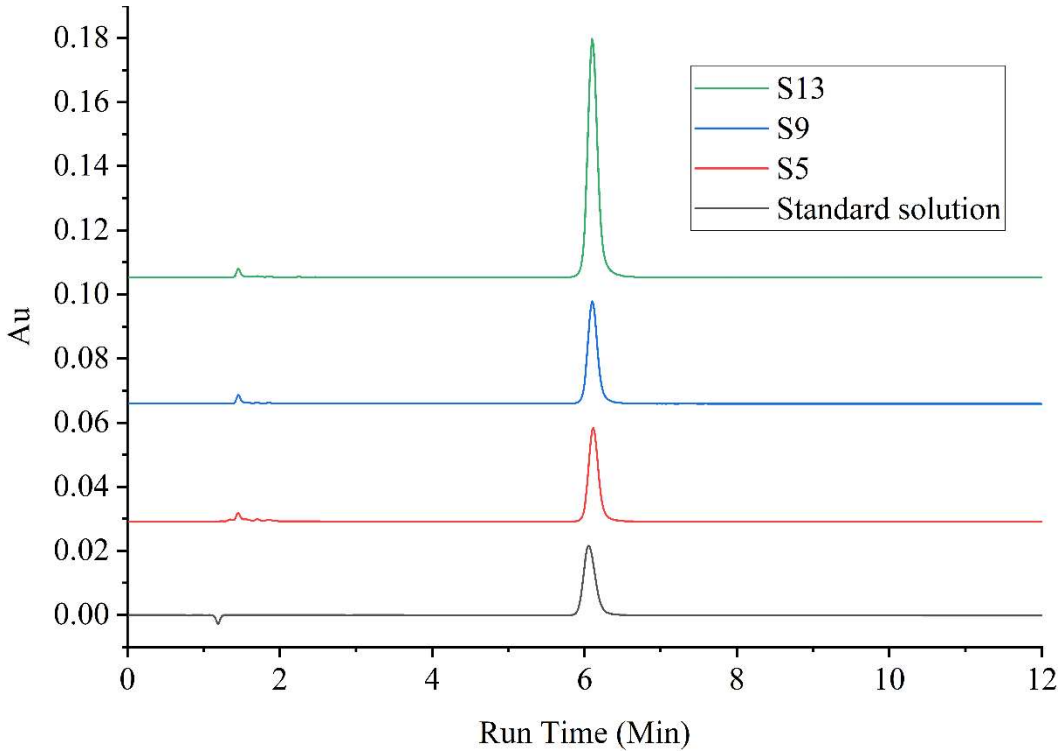

Figure 4-21 HPLC chromatograph of fenofibrate from the standard solution and extruded solid dispersions formulation (n=3).

Table 4-8 Uniformity of fenofibrate content of hot melt extruded solid dispersions (n=3).

Formulation	Real Drug Content (%) ±Std Err	Nominal (%)	Formulation	Real Drug Content (%) ±Std Err	Nominal (%)
s5	2.16±0.45	5	s37	2.21±0.64	5
s6	2.92±0.38	5	s38	3.33±0.13	5
s9	5.60±1.54	10	s41	6.02±0.52	10
s10	7.91±2.63	10	s42	7.58 ±2.97	10
s13	14.68±2.81	20	s45	10.45±6.47	20
s14	14.37±1.87	20	s46	14.37±1.83	20
s21	2.15±0.51	5	s53	2.22±1.12	5
s22	2.87±1.33	5	s54	3.53±0.33	5
s25	6.89±1.59	10	s57	5.87±0.84	10
s26	7.02±1.84	10	s58	6.57±2.11	10
s29	14.96±2.93	20	s61	11.13±6.25	20
s30	13.85±4.19	20	s62	13.48±4.41	20

The results of the dissolution studies of the fenofibrate-Shellac SSB 55 Pharma FL solid dispersions in pH 7.4 are shown in Figure 4-22. In general, the drug dispersions exhibited a significantly faster rate and higher drug dissolution compared to the physical mixture of fenofibrate. The physical mixture of fenofibrate does not dissolve in the dissolution media. Also, dispersions with a lower content of fenofibrate exhibited a faster and higher drug release which may be related to the low drug concentration. The formulation with higher drug loading presented a slightly slower dissolution rate (14.6% at 60 min) when compared with the lower drug loading formulation (46.4% at 60 min). After 180 min, the spring-parachute effect occurs, and precipitation of the drug from the dissolution solution was recorded for lower drug loading dispersions. This behaviour has been reported for other low solubility drug systems (Bavishi and Borkhataria, 2016)(Baghel, Cathcart and O'Reilly, 2016).

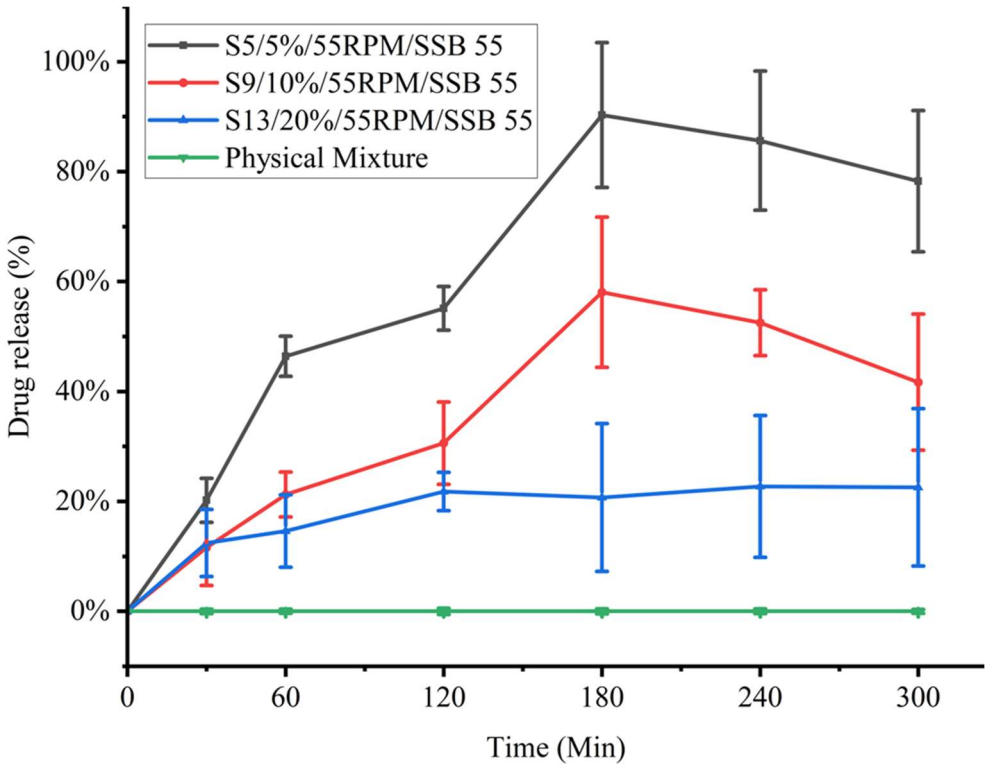

Figure 4-22 Dissolution profile of drug formulation with shellac SSB 55 Pharma FL in pH 7.4 phosphate buffer solution (n=3, $p<0.05$).

The increase in solubility of the formulation was attributed to the amorphous nature of the drug substance in the formulation. However, the pure amorphous state is not stable in solution, drug substance will precipitate and recrystallise rapidly. Nevertheless, the existence of a polymer matrix, even at very low concentrations, can be used to inhibit crystallisation from supersaturated solutions. The amorphous nature of fenofibrate in the drug formulation resulted in a higher and faster dissolution behaviour, however, the drug molecules are prone to aggregate and nucleate. Then the metastable amorphous drug would recrystallise to a more stable but less soluble form (Ilevbare, Marsac and Mitra, 2015)(Xavier, 2015)(Guzmán *et al.*, 2007). Moreover, because fenofibrate does not have any ionisable group, it is not ionised in the phosphate buffer solution, preferring the self-association and subsequent precipitation of the fenofibrate molecules (Jamzad and Fassihi, 2006)(Pezzoli *et al.*, 2019).

The dissolution behaviour of amorphous solid dispersion depends on the drug concentration and the polymeric carrier. Typically, for low drug loads, dissolution occurs

quickly, and a highly supersaturated solution is generated in which drug nano precipitates, in the amorphous or crystalline form, may coexist and be stabilised by the polymer. The dissolution mechanism is then controlled by the water-soluble carrier (Craig, 2002). A second scenario involves a slower dissolution due to higher drug loads resulting in a more sustained release. Water continuously penetrates the solid dispersion particles, mobility increases, and phase separation occurs. If on the surface of the undissolved particles the drug remains amorphous due to the stabilising effect of the polymer, the drug concentration in the media would be equal to the solubility of the amorphous drug (Huang and Dai, 2014).

To determine the effect of the screw speed, the dissolution profile of two formulations produced with the same type of shellac material but by different screw, speeds were shown in Figure 4-23. With increasing the screw speed, the S14 shows a higher dissolution rate (19.9% at 60min) than S13 (14.6 % at 60 min). However, the drug concentration quickly decreased due to the occurrence of the spring-parachute effect. Moreover, S13 shows more sustained release than formulation S14. As for samples S29 and S30 Figure 4-24, from the PXRD result, there is a lesser amount of drug crystal that exists in S29 and would form in an amorphous state when the processing speed increased. S30 also show a higher dissolution rate than S29 in the first 60min, which is similar to SSB 55 pharma Fl base formulation. However, after 120min these two samples have identical release profiles, meaning that the maximum solubility of the drug was reached in the dissolution solution, and the drug concentration in the media would be equal to the solubility of the amorphous drug (Huang and Dai, 2014).

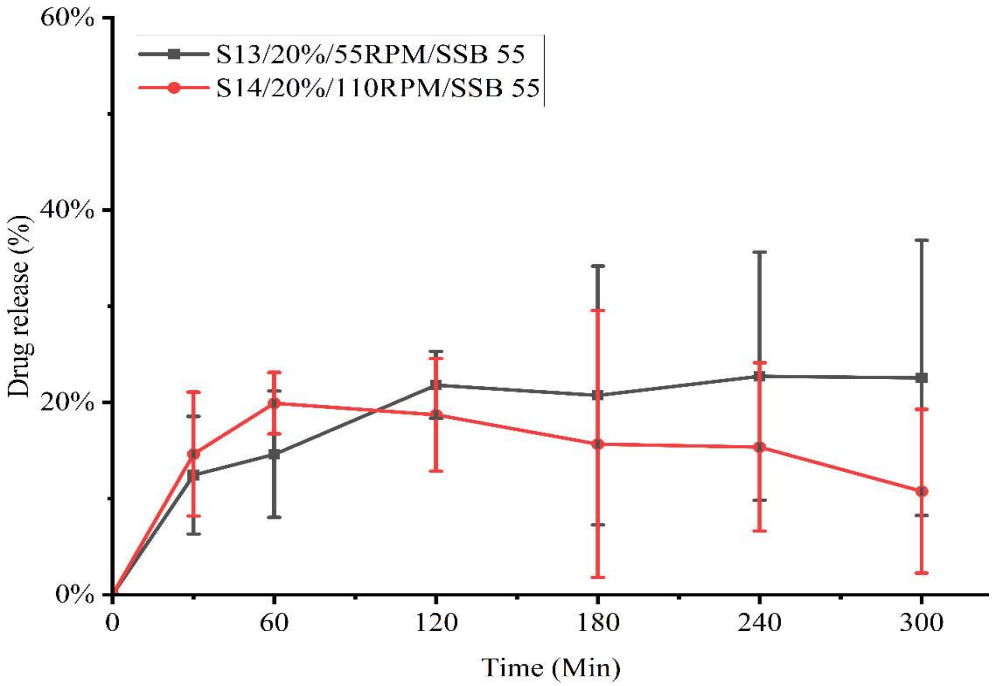

Figure 4-23 Dissolution profile of shellac SSB 55 Pharma FL drug formulation produced with different screw speeds in pH 7.4 phosphate buffer solution (n=3, $p<0.05$).

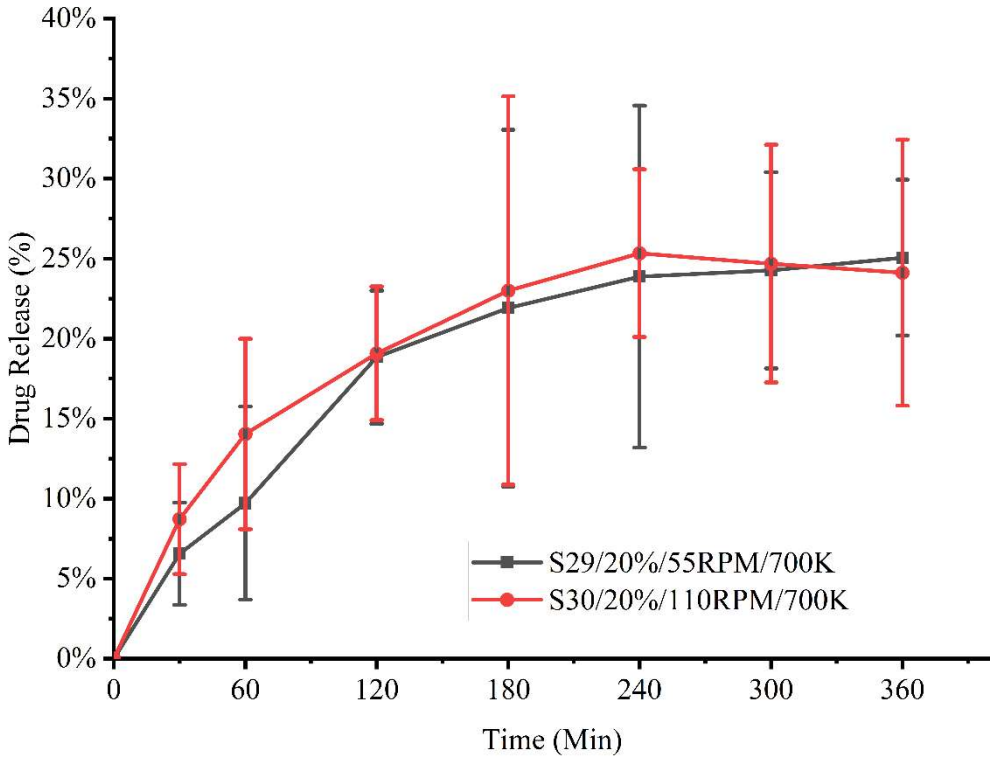

Figure 4-24 Dissolution profile of Dewaxed shellac AFS HS 700K drug formulation produced with different screw speeds in pH 7.4 phosphate buffer solution (n=3, $p<0.05$).

When compared to the formulation produced by a different type of shellac material Figure 4-25, At the first stage of 60min, formulation S13 shows a faster dissolution rate (14.6 % at 60 min) than sample S29 (9.7% at 60min), this is as expected, cause shellac SSB 55 pharma FL have a faster dissolution rate than Dewaxed shellac AFS HS 700K, as shown in section 4.1. after that the maximum solubility reached the drug concentration was equal to the solubility of an amorphous drug (Huang and Dai, 2014).

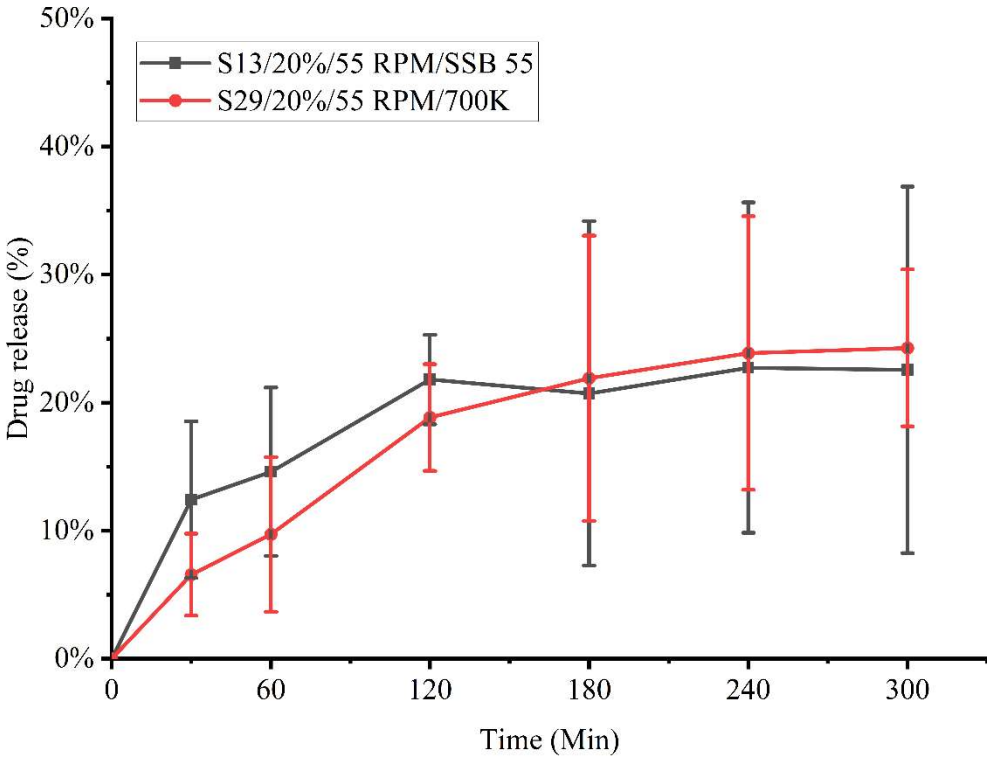

Figure 4-25 Dissolution profile of formulation produced with a different type of shellac (n=3, $p<0.05$)

The variability of the dissolution analysis confirmed that the uniformity of the extruded sample is varied. This is because the calculation is performed by a constant value of drug content, which means that if the tested extrudate is not uniform dispersed, the calculation result will vary. There may be many reasons for the variance, and one of the key factors is the screw design for the extrusion process to optimise the drug mixing and distribution in the matrix. The distinct types of screw elements on any extruder screw have divergent functions. In this study, a universal screw design was used in the processing, it has one single kneading block as a mixing zone, which consists of a 30º angle. This setup has more

conveying ability than mixing. A new optimized screw design is required for formulation production to enhance the mixing and distribution of the drug molecules in the matrix.

4.2.3 **Summary**

In this section, the formulation of fenofibrate as an amorphous solid dispersion with shellac by the hot melt extrusion process was investigated. This section of work demonstrates that additional processing aids were not necessary to increase the solubility of fenofibrate. Increased solubility of Fenofibrate can help to reduce the required dose and improve therapeutic outcomes, with the use of either shellac SSB 55 pharma FL or Dewaxed shellac AHS HS 700K. The improvement in the extent of solubility, as well as the rate of dissolution over that of fenofibrate, have been achieved. The amorphous solid dispersion formulation improved the solubility by over 8-times relative to untreated fenofibrate. The fenofibrate-shellac binary system provides a different approach from the traditional strategies and can be considered a convenient choice for optimizing the oral delivery of fenofibrate. Moreover, shellac base drug delivery system has an innate advantage due to its pH-sensitive nature and can be potentially used as a colon target delivery system. However, this section highlights the disadvantages of a universal screw configuration due to insufficient mixing of the kneading elements section. Based on the data it was found that the rug was poorly dispersed within the shellac matrix. There are several possible routes to enhance dispersion in this work it was decided to optimize the design of the mixing screw to enhance dispersion due to the shear sensitivity of Shellac and the requirements for pharmaceutical applications in terms of other additives which may enhance dispersion. Moreover, the dissolution profiles were identical when the maximum solubility of the drug in the aqueous solution was reached. One potential solution to increase the maximum solubility in the aqueous solution is to add a surfactant (Sodium Dodecyl Sulfate (SDS)) into the dissolution media.

4.3 Screw design and simulation

4.3.1 **Introduction**

Modular mesh co-rotating twin-screw extruders are widely used in modern processing technology because of their excellent mixing performance and the flexible combination of screw elements (Bouvier and Campanella, 2014)(do Val Siqueira *et al.*, 2021). For a specific mixing process, it is essential to find the best combination of screw elements, however, in practice, performing screw combination tests is a very time-consuming and labour-intensive process (Pandey and Maia, 2021). The entire process is very arduous, including screw assembly, extruder preheating, extruder operation, experimental data measurement, residual material cleaning, shutdown to screw disassembly and reassembly. Furthermore, a high degree of precision is required in the assembly of the screw, and repeated attempts are often required to adjust the centreline distance, to ensure that the two screws do not interfere with each other and to avoid hard sweeping. Therefore, most of the experimental findings in the literature on twin-screw extrusion are based on limited experimental data and a small range of process conditions (Zhu and Jaluria, 2001)(Hyvärinen, Jabeen and Kärki, 2020). In this respect, the use of numerical simulations is highly advantageous.

While previous studies on the extrusion performance of conveying screw elements are relatively consistent, there is a wide range of opinions on the extrusion performance of meshing block elements (conveying element, backwards-conveying element, kneading element, etc.) Some researchers have summarized the conveying or compounding properties of various screw elements without clarifying the prerequisites for their conclusions. Manas-Zloczower has shown that for a unit length of a kneading block element, the dispersion and mixing capacity increases and the distribution and mixing capacity decreases when the misalignment angle is constant and the thickness of the kneading block disc's increases (Manas-Zloczower, 2012). Ishikawa's study shows that the dispersion and mixing capacity of a smaller, thicker kneading disc with a larger misalignment angle has a better dispersion and mixing capacity (Ishikawa, Kihara and Funatsu, 2000). In 2001, Chen Zhiqiang et al.

reported on studying the influence of the kneading block element configuration on the co-rotating twin screw extruders that when the thickness of the kneading disk is small, the conveying ability is strong, the distributive mixing performance is better, but the dispersing and mixing ability is poor. Both the distributive mixing ability and the dispersing mixing ability are better than the forward kneading disc (Chen Zhiqiang, Chunfen and Wwang Yi, 2001).

The experimental study by Shearer et al concluded that when the thickness of the kneading disc is constant the order of local distributed mixing performance is forward kneading disc > neutral kneading disc > reverse kneading disc. In terms of overall distributed mixing performance, the mixing capacity of the kneading block components varies with the process conditions (Shearer and Tzoganakis, 2001). In the experimental results in the previous section 4.2, it was found that the uniformity of content of Fenofibrate in the extrudate formulations varied greatly, which is because the mixing area of the screw is only configured by the 30° kneading disc. Therefore, this section examines the conveying element and kneading block elements and simulates the transient flow field after the combination of kneading block elements with different staggered angles and thread block elements in the combined meshing co-rotating twin-screw extruder Prism 16. The kneading block elements and their melt transport characteristics, extrusion stability and transient mixing characteristics in the combined screw are comprehensively analysed and discussed. Furthermore, an actual mixing section was built based on the simulations and analysed, and the mixing performance and transition flow field were evaluated.

4.3.2 **Result and discussion**

4.3.2.1 *Screw conveying capacity*

Figure 4-26 shows the natural flow rate through each combination of screws configuration at zero differential pressure. For the positive conveying screw element, the conveying capacity is stronger, while the screw speed increases. However, the kneading elements with a 30º stagger angle have a larger conveying capacity than other screw

combinations which means this screw setup can transport material rather than mix materials. Furthermore, since the flow resistance of the kneading element with 90º stagger is very large, a reverse flow is formed, and the volume flow rate of this combination for each time step is a negative value, as a result, it is not shown in the figure.

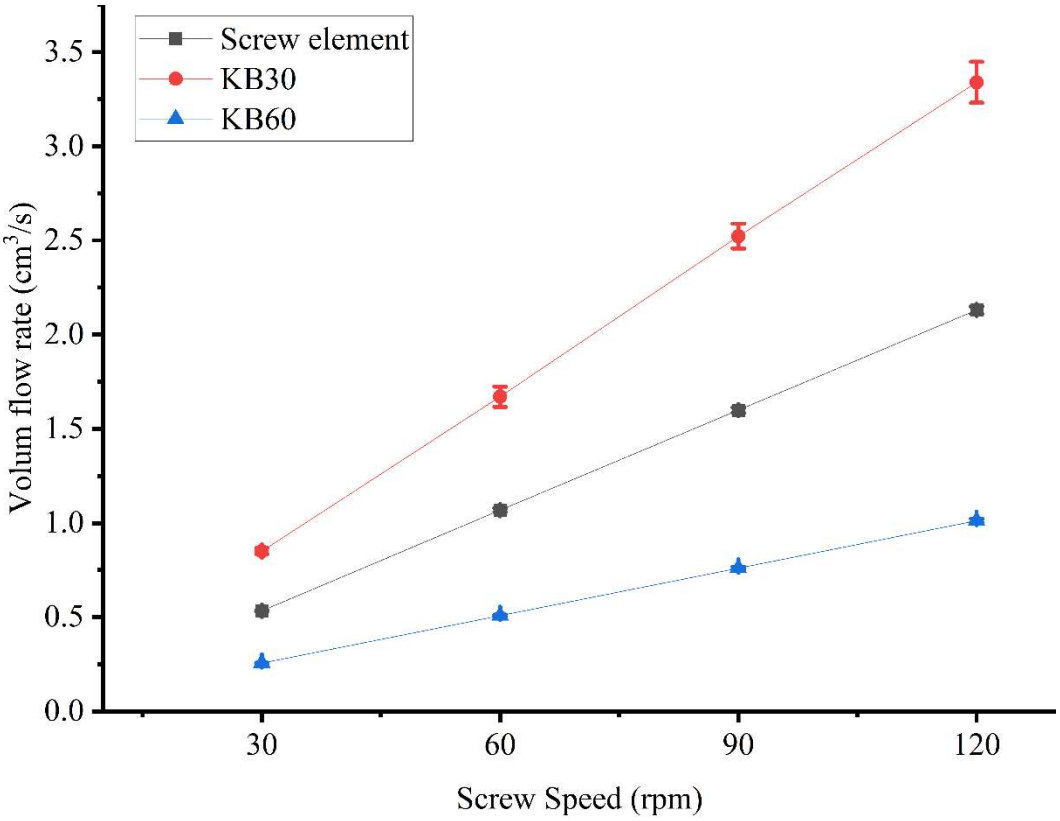

Figure 4-26 Natural flow rate through each combination of screws configuration at zero differential pressure.

4.3.2.2 *Screw speed and pressure distribution*

Figure 4-27 are the pressure and viscosity field distributions of the screw element calculated when the inlet and outlet pressure difference, grid, material characteristic parameters, and model geometric size remain constant, but screw speed changes.

In the pressure distribution diagram, distinct colours represent different pressure values, blue represents low pressure, red represents high pressure, and the colour from blue to red represents increasing pressure. Figure 4-27 shows that under four groups of different screw speed conditions, the colour cloud diagram of the pressure in the flow field is almost consistent, that is, the difference between the pressure at each position in the flow field and the pressure at the inlet and outlet section is unchanged. The pressure value of each point in the flow field is determined by the pressure difference between the outlet section and the inlet section; When the inlet and outlet pressure difference is a fixed value, no matter how screw speed changes, the pressure colour cloud diagram is certain, that is, the relative value of pressure at each point in the flow field will not change.

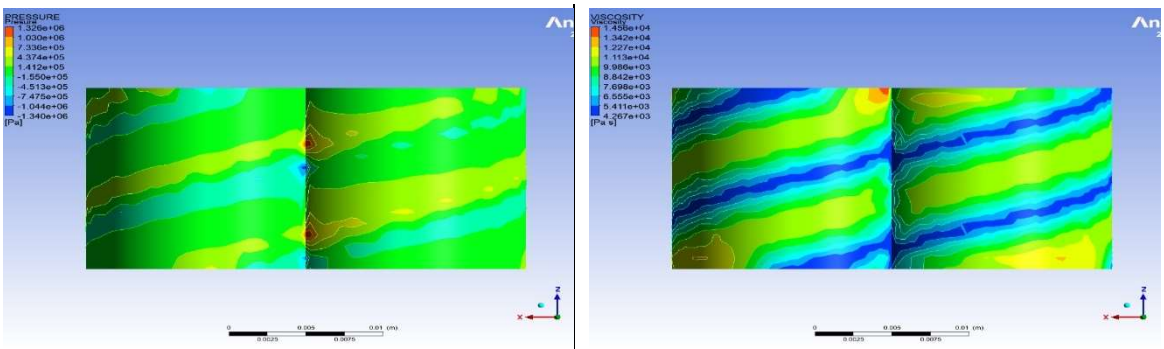

30RPM 30RPM

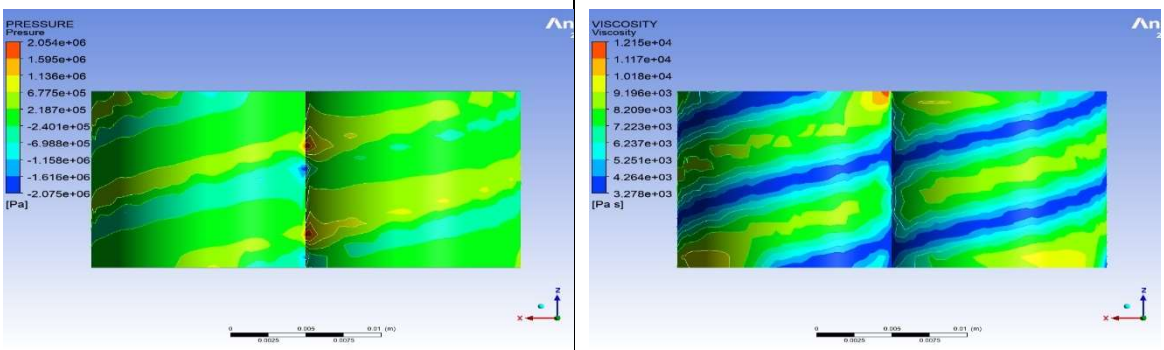

60RPM 60RPM

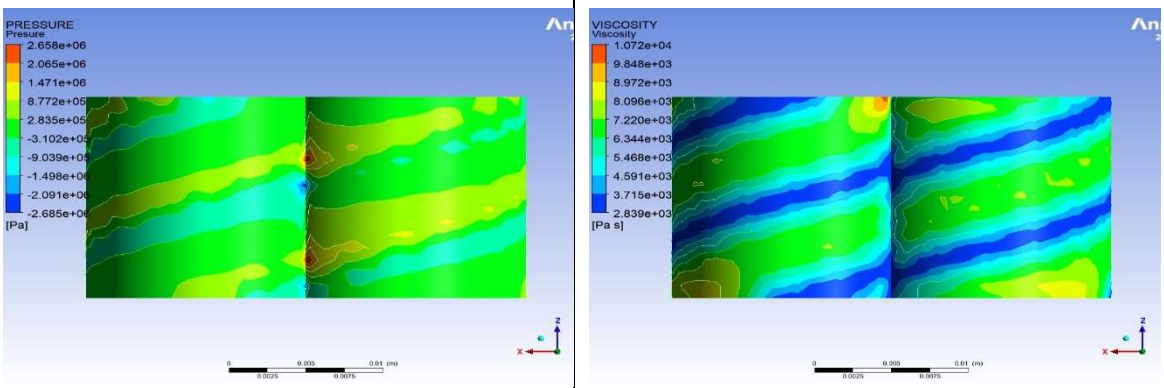

90RPM 90RPM

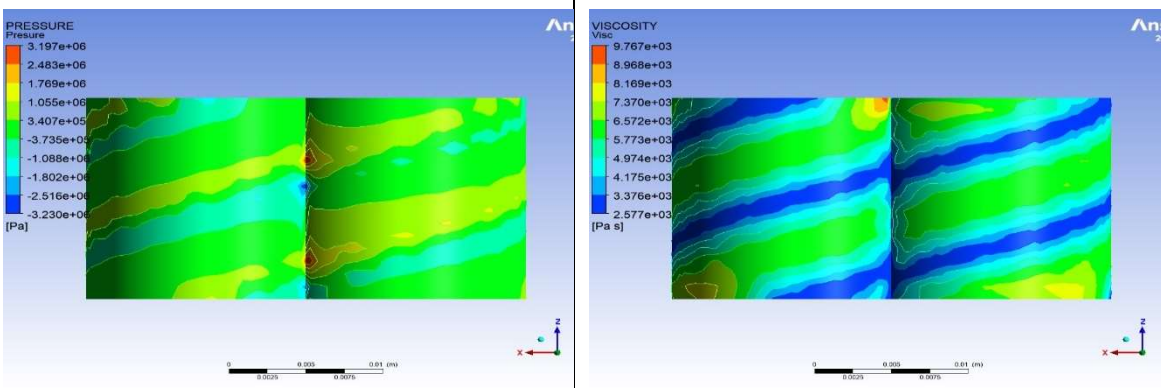

120RPM 120RPM

A (Pressure distribution) B (Viscosity distribution)

Figure 4-27 Pressure and viscosity field distributions of the screw element at various speeds.

Since the formulas of viscosity η and shear stress τ are η =mγ and τ=mγ, the viscosity η decreases with the increase of shear rate γ, and shear stress increases with the increase of shear rate γ (Mezger, 2012). The shear condition of the material can be found by viscosity distribution in the flow channel. In the viscosity distribution diagram, distinct colours represent different viscosity values, blue represents low viscosity, the shear stress of materials in this section is large, this area is a high shear area, red represents high viscosity, the shear stress of materials in this section is small, and this area is a low shear area. From the figure, under four groups of different screw speed conditions, the colour cloud diagram of viscosity distribution in the flow field is quite close. Considering the calculation error (converged error 0.01%), it can be considered that the viscosity distribution in the flow channel is consistent in these four cases. That is, the viscosity value at each position in the flow field is certain. It can be concluded that the viscosity of each point in the flow field is determined by the pressure difference between the outlet and the inlet; When the pressure difference between the inlet and outlet is a fixed value, no matter how the pressure at both ends changes, the viscosity distribution nephogram does not change, that is, the viscosity field is only related to the pressure difference between the inlet and outlet, and has nothing to do with the algebraic value of the end face pressure at the inlet and outlet.

4.3.2.3 *Screw speed and velocity distribution*

The velocity field of the calculated partial velocity V_x is shown in Figure 4-28a. It can be seen from the V_x distribution diagram that the velocity distribution on the screw surface conforms to the distribution law of $V_x = \omega * y$. due to the small value of Y in the meshing area, the material velocity V_x in the meshing area is smaller than in other areas.

The velocity field of the calculated partial velocity V_y is shown in Figure 4-28b. It can be seen from the V_y distribution diagram the value of V_y in the meshing area is relatively large than in other areas, and the velocity of V_y of the left and right screws is very large, which has a certain impact on the V_y value of materials in the whole flow channel.

The velocity field of the calculated partial velocity V_z is shown in Figure 4-28c. The distribution of V_z determines the flow rate. The production capacity of the twin-screw extruder can be obtained by analysing V_z. It can be seen from the V_z distribution diagram that the axial speed of the material sandwiched between the screw edges is large, while the axial speed of the material in contact with the barrel and screw surface is zero this is because of the boundary condition setting. All the material contact to the out surface is zero velocity.

The distribution of the synthetic velocity field in the channel of the screw element is shown in Figure 4-28d. In the figure, blue represents low speed, red represents high speed, and the colour changes from blue to red representing that the speed gradually increases. It can be seen from the figure that the material speed at the barrel is zero and the speed on the top surface of the screw element is high. The synthesis speed at the bottom of the screw is lower than that at the top of the screw.

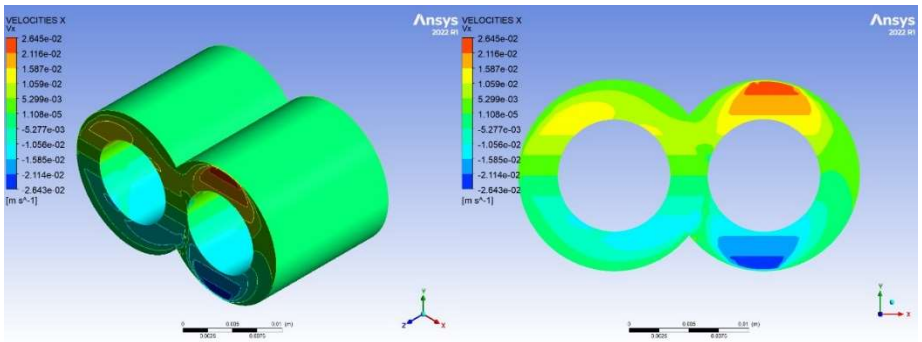

a

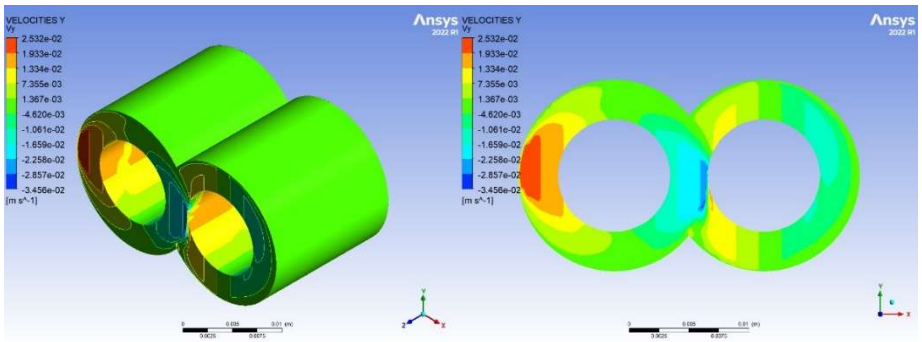

b

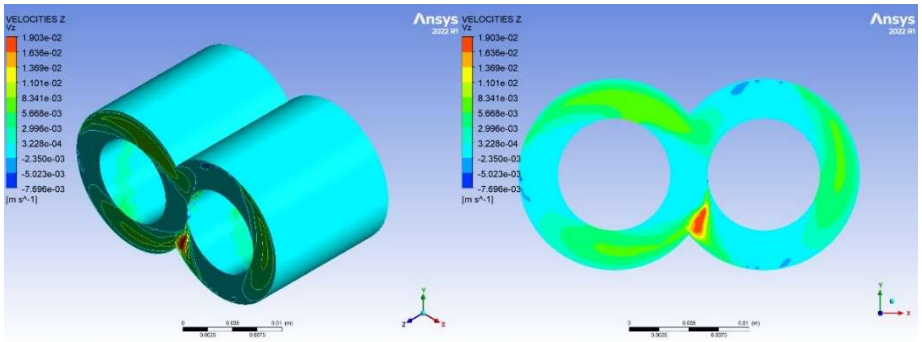

c

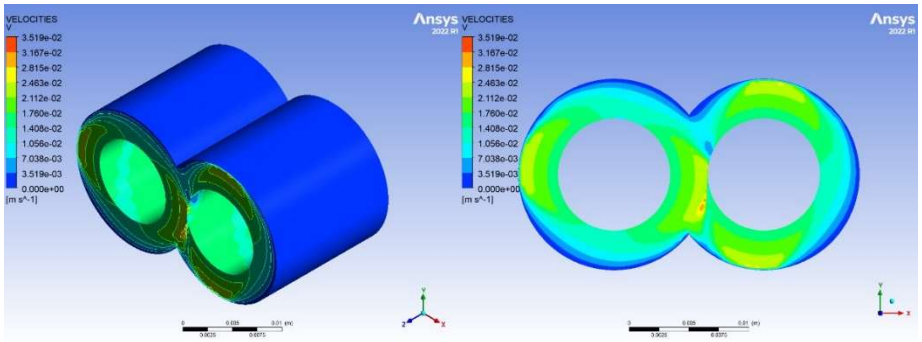

d

Figure 4-28 Velocity field of the screw element a) Vx, b) V_y c) V_z d) V.

4.3.2.4 *Visualisation of the mixing process*

Polystat's EXTRACT function may be used to examine the tracking particles' motion at any point in time and the resulting data can be utilized to determine the dispersion of particles in the flow field. Figure 4-29 illustrates the tracking particles during a single rotation cycle. The following parameters are used in this simulation: rotation speed n=30RPM, radius R =15.8 mm, pitch=16 mm. At 0s, 2000 tracking particles of various colours were injected instantaneously into the inlet zoon. Two different particle colours signify dissimilar materials. The particles progressively dispersed as the screw rotated.

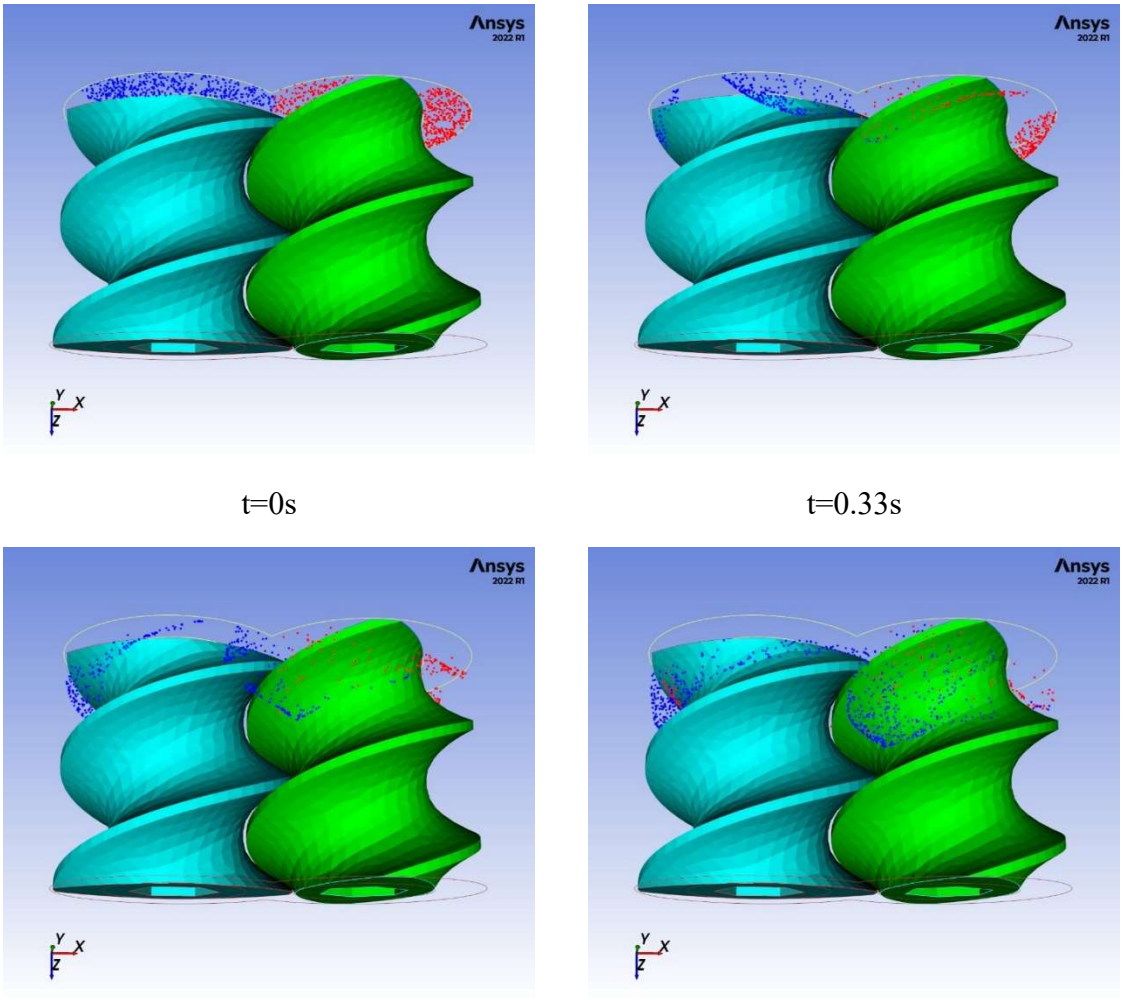

t=0s t=0.33s

t=0.66s t=0.99s

Figure 4-30 Tracking particles dispersion inside the screw element during a single rotation cycle with a screw speed of 30 RPM.

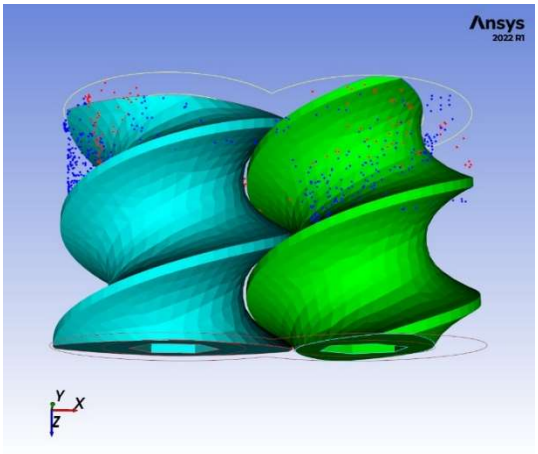

t=1.33s

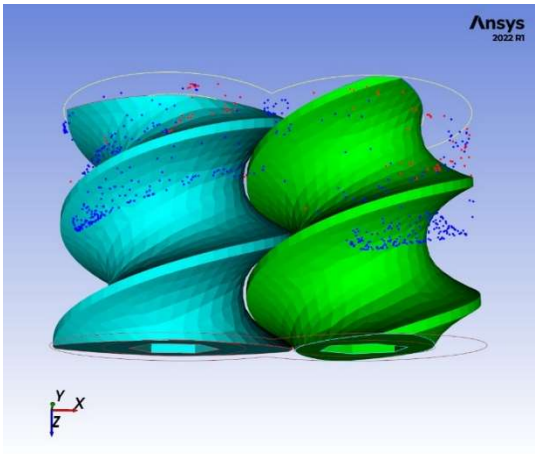

t=1.66s

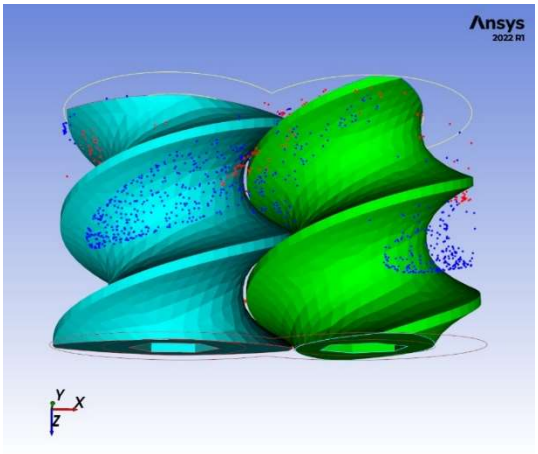

t=1.99s

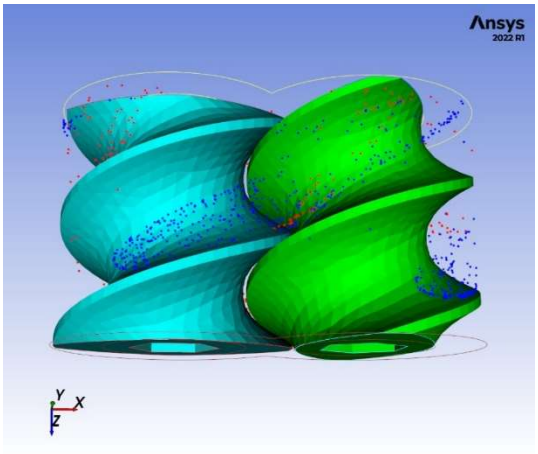

t=2.33s

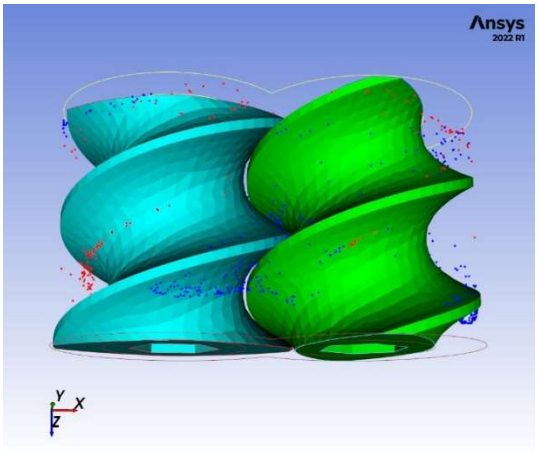

t=2.66s

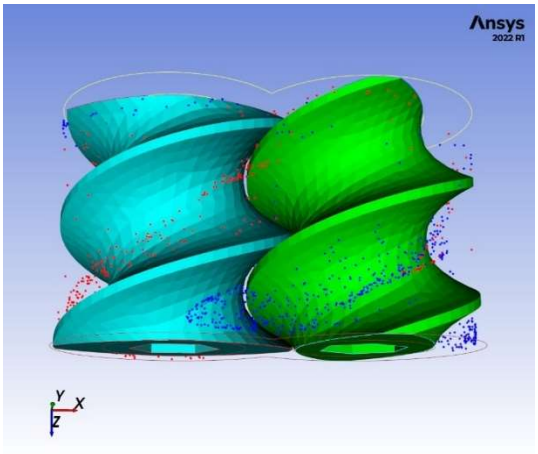

t=2.99s

Figure 4-29 Tracking particles dispersion inside the screw element during a single rotation cycle with a screw speed of 30 RPM.

The segregation scale of the screw mixing was shown in Figure 4-30. All points were initially at the side of the screw. Following that, when points were distributed, the distance between particles decreases as the rotor rotates. However, due to the confluence effect of the screw, the segregation scale would increase at some point. Then, it would decrease again with the dispersive mixing progress. The percentile represents the outcomes of applying mathematical statistics to the parameters defining the mixing characteristic. A percentile value is the value of a variable below which a certain percentage of observations fall. For example, if the highest shear rate corresponding to the 10% percentile is $100/s^{-1}$, it signifies that 10% of the particles experience shear rates less than or equal to $100/s^{-1}$, while 90% of the particles experience shear rates more than $100/s^{-1}$. The effect of screw rotation speed and structural characteristics on mixing performance was investigated in this study using the maximum shear rate, stretching rate, time-averaged efficiency, mixing index, and residence time distribution. The results are presented as 10%, 50%, and 90% percentile curves to illustrate the distribution of the mixing characteristic values. The three percentiles denote the largest, medium, and smaller values.

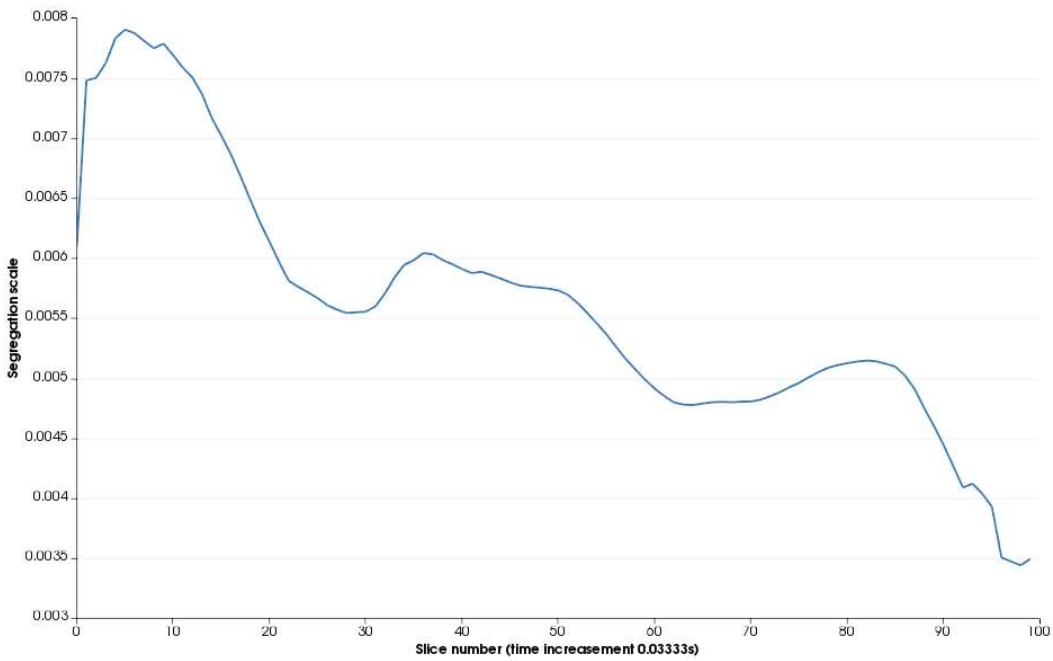

Figure 4-30 Segregation scale of the screw element with 30-degree stagger at screw speed 30 RPM.

4.3.2.5 *The influence of screw speed on the mixing properties of the screw element*

A rotation cycle was used to determine the percentile of the mixing characteristic parameters at various rotational speeds. The selected speed for the analysis was 30 RPM, 60 RPM, 90 RPM, and 120 RPM. Figure 4-31 to Figure 4-32 illustrates the mixing characteristic parameters of screw elements at various rotational speeds.

Figure 4-31 illustrates the maximum shear rate and maximum stretching rate of the particles at various percentiles of rotating speeds, respectively. The maximum shear and stretching rates gradually increased as the rotating speed increased for each of the three percentiles. When the percentile is 10% or 50%, maximum shear and stretching rates both increase linearly. When the percentile is 90%, the maximum shear and stretching rates increased the fastest from 90 RPM to 120 RPM and from 60 RPM to 120 RPM, respectively. This indicates that the maximum stretching and shear rates of 90% of the particles increased at the fastest rate. When the rotational speed is between 90 RPM to 120 RPM, the speed at which mixing performance may be improved through a comparative analysis of three percentiles is most visible.

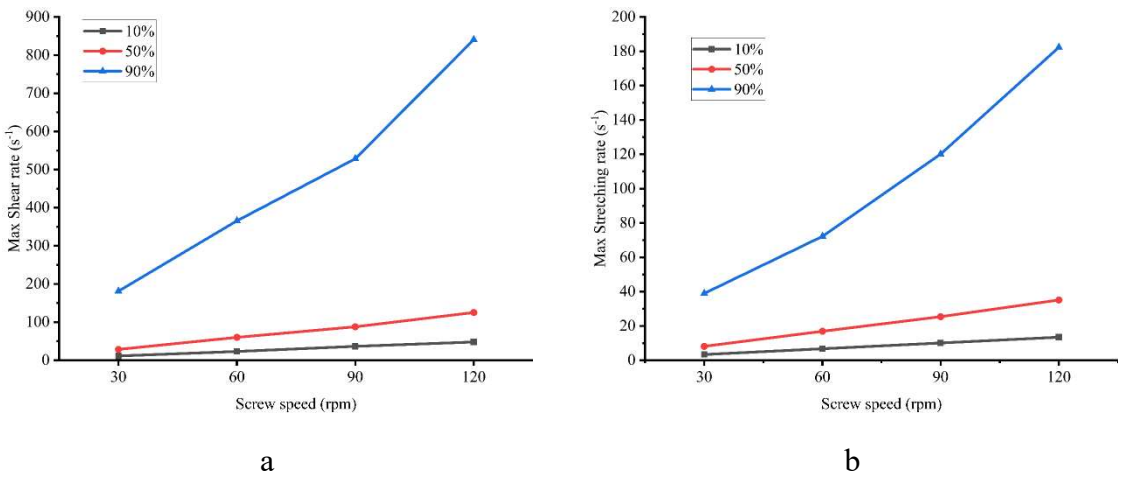

Figure 4-31 Influence of screw speed on the a) maximum shear rate and b) maximum stretching rate (Screw element).

Figure 4-32 depicts the maximum time-average efficiency and mixing index experienced by particles in the three percentiles at various rotational speeds. All the graphs'

maximum time-averaged efficiency curves were more than 0, showing that all particles were exposed to the stretching flow. At the 90th percentile, the maximum time-averaged efficiency was greater than 0.57, indicating that approximately 57% of the mechanical energy in these particles was utilized to cause stretching. When the speed is 90rpm, the most mechanical energy is employed to stretch the melt. The maximum mixing indexes under different speeds were greater than 0.79 in the 90th percentile, which means that more particles experienced extensional flow. In the 10% and 50% percentile, the mixing index value did not vary much and showed a zigzag change as the speed increased and reached the maximum at the speed of 90 RPM.

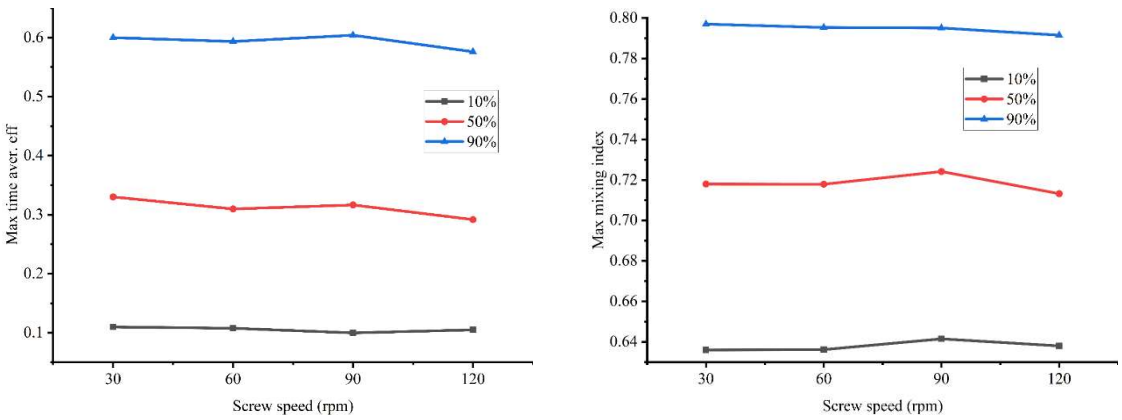

a b

Figure 4-32 Influence of screw speed on the maximum time-average efficiency and mixing index (Screw element).

Increased rotational speed increases the intensity of the flow field but decreases the duration the material remains in the extruder. As a result, when evaluating the mixing performance, the residence time distribution should be considered.

Each residence time distribution curve contained multiple wave peaks, indicating that the particles exited in a batch. And the first wave peak on each curve occurred approximately 1.5 times through the rotating period. In addition, the overall width of residence time distribution narrowed with the rotational speed increased. The residence time distribution of 30 RPM was better than other rotational speeds, and the width of the 60 RPM residence time

distribution was greater than that of 90 RPM or 120 RPM, as indicated by the width of the peak residence time distribution curve in Figure 4-33.

In general, shear and stretching rates increase as rotational speed increases, with the fastest rise occurring between 60 RPM to 120 RPM. The mixing index and time average mixing efficiency were not significantly affected by the rotational speed. As the speed increases, the residence time of the material in the screw element decreases. The material at 60 RPM speed has a longer residence time than 90rpm and 120 RPM. In summary, the screw element performs optimally when rotated at a speed of 60 RPM.

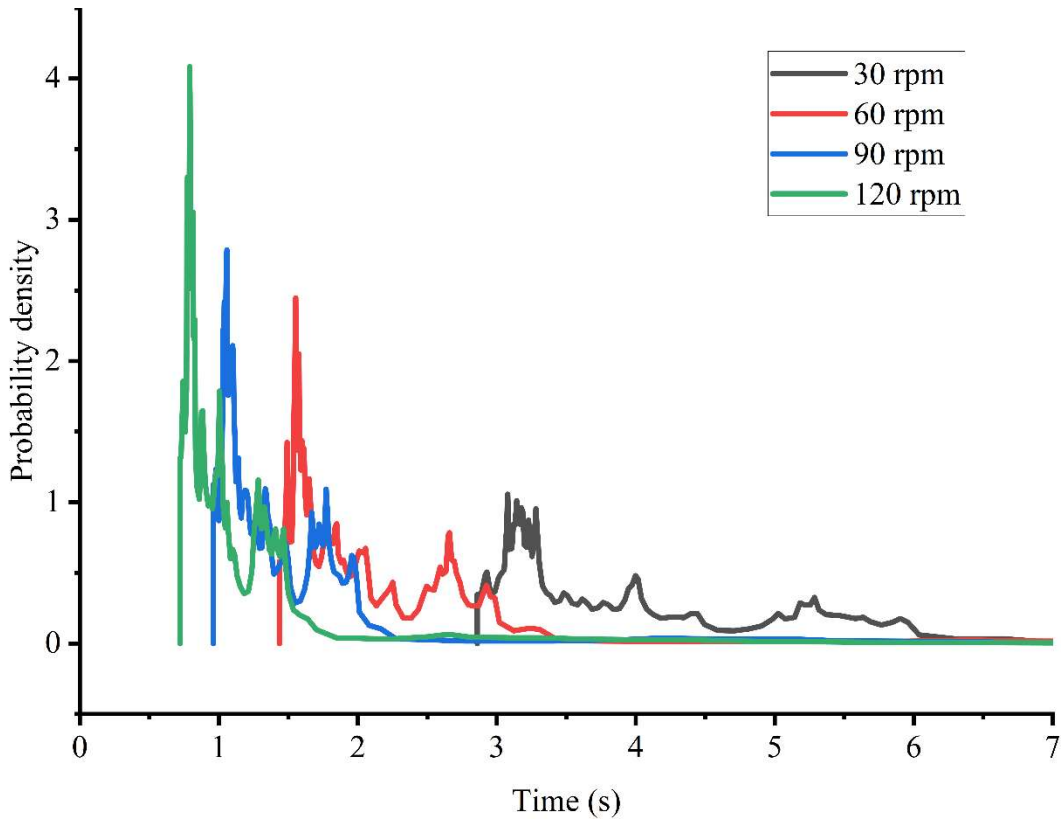

Figure 4-33 Influence of screw speed on the residence time distribution (Screw element).

4.3.2.6 *The influence of rotation speed on mixing properties of the kneading blocks.*

The segregation scale of the kneading blocks with 30º stagger at 30 RPM was shown in Figure 4-34. All points were initially at the side of the element. When points were distributed, the distance between particles decreases as the rotor rotates. Moreover, compared to the screw element, the 30º kneading blocks have less confluence effect, and the

segregation scale would decrease faster than the screw element. This means that when distribution improves, the distribution of particles in the extruder becomes faster. The percentile represents the outcomes of applying mathematical statistics to the parameters defining the mixing characteristic.

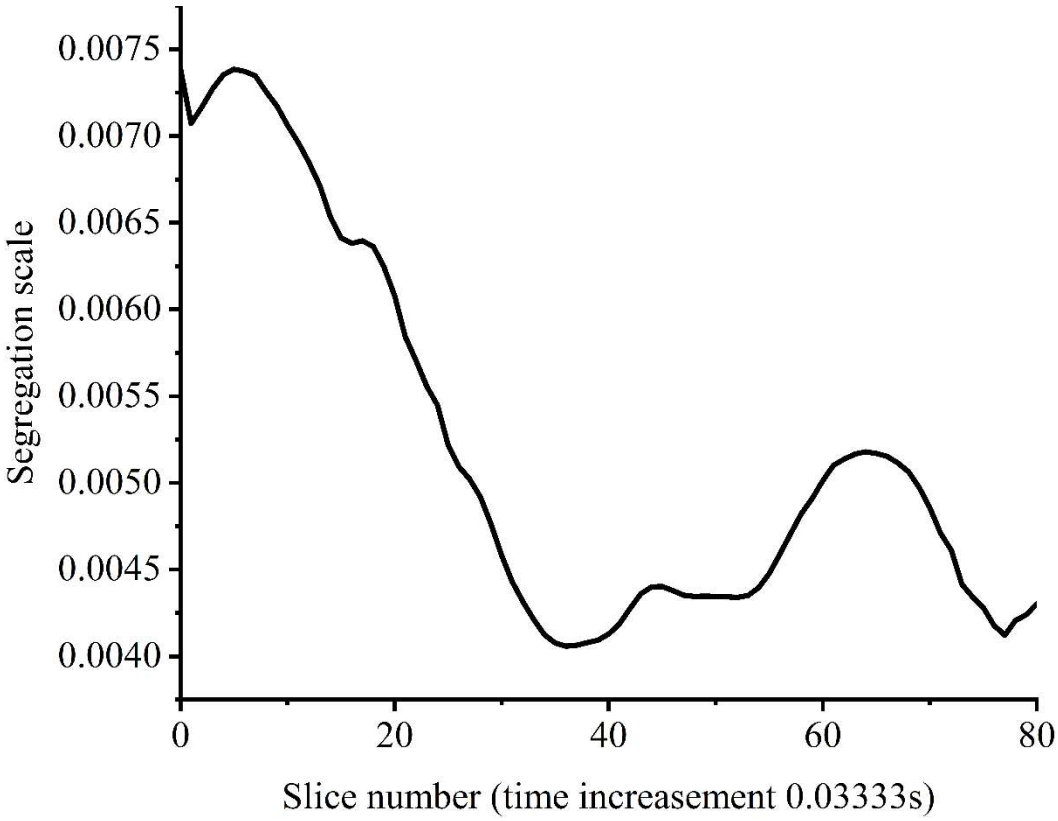

Figure 4-34 Segregation scale of the kneading blocks with 30-degree stagger at screw speed 30 RPM.

Figure 4-35 illustrates the maximum shear rate and maximum stretching rate of the particles at various percentiles of rotating speeds for the kneading blocks. It shows the same trend as screw elements, while the rotating speed increased the maximum shear and stretching rates gradually increased for each of the three percentiles. Maximum shear and stretching rates both rise linearly when the percentile is 10% or 50%. When the percentile is 90%, the maximum shear and stretching rates increased the quickest from 60 RPM to 90 RPM and from 30 RPM to 60 RPM, respectively. For the kneading blocks with 30º stagger angles, when the rotational speed is around 60 RPM, the speed at which mixing performance may be improved through comparative analysis of three percentiles is most visible.

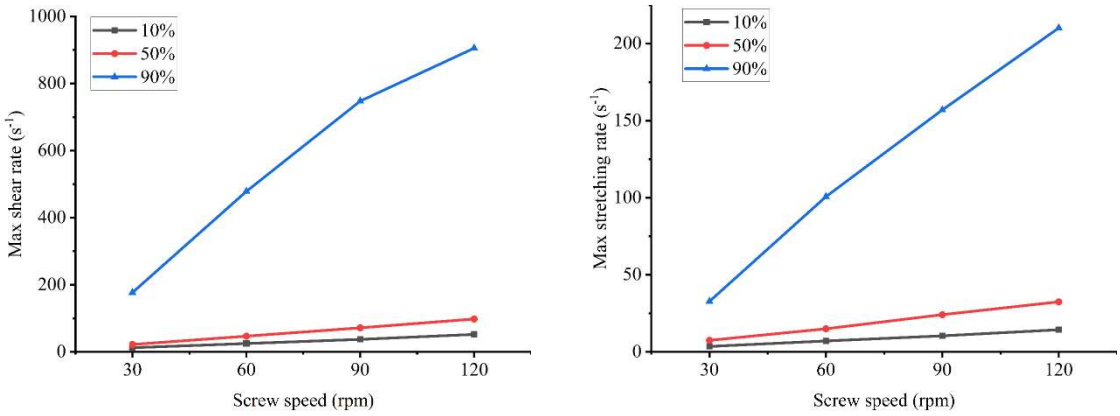

a b

Figure 4-35 Influence of screw speed on the a) maximum shear rate and b) maximum stretching rate (Kneading blocks).

As shown in Figure 4-36, the effect of screw speed on the maximum time-averaged efficiency and mixing index of kneading blocks. All the percentile shows a single peak in the line. The highest value is sitting around 60 RPM to 90 RPM. Meanwhile, the maximum time-averaged mixing efficiency and mixing indexes of various percentiles were all above 0 and 0.5 respectively, illustrating that there was a strong stretching flow field in kneading blocks with different screw speeds.

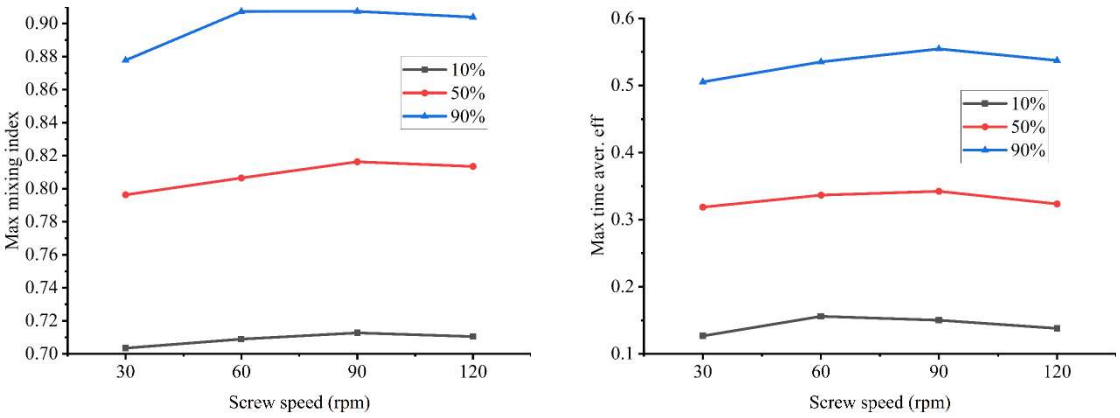

a b

Figure 4-36 Influence of screw speed on the a) maximum mixing index and b) maximum time average efficiency (Kneading blocks).

It can be seen from Figure 4-37 that the curves of residence time distribution under different screw speeds have a similar trend as the screw element. This is because the 30º

stagger angle is gentler than the other type of kneading blocks. Thus, the conclusion is that the change of the screw speed on kneading blocks has a similar effect on the screw element. In summary, the effect of screw speed for the 30º stagger angle kneading element is the same as the screw element. In general, shear and stretching rates increase as rotational speed increases, with the fastest rise occurring between 60 RPM to 90 RPM. The mixing index and time average mixing efficiency were not significantly affected by rotating speed. As the speed increased, the residence time of the material in the 30º kneading element decreased. In summary, the 30º stagger angle kneading element performs optimally when rotated at a speed of 60 RPM.

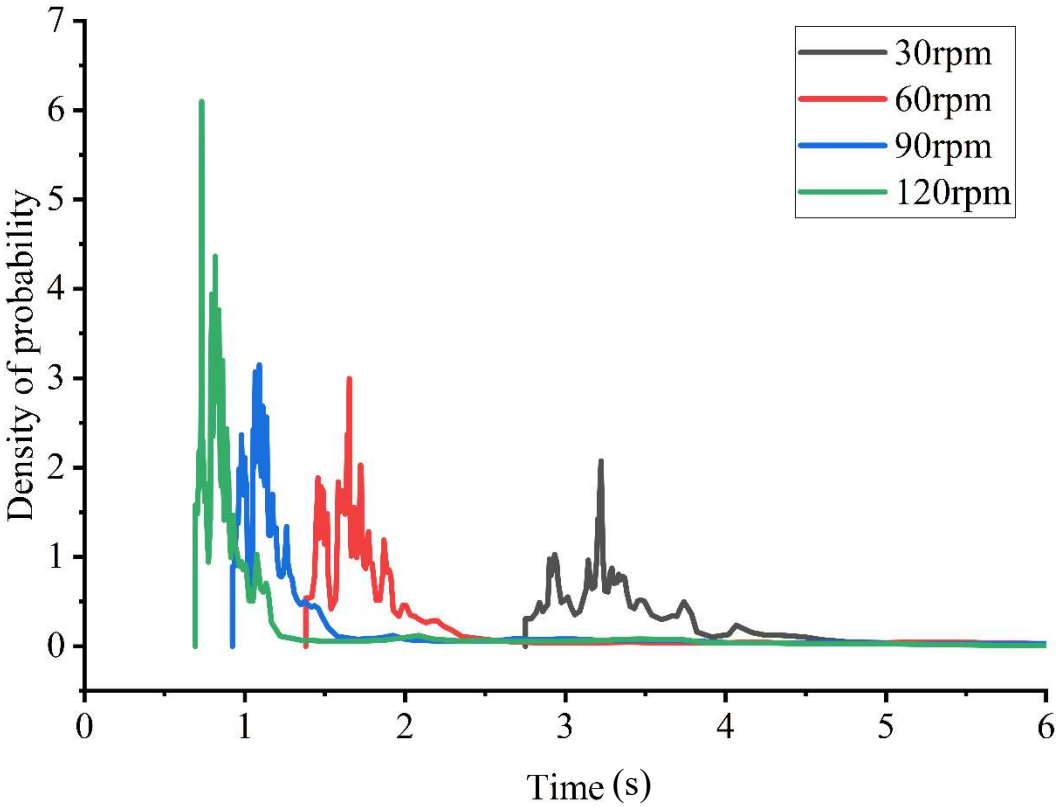

Figure 4-37 Influence of screw speed on the residence time distribution (Kneading blocks).

4.3.2.7 *The influence of stagger angle on mixing properties of the kneading blocks*

Figure 4-38 illustrates the maximum shear rate and maximum stretching rate of the particles at various percentiles of stagger angle for the kneading blocks. All the analysis was done at screw speed 30 RPM. While the stagger angle increased the maximum shear and

stretching rates gradually increased for each of the three percentiles. Maximum shear and stretching rates both rise slowly when the percentile is 10%. When the percentile is 90%, the maximum shear and stretching rates both increased at a faster rate from 30º to 60º and have a maximum value when the stagger angle is 90º. Such an observation can be directly linked to the ability to perform dispersive mixing. Moreover, because the stretching flow is more conducive to improving the performance of a mixture than shear flow, for the kneading blocks with 90º stagger angles, mixing performance may be improved through comparative analysis of three percentiles is most visible (Xie *et al.*, 2017).

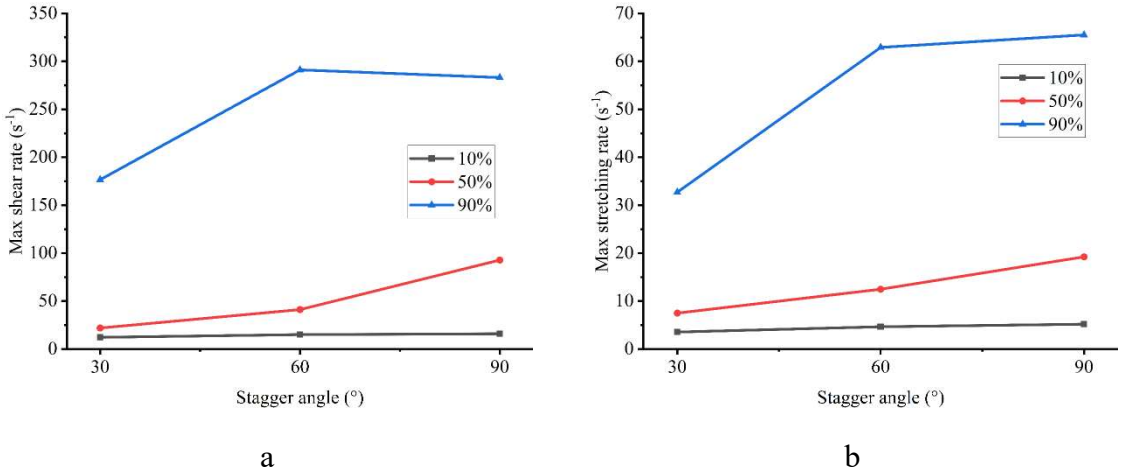

Figure 4-38 Influence of stagger angle on a) the maximum shear rate and b) maximum stretching rate (Kneading blocks).

The maximum mixing index experienced by the particles in the 10%, 50% and 90% percentiles for the different arrangement modes of the kneading blocks are shown in Figure 4-39 a). When the percentiles are 90%, the maximum mixing index increases with increasing stagger angle and the maximum value is over 0.92, which indicates almost 100% extensional flow in 90º stagger angle kneading blocks. However, when percentiles are at 10% or 50%, it has a single peak when the stagger angle is at 60º. However, the maximum mixing indexes experienced by particles for even the 10th percentile were all above 0.65, illustrating that regardless of the stagger angle, almost all particles will experience extensional flow.

As shown in Figure 4-39 b, all the graph's maximum time-averaged efficiency lines

were more than 0, showing that all particles were exposed to the stretching flow. At the 90th percentile, the maximum time-averaged efficiency was greater than 0.50, indicating that over 50% of the mechanical energy in these particles was utilized to cause stretching. When at 90% percentiles the average time efficiency increases when the stagger angle increased. However, 10% and 50% percentiles lines show a single peak around 60º.

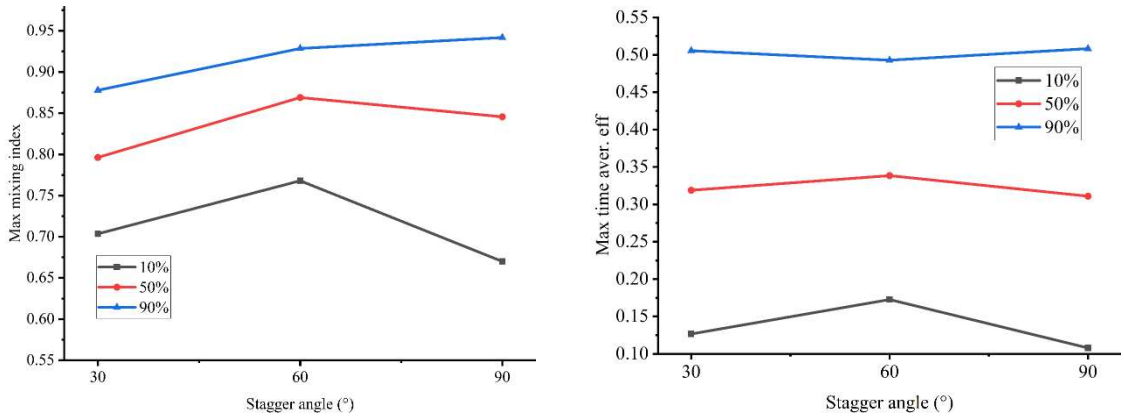

a b

Figure 4-39 Influence of stagger angle on the maximum mixing index and maximum time average efficiency (Kneading blocks).

It can be seen in Figure 4-40. that the curves of residence time distribution for different kneading blocks. The residence time increase with the increase of stagger angle. For 90˚ kneading blocks, no particle can go through the whole blocks during the calculation lifetime with this boundary condition, (free flow in the inlet and outlet boundary). Compared to the conveying elements, the staggering of two sequential discs permits materials exchange between adjacent screw channels. Therefore, a backflow is created and the amount of the positive axial transport is decreased upon increasing the staggering angle (Sarhangi Fard and Anderson, 2013). In summary, the 90˚ stagger angle kneading block has the best mixing performance compared to any other part as well as increasing the upper limit of mixing capacity. However, the use of 90˚ kneading elements would cause a significantly increased residence time. The most critical distributions for the distributive efficiency are the total shear experienced in the barrel. Therefore, to reach a high total shear, a particle must have a high residence time or exhibit a remarkably high shear rate. A combination of both effects is

the best case obtained by the 60˚ and 90˚ kneading element for the same number of discs.

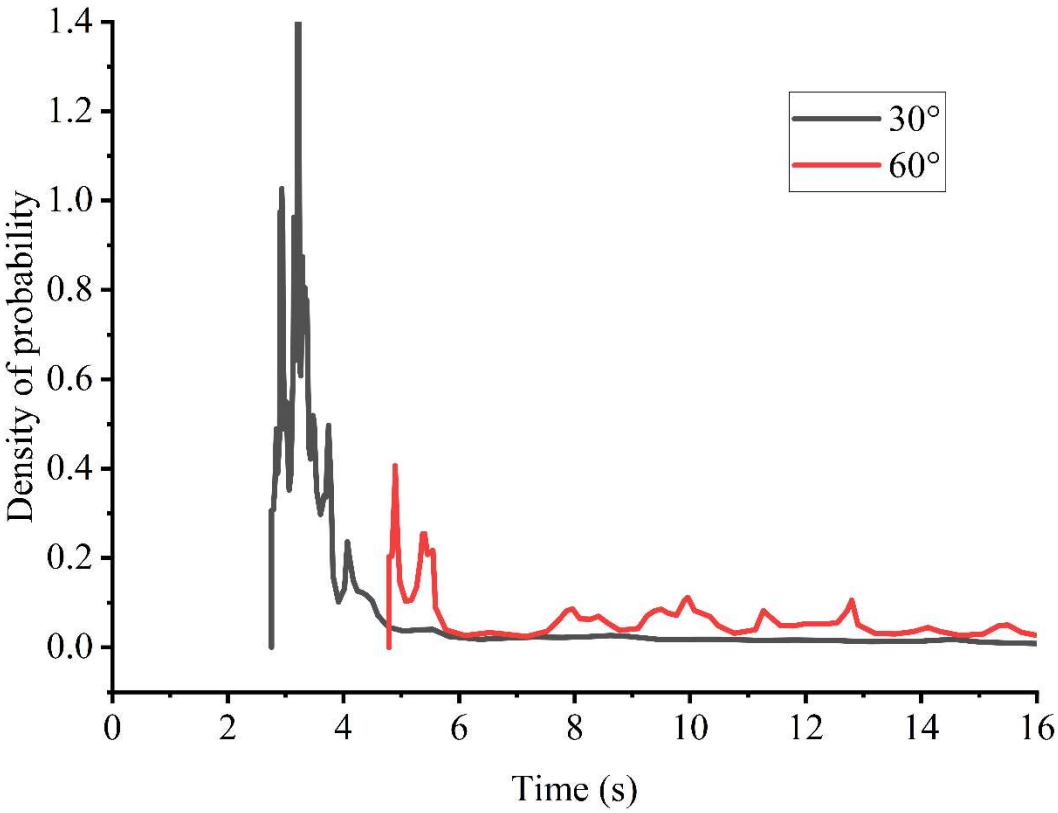

Figure 4-40 Influence of stagger angle on the residence time distribution (Kneading blocks).

4.3.3 **Summary**

The mixing of different compounds is a key step in extrusion processes. The quality of the final product obtained with a twin-extruder depends, in the main, on the dispersive and distributive mixing generated by the kneading blocks. Numerical simulation was used to understand the impact of two classical geometrical parameters on the mixing: the influence of different screw speeds and stagger angle of a twin-screw extruder on mixing performance was studied based on some mixing characteristic parameters such as the maximum shear rate, stretching rate, mixing index, time-averaged efficiency, and the residence time distribution. The intensity of shear and elongational flow strengthened when the rotational speed increased, but the time for the material to stay in the twin-screw extruder will be reduced. From the analysis result, this twin-screw extruder has the best mixing performance when the

rotational speed is around 60 RPM overall consideration when processing shellac material because it has the highest flow intensity and the optimal residence time distribution. In the aspect of kneading block stagger angle parameters, the increase of stagger angle can promote the mixing performance of the extruder. On the contrary, the residence time increase with the increase of the stagger angle. As a result, a combination of three different stagger angles is needed, the 30˚ stagger angle kneading section can bring up enough material to the next section, and the 60˚ stagger angle has the best overall mixing performance. And the last section is a 90˚ stagger kneading block attached at the end of the mixing section, to ensure all the material has undergone high shear and dispersive mixing. The conclusions from the numerical experiences appear to correlate with the global classical interpretation of the flow (Alsteens, Legat and Avalosse, 2004). It is straightforward to extend this type of sensibility analysis to other geometric parameters. Moreover, finite element simulations are an effective method for deciphering complex mixing characteristics and for extracting global and local information. These data are virtually inaccessible via the experimental method. Additionally, it is required to verify that the simulation maintains physical relevance and appropriate accuracy. Even when using certified numerical software, such a compromise is still difficult to achieve. Nevertheless, based on these simulations it is predicted that enhanced dispersion will occur if this optimized screw design was employed in the mixing of different shellac types with a class 2 drug, the next chapter will investigate this experimentally.

4.4 Optimized formulation production and characterisation based on the new screw design

4.4.1 **Introduction**

From section 4.2, the drug content of the extrudate was extremely varied during the extrusion process, referring to the uniformity of the extrudate formulation not being optimised. The first trial process of the formulation is produced using a universal screw configuration setup. One 30° forwarding mixing zone is composed of several kneading discs, as shown in Figure 3-16a. Based on the simulation findings in section 4.3, the universal screw configuration setup would provide less shearing but more conveying to the material and is a benefit for the drug which is shear sensitive. However, this set-up would result in reduced mixing inside the barrel. Furthermore, the 30° mixing zone set-up is likely to have a lower residence time compared to other screw setups (60°/90°) during the process.

From the simulation study in the previous section, the 90˚ stagger kneading block provides the best result in shearing and dispersive mixing. However, the material transport capacity is the drawback to this setup. As a result, a combination of three different stagger angles is needed, the 30˚ stagger angle kneading section can bring up enough material to the next section, and the 60˚ stagger angle has the best overall mixing performance. And the last section is a 90˚ stagger kneading block attached at the end of the mixing section, to ensure all the material has undergone high shear and dispersive mixing.

In this section, the modified screw setup was built and employed in the small-scale production run as shown in Figure 3-16b. The uniformity and properties of the formulation were evaluated. Moreover, because the two wax-containing shellac materials are not certified for pharmaceutical application, and are not pharmaceutical grade materials, both materials were not carried forward in this section. However, A.F. Suter had launched two new pharmaceutical-grade shellac materials AFS HS 702MB and HS SWANLAC. Both new pharmaceutical-grade shellacs were purchased and included in this section.

4.4.2 **Result and discussion**

4.4.2.1 *Differential scanning calorimeter of new shellac material*

In this section, four types of shellac materials were used as the formulation carrier, including Shellac SSB 55 Pharma FL, AFS shellac 700K, AFS shellac 702MB and AFS shellac HS SWANLAC. The raw material DSC analysis result is shown in Figure 4-41. As well as Table 4-9, all T_g values are in a range between 42°C and 49°C. Because these are all dewaxed shellac, all four types of shellac grades show similar thermal behaviour and have a similar glass transition temperature. SSB 55 Pharma FL, based on Kushmi seedlac, has the lowest T_g (41.72°C). The T_g value of Shellac HS 700K, refined by the solvent extraction and based on Kushmi seedlac but early production date, is at 43.84°C, which is higher than SSB 55 Pharma FL. Moreover. AFS shellac HS 702MB based on different seedlac (Bysakhi) have a higher T_g value (48.52°C) than SSB 55 and 700K, even though they are refined by the same process solvent extrusion, Bleached shellac SWANLAC has the highest T_g value which is expected because the bleaching processing would significantly affect the physical properties of the shellac material (Farag and Leopold, 2009).

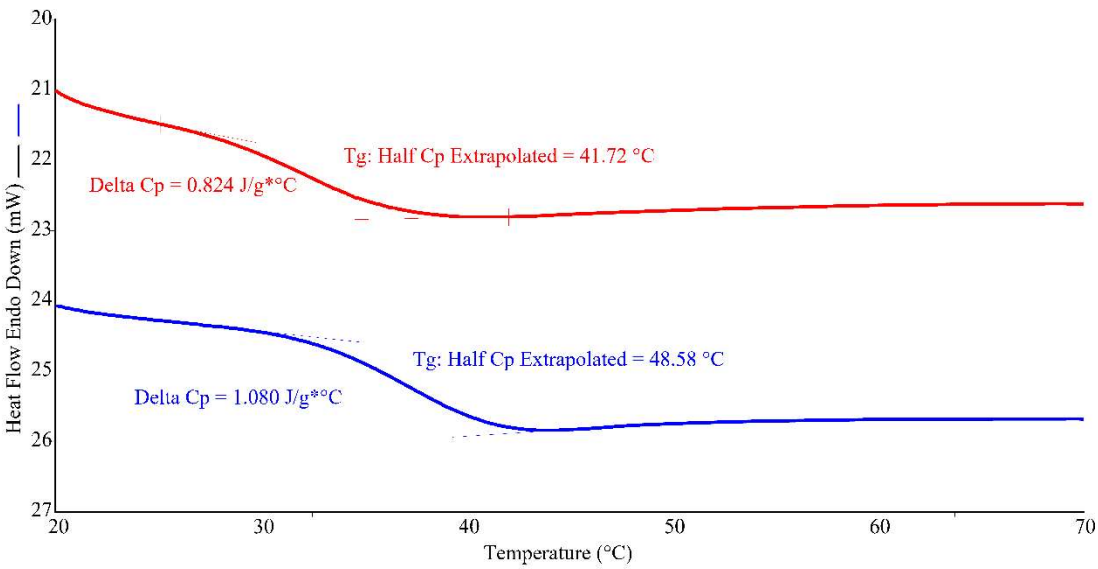

Figure 4-41 DSC thermograms of virgin shellac material (Red: Shellac SSB 55 Pharma FL; Blue: AFS Shellac HS 702MB) (n=2).

Table 4-9 *T*g value of each shellac material used in this section (n=2).

Material	T_g (°C) ± Std Err	T_m (°C)
Shellac SSB 55 Pharma FL	41.72±0.97	-
Dewaxed Shellac HS 700K	43.84±0.68	-
AFS Shellac HS 702MB	48.58±0.61	-
AFS shellac HS SWANLAC	48.97±0.58	-

4.4.2.2 *Fourier transform infrared spectroscopy (FTIR)*

The FTIR spectra (4000-650cm^{-1}) of the fenofibrate, along with drug formulations with different types of shellac are presented in Figure 4-42. The band assignments of each fenofibrate and shellac are listed in Table 4-10. The observed broader band shapes and less well-resolved peaks in the FTIR spectra of the fenofibrate solid dispersion formulation suggest the presence of amorphous fenofibrate (Heinz *et al.*, 2009). As discussed in section 4.2, the fenofibrate FTIR spectra showed characteristic peaks at 1725cm^{-1}, 2985cm^{-1} 1648cm^{-1}, 1596cm^{-1}, 1502cm^{-1}, 858 and 1246cm^{-1}. Also, the presence of CH_2Cl group is indicated by a peak at 1286cm^{-1}. There are two carbonyl peaks shown in the original fenofibrate, one from the C=O, and the other from the methyl ester carbonyl group. These functional groups can act as proton acceptors, however, fenofibrate does not have proton donors. As a result, there is very little hydrogen bonding in fenofibrate drug substances (Heinz *et al.*, 2009). Moreover, there are few reports about fenofibrate forming hydrogen bonds with polymers typically used in pharmaceutical compositions (Huang *et al.*, 2009). In 2009, Wang et al. found that the hydrogen bond between drug and carriers may be relevant to the stabilization of the solid dispersion in the high-energy amorphous state (Wang, Pellerin and Lebel, 2009). The original fenofibrate showed two peaks in 1725.54cm^{-1} and 1648.88cm^{-1}, respectively. But in the solid dispersion formulation two peaks were seen at 1711.91cm^{-1} and 1655.96cm^{-1}, respectively. This is suggested to be due to the formation of hydrogen bond, the carbonyl peak position shifted to a lower wave number. In the amorphous phase, only one carbonyl group took part in the hydrogen bond formation by a downward shift of 13.63cm^{-1}. The other peak shifted by value of 7.08cm^{-1} to a higher peak position.

The upward shift in the position of the C=O group suggests that the hydrogen bond in the original fenofibrate is stronger than that in the formulation. The original fenofibrate and its formulation dose showed different strengths of hydrogen bonding (Sailaja *et al.*, 2016)(Tang, Pikal and Taylor, 2002)(Wang, Pellerin and Lebel, 2009)(Silverstein and Bassler, 1962). Also, the shifts in the spectra of solid dispersions indicate that the strength of the fenofibrate–shellac hydrogen bonding was in the order of SSB 55 Pharma FL<AFS shellac 702MB< AFS shellac 700K<AFS shellac HS SWANLAC. However, even the largest spectral shift found in the AFS shellac SWANLAC solid dispersion, between 1725.54 and 1710.47cm^{-1}, represented very weak drug-polymer interactions (Zhang *et al.*, 2012). Furthermore, the shift differences between various types of shellac are small which further confirmed that for all the shellac materials, there are few chemical differences. The minor change in wavenumber explains why the FTIR spectra of solid dispersions formulation showed no obvious differences compared to those of the corresponding physical mixtures across the entire absorption bands of fenofibrate.

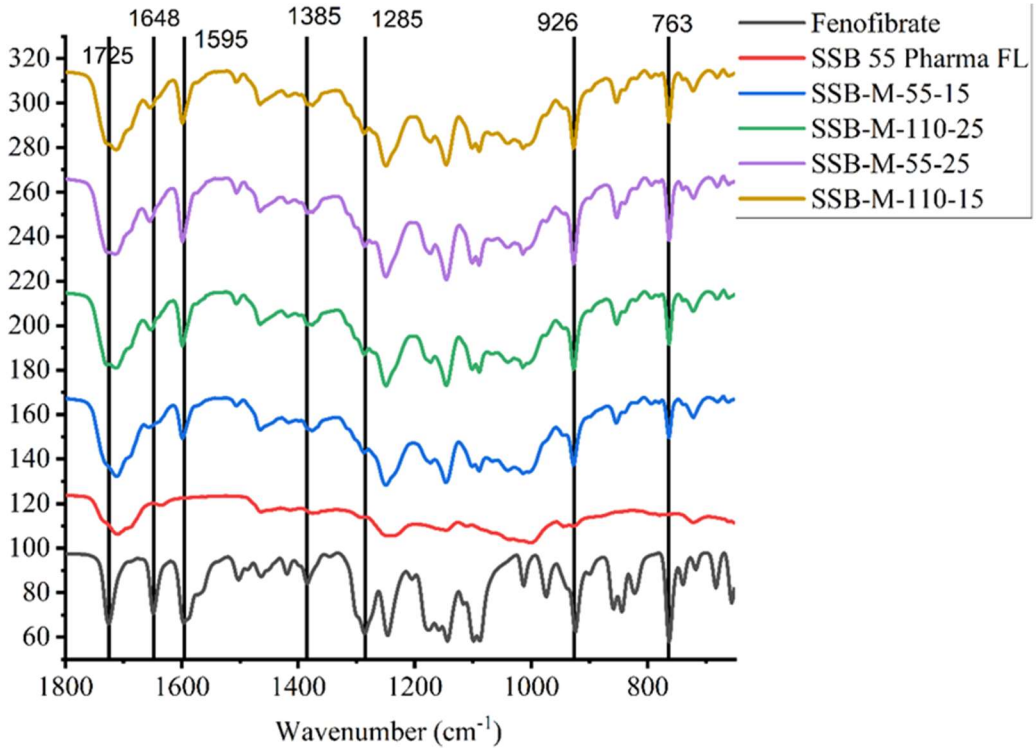

Figure 4-42 FTIR spectra of fenofibrate and formulation produced by modified screw profile based on shellac SSB 55 Pharma FL

Table 4-10 The band assignments of each type of shellac, fenofibrate and formulation (SSB-M-55-15).

FTIR wavenumber cm^{-1}						FTIR band assignment
SSB 55	700K	702MB	SWANLAC	Fenofibrate	Formulation	
3380.63	3418.22	3411.2	3381.31		3414.86	O-H stretching
				2985.14		benzene ring
2928.81	2928.32	2928.91	2929.07		2929.96	CH Stretching
2857.03	2856.71	2857.06	2857.56		2857.76	C–H stretching
1709.80	1709.98	1709.26	1709.45	1725.54	1711.91	C=O stretching
1637.00	1634.27	1637.4	1637.45	1648.88	1655.96	C=O stretching
				1596.31	1598.32	C=O stretching
				1502.57	1506.06	C----O stretching
1464.14	1464.44	1464.36	1463.84	1463.89	1465.33	C----O stretching
1413.69	1415.57	1413.97	1412.44	1419.07	1416.17	CH3 deformation
1374.86	1373.10	1371.42	1374.43	1384.45	1375.7	CH3 deformation
				1286.09	1286.88	CH2Cl stretching
1246.49	1247.32	1246.28	1248.07	1246.5	1249.71	C-O stretching
				1175.88	1172.91	C-C-H in plane deformation
1145.81	1148.29	1145.82	1146.73	1143.89	1146.23	O-H in plane deformation
				1115.94	1101.42	C-C-H in plane deformation
1110.89	1111.14	1112.16	1110.44	1098.95	1089.83	C-C-H in plane deformation
				1088.34	1066.43	C-C-H in plane deformation
1000.71	1002.15	1001.46	1001.24	1012.87	1014.02	C-C-H in plane deformation
944.32	944.00	943.47	827.17	974.3	927.41	C-C-H in plane deformation
				858.59	853.62	C-O stretching
779.61	780.26	779.44	779.97	763.26	763.61	C-H out of plane deformation
721.87	722.68	721.96	722.31		721.97	C-H out of plane deformation
				682.59	680.26	C=C bending
				655.53	661.47	O-H out of plane deformation

4.4.2.3 *Differential scanning calorimetry (DSC)*

The DSC result for drug formulations is shown in Table 4-11. Overall, all the formulation shows a lower T_g value than the virgin shellac material. This is because fenofibrate has a much lower T_g (-19.9°C) value than shellac material and according to the Gordon-Taylor equation, the T_g of the formulation depends on the T_g of individual components (Lang, McGinity and Williams, 2014). This means the result T_g value of formulation is higher than fenofibrate but lower than the shellac material. Moreover, the T_g value would decrease with the increase of fenofibrate contain. This could be attributed to

higher drug concentration and uniform distribution of the drug in the matrix of polymer, resulting in complete miscibility of the molten drug in shellac polymer (Kallakunta *et al.*, 2020).

Furthermore, comparing the formulations which are produced with a universal screw design, those formulations produced with a new configuration screw design show a significantly lower T_g value (Modi and Tayade, 2006). The presence of drug molecules acts as a plasticiser, decreasing the T_g value of the shellac material and increasing the chain mobility at the same time. As shown in Figure 4-43, formulations SSB-M-55-15 and SSB-U-55-15, SSB-M-110-15 and SSB-U-110-15 were produced using the same formulation design and screw speed but different screw designs, SSB-M-55-15 and SSB-M-110-15 have a much lower T_g value than SSB-U-55-15 and SSB-U-110-15, respectively. This is due to the poor dispersion of fenofibrate which would lead to fenofibrate-rich and fenofibrate-poor regions resulting in changes in T_g value depending on the sampling region used for the test (Wang *et al.*, 2015). Furthermore, SSB-M-55-15 and SSB-M-110-15, SSB-U-55-15 and SSB-U-110-15, produced with the same screw design and formulation, but different screw speed, results in the higher processing speed batches having a lower T_g value. This is because the higher screw speed would have more shear rate and heat generation to the extrudate, resulting in polymer degradation because of chain scission and reductions in molecular weight (Farahanchi, Malloy and Sobkowicz, 2016). DSC was also performed to investigate the stability of amorphous fenofibrate over time. The formulation was stored in room condition (Room temperature 20-23°C, without control of %RH) for up to 8 months. DSC thermographs did not indicate recrystallisation had occurred over the 8-month timeframe assessed (Figure 4-44). This indicates that the amorphous shellac polymer matrix prevents recrystallisation and drug-drug interaction from occurring due to the amorphous nature of the shellac material.

Table 4-11 T_g Value of each batch of formulation (n=2).

Batch name	T_g (℃) ± Std Err	Batch name	T_g (℃) ± Std Err
SSB-M-55-15	22.03±0.35	SSB-U-55-15	24.62±0.06
SSB-M-110-25	20.58±0.26	SSB-U-110-15	23.54±0.20
SSB-M-55-25	19.54±0.37	SSB-U-55-25	22.98±0.09
SSB-M-110-15	21.61±0.16	702-M-55-15	28.00±0.09
702-M-110-15	37.47±0.20	702-M-110-25	24.12±0.30
SSB-U-110-25	24.31±0.28	702-M-55-25	25.17±0.33

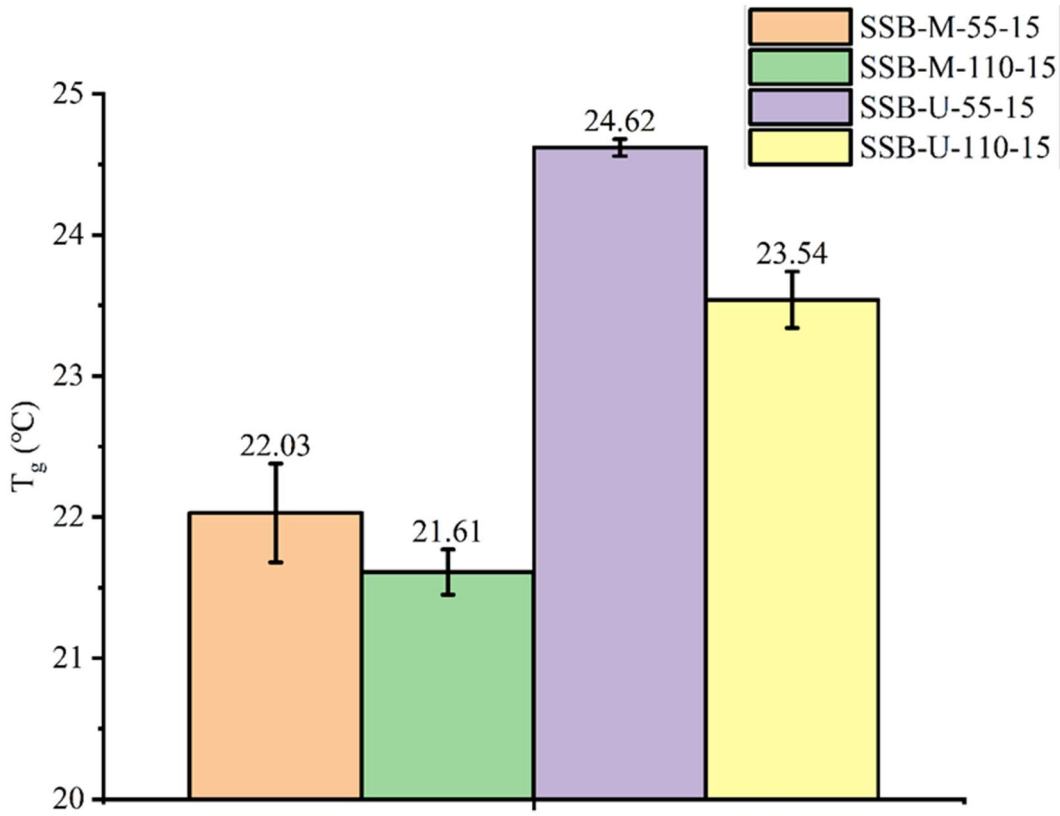

Figure 4-43 T_g value of the same formulation produced with different screw configurations (n=2)

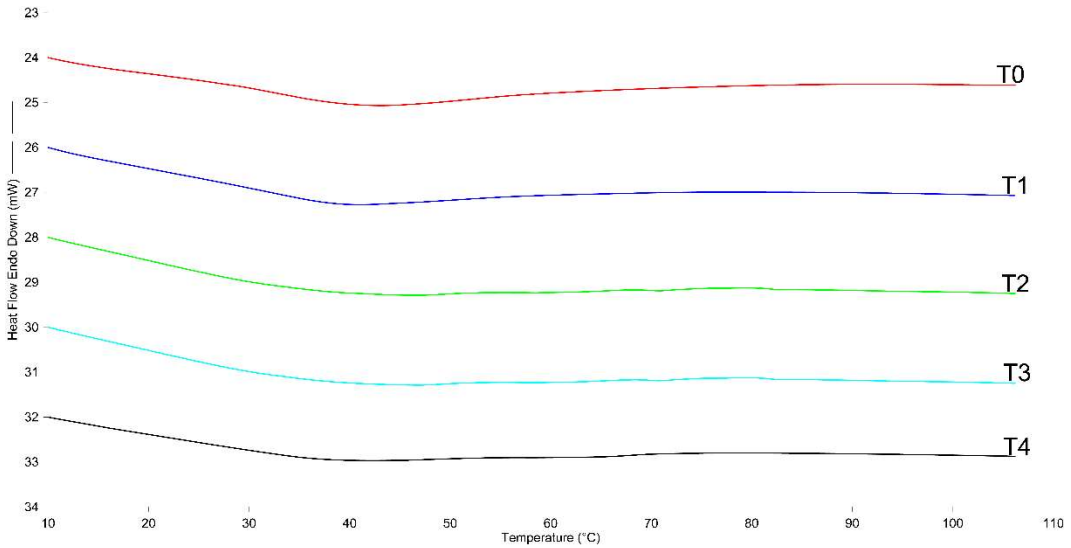

Figure 4-44 DSC thermograms of P1 (Produced by modified screw design, 55RPM, 15% Drug loading) Storage at room temperature. (T1=4 weeks, T2=12 weeks, T3=24 weeks, T4=32 weeks. n=2)

4.4.2.4 *Powder X-ray diffraction (PXRD)*

As shown in Figure 4-45 fenofibrate is a highly crystalline hydrophobic molecule with characteristic crystalline peaks at 14.392°,16.144°,16.624°, 18.004°, 19.156°, 20.788°, 22.18°, 24.604°, and 26.236° (Zhang *et al.*, 2012). The crystallinity of virgin fenofibrate and fenofibrate/shellac solid dispersions was examined by PXRD, and the patterns (Figure 4-46) illustrated that the crystalline peaks of fenofibrate were absent in the solid dispersions composed of all types of shellac formulation, confirming amorphous fenofibrate in the solid dispersions. This result is comparable to that from the DSC thermogram of the crystal fenofibrate raw material, indicating that the amorphous state of fenofibrate was formed by the hot melt extrusion processing. Additionally, the ability of shellac material to provide superior stability of formulation may be because the T_g value of shellac is higher than the room temperature can obstruct fenofibrate from interactions that could result in recrystallisation (Hancock and Zografi, 1997). These results support the DSC results and infer that the drug polymers were miscible at the molecular levels. The reason for this amorphous nature may also be attributed to the amorphous nature of the polymer which prevents interactions leading to recrystallisation (Kallakunta *et al.*, 2020).

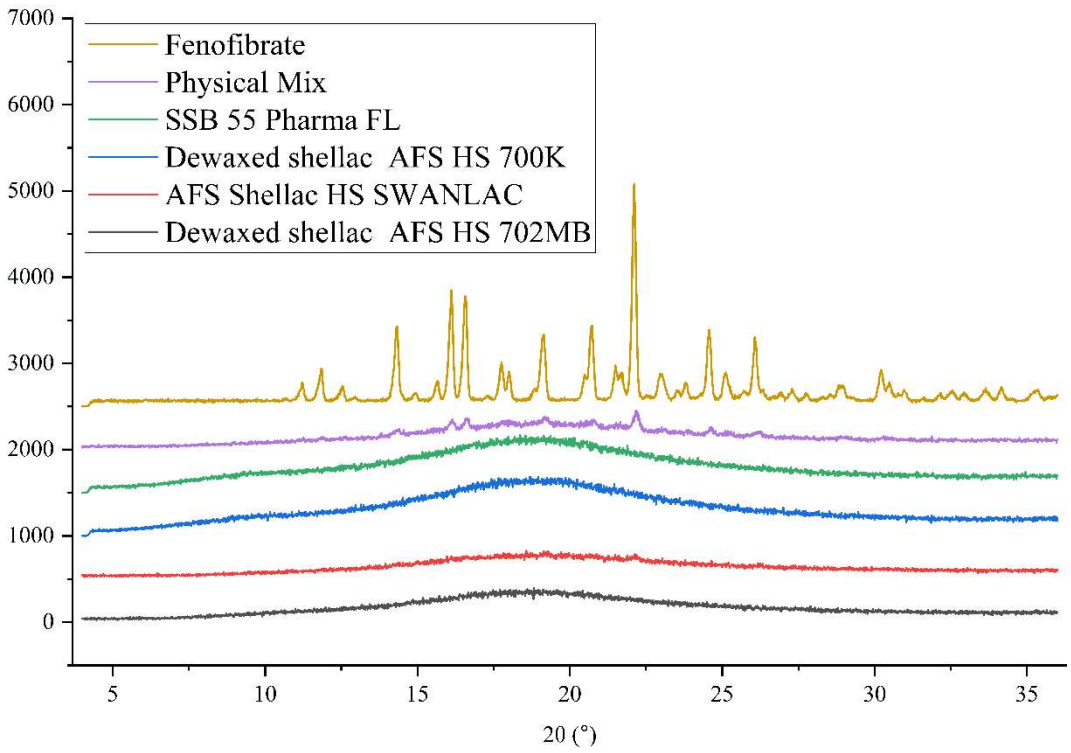

Figure 4-45 PXRD patterns of fenofibrate, shellac, and their physical mixture.

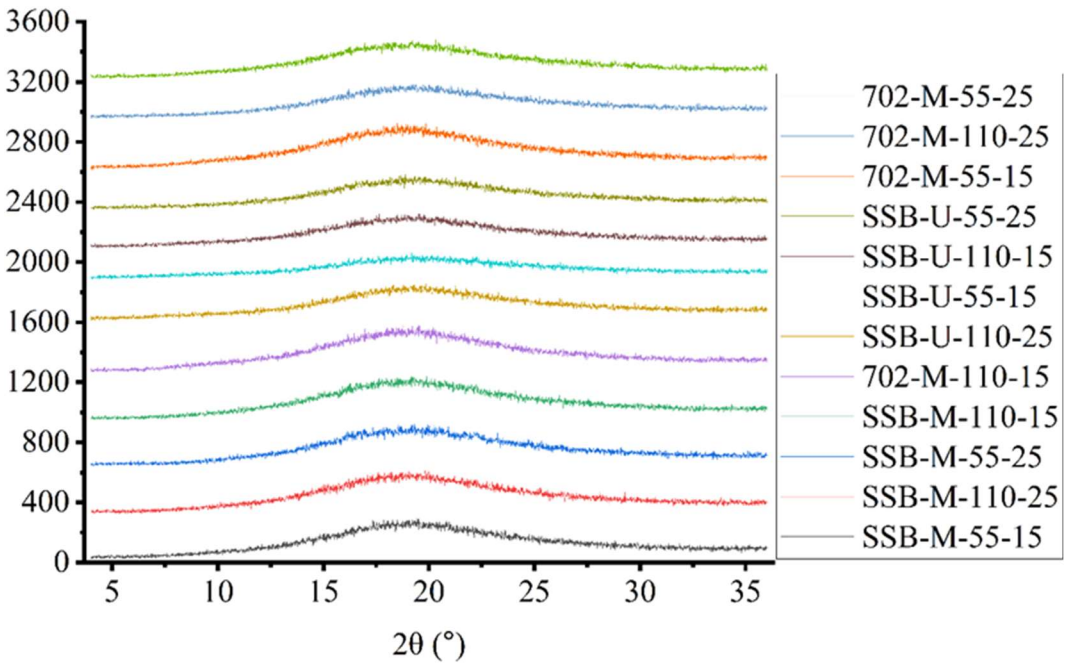

Figure 4-46 PXRD patterns of each formulation.

4.4.2.5 *Dissolution study*

To evaluate the dissolution profile of the dispersions, the content of fenofibrate and its chemical purity was confirmed using HPLC. During the manufacture of the ASDs using HME, due to the higher shear and temperatures applied to the systems, the drug has a higher possibility of degradation. It is then important to determine the effect of the extrusion process on the distribution and stability of the drug. The FEB chromatographs obtained from the extruded solid dispersions showed a single peak with an elution time equal to the standard solutions at 6.3 ± 0.007 min (see Figure 4-47). The results support the chemical integrity of the active ingredient after the thermal and mechanical treatment applied during processing. The concentration of FEB on the different dispersions was quantified to evaluate the drug uniformity of content on the extrudates. The results are presented in Table 4-12 and these values obtained for the actual content of fenofibrate were used for the calculation of the dissolution studies. From Table 4-12, the standard error for the formulation using a new screw design is lower than the formulation using the universal design. Likewise, for the formulation using the universal screw design, the standard error would decrease when using a lower screw speed. This is because the lower screw would increase the residence time which also allows the material stays longer inside the barrel. This will also help improve the mixing efficiency and uniformity of the formulation. This result was confined to the simulation result in section 4.3, The optimised screw design consists of a 60˚ and 90˚ stagger angle kneading element which would result in higher mixing efficiency than the universal screw. Moreover, the lower screw speed would significantly increase the residence time of the material, which would help improve the mixing efficiency as well.

Table 4-12 Drug content of the ASDs formulation as determined by HPLC (n=3).

Batch name	Real fenofibrate (%) ± Std Err	Nominal (%)
SSB-M-55-15	14.93±0.43	15
SSB-M-110-25	22.06±0.50	25
SSB-M-55-25	24.51±1.97	25
SSB-M-110-15	24.61±1.33	15
SSB-U-110-25	19.05±6.09	25
SSB-U-55-15	14.78±2.50	15
SSB-U-110-15	12.69±5.00	15
SSB-U-55-25	22.39±2.59	25
702-M-110-15	12.72±0.87	15
702-M-55-15	14.95±0.17	15
702-M-110-25	21.98±2.97	25
702-M-55-25	24.17±0.33	25

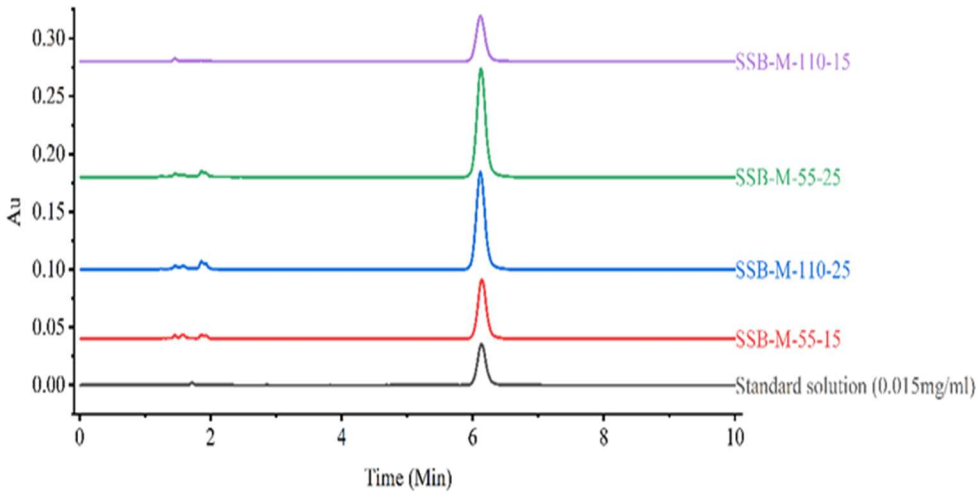

Figure 4-47 HPLC chromatograph of fenofibrate from the standard solution and extruded solid dispersions formulation (n=3).

Dissolution of different batches of fenofibrate solid dispersion and the physical mixture was carried out in phosphate buffer solution with 0.3% SDS added. In general, the drug dispersions exhibited a significantly faster rate and higher drug dissolution than the physical mixture of fenofibrate. The fenofibrate's physical mixture only dissolves around 10% maximum in the sink condition. The increase in the formulation's solubility resulted from the amorphous nature of the drug substance in the formulation. However, the pure amorphous state is not stable in solution, and drug substances will precipitate and recrystallise rapidly.

Nevertheless, the existence of a polymer matrix, even at very low concentrations, can be used to inhibit crystallisation from supersaturated solutions. The amorphous nature of fenofibrate in the drug formulation results from the higher and faster dissolution behaviour. However, the drug molecules are prone to aggregate and nucleate. Then the metastable amorphous drug would recrystallise to a more stable but less soluble form (Guzmán *et al.*, 2007; Ilevbare, Marsac and Mitra, 2015; Xavier, 2015). Moreover, because fenofibrate does not have any ionisable group, it is not ionised in the phosphate buffer solution, preferring the self-association and subsequent precipitation of the fenofibrate molecules (Jamzad and Fassihi, 2006)(Pezzoli *et al.*, 2019).

For twin-screw extrusion processing, the residence time is a very important parameter as it can determine the performance of the extrudate to a certain extent. The higher the residence time means more shear and heat are applied to the resultant extrudate, and better mixing performance can be achieved. Batches SSB55-M-55-15 to SSB55-M-110-15 are using the same screw configuration setup. However, SSB55-M-55-15 had a lower screw speed, indicating a longer residence time. The comparison of the profiles obtained from dissolution revealed a significant increase in the dissolution rates of SSB55-M-55-15 (Figure 4-48). For SSB55-M-55-15, over 25% of the drug was dissolved at 30 min. In comparison, the SSB55-M-110-25 and SSB55-M-110-15 showed dissolution of approximately 12.17% and 16.72%, respectively. Compared to SSB55-M-55-15, SSB55-M-55-25 had the same production screw speed but higher drug loading, which also showed a lower dissolution rate. This may be due to higher drug loading. The dissolution rate had enhanced due to the lower screw speed. Hence, SSB55-M-55-25 showed higher saturation solubility among different batches. In the dissolution test, only dissolved drug substance can be detected with the UV spectrophotometer, meaning that even though the formulation is fully degraded in dissolution media, it cannot be detected if the drug substance is not dissolved in dissolution media. As for SSB55-M-110-15, it shows a lower saturated drug concentration, which could be because the particle size of fenofibrate in formulation SSB55-M-110-15 is larger than

others. This is confirmed by SEM analysis in later result section 4.4.2.7.

The dissolution profile of SSB55-M-55-25 and SSB55-U-55-25 are shown in Figure 4-49, which were produced by the same screw speed but a different screw design with SSB55-M-55-25 being produced by the modified screw design. SSB55-M-55-25 shows a faster dissolution rate at the beginning owing to the new screw design, providing more shear, and mixing during the processing, a similar effect as reducing the screw speed and increasing the residence time. Also, the lower T_g value would have a higher dissolution rate than others (Farag and Leopold, 2009). Moreover, the error bars for batch SSB-U-55-25 are larger than SSB55-M-55-25 which further supports that the newly designed screw profile has a higher mixing efficiency than the universal screw design. It has a narrower error bar deviation than SSB-U-55-25, which indicates a more uniform dispersion for the extrudate. Figure 4-50 illustrates the dissolution profile of the fenofibrate formulation produced with different types of shellac materials. SWA-M-110-15 shows a higher dissolution rate compared to the other three formulations with 34% dissolved after the first 30 min and over 88% after 120min. This means the Bleached shellac SWANLAC has the highest dissolution rate than other types of shellac. Also, from section 4.1, the viscosity of 700K is higher than shellac SSB 55. With the same processing conditions, when materials have a higher viscosity would result in a more shear force during the process. This was also confirmed by the screw torque during processing. Shellac SSB 55 pharma FL have the lowest screw torque (10NM). The dissolution profile of formulations SSB55-M-55-15 and 702-M-55-15 was shown in Figure 4-51, these two batches were produced with lower processing screw speed (55RPM) and low drug loading with different shellac materials. SSB55-M-55-15 shows a higher dissolution rate than 702-M-55-15. However, the saturated concentration is higher than SSB55-M-55-15. This could also be confirmed by SEM analysis, 702-M-55-15 has a smaller fenofibrate particle size than SSB55-M-55-15.

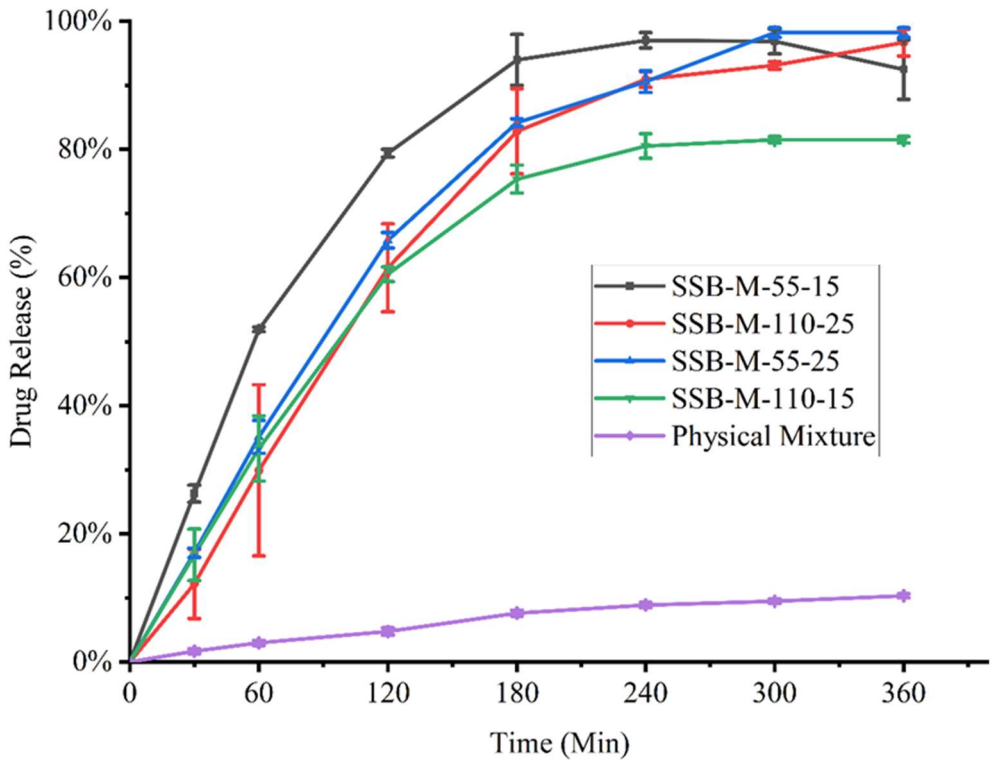

Figure 4-48 Dissolution profile of formulation produced by newly designed screw (n=3, $p<0.05$).

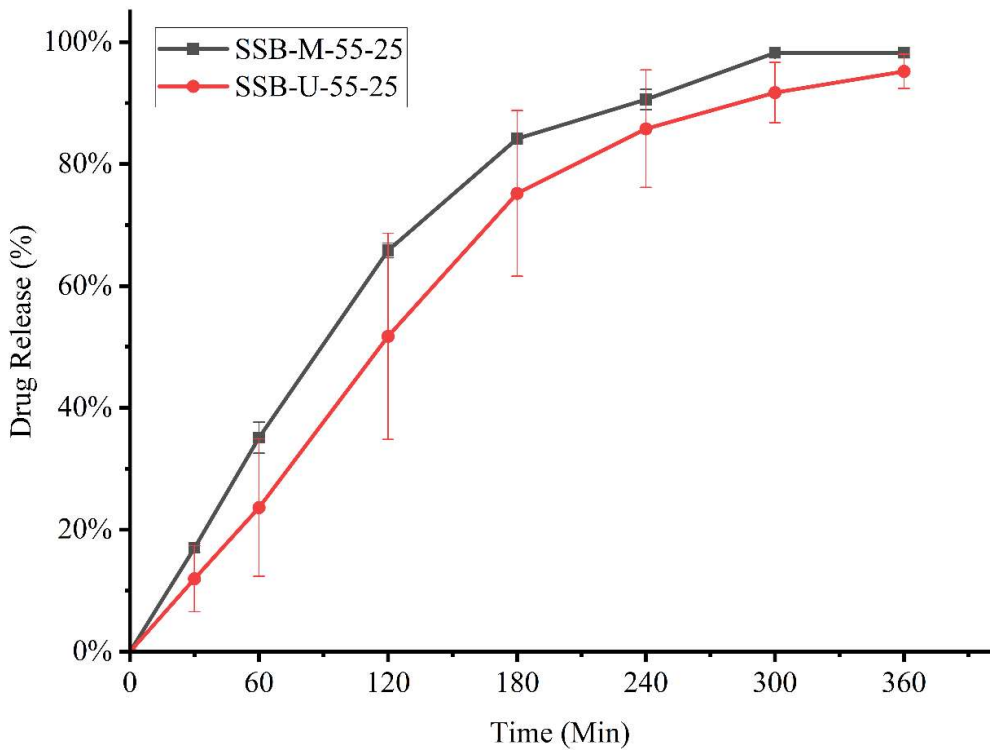

Figure 4-49 Dissolution profile of formulation produced by different screw designs (n=3, $p<0.05$).

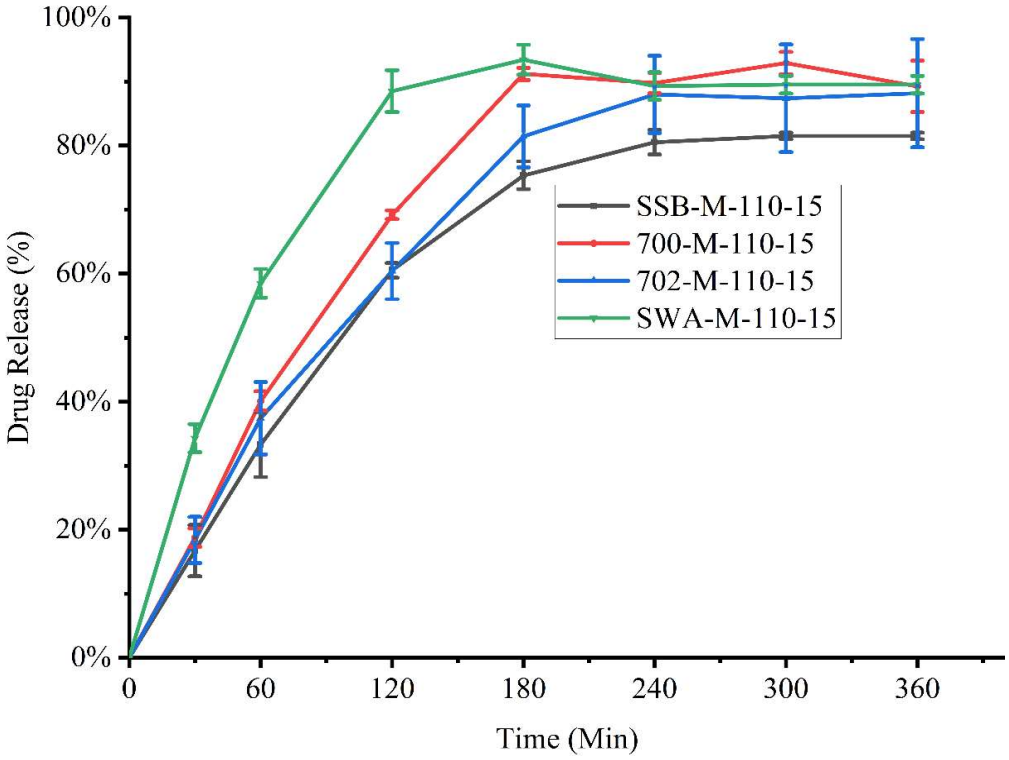

Figure 4-50 Dissolution profile of formulation produced by a different type of shellac (n=3, $p<0.05$).

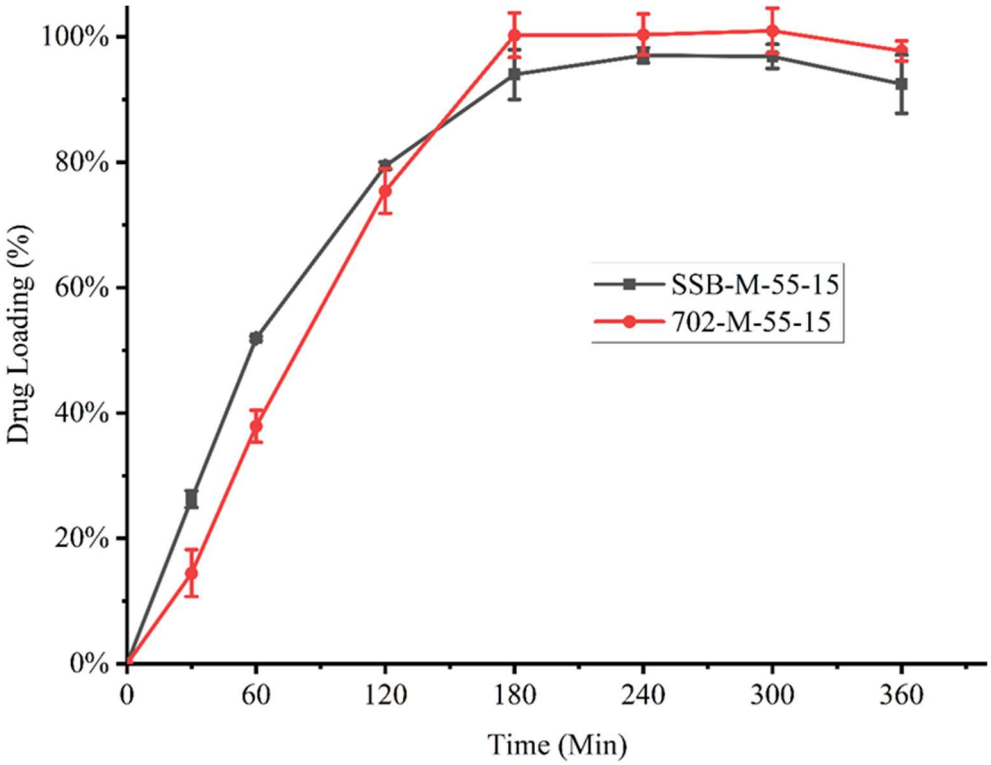

Figure 4-51 Dissolution profile of formulation produced by same formulation and screw design but a different type of shellac (n=3, $p<0.05$).

In the past three decades, with the development of controlled-release dosage forms, great progress has been made in the field of drug delivery (Wang et al., 2021) (Fu & Kao, 2010). Drug release is an important property of the treatment system, which is not only a prerequisite for drug absorption but also an important factor to determine the speed and degree of effective utilization of the body. The release modes include zero-order release, and first-order release and some drugs provide an initial rapid dissolution, followed by zero or first-order release of persistent components (Dash et al., 2010). The purpose of these systems is to keep the concentration of the therapeutic agent in blood or target tissue at an ideal value for as long as possible and control the drug release rate and duration (Langer & Wise, 2019).

By comparing the release data using different mathematical models, the physical mechanism of drug release can be identified. The release kinetics of each formulation in this study were evaluated by fitting the release data to a variety of standard kinetic models, including zero-order, first-order, Higuchi, Hixson-Crowell, Peppas-Sahlin and Korsmeyer-Peppas, Equations 3-1 to Equation 3-6 by DDsolver. The results are shown in Table 4-13 and Table 4-14.

DDSolver provides several statistical criteria for evaluating the 'goodness of fit' of a model, including the adjusted coefficient of determination (Rsqr adj or R2 adjusted), the Akaike Information Criterion (AIC), and the Model Selection Criterion (MSC). The model with a lower AIC value when comparing two models with different numbers of parameters can be thought of as being a better fit, but it is impossible to determine how much lower the value must be for the difference between the models to be statistically significant because the distribution of the AIC values is unknown. Moreover, the MSC has been standardized to be independent of the scaling of the data points and is a modified reciprocal form of the AIC. The model with the largest MSC will be the most suited model when comparing several models. Typically, a good fit is indicated by an MSC value of greater than two to three (Mayer et al., 1999). However, it should be noted that when mechanistic models are evaluated, model selection should be based, not only on the 'goodness of fit' but also on the

mechanistic plausibility of the model.

As shown in Table 4-13, statistical criteria data demonstrates that the drug release profile of SSB 55 pharma FL-based matrix was the best fit by the Peppas Sahlin model when assessed in a phosphate buffer solution having an R^2 value over 0.98 except SSB55-M-55-25 and SSB-U-110-15. Moreover, in the first 60 min, all the dissolution systems were best fit to the zero-order model with a high MSC value and low AIC number. All the kinetics models are valid only for the first 60% of the drug release (Statistical criteria) (Costa and Sousa Lobo, 2001). The diffusional exponent (m) and release constant (k_1, k_2) for fenofibrate release from the shellac matrix are shown in Table 4-14. All the formulations, except the SSB55-M-55-25 and SSB-U-110-15, showed values over 0.89. According to Peppas and Sahlin, when m = 0.45 the drug release mechanism is governed by the Fickian diffusion, when $0.45 < m < 0.89$ it is anomalous (non-Fickian) transport, and when m = 0.89 it is case II transport (Peppas and Sahlin, 1989; Bruschi, 2015; Unagolla and Jayasuriya, 2018). This means most of the formulation dissolution was governor by case 2 transport. Case 2 transport and Fickian transport are the limiting cases for the transport of an organic penetrant through an amorphous glassy polymer. When the stress relaxations controlled the dissolution, this release happens at a sharp boundary separating an outer surface of the polymer, which is called Case 2 transport. Moreover, this sharp boundary will move through the polymer at a constant velocity during dissolution (Jacques, Hopfenberg and Stannett, 1974). SSB55-M-55-15 and SSB-U-110-15 show an 'm' value lower than 0.89 but larger than 0.45, which indicates the anomalous transport happened. This is the combination of diffusion and erosion relaxation dissolution. In 2008, Sontaya also reported that the increased amount of shellac decreased the 'm' value of the shellac base formulation, from Case II transport (relaxation-controlled release) to Fickian transport (diffusion-controlled release) (Limmatvapirat, Limmatvapirat, *et al.*, 2008). In addition, this result also shows that the SSB55-M-55-25 and SSB-U-110-15 were the best fit by the Hixson Crowell model with R^2 values of 0.997 and 0.993, respectively. In this model the dissolution happens in planes parallel to the surface of

the dosage form, moreover, this surface decreases proportionally over time and the geometrical form maintains constant. For the formulation produced by different types of shellac material, the best fit model is unchanged, Peppas-Sahlin. However, Shellac AFS SWANLAC formulation has a lower m value smaller than 0.89. which means the drug is transported by Fickian diffusion and swelling and relaxation of the drug delivery system matrix.

A potential kinetic model of the developed drug platforms was assessed in the above findings. From the result, it can be found that the release of the drug in the formulation is only affected by time at the first 60 minutes. Which means the dissolution was determined by the dissolution of shellac material in dissolution media. With the dissolution progress, the drug release rate decrease, the amount of drug released form the material would affect by more factors, even limited by the precipitation of the drug itself. Therefore, mathematical models that describe the drug release in dissolution media accurately will be difficult or impossible due to this. The transport of drugs inside pharmaceutical dosage forms is governed by several phases which are influenced by physical and chemical factors. It is also possible that the type of drug(s), polymer(s), and the ratio of drug-polymer may affect the rate of release from the dosage generated, changing the kinetics of release.

Table 4-13 Statistical criteria for evaluating mathematic modelling and drug release kinetics from the shellac-based formulation (n=3).

				Zero order			First Order			Higuchi			Korsmeyer-Peppas			Hixson-Crowell			Peppas-Sahlin			Zero order in first 60min		
	Batch	Drug load	Screw speed	R^2 Adj	AIC	MSC	R^2 Adj	AIC	MSC	R^2 Adj	AIC	MSC	R^2 Adj	AIC	MSC	R^2 Adj	AIC	MSC	R^2 Adj	AIC	MSC	R^2 Adj	AIC	MSC
Modified Screw	P1	Low	55.000	0.491	70.032	-0.198	0.987	38.330	3.765	0.900	56.891	1.445	0.913	56.406	1.505	0.987	39.801	3.581	**0.993**	**36.505**	**3.993**	0.999	-0.697	6.737
	P2	high	110.000	0.813	62.181	1.124	0.971	46.175	3.125	0.928	54.860	2.039	0.937	54.978	2.025	0.983	42.157	3.627	**0.988**	**41.502**	**3.630**	0.979	4.885	3.725
	P3	high	55.000	0.800	63.188	0.926	0.986	41.476	3.640	0.981	50.748	2.481	0.955	52.120	2.309	**0.997**	**30.756**	**4.980**	0.995	34.261	4.541	0.998	1.877	5.121
	P4	low	110.000	0.701	63.538	0.484	0.974	44.196	2.902	0.940	50.833	2.073	0.933	52.446	1.871	0.942	50.450	2.120	**0.993**	**33.904**	**4.189**	0.997	2.063	4.925
Universal Screw	P9	low	55.000	0.748	67.787	0.646	0.915	59.017	1.743	0.958	53.110	2.481	0.952	55.084	2.234	0.955	53.955	2.375	**0.995**	**35.498**	**4.683**	0.993	-5.851	8.404
	P8	high	110.000	0.510	69.699	-0.076	0.965	48.666	2.553	0.875	58.869	1.278	0.878	59.487	1.201	0.968	47.802	2.661	**0.981**	**42.932**	**3.270**	0.998	1.299	5.705
	P11	high	55.000	0.870	56.224	1.875	0.964	48.617	2.826	0.915	56.122	1.887	0.952	51.471	2.469	0.981	43.818	3.426	**0.983**	**44.217**	**3.376**	0.998	-7.598	7.304
	P10	low	110.000	0.583	68.479	0.038	0.991	37.258	3.940	0.929	54.215	1.821	0.932	54.688	1.762	**0.993**	**35.391**	**4.174**	0.993	36.892	3.986	0.992	7.991	3.536
700K	P5	low	high	0.644	67.059	0.284	0.978	44.507	3.103	0.918	55.279	1.757	0.907	57.026	1.539	0.975	45.517	2.977	**0.988**	**41.177**	**3.520**	0.998	1.194	5.642
702MB	P6	low	high	0.709	64.342	0.505	0.984	40.769	3.452	0.943	51.139	2.156	0.936	52.974	1.926	0.968	46.769	2.702	**0.989**	**38.049**	**3.792**	1.000	-1.485	6.358
SWANLAC	P7	low	high	0.200	72.397	-0.831	0.965	47.248	2.312	0.806	61.002	0.593	0.896	56.786	1.120	0.936	52.111	1.704	**0.974**	**46.206**	**2.442**	0.987	10.826	3.038
702MB	P12	low	Low	0.683	68.142	0.521	0.943	54.573	2.218	0.891	59.960	1.544	0.879	61.504	1.351	0.970	49.309	2.876	**0.982**	**44.529**	3.473	0.969	9.841	2.775
	P13	high	high	0.837	61.757	1.205	0.972	47.939	2.932	0.940	53.919	2.184	0.944	53.992	2.175	**0.988**	**40.971**	**3.803**	0.982	45.485	3.239	0.992	6.041	3.569
	P14	high	Low	0.836	62.336	1.181	0.970	48.525	2.908	0.938	54.580	2.151	0.941	54.968	2.102	0.988	41.083	3.838	**0.990**	**41.431**	**3.775**	0.968	10.372	2.269
	Mixture			0.918	19.135	1.912	0.930	17.802	2.079	0.953	14.512	2.490	0.980	8.817	3.202	0.926	18.253	2.023	**0.985**	**7.189**	**3.406**	0.991	-9.394	3.853

Table 4-14 Mathematic modelling parameter for shellac-based formulation (n=3).

				Zero order	First Order	Higuchi	Korsmeyer-Peppas		Hixson-Crowell	Peppas-Sahlin			Zero order in first 60min
	Batch	Drug load	Screw speed	k_0	k_1	k_H	k_{KP}	n	k_{HC}	k_1	k_2	m	k_0
Modified Screw	P1	Low	Low	0.353	0.012	5.901	11.264	0.381	0.003	**2.008**	**-0.010**	**0.829**	0.867
	P2	high	High	0.332	0.008	5.379	3.594	0.601	0.002	**0.797**	**-0.002**	**0.973**	0.480
	P3	high	Low	0.342	0.009	5.569	4.297	0.548	**0.002**	0.779	-0.002	0.965	0.582
	P4	low	High	0.294	0.007	4.829	5.311	0.488	0.002	**0.876**	**-0.002**	**0.938**	0.555
Universal Screw	P9	low	Low	0.414	0.014	6.789	6.602	0.506	0.004	**1.296**	**-0.004**	**0.913**	0.805
	P8	high	High	0.343	0.011	5.721	9.869	0.405	0.003	**1.397**	**-0.006**	**0.915**	0.744
	P11	high	Low	0.316	0.007	5.076	2.559	0.698	0.002	**0.868**	**-0.002**	**0.957**	0.395
	P10	low	High	0.351	0.011	5.830	9.246	0.415	**0.003**	1.741	-0.008	0.843	0.794
700K	P5	low	high	0.333	0.009	5.494	6.852	0.460	0.003	**0.955**	**-0.002**	**0.946**	0.660
702MB	P6	low	high	0.313	0.008	5.149	5.583	0.488	0.002	0.941	-0.003	0.928	0.621
SWANLAC	P7	low	high	0.342	0.015	5.811	18.579	0.286	0.004	4.136	-0.045	0.698	1.008
702MB	P12	low	Low	0.367	0.011	6.021	6.022	0.512	0.003	**0.643**	**-0.001**	**1.072**	0.602
	P13	high	high	0.338	0.008	5.467	3.217	0.600	**0.002**	0.595	-0.001	1.016	0.503
	P14	high	Low	0.343	0.009	5.553	3.226	0.601	0.002	0.509	-0.001	1.044	0.495
	Mixture			0.033	0.000	0.530	0.211	0.677	0.000	-6.059	4.063	0.160	0.051

4.4.2.6 *Rheology*

Complex viscosity versus angular frequency (rad/s) curve at 90 ºC for virgin shellac SSB 55 Pharma FL and formulation SSB55-M-110-15, SSB-U-110-15 were illustrated in Figure 4-52. A dramatic decrease in complex viscosity is observed with the incorporation of the fenofibrate. For all the samples tested, with increasing angular frequency, their complex viscosity decreases at lower test angular frequency. However, when the frequency continues to increase the viscosity remains steady state because the material has reached its second steady platform. All the molecular chains have been completely disentangled (Mezger, 2012). Formulation SSB55-M-110-15 had a lower viscosity than SSB-U-110-15 in all the ranges tested, mainly because SSB55-M-110-15 has a better dispersion than SSB-U-110-15, HPLC analysis also supports the result that SSB55-M-110-15 has a lower standard error than SSB-U-110-15. Additionally, higher content of melting fenofibrate appears to help the shellac chain to flow more (Mezger, 2006)(Mezger, 2020).

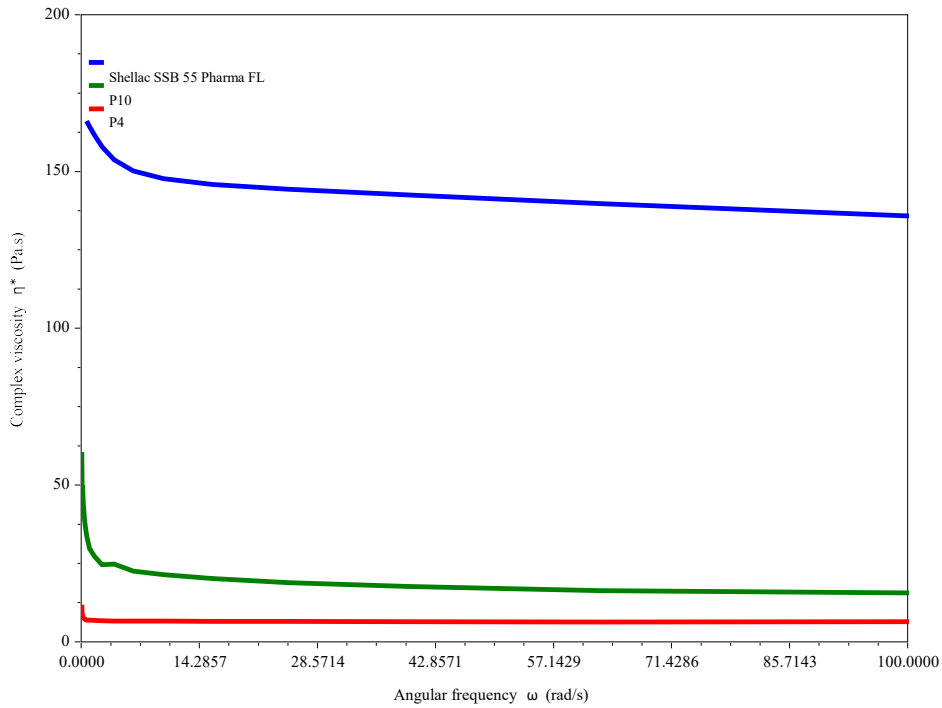

Figure 4-52 Complex viscosity versus angular frequency (rad/s) curves at 90 ºC for shellac SSB 55 Pharma Fl and formulation SSB55-M-110-15 (New screw design), SSB-U-110-15 (Universal screw design) (n=3).

4.4.2.7 *Scanning electron microscopy (SEM)*

To study the surface morphology of various solid dispersion formulations, an SEM analysis was carried out, and these images are depicted in Figure 4-53. SEM was employed to investigate the surface morphology of the samples. A physical mixture, the image of the virgin fenofibrate mixture exhibited large, compact crystals at the micron scale and physically adsorbed on the surface of the carrier particles. However, a clear boundary between them can be found. As for the shellac a smooth surface was observed, moreover, for Shellac 700K, 702MB and SSB 55 the existence of scratches was caused by the blade when grinding them to powder. However, shellac HS SWANLAC was received as powder form without further grinding process, they show an irregular spherical shape rather than a flat surface. This is due to the processing method difference, HS SWANLAC was precipitated from the shellac solution by adding dilute sulphuric acid. All the solid dispersion of fenofibrate and shellac formulation showed a homogeneous dispersion indicating that the fenofibrate molecules were dispersed uniformly in carrier matrices. No crystals of fenofibrate were observed because of the homogeneous blending of fenofibrate and shellac polymers during the melt extrusion process used to prepare the solid dispersions and the ability of the shellac polymers to inhibit crystal growth. The P-XRD and DSC results confirmed that fenofibrate was molecularly dispersed within polymers. Compared to the physical mixture, the SEM image of this processed formulation also indicates the reduced particle size of the drug substance. Thus, the improvement in solubility and dissolution rate was attributed to the conversion of the crystalline drug into the amorphous state and the reduced particle size.

For batches SSB55-M-55-15, SSB55-M-110-25 and SSB55-M-110-15, produced by the same screw design but with different screw speeds and mixing methods, the size of fenofibrate spherical particles in SSB55-M-110-15 is larger than in the other two, which may be because of the higher screw speed resulting in lower residence time. From the dissolution result, SSB55-M-110-15 shows a lower saturated drug concentration. In Figure 4-54,

formulations SSB55-M-110-15 and SSB-U-110-15, produced by different screw configurations are depicted. The SEM image shows that fenofibrate is evenly dispersed in the formulation. However, for formulation SSB-U-110-15 there is one area had much less fenofibrate dispersed on it compared to other areas (Figure 4-54). This phenomenon further confirmed that; the newly designed screw configuration has a better mixing efficiency than the universal screw design.

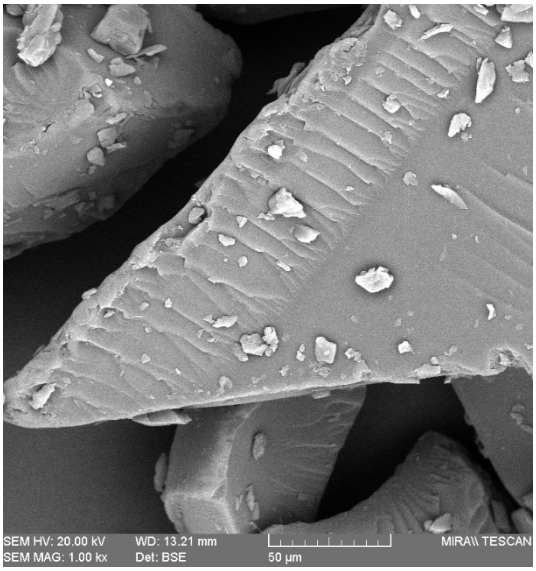

Dewaxed shellac AFS HS 700K

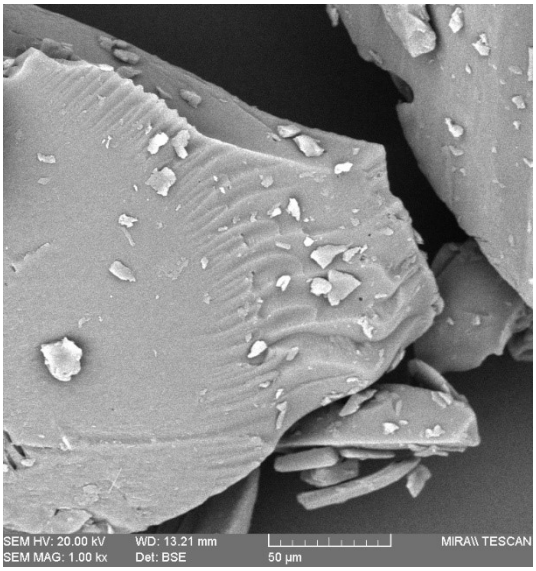

Dewaxed shellac AFS HS 702MB

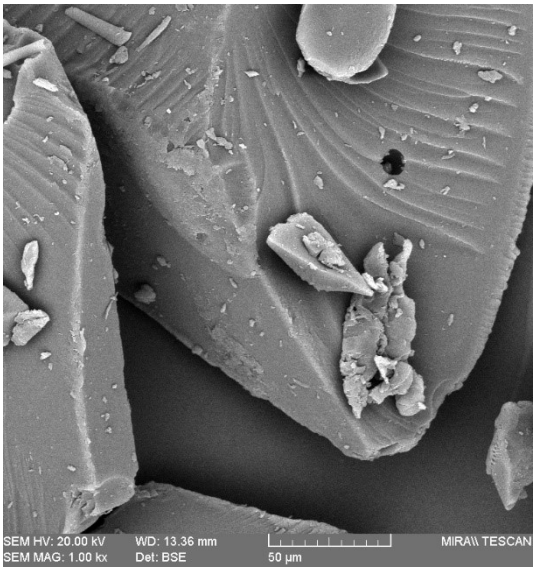

Shellac SSB 55 Pharma FL

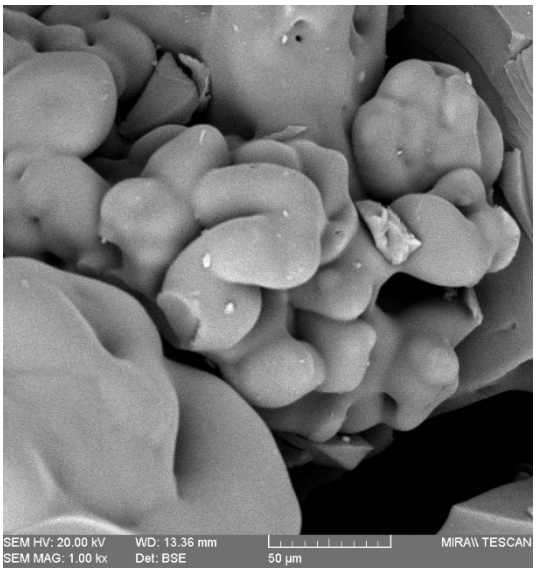

AFS shellac HS SWANLAC

Figure 4.54 SEM image of the unprocessed shellac (Dewaxed shellac AFS HS 700K, 702MB, SSB 55,

AFS HS SWALAC)

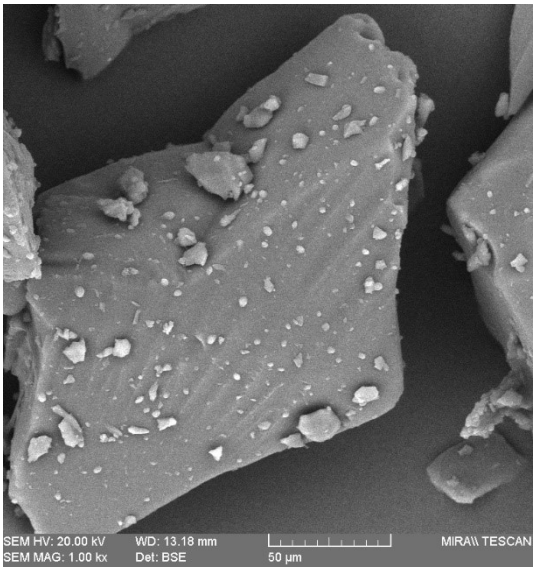

SSB55-M-55-15

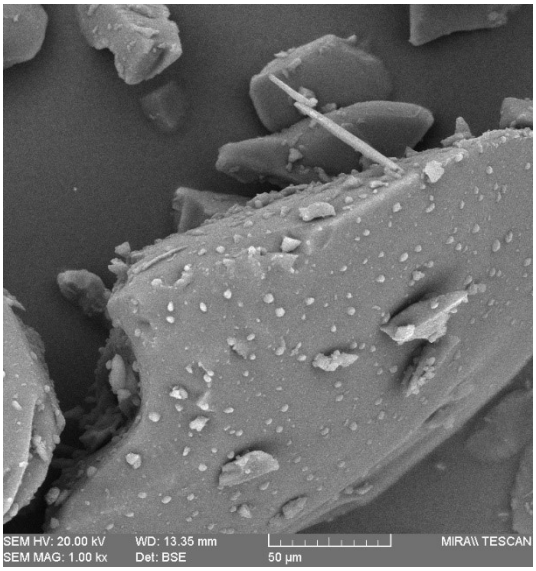

SSB55-M-110-25

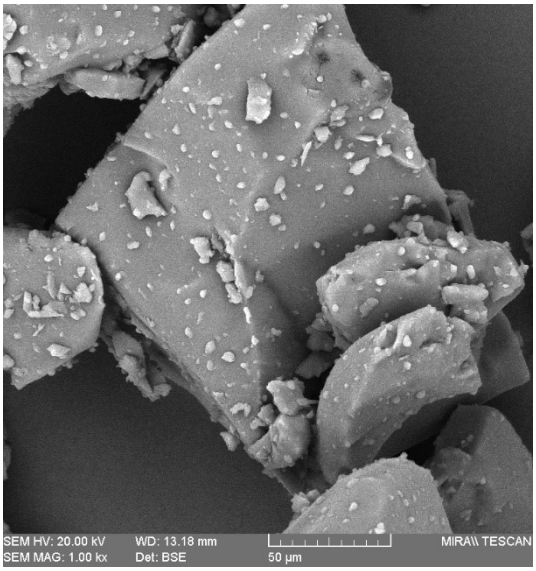

SSB55-M-110-15

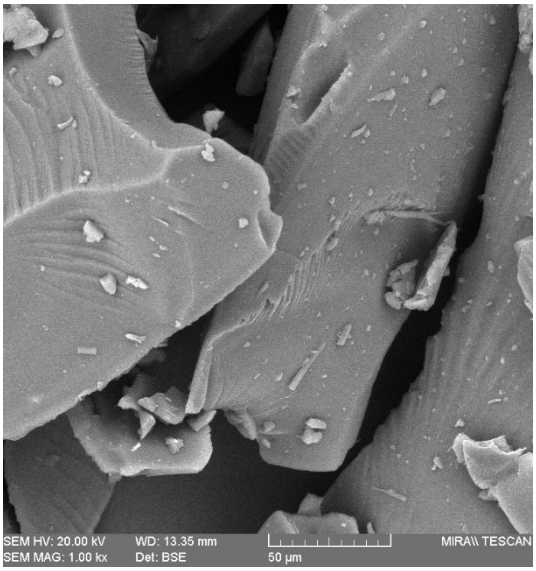

700-M-110-15

Figure 4.54 SEM image of the drug formulation (SSB55-M-55-15, SSB55-M-110-25, SSB55-M-110-15, 700-M-110-15

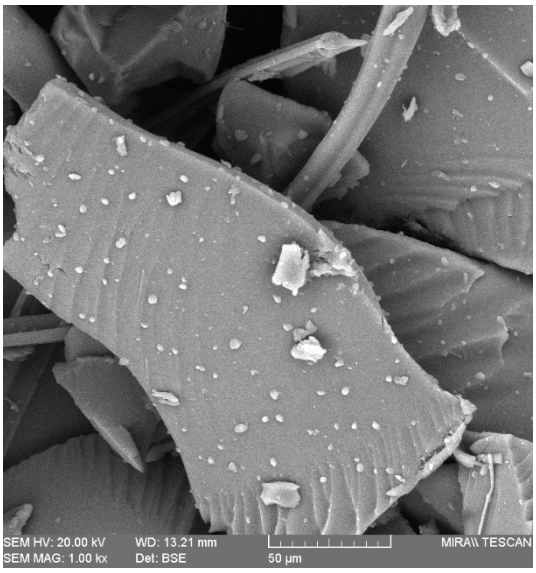

702-M-110-15

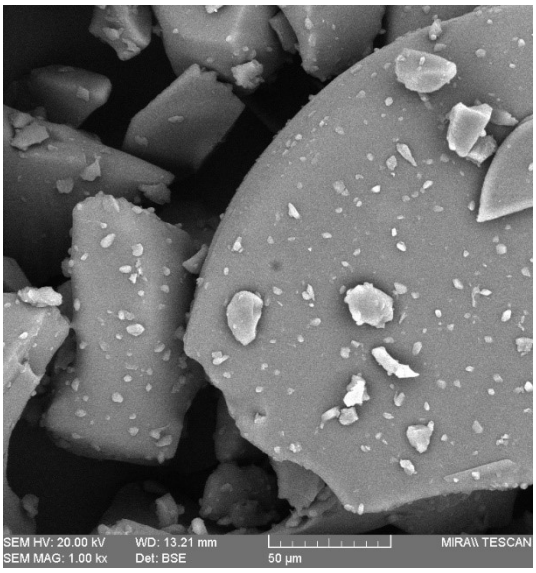

SWA-M-110-15

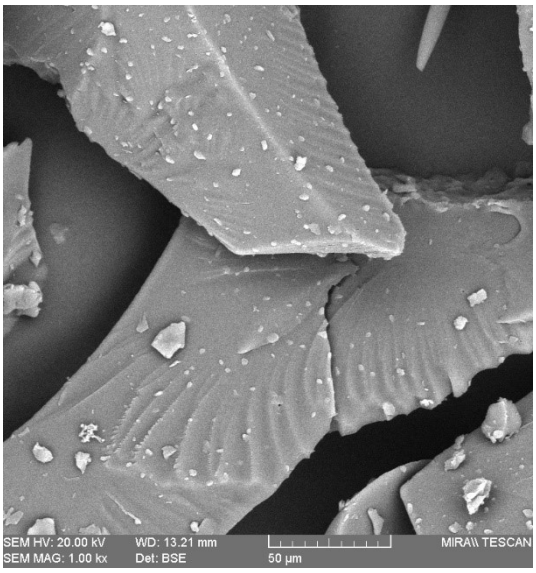

702-M-55-15

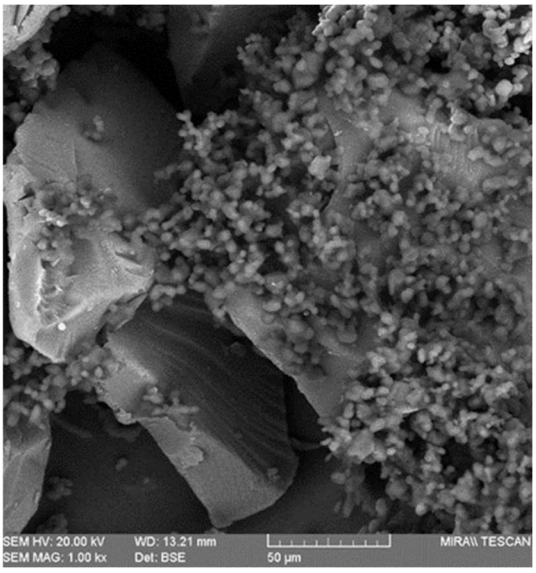

Physical mixture

Figure 4-53 SEM image of the unprocessed shellac (Dewaxed shellac AFS HS 700K, 702MB, SSB 55, AFS HS SWALAC), drug formulation (SSB55-M-55-15, SSB55-M-110-25, SSB55-M-110-15, 700-M-110-15, 702-M-110-15, SWA-M-110-15, 702-M-55-15) and physical mixture (Physical mixture)

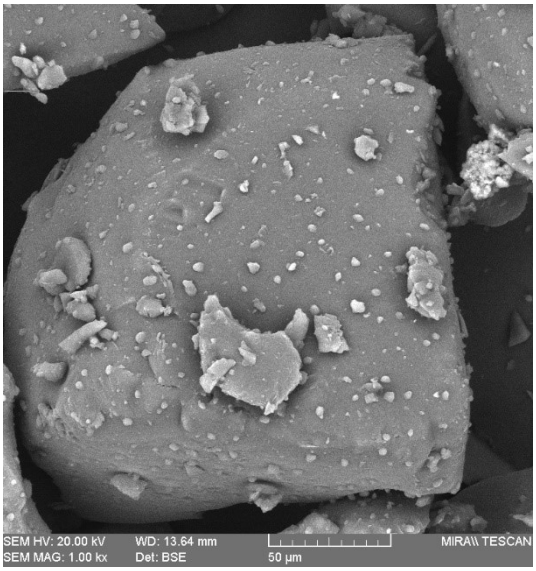

SSB55-M-110-15

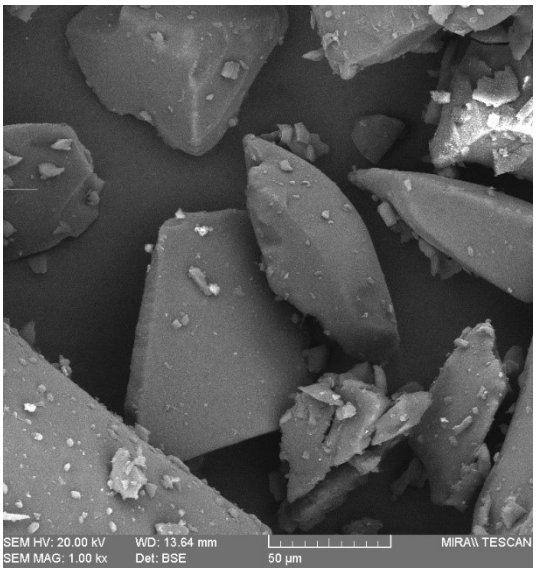

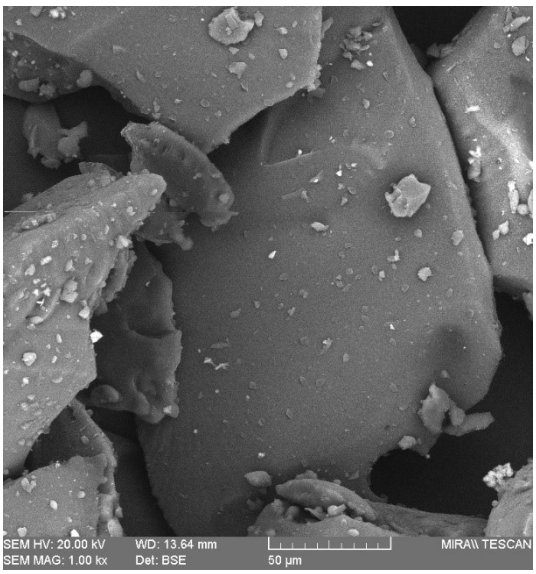

SSB-U-110-15

Figure 4-54 SEM Image of SSB55-M-110-15 and SSB-U-110-15

4.4.3 **Summary**

In this section, the formulation of fenofibrate as an amorphous solid dispersion with different shellac materials by a hot melt extrusion process with two different screw designs has been demonstrated to increase the solubility of fenofibrate. This can help reduce the required dose and improve therapeutic outcomes. With the use of either type of shellac, the improvement in the extent of solubility, and the rate of dissolution over that of fenofibrate have been achieved. The formed amorphous solid dispersion formulation improved the solubility by over 8-times relative to untreated fenofibrate. The fenofibrate-shellac binary

system provides a different approach from the traditional strategies and can be considered as a convenient choice for optimising the oral delivery of fenofibrate. Moreover, shellac base drug delivery system has an innate advantage due to its pH-sensitive nature and can be used as a colon target delivery system. Additionally, this study also confined the success in newly designed screw configurations. Compared to the universal screw design, the new screw design has higher mixing efficiency. The new screw design would result in more shear to the drug formulation during the processing and provide higher mixing efficiency than the universal screw design. This results in a smaller standard error of drug content in the extrudate. By analysing the drug dissolution profile, the best-fit mathematical model for most of the formulations is the Peppas-Sahlin model. The diffusional exponent indicates that the drug release mechanism of most formulations is governed by Case 2 transport. Moreover, the increase in shellac content will change the release mechanism from Case II transport (relaxation-controlled release) to Fickian transport (diffusion-controlled release). However, more study is needed to prove the mechanism of the fenofibrate dissolution in the molten shellac polymer and the mechanism of the dissolution of the formulation in media. Further study is recommended to fully understand the dissolution mechanism of the formulation and inform future work on how to modify the drug release profile.

Chapter 5 Conclusion

Milestones in this study

- Increased the solubility of fenofibrate by over 8 times compared to the virgin drug.
- Created a drug delivery platform which can form amorphous solid dispersion and be used as a colon target drug delivery system.
- The formulation can hold the amorphous state of fenofibrate over 8 months (at room temperature).
- Evaluated the processability of the raw Shellac material.
- Produced shellac polymer-based drug formulation prototypes and evaluated their properties.
- Modelling and simulating the melt extrusion processing and creating a modified screw design.
- Optimized the processing conditions to produce uniform formulations and characterised the new formulations.

Hot Melt Extrusion (HME) has attracted recent interest from the pharmaceutical industry and academia as a technology which can enable innovative drug delivery routes. Although scientists have discovered a large number of potential drug compounds using new technologies, however, many drugs cannot even pass the initial solubility test due to backward formulation technology. As a result, numerous novel processing techniques have been introduced to the pharmaceutical sector, to increase the effectiveness and efficiency of all aspects of the manufacturing process, including design, control, and quality assurance.

The primary aim of this research was to create an advanced drug delivery platform and enhance the solubility and bioavailability of the model drug as an amorphous hot melt

extrusion solid dispersion. Specific objectives included the investigation of different types of shellac polymer, the use of HME to form shellac-based polymeric drug solid dispersions, characterisation of the prototype of the drug formulation, and optimisation of the drug melt extrusion processing.

In section 4.1, various types of shellac material were explored and their physicochemical properties and processability were analysed. Physical, thermal and rheology investigations of the shellac materials were done to support its applicability in hot melt extrusion as a polymer matrix used in drug delivery platforms. All shellac samples were amorphous and had no variation in chemical structure by FTIR. During DSC analysis, the existence of a peak in two wax-containing shellac materials was owing to the presence of the wax. And all the shellac material shows a glass transition temperature of around 40-50˚C. The viscosity of the various shellac materials in this investigation was demonstrated to follow shear-thinning behaviour, typical of many polymer responses, and corresponded well with the melt flow index value. The wax-containing shellac material has a higher viscosity than the dewaxed shellac material. Moreover, based on the rheology results, the processing temperature ranges of different types of shellac for melt extrusion could be identified as around 75-100˚C. Nevertheless, because of the shear-thinning properties, shellac can be extruded at a lower temperature. During the extrusion process, the material experiences a variety of temperatures and shear stress. In addition, the melting behaviour of the material during extrusion is significantly affected by the viscosity of the melted polymer. The processability of materials is significantly affected by how the polymer responds to flow and strain. When determining the extrusion parameters before processing, high viscosity polymers, always require higher melting temperature profiles and resulting in higher shear rates. Additionally, compared to the other shellac materials, shellac SSB 55 Pharma had the lowest process temperature, which implies maximum processability. This section gives critical data to evaluate the process conditions for the hot melt extrusion process employing shellac material in the next section. The content of wax and the ageing process of shellac

have major effects on the physical properties of shellac. However, the ageing behaviour of shellac is based on the self-esterification of one ingredient of the natural resin: aleuritic acid. This shift can be recognized by gas chromatography-mass spectrometry technology. As a result, future investigations are proposed to employ GC-MS or HPLC/MS technology to identify the chemical content differences of the various types of shellac.

In section 4.2, based on the result in section 4.1, the processing condition for the drug formulation was determined, with a screw speed of 55 RPM and 110 RPM, processed with a temperature range from 30 to 90˚C. The formulation of fenofibrate as an amorphous solid dispersion with shellac matrix by hot melt extrusion process was produced and investigated. In this section, it demonstrates that additional processing aids were not necessary to produce the formulation and to increase the solubility of fenofibrate. The amorphous solid dispersion formulation improved the solubility of fenofibrate by over 8-times relative to untreated fenofibrate. Increased solubility of fenofibrate can help to reduce the required dose and improve therapeutic outcomes, with the use of either type of shellac. The fenofibrate-shellac binary system provides a different approach from the traditional strategies and can be considered a convenient choice for optimizing the oral delivery of fenofibrate. Moreover, shellac base drug delivery system has an innate advantage due to its pH-sensitive nature and can be potentially used as a colon target delivery system. Moreover, this section also shows that the processing conditions as well as the different types of shellac can significantly affect the properties of the formulation. Batch 29 was shown to have some fenofibrate crystal still present when processing with the lower screw speed. Conversely, the batch with the same drug loading and shellac type but processed using a higher screw speed resulted in a completely amorphous fenofibrate dispersion. Also, batch 13 with the same drug loading and processed with the same screw speed, shows a completely amorphous formulation. This body of work also supports the results reported in section 4.1, where Shellac SSB 55 Pharma FL had the best processing performance compared to all other shellacs. However, this section shows the limitations of a universal screw structure due to poor mixing of the kneading

elements section. The drug content in the drug formulation is altered, resulting in the error bars in the dissolution data showing a large overlay. Additionally, the dissolution profiles were equivalent when the maximal solubility of the drug in the aqueous solution was reached. One potential solution to increase the maximum solubility in the aqueous solution is to add a surfactant (Sodium Dodecyl Sulfate (SDS)) into the dissolution media.

In section 4.3, the extrusion processing was modelled and simulated, to find out the optimised screw design with improved mixing performance. The mixing of different compounds is a key step in extrusion processes. The quality of the final product obtained with a twin-extruder depends, in the main, on the dispersive and distributive mixing generated by the kneading blocks. This section uses numerical simulation techniques to simulate and understand the impact of two classical geometrical parameters on the mixing: the influence of different screw speeds and staggers angle of a kneading block on mixing performance. The result was analysed based on some mixing characteristic parameters such as the maximum shear rate, stretching rate, mixing index, time-averaged efficiency, and the residence time distribution. With the screw speed increase, the intensity of shear and elongational flow strengthened, but at the same time, the residence time of the material will be reduced. From the simulations, considering various impacts, the twin-screw extruder has the best mixing performance when the screw speed is around 60 RPM because it has the highest flow intensity and the optimal residence time distribution. As for the stagger angle of the kneading blocks, the mixing performance increased with the increased stagger angle. On the contrary, the residence time increase with the increase of the tagger angle. So, a mixture of three distinct stagger angles is needed, the 30˚ stagger angle kneading portion can bring up enough material to the following part, and the 60˚ stagger angle has the best overall mixing performance. And the last section is a 90˚ stagger kneading block attached near the end of the mixing section, to guarantee all the material has undergone high shear and dispersive mixing. The optimised screw design was brought to the next section to verify its performance of the optimised screw design.

In section 4.4, an optimised screw design was used to produce the drug formulation, also two new materials were brought into the production line to find how different type of shellac affects the properties of the drug formulation. The solubility of fenofibrate has been increased over 8 times compared to untreated fenofibrate by using a hot melt extrusion process with two different screw designs. The extent of solubility and rate of dissolution of fenofibrate were improved when any type of shellac was used. From the analysis result, all the fenofibrate in the formulation is in a completely amorphous state. After 8 months of storage, the DSC thermographs did not indicate recrystallisation had occurred. This indicates that the amorphous shellac polymer matrix prevents recrystallisation from occurring due to the amorphous nature of the shellac material. The shellac HS 702MB shows a higher T_g value than other shellacs. Moreover, shellac HS SWANLAC shows a higher dissolution rate than other formulations. This further supported that the properties of the shellac material would be affected by its refining process and type of seedlac. Furthermore, because of the pH sensitivity of shellac material, the shellac-based drug delivery system has an inherent advantage and can be used as a colon target delivery system. This research also confined the success of the optimised designed screw configurations. The new screw design has a higher mixing efficiency than the universal screw design. The new screw design would impart more shear to the drug formulation during processing and improve mixing efficiency over the universal screw design. As a result, the drug content in the extrudate samples had a reduced standard error. Moreover, Peppas-Sahlin is the best fit mathematical model for most formulations based on dissolution profiles. The diffusional exponent indicates that the drug release mechanism of most formulations is governed by Case II transport. Additionally, higher Shellac content will change the formulation release mechanism from Case II transport (relaxation-controlled release) to Fickian transport (diffusion-controlled release). It is, however, recommended to conduct more research in follow on studies to determine how fenofibrate dissolves in molten shellac polymer and how the formulation dissolves in dissolution media. To better understand the dissolution mechanism of the formulation and

modify drug release profiles in the future, it is recommended that further research be conducted.

Chapter 6 Recommendations for future work

To gain an improved understanding of the processes and formulations developed during this work, the following further work is recommended:

- To examine existing downstream technologies to develop a novel functional downstream tabletting/palletisation technology.
- Developed fenofibrate solid dispersion formulations can be suitably converted to patient-compliant oral dosage forms by the novel downstream technology.
- Quantification of the mechanical properties of the prepared fenofibrate solid dispersion formulation would be useful to gain further insight into the extrusion process.
- Fully understand the mechanism of solubility enhancement by shellac base drug delivery platform.
- Particle size analysis for the raw material and result formulation would be of benefit to gain insight into the mechanism of solubility enhancement.
- Alternative test method for material temperature stability, Isothermal temperature study in TGA analysis. Instead of heating the material to a very high temperature at a constant speed, heat the material at a specific temperature and maintain that temperature for a longer time period.
- *In VIVO* analysis needs to be carried out for the model drug, the appropriate dosage loading for the drug formulation would change because of the increased solubility.
- In this study, only one single drug fenofibrate was investigated in detail. It is therefore suggested that other poorly soluble APIs would be interesting to study in greater detail. Fenofibrate is a low melting point drug (80˚C), and the processing temperature is above its melting temperature. As a result, fenofibrate is fully melted during the process and forms the amorphous solid dispersion upon cooling. In the case of Nifedipine, its melting temperature is much higher than the processing

temperature. Therefore, a study of the solubility of the different drugs in shellac material is recommended.

- The natural ageing processing of the shellac material is inevitable; therefore, the optimising of the shellac material is a useful strategy to minimise this effect. Also, the drug release profile can be optimised by the modification of shellac material.
- Due to the limitation of computer performance, the simulation calculation is not calculated according to the actual length of the screw, but one pitch of the screw instead. Therefore, a full length of screw simulation or periodic boundary conditions is recommended in the future to have more accurate simulation data.
- Establish the mechanism of fenofibrate dissolution in molten shellac polymer and the mechanism of formulation dissolution in media which inform future work on how to modify the drug release profile.
- Investigate the possibility of pre-dissolve the shellac material and model drug into the solution to obtain a homogeneous mixture before hot melt extrusion processing.
- The stability analysis of the formulation was performed by DSC only, which needs more analysis to confirm its phase state and drug content. Also, the chemical stability of the model drug would need to be assessed.

Chapter 7 References

Abuzar, S.M. *et al.* (2018) 'Enhancing the solubility and bioavailability of poorly water-soluble drugs using supercritical antisolvent (SAS) process', *International Journal of Pharmaceutics*, 538(1–2), pp. 1–13. Available at: https://doi.org/10.1016/j.ijpharm.2017.12.041.

Adeli, E. (2014) 'A comparative evaluation between utilizing SAS supercritical fluid technique and solvent evaporation method in preparation of Azithromycin solid dispersions for dissolution rate enhancement', *Journal of Supercritical Fluids*, 87, pp. 9–21. Available at: https://doi.org/10.1016/j.supflu.2013.12.020.

Agrawal, S. *et al.* (2022) 'Quality aspects in the development of pelletized dosage forms', *Heliyon*, 8(2), p. e08956. Available at: https://doi.org/10.1016/j.heliyon.2022.e08956.

Aho, J. *et al.* (2015) 'Rheology as a tool for evaluation of melt processability of innovative dosage forms', *International Journal of Pharmaceutics*, 494(2), pp. 623–642. Available at: https://doi.org/10.1016/j.ijpharm.2015.02.009.

Al-Gousous, J., Penning, M. and Langguth, P. (2015) 'Molecular insights into shellac film coats from different aqueous shellac salt solutions and effect on disintegration of enteric-coated soft gelatin capsules', *International Journal of Pharmaceutics*, 484(1–2), pp. 283–291. Available at: https://doi.org/10.1016/j.ijpharm.2014.12.060.

Alavijeh, M.S. and Palmer, A.M. (2004) 'The pivotal role of drug metabolism and pharmacokinetics in the discovery and development of new medicines', *IDrugs*, 7(8), pp. 755–763.

Alsteens, B., Legat, V. and Avalosse, T. (2004) 'Parametric study of the mixing efficiency in a kneading block section of a twin-screw extruder', *International Polymer Processing*, 19(3), pp. 207–217. Available at: https://doi.org/10.3139/217.1836.

Alzahrani, H., Bedir, Y. and Al-Hayani, A. (2013) 'Efficacy of shellac, a natural product, for the prevention of wet gangrene', *Journal of International Medical Research*, 41(3), pp. 795–

803. Available at: https://doi.org/10.1177/0300060513483391.

Amidon, G.L. *et al.* (1995) 'A Theoretical Basis for a Biopharmaceutic Drug Classification: The Correlation of in Vitro Drug Product Dissolution and in Vivo Bioavailability', *Pharmaceutical Research: An Official Journal of the American Association of Pharmaceutical Scientists*, pp. 413–420. Available at: https://doi.org/10.1023/A:1016212804288.

Amstad, E., Spaepen, F. and Weitz, D.A. (2015) 'Crystallization of undercooled liquid fenofibrate', *Physical Chemistry Chemical Physics*, 17(44), pp. 30158–30161. Available at: https://doi.org/10.1039/c5cp04958j.

Angadi, G. *et al.* (2017) 'Effect of screw configuration on the dispersion of nanofillers in thermoset polymers', *Journal of Polymer Engineering*, 37(8), pp. 815–825. Available at: https://doi.org/10.1515/polyeng-2015-0427.

Ansys (2015) 'Example 37 Mixer 2-D'. Lebanon,New Hampshire: ANSYS, Inc.

Ansys (2022) *ANSYS Polystat User's Guide*. Lebanon,New Hampshire: ANSYS, Inc.

ANSYS (2022a) *Ansys Polyflow Polymer Processing Simulation Software*. Available at: https://www.ansys.com/en-gb/products/fluids/ansys-polyflow#tab1-1 (Accessed: 15 September 2022).

ANSYS (2022b) *Brand Story Tell Us It's Impossible*. Available at: https://www.ansys.com/en-gb/the-ansys-story (Accessed: 15 September 2022).

ANSYS, I. (2021) 'ANSYS Polyflow user's guide'. ANSYS, Inc. Available at: http://www.ansys.com.

Anton, F. (1938) 'Method and apparatus for the production of fibers'. Available at: https://patentimages.storage.googleapis.com/24/1a/6b/afe03b025f711d/US2123992.pdf (Accessed: 26 July 2018).

Ardelean, M. *et al.* (2018) *In Vitro Dissolution Methodology And Estimated Consequences Of Biowaiver Extension For Immediate Release Solid Oral Dosage Forms With Metformin Hydrochloride*, *FARMACIA*. Available at: http://www.revistafarmacia.ro/201801/art-03-

Ardelean_Stoicescu_Miron_18-25.pdf (Accessed: 16 August 2018).

Arnautov, A., Korhov, V. and Faitelson, F. (2013) 'Physicomechanical Properties of Shellac Films', *Mechanics of Composite Materials*, 49(2), pp. 163–171.

Austen Angell, C. and Sivarajan, S. (2017) 'Glass Transition', in *Reference Module in Materials Science and Materials Engineering*. Elsevier. Available at: https://doi.org/10.1016/B978-0-12-803581-8.03155-6.

Azouka, A., Huggett, R. and Harrison, A. (1993) 'The production of shellac and its general and dental uses: a review', *Journal of Oral Rehabilitation*, 20(4), pp. 393–400. Available at: https://doi.org/10.1111/j.1365-2842.1993.tb01623.x.

Badens, E. *et al.* (2017) 'Current situation and perspectives in drug formulation by using supercritical fluid technology', *Journal of Supercritical Fluids, The*, (November 2017), pp. 0–1. Available at: https://doi.org/10.1016/j.supflu.2017.12.038.

Baghel, S., Cathcart, H. and O'Reilly, N.J. (2016) 'Polymeric Amorphous Solid Dispersions: A Review of Amorphization, Crystallization, Stabilization, Solid-State Characterization, and Aqueous Solubilization of Biopharmaceutical Classification System Class II Drugs', *Journal of Pharmaceutical Sciences*, 105(9), pp. 2527–2544. Available at: https://doi.org/10.1016/j.xphs.2015.10.008.

Baird, J.A. and Taylor, L.S. (2012) 'Evaluation of amorphous solid dispersion properties using thermal analysis techniques', *Advanced Drug Delivery Reviews*, 64(5), pp. 396–421. Available at: https://doi.org/10.1016/j.addr.2011.07.009.

Balendiran, G.K. *et al.* (2012) 'Biomolecular Chemistry of Isopropyl Fibrates', *Journal of Pharmaceutical Sciences*, 101(4), pp. 1555–1569. Available at: https://doi.org/10.1002/jps.23040.

Barnes, H.A., Hutton, J.F. (John F. and Walters, K. (1989) *An introduction to rheology*. Elsevier. Available at: https://books.google.ie/books/about/An_Introduction_to_Rheology.html?id=B1e0uxFg4oYC&redir_esc=y (Accessed: 31 July 2018).

Bates, S. *et al.* (2006) 'Analysis of Amorphous and Nanocrystalline Solids from Their X-Ray Diffraction Patterns', *Pharmaceutical Research*, 23(10), pp. 2333–2349. Available at: https://doi.org/10.1007/s11095-006-9086-2.

Bavishi, D.D. and Borkhataria, C.H. (2016) 'Spring and parachute: How cocrystals enhance solubility', *Progress in Crystal Growth and Characterization of Materials*, 62(3), pp. 1–8. Available at: https://doi.org/10.1016/j.pcrysgrow.2016.07.001.

Bedoya, D.A. *et al.* (2020) 'Stimuli-Responsive Polymeric Systems for Smart Drug Delivery', in. Springer International Publishing, pp. 115–134. Available at: https://doi.org/10.1007/978-3-030-46923-8_5.

Belyatskaya, A. V. *et al.* (2019) 'Dissolution of Ketoprofen from Poly(Ethylene Glycol) Solid Dispersions', *Pharmaceutical Chemistry Journal*, 52(12), pp. 1001–1006. Available at: https://doi.org/10.1007/s11094-019-01941-0.

Beneš, M. *et al.* (2017) 'Methods for the preparation of amorphous solid dispersions – A comparative study', *Journal of Drug Delivery Science and Technology*, 38, pp. 125–134. Available at: https://doi.org/10.1016/j.jddst.2017.02.005.

Benjamin, E.J. *et al.* (2018) *Heart disease and stroke statistics - 2018 update: A report from the American Heart Association*, *Circulation*. Available at: https://doi.org/10.1161/CIR.0000000000000558.

Bhowmik, D., Sahu, S. and Sahu, C. (2016) *Recent Trends in Sustained Release Drug Delivery System-an overview*. Uttar Pradesh. Available at: https://www.farmavita.net/documents/Matrix Drug Delivery System.pdf.

Bochmann, E.S. *et al.* (2017) 'Predicting melt rheology for hot-melt extrusion by means of a simple Tg-measurement', *European Journal of Pharmaceutics and Biopharmaceutics*, 119, pp. 47–55. Available at: https://doi.org/10.1016/j.ejpb.2017.05.010.

Booy, M.L. (1978) 'Geometry of fully wiped twin-screw equipment', *Polymer Engineering & Science*, 18(12), pp. 973–984. Available at: https://doi.org/10.1002/pen.760181212.

Booy, M.L. (1980) 'Isothermal flow of viscous liquids in corotating twin screw devices',

Polymer Engineering and Science, 20(18), pp. 1220–1228. Available at: https://doi.org/10.1002/pen.760201808.

Bouvier, J.-M. and Campanella, O.H. (2014) *Extrusion Processing Technology*, *Extrusion Processing Technology*. Available at: https://doi.org/10.1002/9781118541685.

Bravo, V.L., Hrymak, A.N. and Wright, J.D. (2000) 'Numerical simulation of pressure and velocity profiles in kneading elements of a co-rotating twin screw extruder', *Polymer Engineering and Science*, 40(2), pp. 525–541. Available at: https://doi.org/10.1002/pen.11184.

Brazel, C.S. and Rosen, S.L. (2012) *Fundamental Principles of Polymeric Materials*. John Wiley & Sons.

Breitenbach, J. and Gmbh, A. (2002) 'Melt extrusion: from process to drug delivery technology ¨', *European Journal of Pharmaceutics and Biopharmaceutics*, 54(2), pp. 107–117. Available at: https://doi.org/10.1016/S0939-6411(02)00061-9.

Brown, M.E. (1988) *Introduction to Thermal Analysis : Techniques and applications*. Dordrecht: Springer Netherlands. Available at: https://doi.org/10.1007/978-94-009-1219-9.

Bruschi, M.L. (ed.) (2015) '5 - Mathematical models of drug release', in *Strategies to Modify the Drug Release from Pharmaceutical Systems*. Woodhead Publishing, pp. 63–86. Available at: https://doi.org/10.1016/B978-0-08-100092-2.00005-9.

Buch, K. *et al.* (2009) 'Investigation of various shellac grades: Additional analysis for identity', *Drug Development and Industrial Pharmacy*, 35(6), pp. 694–703. Available at: https://doi.org/10.1080/03639040802563253.

Buch, P. *et al.* (2010) 'IVIVC for Fenofibrate Immediate Release Tablets Using Solubility and Permeability as In Vitro Predictors for Pharmacokinetics', *Journal of Pharmaceutical Sciences*, 99(10), pp. 4427–4436. Available at: https://doi.org/10.1002/jps.22148.

Buchbauer, G. *et al.* (1993) 'Headspace Constituents of Shellac', *Zeitschrift für Naturforschung B*, 48(2), pp. 247–248. Available at: https://doi.org/10.1515/znb-1993-0223.

Butler, J.M. and Dressman, J.B. (2010) 'The Developability Classification System:

Application of Biopharmaceutics Concepts to Formulation Development', *Journal of Pharmaceutical Sciences*, 99(12), pp. 4940–4954. Available at: https://doi.org/10.1002/jps.22217.

Cal, K. and Sollohub, K. (2010) 'Spray Drying Technique. I: Hardware and Process Parameters', *Journal of Pharmaceutical Sciences*, 99(2), pp. 575–586. Available at: https://doi.org/10.1002/jps.21886.

Cao, Z. *et al.* (2016) 'Synthesis and characterization of high density polyethylene/peat ash composites', *Composites Part B: Engineering*, 94, pp. 312–321. Available at: https://doi.org/10.1016/j.compositesb.2016.03.009.

Carley, J.F. and McKelvey, J.M. (2005) 'Extruder Scale-Up Theory and Experiments', *Industrial & Engineering Chemistry*, 45(5), pp. 989–992. Available at: https://doi.org/10.1021/ie50521a036.

Chapman, M.J. (2003) 'Fibrates in 2003: Therapeutic action in atherogenic dyslipidaemia and future perspectives', *Atherosclerosis*, 171(1), pp. 1–13. Available at: https://doi.org/10.1016/S0021-9150(03)00156-4.

Charles Hatchett, E.F.R.S. (1804) 'Analytical experiments and observations on lac', *Philosophical Transactions*, (January), pp. 191–218.

Chaudhari, S.P. and Patil, P.S. (2012) 'Pharmaceutical Excipients : A review', *International Journal of Advances in Pharmacy, Biology and Chemistry*, 1(1), pp. 21–34.

Chauhan, V.S. *et al.* (1973) 'Chromatographic separation of the alkaline hydrolysis products of shellac', *Journal of Chromatography A*, 84(1), pp. 51–58. Available at: https://doi.org/10.1016/S0021-9673(01)85368-1.

Chen, B. *et al.* (2017) 'Process Development and Scale-Up', in *Developing Solid Oral Dosage Forms*. Elsevier, pp. 821–868. Available at: https://doi.org/10.1016/B978-0-12-802447-8.00031-5.

Chen, L. *et al.* (2018) 'Preparation and characterization of solid dispersion of novel dual antiplatelet agent BF061 for oral use', *Journal of Drug Delivery Science and Technology*,

43(October 2017), pp. 311–317. Available at: https://doi.org/10.1016/j.jddst.2017.10.007.

Chen, R. and McKeever, S.W.S. (1997) *Theory of Thermoluminescence and Related Phenomena*. World Scientific. Available at: https://books.google.ie/books?id=jcmFRLktMPQC.

Chen Zhiqiang, Chunfen, W. and Wwang Yi (2001) 'Performance and Application of New Type Mixing Elements in Co-Rotating Twin Screw Extruders'. Available at: https://doi.org/10.19491/j.issn.1001 -9278.2001.06.020.

Cheng, H. and Manas-Zloczower, I. (1997) 'Study of Mixing Efficiency in Kneading Discs of Co-Rotating Twin-Screw Extruders', 37(6). Available at: https://doi.org/10.1002/pen.11753.

Cheng, Y.-T. and Johnson, W.L. (1987) 'Disordered Materials: A Survey of Amorphous Solids', *Science*, 235(4792), pp. 997–1002. Available at: https://doi.org/10.1126/science.235.4792.997.

Chiavari, G. *et al.* (1995) 'Pyrolysis gas chromatography-mass spectrometry of natural resins used for artistic objects', *Chromatographia*, 41(5–6), pp. 273–281. Available at: https://doi.org/10.1007/BF02688040.

Chiavari, G., Fabbri, D. and Prati, S. (2002) 'Characterisation of Natural Resins by Pyrolysis - Silylation', *Chromatographia*, 55, pp. 611–616. Available at: https://doi.org/10.1007/BF02492910.

Chiou, W.L. and Riegelman, S. (1971) 'Pharmaceutical applications of solid dispersion systems', *Journal of Pharmaceutical Sciences*, 60(9), pp. 1281–1302. Available at: https://doi.org/10.1002/jps.2600600902.

Chokshi, R. and Zia, H. (2004) 'Hot-Melt Extrusion technique: A Review', *Iranian Journal of Pharmaceutical Research*, 3(December 2003), pp. 3–16.

Coelho, C. *et al.* (2012) 'Molecular changes during natural biopolymer ageing - The case of shellac', *Polymer Degradation and Stability*, 97(6), pp. 936–940. Available at: https://doi.org/10.1016/j.polymdegradstab.2012.03.024.

Cole, G., Hogan, J. and Holton, M. (1995) *Pharmaceutical coating technology*. Taylor & Francis.

Colin, S. *et al.* (2013) 'Activation of intestinal peroxisome proliferator-activated receptor-α increases high-density lipoprotein production', *European Heart Journal*, 34(32), pp. 2566–2574. Available at: https://doi.org/10.1093/eurheartj/ehs227.

Cornell, E.W. *et al.* (2007) 'Using optical metrology to reconstruct sound recordings', *Nuclear Instruments and Methods in Physics Research, Section A: Accelerators, Spectrometers, Detectors and Associated Equipment*, 579(2 SPEC. ISS.), pp. 901–904. Available at: https://doi.org/10.1016/j.nima.2007.05.316.

Costa, P. and Sousa Lobo, J.M. (2001) 'Modeling and comparison of dissolution profiles', *European Journal of Pharmaceutical Sciences*, 13(2), pp. 123–133. Available at: https://doi.org/10.1016/S0928-0987(01)00095-1.

Craig, D.Q.M. (2002) 'The mechanisms of drug release from solid dispersions in water-soluble polymers', *International Journal of Pharmaceutics*, 231(2), pp. 131–144. Available at: https://doi.org/10.1016/S0378-5173(01)00891-2.

Crowley, M.M., Zhang, F., *et al.* (2007) 'Pharmaceutical Applications of Hot-Melt Extrusion: Part I', *Drug Development and Industrial Pharmacy*, 33(9), pp. 909–926. Available at: https://doi.org/10.1080/03639040701498759.

Crowley, M.M., Kumar Battu, S., *et al.* (2007) 'Pharmaceutical Applications of Hot-Melt Extrusion: Part I', *Drug Development and Industrial Pharmacy*, 33(9), pp. 909–926. Available at: https://doi.org/10.1080/03639040701498759.

Cunningham, A.F., Furneaux, G.C. and Hillman, D.E. (1976) 'Determination of Rosin in Shellac by High Performance Liquid Chromatography and by Gel Permeation Chromatography', *Analytical Chemistry*, 48(14), pp. 2192–2194. Available at: https://doi.org/10.1021/ac50008a035.

Cutler, L. *et al.* (2006) 'Development of a P-Glycoprotein Knockout Model in Rodents to Define Species Differences in its Functional Effect at the Blood–brain Barrier', *Journal of*

Pharmaceutical Sciences, 95(9), pp. 1944–1953. Available at: https://doi.org/10.1002/jps.20658.

D'Este, M., Alini, M. and Eglin, D. (2012) 'Single step synthesis and characterization of thermoresponsive hyaluronan hydrogels', *Carbohydrate Polymers*, 90(3), pp. 1378–1385. Available at: https://doi.org/10.1016/J.CARBPOL.2012.07.007.

Dahan, A., Wolk, O. and Agbaria, R. (2014) 'Provisional in-silico biopharmaceutics classification (BCS) to guide oral drug product development', *Drug Design, Development and Therapy*, 8, p. 1563. Available at: https://doi.org/10.2147/DDDT.S68909.

Das, S. and Jacob, S.E. (2011) 'Shellac', *Dermatitis*, 22(4), pp. 220–222. Available at: https://doi.org/10.2310/6620.2011.10091.

David B. Hedden and Monthira Reodacha (2013) *Hot Melt Extrusion - Meeting the solubility challenge*, *UPM Pharmaceuticals*. Available at: https://www.contractpharma.com/issues/2013-09/view_features/hot-melt-extrusion (Accessed: 11 June 2018).

Davis, M. and Walker, G. (2017) 'Recent strategies in spray drying for the enhanced bioavailability of poorly water-soluble drugs', *Journal of Controlled Release*, 269(November 2017), pp. 110–127. Available at: https://doi.org/10.1016/j.jconrel.2017.11.005.

Dealy, J.M. *et al.* (2013) *Melt rheology and its applications in the plastics industry*. Springer.

Dealy, J.M. and Wissbrun, K.F. (1990) *Melt Rheology and Its Role in Plastics Processing*, *Journal of Vinyl and Additive Technology*. Dordrecht: Springer Netherlands. Available at: https://doi.org/10.1007/978-94-009-2163-4.

Deloitte (2021) *Average R&D cost to develop a pharmaceutical compound from discovery to launch from 2010 to 2020, by study cohort*, *Statista*. Available at: https://www.statista.com/statistics/825727/randd-cost-for-new-pharma-compounds-by-cohort/ (Accessed: 5 June 2022).

Denson, C.D. and Hwang, B.K. (1980) 'The influence of the axial pressure gradient on flow

rate for Newtonian liquids in a self wiping, co-rotating twin screw extruder', *Polymer Engineering & Science*, 20(14), pp. 965–971. Available at: https://doi.org/10.1002/pen.760201408.

Derry, J. (2012) *Investigating Shellac: Documenting the Process, Defining the Product*. University of Oslo.

Dinesen, B. *et al.* (2019) 'Integration of Rehabilitation Activities Into Everyday Life Through Telerehabilitation: Qualitative Study of Cardiac Patients and Their Partners', *Journal of Medical Internet Research*, 21(4). Available at: https://doi.org/10.2196/13281.

Ding, C. *et al.* (2016) 'Recent advances in stimuli-responsive release function drug delivery systems for tumor treatment', *Molecules*, 21(12). Available at: https://doi.org/10.3390/molecules21121715.

Djuris, J. *et al.* (2019) 'Selection of the suitable polymer for supercritical fluid assisted preparation of carvedilol solid dispersions', *International Journal of Pharmaceutics*, 554, pp. 190–200. Available at: https://doi.org/10.1016/j.ijpharm.2018.11.015.

Douroumis, D. (2012) *Hot-melt Extrusion: Pharmaceutical Applications*, *Hot-Melt Extrusion: Pharmaceutical Applications*. Edited by D. Douroumis. Greenwich: John Wiley & Sons. Available at: http://doi.wiley.com/10.1002/9780470711415.ch5.

Van Drooge, D.J. *et al.* (2006) 'Characterization of the molecular distribution of drugs in glassy solid dispersions at the nano-meter scale, using differential scanning calorimetry and gravimetric water vapour sorption techniques', *International Journal of Pharmaceutics*, 310(1–2), pp. 220–229. Available at: https://doi.org/10.1016/j.ijpharm.2005.12.007.

Duflot, A. V., Kitaeva, N.K. and Duflot, V.R. (2015) 'Radiation-chemical preparation of poly(vinyl alcohol) hydrogels', *Radiation Physics and Chemistry*, 107, pp. 1–6. Available at: https://doi.org/10.1016/J.RADPHYSCHEM.2014.08.002.

Dynisco (2017) *An Introduction to Single Screw Extrusion*, *Azo Materials*. Available at: https://www.azom.com/article.aspx?ArticleID=13566 (Accessed: 14 September 2022).

Eckert, C.A., Knutson, B.L. and Debenedetti, P.G. (1996) 'Supercritical fluids as solvents

for chemical and materials processing', *Nature*, 383(6598), pp. 313–318. Available at: https://doi.org/10.1038/383313a0.

Engelman, M.S. (1983) 'Fidap - Fluid Dynamics Analysis Program.', 4(4), pp. 255–265.

Englert, C. *et al.* (2018) 'Pharmapolymers in the 21st century: Synthetic polymers in drug delivery applications', *Progress in Polymer Science*, 87, pp. 107–164. Available at: https://doi.org/10.1016/j.progpolymsci.2018.07.005.

Erdmenger, R. (1964) 'Mehrwellen-Schnecken in der Verfahrenstechnik', *Chemie Ingenieur Technik - CIT*, 36(3), pp. 175–185. Available at: https://doi.org/10.1002/cite.330360303.

Fan, D. *et al.* (2019) 'Numerical Simulation of Mixing Characteristics in the Eccentric Rotor Extruder with Different Process Conditions and Structural Parameters', *Advances in Polymer Technology*, 2019, pp. 1–11. Available at: https://doi.org/10.1155/2019/8132308.

Farag, Y. (2010) *Characterization of different shellac types and development of shellac coated dosage forms, Dissertation*. Available at: http://ediss.sub.uni-hamburg.de/volltexte/2010/4814/.

Farag, Y. and Leopold, C.S. (2009) 'Physicochemical properties of various shellac types', *Dissolution Technologies*, 16(2), pp. 33–39. Available at: https://doi.org/10.14227/DT160209P33.

Farag, Y. and Leopold, C.S. (2011) 'Development of shellac-coated sustained release pellet formulations', *European Journal of Pharmaceutical Sciences*, 42(4), pp. 400–405. Available at: https://doi.org/10.1016/j.ejps.2011.01.006.

Farahanchi, A., Malloy, R. and Sobkowicz, M.J. (2016) 'Effects of ultrahigh speed twin screw extrusion on the thermal and mechanical degradation of polystyrene', *Polymer Engineering & Science*, 56(7), pp. 743–751. Available at: https://doi.org/10.1002/pen.24301.

Febriyenti, F., Rahmi, S. and Halim, A. (2019) 'Study of gliclazide solid dispersion systems using PVP K-30 and PEG 6000 by solvent method', *Journal of Pharmacy And Bioallied Sciences*, 11(3), p. 262. Available at: https://doi.org/10.4103/jpbs.JPBS_87_18.

Flumerfelt, R.W. *et al.* (1969) 'Generalized Plane Couette Flow of a Non-Newtonian Fluid',

Industrial & Engineering Chemistry Fundamentals, 8(2), pp. 354–357. Available at: https://doi.org/10.1021/i160030a028.

Forster, A. *et al.* (2001) 'Selection of excipients for melt extrusion with two poorly water-soluble drugs by solubility parameter calculation and thermal analysis', *International Journal of Pharmaceutics*, 226(1–2), pp. 147–161. Available at: https://doi.org/10.1016/S0378-5173(01)00801-8.

Forster, A., Hempenstall, J. and Rades, T. (2001) 'Characterization of glass solutions of poorly water-soluble drugs produced by melt extrusion with hydrophilic amorphous polymers', *Journal of Pharmacy and Pharmacology*, 53(3), pp. 303–315. Available at: https://doi.org/10.1211/0022357011775532.

Frazza, E.J. and Schmitt, E.E. (1971) 'A new absorbable suture', *Journal of Biomedical Materials Research*, 5(2), pp. 43–58. Available at: https://doi.org/10.1002/jbm.820050207.

Frost & Sullivan (2019) *Global pharmaceutical R&D spending compared to the U.S. and China from 2014 to 2023*, *Statista*. Available at: https://www.statista.com/statistics/1085586/pharma-randd-spending-global-china-us/ (Accessed: 6 May 2022).

Gabbott, P. (ed.) (2008) *Principles and Applications of Thermal Analysis*. Oxford, UK: Blackwell Publishing Ltd. Available at: https://doi.org/10.1002/9780470697702.

Gajda, M. *et al.* (2018) 'The role of the polymer matrix in solvent-free hot melt extrusion continuous process for mechanochemical synthesis of pharmaceutical cocrystal', *European Journal of Pharmaceutics and Biopharmaceutics*, 131(April), pp. 48–59. Available at: https://doi.org/10.1016/j.ejpb.2018.07.002.

Gale, M. (2009) *Mixing in Single Screw Extrusion*. Shropshire: iSmithers Rapra Publishing. Available at: http://www.ncbi.nlm.nih.gov/pubmed/21298581.

Gandhi, N.K. (2016) 'Various approaches for particle size reduction for improvement of oral bioavailability of hydrophobic drugs', 3(8), pp. 222–229.

Gately, N. (2011) *The development of a polymeric colon targeted therapeutic delivery device*

to aid in the treatment of irritable bowel syndrome. Athlone Institute of Technology.

Gately, N.M. and Kennedy, J.E. (2017) 'The development of a melt-extruded shellac carrier for the targeted delivery of probiotics to the colon', *Pharmaceutics*, 9(4), pp. 1–12. Available at: https://doi.org/10.3390/pharmaceutics9040038.

Ghebre-Sellassie, I. *et al.* (2018) *Pharmaceutical extrusion technology*. Second Edi. CRC Press. Available at: http://ir.obihiro.ac.jp/dspace/handle/10322/3933.

Goffart, D. *et al.* (1996) 'Three-dimensional flow modeling of a self-wiping corotating twin-screw extruder. Part II: The kneading section', *Polymer Engineering and Science*, 36(7), pp. 912–924. Available at: https://doi.org/10.1002/pen.10479.

Gohel, M.C. and Jogani, P.D. (2005) 'A review of co-processed directly compressible excipients', *Journal of Pharmacy and Pharmaceutical Sciences*, 8(1), pp. 76–93.

Göke, K. *et al.* (2018) 'Novel strategies for the formulation and processing of poorly water-soluble drugs', *European Journal of Pharmaceutics and Biopharmaceutics*, 126, pp. 40–56. Available at: https://doi.org/10.1016/j.ejpb.2017.05.008.

Górniak, A. *et al.* (2011) 'Phase diagram and dissolution studies of the fenofibrate-acetylsalicylic acid system', *Journal of Thermal Analysis and Calorimetry*, 104(3), pp. 1195–1200. Available at: https://doi.org/10.1007/s10973-010-1148-3.

Goswami, D.N. (1985) 'The Dielectric Behavior of Shellac-Urea-Formaldehyde Resins', *Angewandte Makromolekulare Chemie*, 135(Oct), pp. 33–40. Available at: https://doi.org/10.1002/apmc.1985.051350104.

Graeser, K.A. *et al.* (2010) 'The Role of Configurational Entropy in Amorphous Systems', *Pharmaceutics*, 2(2), pp. 224–244. Available at: https://doi.org/10.3390/pharmaceutics2020224.

Guichard, J.P. and Levy-Prades Sauron, R. (1993) 'A comparison of the bioavailability of standard or micronized formulations of fenofibrate', *Current Therapeutic Research*, 54(5), pp. 610–614. Available at: https://doi.org/10.1016/S0011-393X(05)80682-4.

Gullan, P.J. and Kondo, T. (2007) 'The morphology of lac insects (Hemiptera: Coccoidea:

Kerriidae)', *of the XIth International Symposium on*, pp. 63–70. Available at: http://people.scalenet.info/wp-content/uploads/2009/11/GullanKondo_Lac_PDF.pdf.

Gunasekaran, S., Renuga Devi, T.S. and Sakthivel, P.S. (2008) 'Qualitative and quantitative analysis on fibrates - A spectroscopic study', *Asian Journal of Chemistry*, 20(6), pp. 4249–4268.

Gupta, B.P. *et al.* (2010) 'Osmotically controlled drug delivery system with associated drugs.', *Journal of pharmacy & pharmaceutical sciences : a publication of the Canadian Society for Pharmaceutical Sciences, Societe canadienne des sciences pharmaceutiques*, 13(4), pp. 571–88. Available at: http://www.ncbi.nlm.nih.gov/pubmed/21486532 (Accessed: 7 June 2018).

Gupta, S., Kesarla, R. and Omri, A. (2013) 'Formulation Strategies to Improve the Bioavailability of Poorly Absorbed Drugs with Special Emphasis on Self-Emulsifying Systems', *ISRN Pharmaceutics*, 2013(16), pp. 1–16. Available at: https://doi.org/10.1155/2013/848043.

Gupta, S.S. *et al.* (2014) 'Investigation of thermal and viscoelastic properties of polymers relevant to hot melt extrusion - I: Polyvinylpyrrolidone and related polymers. Simerdeep', *Journal of Excipients and Food Chemicals*, 5(1), pp. 32–45. Available at: https://doi.org/10.1208/s12249-015-0426-6.

Gupta, S.S. *et al.* (2015) 'Effect of carbamazepine on viscoelastic properties and hot melt extrudability of Soluplus®', *International Journal of Pharmaceutics*, 478(1), pp. 232–239. Available at: https://doi.org/10.1016/j.ijpharm.2014.11.025.

Gupta, S.S., Solanki, N. and Serajuddin, A.T.M.M. (2016) 'Investigation of Thermal and Viscoelastic Properties of Polymers Relevant to Hot Melt Extrusion, IV: Affinisol™ HPMC HME Polymers', *AAPS PharmSciTech*, 17(1), pp. 148–157. Available at: https://doi.org/10.1208/s12249-015-0426-6.

Guzmán, H.R. *et al.* (2007) 'Combined Use of Crystalline Salt Forms and Precipitation Inhibitors to Improve Oral Absorption of Celecoxib from Solid Oral Formulations', *Journal*

of Pharmaceutical Sciences, 96(10), pp. 2686–2702. Available at: https://doi.org/10.1002/jps.20906.

Hagenmaier, R.D. and Shaw, P.E. (1991) 'Permeability of Shellac Coatings to Gases and Water Vapor', *Journal of Agricultural and Food Chemistry*, 39(5), pp. 825–829. Available at: https://doi.org/10.1021/jf00005a001.

Hammond, R.B. *et al.* (2007) 'Quantifying solubility enhancement due to particle size reduction and crystal habit modification: Case study of acetyl salicylic acid', *Journal of Pharmaceutical Sciences*, 96(8), pp. 1967–1973. Available at: https://doi.org/10.1002/jps.20869.

Hancock, B.C. and Zografi, G. (1997) 'Characteristics and Significance of the Amorphous State in Pharmaceutical Systems', *Journal of Pharmaceutical Sciences*, 86(1), pp. 1–12. Available at: https://doi.org/10.1021/js9601896.

Harrison, K. (2007) 'Introduction to polymeric drug delivery systems', in *Biomedical Polymers*. UK: Elsevier, pp. 33–56. Available at: https://doi.org/10.1533/9781845693640.33.

Hauss, J.D. (2013) *Oral lipid-based formulations: Enhancing the bioavailability of poorly Water-soluble drugs*, *Drugs and the Pharmaceutical Sciences*. Informa Healthcare. Available at: https://doi.org/10.1017/CBO9781107415324.004.

Heinz, A. *et al.* (2009) 'Understanding the solid-state forms of fenofibrate - A spectroscopic and computational study', *European Journal of Pharmaceutics and Biopharmaceutics*, 71(1), pp. 100–108. Available at: https://doi.org/10.1016/j.ejpb.2008.05.030.

Hixson, J.E. *et al.* (2017) 'Whole Exome Sequencing to Identify Genetic Variants Associated with Raised Atherosclerotic Lesions in Young Persons', *Scientific Reports*, 7(1), pp. 1–9. Available at: https://doi.org/10.1038/s41598-017-04433-x.

Hu, X.Y., Lou, H. and Hageman, M.J. (2018) 'Preparation of lapatinib ditosylate solid dispersions using solvent rotary evaporation and hot melt extrusion for solubility and dissolution enhancement', *International Journal of Pharmaceutics*, 552(1–2), pp. 154–163. Available at: https://doi.org/10.1016/j.ijpharm.2018.09.062.

Hua Linga, Luomab, J.T. and Hillemanc, D. (2013) 'A Review of Currently Available Fenofibrate and Fenofibric Acid Formulations', *Cardiology Research*, 4(2), pp. 47–55. Available at: https://doi.org/10.4021/cr270w.

Huang, Q.P. *et al.* (2009) 'Preparation of ultrafine fenofibrate powder by solidification process from emulsion', *International Journal of Pharmaceutics*, 368(1–2), pp. 160–164. Available at: https://doi.org/10.1016/j.ijpharm.2008.10.015.

Huang, Y. and Dai, W.-G. (2014) 'Fundamental aspects of solid dispersion technology for poorly soluble drugs', *Acta Pharmaceutica Sinica B*, 4(1), pp. 18–25. Available at: https://doi.org/10.1016/J.APSB.2013.11.001.

Hughes, J. *et al.* (2011) 'Principles of early drug discovery', *British Journal of Pharmacology*, 162(6), pp. 1239–1249. Available at: https://doi.org/10.1111/j.1476-5381.2010.01127.x.

Hyvärinen, M., Jabeen, R. and Kärki, T. (2020) 'The modelling of extrusion processes for polymers-A review', *Polymers*, 12(6). Available at: https://doi.org/10.3390/polym12061306.

Ignatious, F. *et al.* (2010) 'Electrospun Nanofibers in Oral Drug Delivery', *Pharmaceutical Research*, 27(4), pp. 576–588. Available at: https://doi.org/10.1007/s11095-010-0061-6.

Ilevbare, G., Marsac, P. and Mitra, A. (2015) 'Performance and Characterization of Amorphous Solid Dispersions: An Overview', in *Discovering and Developing Molecules with Optimal Drug-Like Properties*, pp. 287–343. Available at: https://doi.org/10.1007/978-1-4939-1399-2_10.

Irimia-Vladu, M. *et al.* (2013) 'Natural resin shellac as a substrate and a dielectric layer for organic field-effect transistors', *Green Chemistry*, 15(6), p. 1473. Available at: https://doi.org/10.1039/c3gc40388b.

Ishikawa, T., Kihara, S.I. and Funatsu, K. (2000) '3-D numerical simulations of nonisothermal flow in co-rotating twin screw extruders', *Polymer Engineering and Science*, 40(2), pp. 357–364. Available at: https://doi.org/10.1002/pen.11169.

Jacques, C.H.M., Hopfenberg, H.B. and Stannett, V. (1974) 'Super Case Ii Transport of

Organic Vapors in Glassy Polymers.', *Am Chem Soc, Div Org Coatings Plast Chem1974*, 34(1), pp. 452–456.

Jain, K.K. (2008) 'Drug Delivery Systems - An Overview', in, pp. 1–50. Available at: https://doi.org/10.1007/978-1-59745-210-6_1.

Jaluria, Y. (2003) 'Thermal Processing of Materials: From Basic Research to Engineering', *Journal of Heat Transfer*, 125(6), p. 957. Available at: https://doi.org/10.1115/1.1621889.

Jamzad, S. and Fassihi, R. (2006) 'Role of surfactant and pH on dissolution properties of fenofibrate and glipizide—A technical note', *AAPS PharmSciTech*, 7(2), pp. E17–E22. Available at: https://doi.org/10.1208/pt070233.

Janssen, L., JJ, P. and JM, S. (1976) 'DRUCKAUFBAU UND AUSSTOSSLEISTUNG EINES DOPPELSCHNECKENEXTRUDERS.'

Jermain, S. V., Brough, C. and Williams, R.O. (2018) 'Amorphous solid dispersions and nanocrystal technologies for poorly water-soluble drug delivery – An update', *International Journal of Pharmaceutics*, 535(1–2), pp. 379–392. Available at: https://doi.org/10.1016/j.ijpharm.2017.10.051.

Jonathan, P. (2015) *Analysis on Light Transmission and Thermal Conductivity of Functional Secondary Optical Elements by Injection Molding of PMMA-TiO2 Composites*. National Taiwan University of Science and Technology. Available at: https://doi.org/10.13140/RG.2.2.19369.08802.

De Jong, W.H. and Borm, P.J.A. (2008) 'Drug delivery and nanoparticles:applications and hazards.', *International journal of nanomedicine*, 3(2), pp. 133–49. Available at: http://www.ncbi.nlm.nih.gov/pubmed/18686775 (Accessed: 16 August 2018).

Kaboorani, A. and Blanchet, P. (2014) 'Determining the linear viscoelastic region of sugar maple wood by dynamic mechanical analysis', *BioResources*, 9(3), pp. 4392–4409. Available at: https://doi.org/10.15376/biores.9.3.4392-4409.

Kallakunta, V.R. *et al.* (2020) 'Stable amorphous solid dispersions of fenofibrate using hot melt extrusion technology: Effect of formulation and process parameters for a low glass

transition temperature drug', *Journal of Drug Delivery Science and Technology*, 58(August 2019), p. 101395. Available at: https://doi.org/10.1016/j.jddst.2019.101395.

Kalyon, D.M. and Aktaş, S. (2014) 'Factors Affecting the Rheology and Processability of Highly Filled Suspensions', *Annual Review of Chemical and Biomolecular Engineering*, 5(1), pp. 229–254. Available at: https://doi.org/10.1146/annurev-chembioeng-060713-040211.

Karavas, E. *et al.* (2006) 'Effect of hydrogen bonding interactions on the release mechanism of felodipine from nanodispersions with polyvinylpyrrolidone', *European Journal of Pharmaceutics and Biopharmaceutics*, 63(2), pp. 103–114. Available at: https://doi.org/10.1016/j.ejpb.2006.01.016.

Karsa, D.R. *et al.* (1996) *Chemical aspects of drug delivery systems*. Royal Society of Chemistry. Available at: https://books.google.ie/books?hl=zh-CN&lr=&id=qGwoDwAAQBAJ&oi=fnd&pg=PA146&dq=Aqueous+shellac+solutions+for+controlled+release+coatings&ots=X7OV6S2cyq&sig=bz8J7a1Ax5UcQ9oFqPrhmjBE6L4&redir_esc=y#v=onepage&q=Aqueous shellac solutions for controlled release (Accessed: 31 July 2018).

Kawakami, K. and Pikal, M.J. (2005) 'Calorimetric investigation of the structural relaxation of amorphous materials: Evaluating validity of the methodologies', *Journal of Pharmaceutical Sciences*, 94(5), pp. 948–965. Available at: https://doi.org/10.1002/jps.20298.

Kendre, P.N., Pande, V. V and Chavan, K.M. (2014) 'Novel Formulation Strategy to Enhance Solubility of Quercetin', *Pharmacophore International Research Journal*, 5(3), pp. 358–370. Available at: http://www.pharmacophorejournal.com/.

Khadka, P. *et al.* (2014) 'Pharmaceutical particle technologies: An approach to improve drug solubility, dissolution and bioavailability', *Asian Journal of Pharmaceutical Sciences*, 9(6), pp. 304–316. Available at: https://doi.org/10.1016/j.ajps.2014.05.005.

Khairuddin, Pramono, E., *et al.* (2016) 'FTIR studies on the effect of concentration of

polyethylene glycol on polimerization of Shellac', *Journal of Physics: Conference Series*, 776(1). Available at: https://doi.org/10.1088/1742-6596/776/1/012053.

Khairuddin, Pramono, Edi, *et al.* (2016) 'The effect of polyethylene glycol on shellac stability', *IOP Conference Series: Materials Science and Engineering*, 107(1). Available at: https://doi.org/10.1088/1757-899X/107/1/012066.

Khorram, F., Ramezanian, A. and Hosseini, S.M.H. (2017) 'Shellac, gelatin and Persian gum as alternative coating for or[1] F. Khorram, A. Ramezanian, and S. M. H. Hosseini, "Shellac, gelatin and Persian gum as alternative coating for orange fruit," Sci. Hortic. (Amsterdam)., vol. 225, no. July, pp. 22–28, 2017.', *Scientia Horticulturae*, 225(July), pp. 22–28. Available at: https://doi.org/10.1016/j.scienta.2017.06.045.

Klonos, P. *et al.* (2018) 'Morphology, crystallization and rigid amorphous fraction in PDMS adsorbed onto carbon nanotubes and graphite', *Polymer (United Kingdom)*, 139, pp. 130–144. Available at: https://doi.org/10.1016/j.polymer.2018.02.020.

Kohlgrüber, K. (2007a) *Co-Rotating Extruders Twin-Screw Fundamentals, Technology, and Applications*, *Hanser Gardner Pubns*. Available at: https://doi.org/10.1007/978-0-387-30160-0_12006.

Kohlgrüber, K. (2007b) *Co-Rotating Twin-Screw Extruders-Fundamentals, Technology, and Applications*. Ohio: Hanser Gardner Publications.

Kohnke, P.C. (1982) 'ANSYS', in *Finite Element Systems*. Berlin, Heidelberg: Springer Berlin Heidelberg, pp. 19–25. Available at: https://doi.org/10.1007/978-3-662-07229-5_2.

Kolter, K., Karl, M. and Gryczke, A. (2012) *Hot-Melt Extrusion with BASF Pharma Polymers-Extrusion Compendium*. 2rd edn, *BASF SE*. 2rd edn. Pharma Ingredients & Services.

Komarewsky, V.I., Rideal, E.K. and Frankenburg, W.G. (1953) *Advances in Catalysis*. Elsevier Science (Advances in Catalysis). Available at: https://books.google.ie/books?id=f_Oiij4V98cC.

Kompella, U.B. and Koushik, K. (2001) 'Preparation of drug delivery systems using

supercritical fluid technology.', *Critical reviews in therapeutic drug carrier systems*, pp. 173–99. Available at: http://www.ncbi.nlm.nih.gov/pubmed/11325031 (Accessed: 23 July 2018).

Korsmeyer, R.W. *et al.* (1983) 'Mechanisms of solute release from porous hydrophilic polymers', *International Journal of Pharmaceutics*, 15(1), pp. 25–35. Available at: https://doi.org/10.1016/0378-5173(83)90064-9.

Krause, K.P. and Müller, R.H. (2001) 'Production of aqueous shellac dispersions by high pressure homogenisation', *International Journal of Pharmaceutics*, 223(1–2), pp. 89–92. Available at: https://doi.org/10.1016/S0378-5173(01)00730-X.

Kulkarni, C.S. (2013) *Novel Formulations of a Poorly Soluble Drug Using the Extrusion Process*. University of Bradford.

Kwong, E., Higgins, J. and Templeton, A.C. (2011) 'Strategies for bringing drug delivery tools into discovery', *International Journal of Pharmaceutics*, 412(1–2), pp. 1–7. Available at: https://doi.org/10.1016/J.IJPHARM.2011.03.024.

Labuschagne, P.W., Naicker, B. and Kalombo, L. (2016) 'Micronization, characterization and in-vitro dissolution of shellac from PGSS supercritical CO2technique', *International Journal of Pharmaceutics*, 499(1–2), pp. 205–216. Available at: https://doi.org/10.1016/j.ijpharm.2015.12.021.

Lachowicz, M. *et al.* (2016) 'New biopolymer nanoparticles improve the solubility of lipophilic megestrol acetate', *Molecules*, 21(2), pp. 1–8. Available at: https://doi.org/10.3390/molecules21020197.

Lang, B., McGinity, J.W. and Williams, R.O. (2014) 'Hot-melt extrusion-basic principles and pharmaceutical applications', *Drug Development and Industrial Pharmacy*, 40(9), pp. 1133–1155. Available at: https://doi.org/10.3109/03639045.2013.838577.

Larson, R.G. (1999) *The structure and rheology of complex fluids*, *Published in* ***1999*** *in New York (N.Y.) by Oxford university press*. Oxford University Press. Available at: https://lib.ugent.be/en/catalog/rug01:002006527 (Accessed: 31 July 2018).

Law, D. *et al.* (2003) 'Properties of rapidly dissolving eutectic mixtures of poly(ethylene glycol) and fenofibrate: The eutectic microstructure', *Journal of Pharmaceutical Sciences*, 92(3), pp. 505–515. Available at: https://doi.org/10.1002/jps.10324.

Lee, J.H. and Yeo, Y. (2015) 'Controlled Drug Release from Pharmaceutical Nanocarriers.', *Chemical engineering science*, 125, pp. 75–84. Available at: https://doi.org/10.1016/j.ces.2014.08.046.

Leuner, C. and Dressman, J. (2000) 'Improving drug solubility for oral delivery using solid dispersions.', *European journal of pharmaceutics and biopharmaceutics : official journal of Arbeitsgemeinschaft für Pharmazeutische Verfahrenstechnik e.V*, 50(1), pp. 47–60. Available at: https://doi.org/10.1016/S0939-6411(00)00076-X.

Lewandowski, A. and Wilczyński, K. (2022) 'Modeling of Twin Screw Extrusion of Polymeric Materials', *Polymers*, 14(2), p. 274. Available at: https://doi.org/10.3390/polym14020274.

Li, P. and Zhao, L. (2007) 'Developing early formulations: Practice and perspective', *International Journal of Pharmaceutics*, 341(1–2), pp. 1–19. Available at: https://doi.org/10.1016/J.IJPHARM.2007.05.049.

Liming Lu, J.E.K.S. (2009) *elastomer*. Northeast University Press.

Limmatvapirat, S. *et al.* (2004) 'Modification of physicochemical and mechanical properties of shellac by partial hydrolysis', *International Journal of Pharmaceutics*, 278(1), pp. 41–49. Available at: https://doi.org/10.1016/j.ijpharm.2004.02.030.

Limmatvapirat, S. *et al.* (2005) 'Effect of Alkali Treatment on Properties of Native Shellac and Stability of Hydrolyzed Shellac', *Pharmaceutical Development and Technology*, 10(1), pp. 41–46. Available at: https://doi.org/10.1081/PDT-35897.

Limmatvapirat, S. *et al.* (2007) 'Enhanced enteric properties and stability of shellac films through composite salts formation', *European Journal of Pharmaceutics and Biopharmaceutics*, 67(3), pp. 690–698. Available at: https://doi.org/10.1016/j.ejpb.2007.04.008.

Limmatvapirat, S., Panchapornpon, D., *et al.* (2008) 'Formation of shellac succinate having improved enteric film properties through dry media reaction', *European Journal of Pharmaceutics and Biopharmaceutics*, 70(1), pp. 335–344. Available at: https://doi.org/10.1016/j.ejpb.2008.03.002.

Limmatvapirat, S., Limmatvapirat, C., *et al.* (2008) 'Modulation of drug release kinetics of shellac-based matrix tablets by in-situ polymerization through annealing process', *European Journal of Pharmaceutics and Biopharmaceutics*, 69(3), pp. 1004–1013. Available at: https://doi.org/10.1016/j.ejpb.2008.01.027.

Lindenberg, M., Kopp, S. and Dressman, J.B. (2004) 'Classification of orally administered drugs on the World Health Organization Model list of Essential Medicines according to the biopharmaceutics classification system', *European Journal of Pharmaceutics and Biopharmaceutics*, 58(2), pp. 265–278. Available at: https://doi.org/10.1016/j.ejpb.2004.03.001.

Liptak, B.G. (2003) *Instrument Engineers' Handbook, Volume One: Process Measurement and Analysis*. CRC Press (Instrument Engineers' Handbook). Available at: https://books.google.ie/books?id=a05NAvaqfcUC.

Liu, D. *et al.* (2016) 'The Smart Drug Delivery System and Its Clinical Potential.', *Theranostics*, 6(9), pp. 1306–23. Available at: https://doi.org/10.7150/thno.14858.

Liu, H. *et al.* (2012) 'Miscibility Studies of Indomethacin and Eudragit® E PO by Thermal, Rheological, and Spectroscopic Analysis', *Journal of Pharmaceutical Sciences*, 101(6), pp. 2204–2212. Available at: https://doi.org/10.1002/jps.23075.

Liu, X. *et al.* (2012) 'Improving the chemical stability of amorphous solid dispersion with cocrystal technique by hot melt extrusion', *Pharmaceutical Research*, 29(3), pp. 806–817. Available at: https://doi.org/10.1007/s11095-011-0605-4.

Liu, X. *et al.* (2014) 'ABCD2 alters peroxisome proliferator-activated receptor α signaling in vitro, but does not impair responses to fenofibrate therapy in a mouse model of diet-induced obesity', *Molecular Pharmacology*, 86(5), pp. 505–513. Available at:

https://doi.org/10.1124/mol.114.092742.

Lubrizol (2020) *Hot melt extrusion*. Available at: https://www.particlesciences.com/news/technical-briefs/2011/hot-melt-extrusion.html (Accessed: 16 September 2022).

Luo, Y. *et al.* (2013) 'Improvement of dissolution and bioavailability of Ginsenosides by hot melt extrusion and cogrinding', *Drug Development and Industrial Pharmacy*, 39(1), pp. 109–116. Available at: https://doi.org/10.3109/03639045.2012.659189.

M. S. Wadia, R. G. Khurana, V.V.M. and S. dev (1969) 'CHEMISTRY OF LAC RESIN-I LAC ACIDS (Part 1): BUTOLIC, JALARIC AND LAKSHOLIC ACIDS', 25(1969), pp. 3841–3854.

Maas, J., Kamm, W. and Hauck, G. (2007) 'An integrated early formulation strategy – From hit evaluation to preclinical candidate profiling', *European Journal of Pharmaceutics and Biopharmaceutics*, 66(1), pp. 1–10. Available at: https://doi.org/10.1016/J.EJPB.2006.09.011.

Macheras, P., Karalis, V. and Valsami, G. (2013) 'Keeping a Critical Eye on the Science and the Regulation of Oral Drug Absorption: A Review', *Journal of Pharmaceutical Sciences*, 102(9), pp. 3018–3036. Available at: https://doi.org/10.1002/jps.23534.

Madan, Sa and Madan, Su (2012) 'Hot melt extrusion and its pharmaceutical applications', *Asian Journal of Pharmaceutical Sciences*, 7(2), pp. 123–133.

Majerik, V. *et al.* (2007) 'Bioavailability enhancement of an active substance by supercritical antisolvent precipitation', *The Journal of Supercritical Fluids*, 40(1), pp. 101–110. Available at: https://doi.org/10.1016/J.SUPFLU.2006.03.027.

Malik, M., Kalyon, D.M. and Golba, J.C. (2014) 'Simulation of co-rotating twin screw extrusion process subject to pressure-dependent wall slip at barrel and screw surfaces: 3D FEM analysis for combinations of forward- and reverse-conveying screw elements', *International Polymer Processing*, 29(1), pp. 51–62. Available at: https://doi.org/10.3139/217.2802.

Manas-Zloczower, I. (2012) *Mixing and compounding of polymers: theory and practice*. Carl Hanser Verlag GmbH Co KG.

Martena, V. *et al.* (2014) 'Effect of four different size reduction methods on the particle size, solubility enhancement and physical stability of nicergoline nanocrystals', *Drug Development and Industrial Pharmacy*, 40(9), pp. 1199–1205. Available at: https://doi.org/10.3109/03639045.2013.810635.

Di Martino, P., Palmieri, G.F. and Martelli, S. (2000) 'Evidence of a metastable form of fenofibrate.', *Die Pharmazie*, 55(8), pp. 625–6. Available at: http://www.ncbi.nlm.nih.gov/pubmed/10989846.

Maru, S.M. *et al.* (2011) 'Characterization of thermal and rheological properties of zidovidine, lamivudine and plasticizer blends with ethyl cellulose to assess their suitability for hot melt extrusion', *European Journal of Pharmaceutical Sciences*, 44(4), pp. 471–478. Available at: https://doi.org/10.1016/j.ejps.2011.09.003.

Mathur, H.H. and Bhattacharyya, S.C. (1963) '17. Macrocyclic musk compounds. Part II. New syntheses of civetone, isocivetone, and dihydrocivetone from aleuritic acid', *Journal of the Chemical Society (Resumed)*, 0(0), p. 114. Available at: https://doi.org/10.1039/jr9630000114.

Maurice, B.D. (2015) *The Development of Novel Smart Melt Processed Drug Delivery Systems to control the Release Rate of Active Pharmaceutical Ingredients*. Athlone Institute of Technology.

Mayer, B.X. *et al.* (1999) 'Pharmacokinetic-pharmacodynamic profile of systemic nitric oxide-synthase inhibition with L-NMMA in humans', *British Journal of Clinical Pharmacology*, 47(5), pp. 539–544. Available at: https://doi.org/10.1046/j.1365-2125.1999.00930.x.

Meena, A. *et al.* (2014) 'Investigation of thermal and viscoelastic properties of polymers relevant to hot melt extrusion, II: Cellulosic polymers.', *Journal of Excipients and Food Chemicals*, 5(1), pp. 46–55. Available at:

https://ojs.abo.fi/ojs/index.php/jefc/article/view/345.

Menard, K.P. (2008) *Dynamic Mechanical Analysis: A Practical Introduction*. Boca Raton: CRC Press. Available at: https://books.google.ie/books/about/Dynamic_Mechanical_Analysis.html?id=AMCjRtKY17IC&redir_esc=y.

van der Merwe, J. *et al.* (2020) 'The role of functional excipients in solid oral dosage forms to overcome poor drug dissolution and bioavailability', *Pharmaceutics*, 12(5). Available at: https://doi.org/10.3390/pharmaceutics12050393.

Mezger, T.G. (2006) *The Rheology Handbook: For Users of Rotational and Oscillatory Rheometers*. Vincentz Network GmbH & Co KG.

Mezger, T.G. (2012) *The Rheology Handbook: 4th Edition*. Vincentz Network.

Mezger, T.G. (2020) *Applied Rheology with Joe Flow on Rheology Road*. 7th edn. Austria: Anton Paar Gmbh.

Mishra, M.K. (1983) 'Dimers of Aleuritic Acid Derivatives', *Journal of Macromolecular Science: Part A - Chemistry*, 20(5–6), pp. 619–625. Available at: https://doi.org/10.1080/00222338308061796.

Modi, A. and Tayade, P. (2006) 'Enhancement of dissolution profile by solid dispersion (kneading) technique', *AAPS PharmSciTech*, 7(3), pp. 1–6. Available at: https://doi.org/10.1208/pt070368.

Monteyne, T. *et al.* (2016) 'Vibrational spectroscopy to support the link between rheology and continuous twin-screw melt granulation on molecular level: A case study', *European Journal of Pharmaceutics and Biopharmaceutics*, 103, pp. 127–135. Available at: https://doi.org/10.1016/j.ejpb.2016.03.030.

Muhrer, G. *et al.* (2006) 'Use of compressed gas precipitation to enhance the dissolution behavior of a poorly water-soluble drug: Generation of drug microparticles and drug-polymer solid dispersions', *International Journal of Pharmaceutics*, 308(1–2), pp. 69–83. Available at: https://doi.org/10.1016/j.ijpharm.2005.10.026.

Nakayama, Y. *et al.* (2018) 'Improving mixing characteristics with a pitched tip in kneading elements in twin-screw extrusion', *AIChE Journal*, 64(4), pp. 1424–1434. Available at: https://doi.org/10.1002/aic.16003.

Nath Goswami, D. *et al.* (2009) 'Degradation of lac with storage and a simple method to check the same', *Pigment & Resin Technology*, 38(4), pp. 211–217. Available at: https://doi.org/10.1108/03699420910973297.

Nokhodchi, A. *et al.* (2012) 'The role of oral controlled release matrix tablets in drug delivery systems', *BioImpacts*, 2(4), pp. 175–187. Available at: https://doi.org/10.5681/bi.2012.027.

Osman, Z. (2012) *Investigation of Different Shellac Grades and Improvement of Release From Air suspension Coated Pellets*.

Osswald, T.A. and Rudolph, N. (2015) *Polymer Rheology*. Dordrecht: Springer Netherlands. Available at: https://doi.org/10.1063/1.882283.

Panchapornpon, D. *et al.* (2011) 'Fabrication of thermally stabilized shellac through solid state reaction with phthalic anhydride', *Materials Letters*, 65(8), pp. 1241–1244. Available at: https://doi.org/10.1016/j.matlet.2011.01.068.

Pandey, V. and Maia, J.M. (2021) 'Extension-dominated improved dispersive mixing in single-screw extrusion. Part 1: Computational and experimental validation', *Journal of Applied Polymer Science*, 138(4), pp. 1–18. Available at: https://doi.org/10.1002/app.49716.

Park, K. (2014) 'Controlled drug delivery systems: past forward and future back.', *Journal of controlled release : official journal of the Controlled Release Society*, 190, pp. 3–8. Available at: https://doi.org/10.1016/j.jconrel.2014.03.054.

Patil, H., Tiwari, R. V. and Repka, M.A. (2016) 'Hot-Melt Extrusion: from Theory to Application in Pharmaceutical Formulation', *AAPS PharmSciTech*, 17(1), pp. 20–42. Available at: https://doi.org/10.1208/s12249-015-0360-7.

Patterson, J.E. *et al.* (2008) 'Melt extrusion and spray drying of carbamazepine and dipyridamole with polyvinylpyrrolidone/vinyl acetate copolymers', *Drug Development and*

Industrial Pharmacy, 34(1), pp. 95–106. Available at: https://doi.org/10.1080/03639040701484627.

Paudel, A. *et al.* (2013) 'Manufacturing of solid dispersions of poorly water soluble drugs by spray drying: Formulation and process considerations', *International Journal of Pharmaceutics*, 453(1), pp. 253–284. Available at: https://doi.org/10.1016/j.ijpharm.2012.07.015.

Paudel, A., Geppi, M. and Van Den Mooter, G. (2014) 'Structural and dynamic properties of amorphous solid dispersions: The role of solid-state nuclear magnetic resonance spectroscopy and relaxometry', *Journal of Pharmaceutical Sciences*, 103(9), pp. 2635–2662. Available at: https://doi.org/10.1002/jps.23966.

Pearnchob, N., Siepmann, J. and Bodmeier, R. (2003a) 'Pharmaceutical applications of shellac: Moisture-protective and taste-masking coatings and extended-release matrix tablets', *Drug Development and Industrial Pharmacy*, 29(8), pp. 925–938. Available at: https://doi.org/10.1081/DDC-120024188.

Pearnchob, N., Siepmann, J. and Bodmeier, R. (2003b) 'Pharmaceutical applications of shellac: Moisture-protective and taste-masking coatings and extended-release matrix tablets', *Drug Development and Industrial Pharmacy*, 29(8), pp. 925–938. Available at: https://doi.org/10.1081/DDC-120024188.

Penning, M. (1996) 'Aqueous shellac solutions for controlled release coatings', in *Chemical Aspects of Drug Delivery Systems*. Cambridge: Royal Society of Chemistry, pp. 146–154. Available at: https://doi.org/10.1039/9781847550378-00146.

Pepliński, K. and Mozer, A. (2011) 'Design of extrusion die for plastic profile using ansys polyflow software', *Journal of Polish CIMAC*, 6(3), pp. 221–226.

Peppas, N.A. and Sahlin, J.J. (1989) 'A simple equation for the description of solute release. III. Coupling of diffusion and relaxation', *International Journal of Pharmaceutics*, 57(2), pp. 169–172. Available at: https://doi.org/10.1016/0378-5173(89)90306-2.

PerkinElmer (2005) 'FT-IR Spectroscopy Attenuated Total Reflectance (ATR)',

PerkinElmer Life and Analystical Sciences, pp. 1–5. Available at: https://doi.org/007024B_01.

Pezzoli, R. *et al.* (2019) 'Stability studies of hot-melt extruded ternary solid dispersions of poorly-water soluble indomethacin with poly(vinyl pyrrolidone-co-vinyl acetate) and polyethylene oxide', *Journal of Drug Delivery Science and Technology*, 52(November 2018), pp. 248–254. Available at: https://doi.org/10.1016/j.jddst.2019.04.023.

Phaechamud, T. and Choncheewa, C. (2016) 'Double-Layered Matrix of Shellac Wax-Lutrol in Controlled Dual Drug Release', *AAPS PharmSciTech*, 17(6), pp. 1326–1335. Available at: https://doi.org/10.1208/s12249-015-0468-9.

Plastics, I. (2017) *The Difference Between Amorphous & Semi-crystalline Polymers*. Available at: https://blog.impactplastics.co/blog/the-difference-between-amorphous-semi-crystalline-polymers (Accessed: 11 July 2022).

Pokharkar, V.B. *et al.* (2006) 'Development, characterization and stabilization of amorphous form of a low Tg drug', *Powder Technology*, 167(1), pp. 20–25. Available at: https://doi.org/10.1016/j.powtec.2006.05.012.

Pouton, C.W. (2006) 'Formulation of poorly water-soluble drugs for oral administration: Physicochemical and physiological issues and the lipid formulation classification system', *European Journal of Pharmaceutical Sciences*, 29(3–4), pp. 278–287. Available at: https://doi.org/10.1016/J.EJPS.2006.04.016.

PubChem (2005) *Aleuritic acid | C16H32O5 - PubChem*, *PubChem*. Available at: https://pubchem.ncbi.nlm.nih.gov/compound/10790 (Accessed: 30 July 2018).

PubChem (2007) *Jalaric acid | C15H20O5 - PubChem*, *PubChem*. Available at: https://pubchem.ncbi.nlm.nih.gov/compound/12304681#section=Top (Accessed: 30 July 2018).

PubChem (2015) *Shellolic acid | C15H20O6 - PubChem*, *PubChem*. Available at: https://pubchem.ncbi.nlm.nih.gov/compound/102248357#section=Top (Accessed: 30 July 2018).

PubChem (2022a) *Fenofibrate | C20H21ClO4 - PubChem*. Available at: https://pubchem.ncbi.nlm.nih.gov/compound/Fenofibrate#section=Crystal-Structures&fullscreen=true (Accessed: 10 February 2022).

PubChem (2022b) *PubChem Compound Summary for CID 3339, Fenofibrate*, *National Center for Biotechnology Information*. Available at: https://pubchem.ncbi.nlm.nih.gov/compound/Fenofibrate. (Accessed: 10 February 2022).

Punitha, S. *et al.* (2011) 'Solid dispersions: A review', *Research Journal of Pharmacy and Technology*, pp. 331–334. Available at: http://www.ncbi.nlm.nih.gov/pubmed/19339238 (Accessed: 13 July 2018).

Rasenack, N. and Müller, B.W. (2004) 'Micron-Size Drug Particles: Common and Novel Micronization Techniques', *Pharmaceutical Development and Technology*, 9(1), pp. 1–13. Available at: https://doi.org/10.1081/PDT-120027417.

Rauwendaal, C. (2014) *Polymer Extrusion*. 5th Editio. Hanser. Available at: https://doi.org/10.1016/B978-1-56990-516-6.50001-0.

Ravi, V., Pramod Kumar, T.M. and Siddaramaiah (2008) 'Novel colon targeted drug delivery system using natural polymers.', *Indian journal of pharmaceutical sciences*, 70(1), pp. 111–113. Available at: https://doi.org/10.4103/0250-474X.40346.

Ravi, V., Siddaramaiah and Pramod Kumar, T.M. (2008) 'Influence of natural polymer coating on novel colon targeting drug delivery system', *Journal of Materials Science: Materials in Medicine*, 19(5), pp. 2131–2136. Available at: https://doi.org/10.1007/s10856-007-3155-x.

Repka, M.A. *et al.* (2018) 'Melt extrusion with poorly soluble drugs – An integrated review', *International Journal of Pharmaceutics*, 535(1–2), pp. 68–85. Available at: https://doi.org/10.1016/j.ijpharm.2017.10.056.

Rodriguez-Aller, M. *et al.* (2015) 'Strategies for formulating and delivering poorly water-soluble drugs', *Journal of Drug Delivery Science and Technology*, 30, pp. 342–351. Available at: https://doi.org/10.1016/j.jddst.2015.05.009.

Rosenblum, D. *et al.* (2018) 'Progress and challenges towards targeted delivery of cancer therapeutics', *Nature Communications*, 9(1), p. 1410. Available at: https://doi.org/10.1038/s41467-018-03705-y.

Rowe, R., Sheskey, P. and Quinn, M. (2009) 'Handbook of Pharmaceutical Excipients', *Handbook of pharmaceutical excipients, Sixth edition*, pp. 549–553. Available at: https://doi.org/10.1016/S0168-3659(01)00243-7.

Rudra Murthy, B. V. and Gumtapure, V. (2020) 'Thermo-physical analysis of natural shellac wax as novel bio-phase change material for thermal energy storage applications', *Journal of Energy Storage*, 29(April), p. 101390. Available at: https://doi.org/10.1016/j.est.2020.101390.

Sailaja, U. *et al.* (2016) 'Molecular dynamics of amorphous pharmaceutical fenofibrate studied by broadband dielectric spectroscopy', *Journal of Pharmaceutical Analysis*, 6(3), pp. 165–170. Available at: https://doi.org/10.1016/j.jpha.2014.09.003.

Sanganwar, G.P. and Gupta, R.B. (2008) 'Dissolution-rate enhancement of fenofibrate by adsorption onto silica using supercritical carbon dioxide', *International Journal of Pharmaceutics*, 360(1–2), pp. 213–218. Available at: https://doi.org/10.1016/j.ijpharm.2008.04.041.

Sapkale, G.N. *et al.* (2010) 'Supercritical Fluid Extraction', *Int. J. Chem. Sci*, 8(2), pp. 729–743. Available at: http://www.tsijournals.com/articles/supercritical-fluid-extraction--a-review.pdf (Accessed: 23 July 2018).

Saravanan, M. and Domb, A.J. (2013) 'A contemporary review on – polymer stereocomplexes and its biomedical application', *European Journal of Nanomedicine*, 5(2), pp. 81–96. Available at: https://doi.org/10.1515/ejnm-2012-0017.

Sarhangi Fard, A. and Anderson, P.D. (2013) 'Simulation of distributive mixing inside mixing elements of co-rotating twin-screw extruders', *Computers and Fluids*, 87, pp. 79–91. Available at: https://doi.org/10.1016/j.compfluid.2013.01.030.

Sathigari, S.K. *et al.* (2012) 'Amorphous-State Characterization of Efavirenz—Polymer

Hot-Melt Extrusion Systems for Dissolution Enhancement', *Journal of Pharmaceutical Sciences*, 101(9), pp. 3456–3464. Available at: https://doi.org/10.1002/JPS.23125.

Schafroth, N. *et al.* (2012) 'Nano and microparticle engineering of water insoluble drugs using a novel spray-drying process', *Colloids and Surfaces B: Biointerfaces*, 90(1), pp. 8–15. Available at: https://doi.org/10.1016/j.colsurfb.2011.09.038.

Sekiguchi, K. and Obi, N. (1961) 'Studies on Absorption of Eutectic Mixture. I. A Comparison of the Behavior of Eutectic Mixture of Sulfathiazole and that of Ordinary Sulfathiazole in Man.', *Chemical & Pharmaceutical Bulletin*, 9(11), pp. 866–872. Available at: https://doi.org/10.1248/cpb.9.866.

Sekiguchi, K., Obi, N. and Ueda, Y. (1964) 'Studies on Absorption of Eutectic Mixture. II. Absorption of fused Conglomerates of Chloramphenicol and Urea in Rabbits.', *Chemical & Pharmaceutical Bulletin*, 12(2), pp. 134–144. Available at: https://doi.org/10.1248/cpb.12.134.

Serajuddin, A.T.M. (1999) 'Solid dispersion of poorly water-soluble drugs: Early promises, subsequent problems, and recent breakthroughs', *Journal of Pharmaceutical Sciences*, 88(10), pp. 1058–1066. Available at: https://doi.org/10.1021/JS980403L.

Shah, S. *et al.* (2013) 'Melt extrusion with poorly soluble drugs', *International Journal of Pharmaceutics*, 453(1), pp. 233–252. Available at: https://doi.org/10.1016/j.ijpharm.2012.11.001.

Shahiwala, A. and Misra, A. (2014) *Applications of Polymers in Drug Delivery*. Available at: http://eds.b.ebscohost.com.esf.idm.oclc.org/eds/ebookviewer/ebook/ZTAwMHRuYV9fNzk1MjMzX19BTg2?sid=78cd1389-7a58-4083-bb83-7696cd3d1331@sessionmgr102&vid=18&format=EB&rid=1.

Sharma, P., Negi, P. and Mahindroo, N. (2018) 'Recent advances in polymeric drug delivery carrier systems', *Advances in Polymers for Biomedical Applications*, pp. 369–388.

Shearer, G. and Tzoganakis, C. (2001) 'Distributive mixing profiles for co-rotating twin-screw extruders', *Advances in Polymer Technology*, 20(3), pp. 169–190. Available at:

https://doi.org/10.1002/adv.1014.

Shegokar, R. and Müller, R.H. (2010) 'Nanocrystals: Industrially feasible multifunctional formulation technology for poorly soluble actives', *International Journal of Pharmaceutics*, 399(1–2), pp. 129–139. Available at: https://doi.org/10.1016/j.ijpharm.2010.07.044.

Sheng, H.W. *et al.* (2006) 'Atomic packing and short-to-medium-range order in metallic glasses', *Nature*, 439(7075), pp. 419–425. Available at: https://doi.org/10.1038/nature04421.

Shenoy, A. V. (1999) *Rheology of filled polymer systems*, *Polymer*. Available at: https://doi.org/10.1007/s00726-011-1022-z.

Shergill, M. *et al.* (2016) 'Development and characterisation of sustained release solid dispersion oral tablets containing the poorly water soluble drug disulfiram', *International Journal of Pharmaceutics*, 497(1–2), pp. 3–11. Available at: https://doi.org/10.1016/J.IJPHARM.2015.11.029.

Shi, X., Shao, Y. and Sheng, X. (2018) 'A new polymorph of fenofibrate prepared by polymer-mediated crystallization', *Journal of Crystal Growth*, 498(May), pp. 93–102. Available at: https://doi.org/10.1016/j.jcrysgro.2018.05.030.

Shingel, K.I. *et al.* (2017) 'Solid dispersions of drugs in hyaluronan matrix: The role of the biopolymer in modulating drug activity in vivo', *Journal of Drug Delivery Science and Technology*, 39, pp. 140–146. Available at: https://doi.org/10.1016/J.JDDST.2017.03.018.

Sill, T.J. and von Recum, H.A. (2008) 'Electrospinning: Applications in drug delivery and tissue engineering', *Biomaterials*. Elsevier, pp. 1989–2006. Available at: https://doi.org/10.1016/j.biomaterials.2008.01.011.

Silverstein, R.W. and Bassler, G.C. (1962) 'Spectrometric identification of organic compounds', *Journal of Chemical Education*, 39(11), pp. 546–553. Available at: https://doi.org/10.1021/ed039p546.

Simões, M.F., Pinto, R.M.A. and Simões, S. (2019) 'Hot-melt extrusion in the pharmaceutical industry: toward filing a new drug application', *Drug Discovery Today*, 24(9), pp. 1749–1768. Available at: https://doi.org/10.1016/j.drudis.2019.05.013.

Singh, A.N., Mhaskar, V.V. and Dev, S. (1978) 'Chemistry of lac resin-VIII', *Tetrahedron*, 34(5), pp. 595–598. Available at: https://doi.org/10.1016/0040-4020(78)80058-1.

Singh, S., Singh Baghel, R. and Yadav, L. (2011) 'A review on solid dispersion', *Int. J. of Pharm. & Life Sci. (IJPLS)*, 2(9), pp. 1078–1095. Available at: http://www.ijplsjournal.com/issues PDF files/sep2011/11.pdf (Accessed: 2 July 2018).

Singhal, S., Lohar, V.K. and Arora, V. (2011) 'Hot Melt Extrusion Technique', *WebmedCentral PHARMACEUTICAL SCIENCES*, 2(1), pp. 1–20.

Solanki, N., Gupta, S.S. and Serajuddin, A.T.M. (2018) 'Rheological analysis of itraconazole-polymer mixtures to determine optimal melt extrusion temperature for development of amorphous solid dispersion', *European Journal of Pharmaceutical Sciences*, 111(September 2017), pp. 482–491. Available at: https://doi.org/10.1016/j.ejps.2017.10.034.

Solanki, N.G. *et al.* (2019) 'Effects of Surfactants on Itraconazole-HPMCAS Solid Dispersion Prepared by Hot-Melt Extrusion I: Miscibility and Drug Release', *Journal of Pharmaceutical Sciences*, 108(4), pp. 1453–1465. Available at: https://doi.org/10.1016/j.xphs.2018.10.058.

Soradech, S. *et al.* (2017) 'Utilization of shellac and gelatin composite film for coating to extend the shelf life of banana', *Food Control*, 73, pp. 1310–1317. Available at: https://doi.org/10.1016/j.foodcont.2016.10.059.

Soradech, S., Limatvapirat, S. and Luangtana-anan, M. (2013) 'Stability enhancement of shellac by formation of composite film: Effect of gelatin and plasticizers', *Journal of Food Engineering*, 116(2), pp. 572–580. Available at: https://doi.org/10.1016/j.jfoodeng.2012.12.035.

Sosnik, A. and Seremeta, K.P. (2015) 'Advantages and challenges of the spray-drying technology for the production of pure drug particles and drug-loaded polymeric carriers', *Advances in Colloid and Interface Science*, 223, pp. 40–54. Available at: https://doi.org/10.1016/j.cis.2015.05.003.

Speyer, R.F. (1993) *Thermal analysis of materials*. Marcel Dekker. Available at:

https://books.google.ie/books/about/Thermal_Analysis_of_Materials.html?id=5vTPIN_Y_FMC&redir_esc=y (Accessed: 31 July 2018).

Srilalitha, M.D.V. and Prasad, B.B. (2015) 'Structure and Crystallization Behaviour of Amorphous Fe76Tm4B20 Alloy Studied by DSC, SEM and EDS', *Procedia Materials Science*, 10(Cnt 2014), pp. 609–615. Available at: https://doi.org/10.1016/j.mspro.2015.06.013.

Srirangam, R. *et al.* (2008) 'Applications of hot-melt extrusion for drug delivery', *Expert Opinion on Drug Delivery*, 5(12), pp. 1357–1376. Available at: https://doi.org/10.1517/17425240802583421.

Stachurski, Z.H. (2011) 'On Structure and Properties of Amorphous Materials', *Materials*, 4(9), pp. 1564–1598. Available at: https://doi.org/10.3390/ma4091564.

Stanković, M., Frijlink, H.W. and Hinrichs, W.L.J. (2015) 'Polymeric formulations for drug release prepared by hot melt extrusion: application and characterization', *Drug Discovery Today*, 20(7), pp. 812–823. Available at: https://doi.org/10.1016/j.drudis.2015.01.012.

Stegemann, S. *et al.* (2007) 'When poor solubility becomes an issue: From early stage to proof of concept', *European Journal of Pharmaceutical Sciences*, 31(5), pp. 249–261. Available at: https://doi.org/10.1016/j.ejps.2007.05.110.

Steller, R.T. (1990) 'Theoretical model for flow of polymer melts in the screw channel', *Polymer Engineering & Science*, 30(7), pp. 400–407. Available at: https://doi.org/10.1002/pen.760300704.

Sun, D.D. and Lee, P.I. (2013) 'Evolution of Supersaturation of Amorphous Pharmaceuticals: The Effect of Rate of Supersaturation Generation', *Molecular Pharmaceutics*, 10(11), pp. 4330–4346. Available at: https://doi.org/10.1021/mp400439q.

Sun, D.D. and Lee, P.I. (2014) 'Crosslinked hydrogels—a promising class of insoluble solid molecular dispersion carriers for enhancing the delivery of poorly soluble drugs', *Acta Pharmaceutica Sinica B*, 4(1), pp. 26–36. Available at: https://doi.org/10.1016/J.APSB.2013.12.002.

Szafraniec-Szczęsny, J. *et al.* (2021a) 'How Does the Addition of Kollidon®VA64 Inhibit the Recrystallization and Improve Ezetimibe Dissolution from Amorphous Solid Dispersions?', *Pharmaceutics*, 13(2), p. 147. Available at: https://doi.org/10.3390/pharmaceutics13020147.

Szafraniec-Szczęsny, J. *et al.* (2021b) 'How Does the Addition of Kollidon®VA64 Inhibit the Recrystallization and Improve Ezetimibe Dissolution from Amorphous Solid Dispersions?', *Pharmaceutics*, 13(2), p. 147. Available at: https://doi.org/10.3390/pharmaceutics13020147.

Szydlowski, W. and White, J.L. (1987) 'An improved theory of metering in an intermeshing corotating twin-screw extruder', *Advances in Polymer Technology*, 7(2), pp. 177–183. Available at: https://doi.org/10.1002/adv.1987.060070206.

Tadmor, Z. and Gogos, C.G. (2006) *Principles of Polymer Processing*. 2nd edn. John Wiley & Sons, Inc.

Tadmor, Z. and Klein, I. (1970) *Engineering principles of plasticating extrusion*. Van Nostrand Reinhold Co. (Polymer science and engineering series). Available at: https://books.google.ie/books?id=pth_PbbUeZQC.

Tadmor, Z., Lipshitz, S.D. and Lavie, R. (1974) 'Dynamic model of a plasticating extruder', *Polymer Engineering and Science*, 14(2), pp. 112–119. Available at: https://doi.org/10.1002/pen.760140206.

Tahara, K., Yamamoto, K. and Nishihata, T. (1995) 'Overall mechanism behind matrix sustained release (SR) tablets prepared with hydroxypropyl methylcellulose 2910', *Journal of Controlled Release*, 35(1), pp. 59–66. Available at: https://doi.org/10.1016/0168-3659(95)00021-Y.

Tang, X.C., Pikal, M.J. and Taylor, L.S. (2002) 'A spectroscopic investigation of hydrogen bond patterns in crystalline and amorphous phases in dihydropyridine calcium channel blockers', *Pharmaceutical Research*, 19(4), pp. 477–483. Available at: https://doi.org/10.1023/A:1015147729564.

Thakuria, R. *et al.* (2013) 'Pharmaceutical cocrystals and poorly soluble drugs', *International Journal of Pharmaceutics*, 453(1), pp. 101–125. Available at: https://doi.org/10.1016/J.IJPHARM.2012.10.043.

Thombare, N. *et al.* (2022) 'Shellac as a multifunctional biopolymer: A review on properties, applications and future potential', *International Journal of Biological Macromolecules*, 215(March), pp. 203–223. Available at: https://doi.org/10.1016/j.ijbiomac.2022.06.090.

Ting, J.M. *et al.* (2018) 'Advances in Polymer Design for Enhancing Oral Drug Solubility and Delivery', *Bioconjugate Chemistry*, 29(4), pp. 939–952. Available at: https://doi.org/10.1021/acs.bioconjchem.7b00646.

Tiwari, G. *et al.* (2012) 'Drug delivery systems: An updated review.', *International journal of pharmaceutical investigation*, 2(1), pp. 2–11. Available at: https://doi.org/10.4103/2230-973X.96920.

Tiwari, R. V., Patil, H. and Repka, M.A. (2016) 'Contribution of hot-melt extrusion technology to advance drug delivery in the 21st century', *Expert Opinion on Drug Delivery*, 13(3), pp. 451–464. Available at: https://doi.org/10.1517/17425247.2016.1126246.

Todd, D.B. (1998) *Plastics Compounding: Equipment and Processing*. Hanser (Polymer Processing Institute Books from Hanser Publishers). Available at: https://books.google.ie/books?id=CHKOHAAACAAJ.

Tran, P. *et al.* (2019) 'Overview of the manufacturing methods of solid dispersion technology for improving the solubility of poorly water-soluble drugs and application to anticancer drugs', *Pharmaceutics*, 11(3), pp. 1–26. Available at: https://doi.org/10.3390/pharmaceutics11030132.

Tran, P. and Park, J. (2021) 'Application of supercritical fluid technology for solid dispersion to enhance solubility and bioavailability of poorly water-soluble drugs', *International Journal of Pharmaceutics*, 610(October), p. 121247. Available at: https://doi.org/10.1016/j.ijpharm.2021.121247.

Tran, P.H.L., Lee, B.J. and Tran, T.T.D. (2021) 'Recent studies on the processes and

formulation impacts in the development of solid dispersions by hot-melt extrusion', *European Journal of Pharmaceutics and Biopharmaceutics*, 164(February), pp. 13–19. Available at: https://doi.org/10.1016/j.ejpb.2021.04.009.

Tziomalos, K. and Athyros, V.G. (2006) 'Fenofibrate: A novel formulation (Triglide™) in the treatment of lipid disorders: A review', *International Journal of Nanomedicine*, 1(2), pp. 129–147. Available at: https://doi.org/10.2147/nano.2006.1.2.129.

Uhrich, K.E. *et al.* (1999) 'Polymeric Systems for Controlled Drug Release', *Chemical Reviews*, 99(11), pp. 3181–3198. Available at: https://doi.org/10.1021/cr940351u.

Umemoto, Y. *et al.* (2020) 'An effective polyvinyl alcohol for the solubilization of poorly water-soluble drugs in solid dispersion formulations', *Journal of Drug Delivery Science and Technology*, 55(October 2019), p. 101401. Available at: https://doi.org/10.1016/j.jddst.2019.101401.

Ummadi, S. *et al.* (2013) 'Overview on Controlled Release Dosage Form Sathish', *International Journal of Pharma Sciences*, 7, pp. 51–60.

Unagolla, J.M. and Jayasuriya, A.C. (2018) 'Drug transport mechanisms and in vitro release kinetics of vancomycin encapsulated chitosan-alginate polyelectrolyte microparticles as a controlled drug delivery system', *European Journal of Pharmaceutical Sciences*, 114(September 2017), pp. 199–209. Available at: https://doi.org/10.1016/j.ejps.2017.12.012.

United States Pharmacopeial Convention. (2006) *The United States Pharmacopeia : the National Formulary*. United States Pharmacopeial Convention. Available at: https://books.google.ie/books/about/U_S_Pharmacopeia_National_Formulary.html?id=3eEjAQAAMAAJ&redir_esc=y (Accessed: 30 July 2018).

Usher, A.P. (1954) *A History of Mechanical Inventions*. Dover (Dover Books explaining science). Available at: https://books.google.ie/books?id=xuDDqqa8FlwC.

do Val Siqueira, L. *et al.* (2021) 'Starch-based biodegradable plastics: methods of production, challenges and future perspectives', *Current Opinion in Food Science*, 38, pp. 122–130. Available at: https://doi.org/10.1016/j.cofs.2020.10.020.

Vasconcelos, T., Sarmento, B. and Costa, P. (2007) 'Solid dispersions as strategy to improve oral bioavailability of poor water soluble drugs', *Drug Discovery Today*, 12(23–24), pp. 1068–1075. Available at: https://doi.org/10.1016/j.drudis.2007.09.005.

Venkatesh, C. *et al.* (2021) 'Influence of extrusion screw speed on the properties of halloysite nanotube impregnated polylactic acid nanocomposites', *Journal of Polymer Engineering*, 41(6), pp. 499–508. Available at: https://doi.org/10.1515/polyeng-2020-0228.

Vilhelmsen, T., Eliasen, H. and Schæfer, T. (2005) 'Effect of a melt agglomeration process on agglomerates containing solid dispersions', *International Journal of Pharmaceutics*, 303(1–2), pp. 132–142. Available at: https://doi.org/10.1016/j.ijpharm.2005.07.012.

Vimalson, D.C. *et al.* (2016) 'Techniques to Enhance Solubility of Hydrophobic Drugs: An Overview', *Asian Journal of Pharmaceutics*, 10(2), pp. 1–5. Available at: https://doi.org/10.22377/AJP.V10I2.625.

Vogt, M., Kunath, K. and Dressman, J.B. (2008) 'Dissolution enhancement of fenofibrate by micronization, cogrinding and spray-drying: Comparison with commercial preparations', *European Journal of Pharmaceutics and Biopharmaceutics*, 68(2), pp. 283–288. Available at: https://doi.org/10.1016/j.ejpb.2007.05.010.

Wagner, J.R., Mount, E.M. and Giles, H.F. (2014) 'Extrusion Process', in *Extrusion*. William Andrew Publishing, pp. 3–11. Available at: https://doi.org/10.1016/B978-1-4377-3481-2.00001-6.

Wahl, D.A. and Czernuszka, J.T. (2006) 'Collagen-hydroxyapatite composites for hard tissue repair', *European Cells and Materials*, 11(May), pp. 43–56. Available at: https://doi.org/10.22203/eCM.v011a06.

Van Der Wal, D.J. *et al.* (1996) 'Three-dimensional flow modeling of a self-wiping corotating twin-screw extruder. Part II: The kneading section', *Polymer Engineering and Science*, 36(7), pp. 912–924. Available at: https://doi.org/10.1002/pen.10479.

Walker, P.H. and Steele, L.L. (1923) *Shellac*. US Government Printing Office.

Wang, F. *et al.* (2015) 'Mechanical properties and thermal conductivity of graphene

nanoplatelet/epoxy composites', *Journal of Materials Science*, 50(3), pp. 1082–1093. Available at: https://doi.org/10.1007/s10853-014-8665-6.

Wang, H. *et al.* (2013) 'Formulation and particle size reduction improve bioavailability of poorly water-soluble compounds with antimalarial activity.', *Malaria research and treatment*, 2013, p. 769234. Available at: https://doi.org/10.1155/2013/769234.

Wang, L. *et al.* (1999) 'Characterization of natural resin shellac by reactive pyrolysis-gas chromatography in the presence of organic alkali', *Analytical Chemistry*, 71(7), pp. 1316–1322. Available at: https://doi.org/10.1021/ac981049e.

Wang, R., Pellerin, C. and Lebel, O. (2009) 'Role of hydrogen bonding in the formation of glasses by small molecules: A triazine case study', *Journal of Materials Chemistry*, 19(18), pp. 2747–2753. Available at: https://doi.org/10.1039/b820294j.

Wang, X. *et al.* (2006) 'Present research on the composition and application of lac', *Forestry Studies in China*, 8(1), pp. 65–69. Available at: https://doi.org/10.1007/s11632-006-0012-9.

Watterson, S. *et al.* (2014) 'Thermodynamics of fenofibrate and solubility in pure organic solvents', *Fluid Phase Equilibria*, 367, pp. 143–150. Available at: https://doi.org/10.1016/j.fluid.2014.01.029.

Wen, H., Jung, H. and Li, X. (2015) 'Drug Delivery Approaches in Addressing Clinical Pharmacology-Related Issues: Opportunities and Challenges', *The AAPS Journal*, 17(6), pp. 1327–1340. Available at: https://doi.org/10.1208/s12248-015-9814-9.

Werner, H. (1978) 'An analysis of the conveying characteristics of twin screw, co-rotating extruders'.

Whelan, T. and Goff, J. (1988) *The Dynisco Extrusion Processors Handbook*. 2nd edn. Edited by D. Delaney. Available at: https://scholar.google.dk/scholar?hl=en&q=The+Dynisco+Extrusion+Processors+Handbook&btnG=&as_sdt=1%2C5&as_sdtp=#0.

White, J.L. and Chen, Z. (1994) 'Simulation of non-isothermal flow in modular co-rotating twin screw extrusion', *Polymer Engineering & Science*, 34(3), pp. 229–237. Available at:

https://doi.org/10.1002/pen.760340309.

White, J.L., Potente, H. and Berghaus, U. (2003) *Screw Extrusion: Science and Technology*. Hanser.

Williams, H. D. *et al.* (2013) 'Strategies to Address Low Drug Solubility in Discovery and Development', *Pharmacological Reviews*, 65(1), pp. 315–499. Available at: https://doi.org/10.1124/pr.112.005660.

Williams, Hywel D. *et al.* (2013) 'Strategies to Address Low Drug Solubility in Discovery and Development', *Pharmacological Reviews*, 65(1), pp. 315–499. Available at: https://doi.org/10.1124/pr.112.005660.

Williams, M. *et al.* (2010) 'Hot-Melt Extrusion Technology: optimising drug delivery', *European Journal of Parenteral & Pharmaceutical Sciences*, (7), pp. 7–10.

Williams, R.O., Watts, A.B. and Miller, D.A. (2016) *Formulating Poorly Water Soluble Drugs*. Springer International Publishing (AAPS Advances in the Pharmaceutical Sciences Series). Available at: https://books.google.ie/books?id=bbu8DQAAQBAJ.

Wunderlich, B. (2001) 'Thermal Analysis', in *Encyclopedia of Materials: Science and Technology*. Elsevier, pp. 9134–9141. Available at: https://doi.org/10.1016/B0-08-043152-6/01648-X.

Wuxi Weite Machinery Co., L. (2017) *Metal Extrusion Machine Basic Classification*. Available at: http://www.weitepress.com/news/metal-extrusion-machine-basic-classification-6160494.html (Accessed: 27 July 2018).

Xavier, F. (2015) 'Structure-Solubility-Stability Relationships : Solid State Forms of Active Ingredients', *Researchgate Reviews*, (July), pp. 1–32. Available at: https://doi.org/10.13140/RG.2.1.3839.2165.

Xie, H.L. *et al.* (2017) 'Numerical Simulation of Mixing Characteristics and Energy Consumption in Vane Extruders with Different Structure Parameters', *Journal of Macromolecular Science, Part B: Physics*, 56(6), pp. 395–408. Available at: https://doi.org/10.1080/00222348.2017.1316654.

Xu, Zhongbin *et al.* (2014) 'Development and Characterization of a Novel Polymer Microchannel Tube', *Polymer - Plastics Technology and Engineering*, 53(14), pp. 1442–1449. Available at: https://doi.org/10.1080/03602559.2014.909480.

Yan, G. *et al.* (2021) 'Physical properties of shellac material used for hot melt extrusion with potential application in the pharmaceutical industry', *Polymers*, 13(21). Available at: https://doi.org/10.3390/polym13213723.

Yang, H. -H and Manas-Zloczower, I. (1992) 'Flow field analysis of the kneading disc region in a co-rotating twin screw extruder', *Polymer Engineering & Science*, 32(19), pp. 1411–1417. Available at: https://doi.org/10.1002/pen.760321903.

Yang, W.-W. and Pierstorff, E. (2012) 'Reservoir-Based Polymer Drug Delivery Systems', *Journal of Laboratory Automation*, 17(1), pp. 50–58. Available at: https://doi.org/10.1177/2211068211428189.

Yang, Z. (2013) *Development of methods to predict and enhance the physical stability of hot melt extruded solid dispersions*. University of East Anglia.

Yang, Z. *et al.* (2019) 'Development of ibuprofen dry suspensions by hot melt extrusion: Characterization, physical stability and pharmacokinetic studies', *Journal of Drug Delivery Science and Technology*, 54(June), p. 101313. Available at: https://doi.org/10.1016/j.jddst.2019.101313.

Yee, C.S. (2013) *The Development of PVP-based Solid Dispersions using Hot Melt Extrusion for the Preparation of Immediate Release Formulations*, *Core.Kmi.Open.Ac.Uk*. University of East Anglia. Available at: http://core.kmi.open.ac.uk/download/pdf/19086311.pdf.

Yoshihashi, Y. *et al.* (2006) 'Estimation of physical stability of amorphous solid dispersion using differential scanning calorimetry', *Journal of Thermal Analysis and Calorimetry*, 85(3), pp. 689–692. Available at: https://doi.org/10.1007/s10973-006-7653-8.

Yoshinaga, M. *et al.* (2000) 'Mixing mechanism of three-tip kneading block in twin screw extruders', *Polymer Engineering and Science*, 40(1), pp. 168–178. Available at:

https://doi.org/10.1002/pen.11150.

Yu, D.G. *et al.* (2018) 'Electrospun amorphous solid dispersions of poorly water-soluble drugs: A review', *Journal of Controlled Release*, 292, pp. 91–110. Available at: https://doi.org/10.1016/j.jconrel.2018.08.016.

Yu, L. (2001) 'Amorphous pharmaceutical solids: preparation, characterization and stabilization', *Advanced Drug Delivery Reviews*, 48(1), pp. 27–42. Available at: https://doi.org/10.1016/S0169-409X(01)00098-9.

Yuan, Y. *et al.* (2021) 'Shellac: A promising natural polymer in the food industry', *Trends in Food Science and Technology*, 109(January), pp. 139–153. Available at: https://doi.org/10.1016/j.tifs.2021.01.031.

Yun, Y., Lee, B.K. and Park, K. (2014) 'Controlled drug delivery systems: the next 30 years', *Frontiers of Chemical Science and Engineering*, 8(3), pp. 276–279. Available at: https://doi.org/10.1007/s11705-014-1426-x.

Yun, Y.H., Lee, B.K. and Park, K. (2015) 'Controlled Drug Delivery: Historical perspective for the next generation', *Journal of Controlled Release*, 219, pp. 2–7. Available at: https://doi.org/10.1016/j.jconrel.2015.10.005.

Zhang, J. *et al.* (2014) 'Synthesis of oxidized glycerol monooleate-chitosan polymer and its hydrogel formation for sustained release of trimetazidine hydrochloride', *International Journal of Pharmaceutics*, 465(1–2), pp. 32–41. Available at: https://doi.org/10.1016/j.ijpharm.2014.02.001.

Zhang, M. *et al.* (2012) 'Formulation and delivery of improved amorphous fenofibrate solid dispersions prepared by thin film freezing', *European Journal of Pharmaceutics and Biopharmaceutics*, 82(3), pp. 534–544. Available at: https://doi.org/10.1016/j.ejpb.2012.06.016.

Zhang, Y. *et al.* (2010) 'DDSolver: An add-in program for modeling and comparison of drug dissolution profiles', *AAPS Journal*, 12(3), pp. 263–271. Available at: https://doi.org/10.1208/s12248-010-9185-1.

Zheng, H. *et al.* (2011) 'Thermal analysis of four insect waxes based on differential scanning calorimetry (DSC)', *Procedia Engineering*, 18, pp. 101–106. Available at: https://doi.org/10.1016/j.proeng.2011.11.016.

Zhou, D. *et al.* (2002) 'Physical stability of amorphous pharmaceuticals: Importance of configurational thermodynamic quantities and molecular mobility', *Journal of Pharmaceutical Sciences*, 91(8), pp. 1863–1872. Available at: https://doi.org/10.1002/jps.10169.

Zhu, W. and Jaluria, Y. (2001) 'Residence time and conversion in the extrusion of chemically reactive materials', *Polymer Engineering and Science*, 41(7), pp. 1280–1291. Available at: https://doi.org/10.1002/pen.10828.

Chapter 8 Appendices

8.1 Appendix A Technical data of various shellac materials used in this study

Hind Suter Shellac Private Limited
MANUFACTURER & EXPORTER
DE-WAXED SHELLAC, ALEURITIC ACID & BLEACHED LAC.

Regd. Office.
49/K, Dr. Abani Dutta Road
Salkia, Howrah-711 106 (INDIA)
Phone : 2665-7621/7681
Fax : 91-33-2665-4609
E-mail : support@hindsutershellac.com

Certificate of Analysis

Product	Dewaxed Shellac HS 700K	Release Date	13th March 2017
Batch Number	HS700/756	Analysed On	13th March 2017
Batch Size (Kgs)	500	Quantity Sampled	1 Kg
Mfg Date	16 February 2017	Retest date	15 February 2019

Serial No	Tests	Specification	Results
1.	Appearance	Flake form	Flake form
2.	Appearance (20% in EtOH)	Clear solution	Conform
3.	Insolubility (%)	Less than 0.2%	0.187%
4.	Colour	Less than 6	5.8
	Test Report according to E904, EU Reg 231/2012		
5.	Moisture (%)	Less than 2%	1.29%
6.	Acid Value	65 to 89	69.49
7.	Rosin	Absent	Absent
8.	Lead	Less than 2 mg/kg	0.36
9.	Total heavy metals	Less than 10 ppm	Less than 10 ppm
9.	Wax	Less than 0.2 g/ 100g	Less than 0.2 g/ 100g

Storage condition: Store under dark and dry conditions. Maximum storage temperature is 15°C.

Remark: The above sample complies as per specifications.

Analysed and Checked by	Approved by

A. F. Suter & Co Ltd

Certificate of Analysis

Product :	:	**AFS Shellac WL**
Batch Nr.	:	5297
Date of Production	:	05.06.2017
Retest date	:	04.06.2019
Appearance	:	Flake Form

Acid Value	:	68 – 76	74
Loss on Drying	:	max 2 %	1.3
Wax content	:	max 5.5 %	4.5
Lead	:	max 2 ppm	conforms
Rosin	:	absent	absent
Heavy metals	:	< 10 ppm	< 10 ppm

Witham, 20.7.2017

A.F. Suter & Co Ltd

Compass House
Eastways Industrial Estate
Witham
Essex CM8 3YQ

Tel: +44 (0) 1376 514953
Fax: +44 (0) 1376 514080
Email: afsuter@afsuter.com

A. F. Suter & Co Ltd

Certificate of Analysis

Product :	:	**AFS Shellac RTH**
Batch Nr.	:	Sample
Date of Production	:	13.12.2017
Retest date	:	12.12.2019
Appearance	:	Flake Form

Acid Value	:	68 – 76	75
Loss on Drying	:	max 4 %	2.9 %
Wax content	:	max 5.5 %	3.6 %
Flow	:		76 mm
Life	:		40 min/ 150°C
Lead	:	max 2 ppm	conforms
Rosin	:	absent	absent
Heavy metals	:	< 10 ppm	< 10 ppm

Witham, 14.12.2017

A.F. Suter & Co Ltd

Compass House
Eastways Industrial Estate
Witham
Essex CM8 3YQ

Tel: +44 (0) 1376 514953
Fax: +44 (0) 1376 514080
Email: afsuter@afsuter.com

A. F. Suter & Co Ltd

AFS SHELLAC RTH

AFS Shellac RTH is produced from light coloured seedlac by the melting process.

CAS No.	**:**	**9000-59-3**
Appearance	**:**	**Thin, hard brittle transparent, pale yellow flakes**
Storage	**:**	**Cool dry ambient, below 20° C**
Packing	**:**	**25 Kg paper bags**

Acid Value (direct)	:	68 - 76 mg KOH/g
Wax Content	:	5.5% wt. max
Rosin Content	:	Nil
Arsenic	:	<3 ppm
Heavy Metals	:	<10 ppm
Moisture	:	2.0% wt. max

10.2017

Compass House
Eastways Industrial Estate
Witham
Essex CM8 3YQ

Tel: +44 (0) 1376 514953
Fax: +44 (0) 1376 514080
Email: afsuter@afsuter.com

8.2 Appendix B MATLAB program and output graph

```
%% Screw profile for the double head without a gap
clc;
Rs=8,              %Radius of screw
Cl=12.5,           % central distance
S=16,              %Pitch
n=2,               % Number of heads
Rb=Cl-Rs,          %Radius of shaft
Rui=Cl/Rs,
alph=2*(pi/(2*n)-acos(Rui/2)),

Xq= -Rs*cos (alph/2),
Yq= -Rs*sin (alph/2),

figure (10),
theta7=pi*0.5-alph/2:0.0005:pi*0.5+alph/2,
r7(1:length(theta7))=Rs
polar(theta7,r7),
hold on,

theta2=pi/2+alph/2:0.0005:pi-alph/2,
rho2=-Rs*cos(pi-theta2-alph/2)+sqrt(Cl.^2-Rs.^2 * (sin(pi-theta2-alph/2)).^2),
polar(theta2,rho2),
hold on,

theta6=pi-alph/2:0.0005:pi+alph/2,
r6(1:length(theta6))=Rb
polar(theta6,r6),
```

```
hold on,

theta3=pi+alph/2:0.0005:pi*1.5-alph/2,
rho3=-Rs*cos(theta3-pi-alph/2)+sqrt(Cl.^2-Rs.^2 * (sin(theta3-pi-alph/2)).^2),
polar(theta3,rho3),
hold on,

theta8=1.5*pi-alph/2:0.0005:1.5*pi+alph/2,
r8(1:length(theta8))=Rs
polar(theta8,r8),
hold on,

theta4=pi*1.5+alph/2:0.0005:pi*2-alph/2,
rho4=-Rs*cos(2*pi-theta4-alph/2)+sqrt(Cl.^2-Rs.^2 * (sin(2*pi-theta4-alph/2)).^2),
polar(theta4,rho4),
hold on,

theta5=-alph/2:0.0005:alph/2,
r5(1:length(theta5))=Rb
polar(theta5,r5),
hold on,

theta1=alph/2:0.0005:pi*0.5-alph/2,
rho1=-Rs*cos(theta1-alph/2)+sqrt(Cl.^2-Rs.^2 * (sin(theta1-alph/2)).^2),
polar(theta1,rho1),
hold on,

save 111.txt -ascii
```

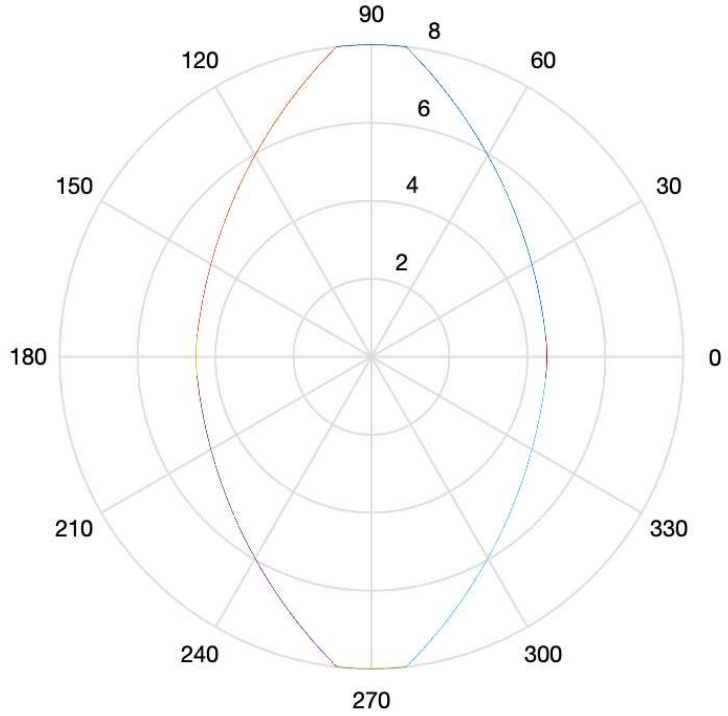


```
%%   Screw profile for the double head with a gap
clc;
Rs=7.8,              %Radius of screw
Cl=12.3,             % central distance
S=16,                %Pitch
n=2,                 % Number of heads
Rb=Cl-Rs,            %Radius of shaft
Rui=Cl/Rs,
alph=2*(pi/(2*n)-acos(Rui/2)),
Xq= -Rs*cos (alph/2),
Yq= -Rs*sin (alph/2),

figure (10),
theta7=pi*0.5-alph/2:0.0005:pi*0.5+alph/2,
```

```
r7(1:length(theta7))=Rs
polar(theta7,r7),
hold on,

theta2=pi/2+alph/2:0.0005:pi-alph/2,
rho2=-Rs*cos(pi-theta2-alph/2)+sqrt(Cl.^2-Rs.^2 * (sin(pi-theta2-alph/2)).^2),
polar(theta2,rho2),
hold on,

theta6=pi-alph/2:0.0005:pi+alph/2,
r6(1:length(theta6))=Rb
polar(theta6,r6),
hold on,

theta3=pi+alph/2:0.0005:pi*1.5-alph/2,
rho3=-Rs*cos(theta3-pi-alph/2)+sqrt(Cl.^2-Rs.^2 * (sin(theta3-pi-alph/2)).^2),
polar(theta3,rho3),
hold on,

theta8=1.5*pi-alph/2:0.0005:1.5*pi+alph/2,
r8(1:length(theta8))=Rs
polar(theta8,r8),
hold on,

theta4=pi*1.5+alph/2:0.0005:pi*2-alph/2,
rho4=-Rs*cos(2*pi-theta4-alph/2)+sqrt(Cl.^2-Rs.^2 * (sin(2*pi-theta4-alph/2)).^2),
polar(theta4,rho4),
hold on,
```

```
theta5=-alph/2:0.0005:alph/2,
r5(1:length(theta5))=Rb
polar(theta5,r5),
hold on,

theta1=alph/2:0.0005:pi*0.5-alph/2,
rho1=-Rs*cos(theta1-alph/2)+sqrt(Cl.^2-Rs.^2 * (sin(theta1-alph/2)).^2),
polar(theta1,rho1),
hold on,

save 111.txt -ascii
```

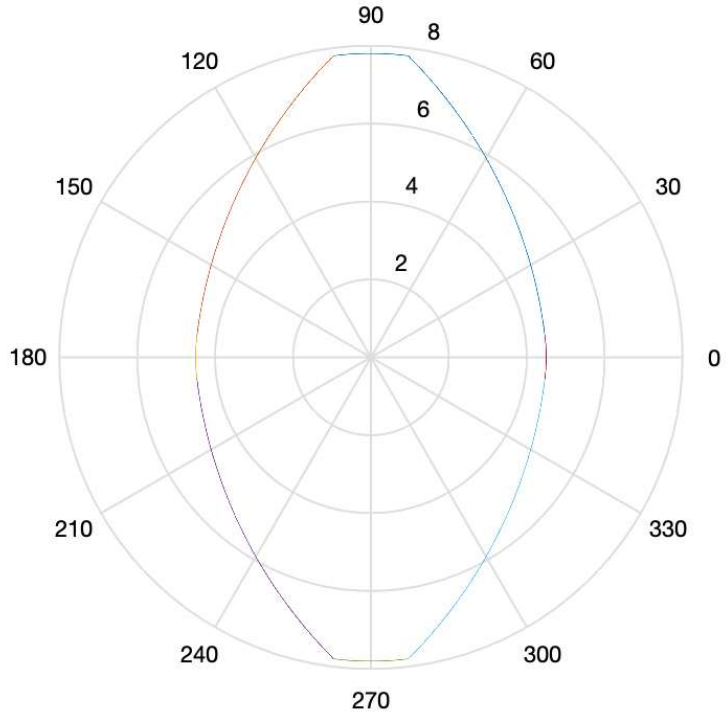

8.3 Appendix C DSC result graphs

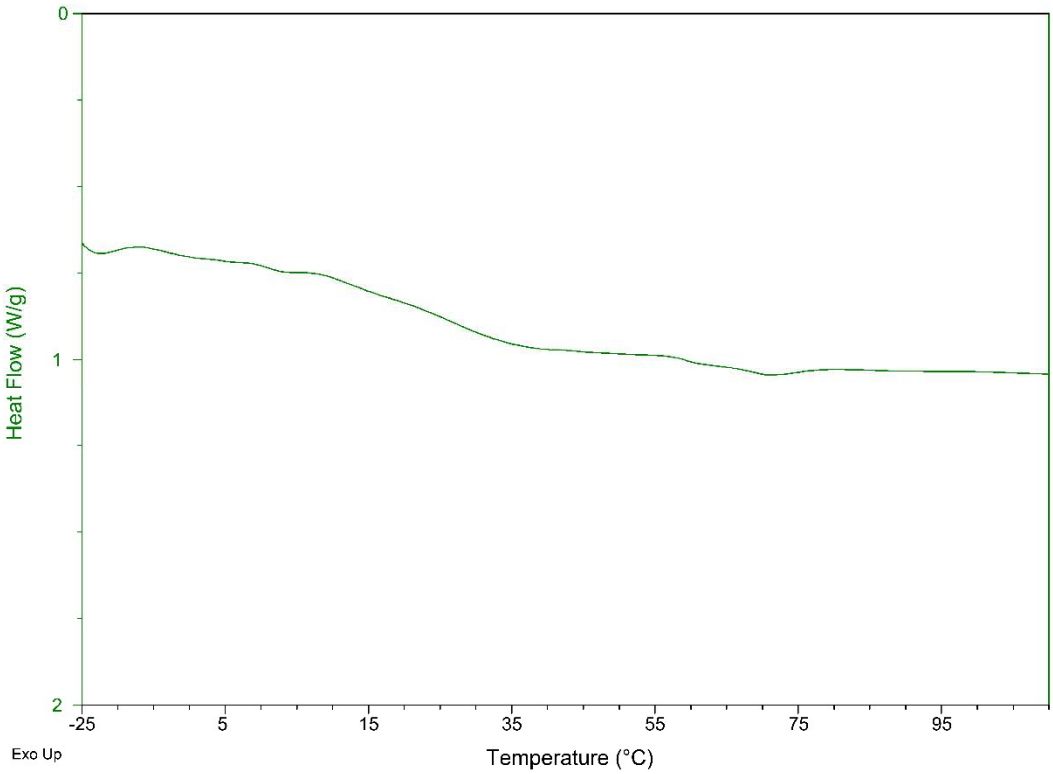

Figure 8-1 Full temperature range DSC result for S13

8.4 Appendix C Miscellaneous

THE SUNDAY TIMES GOOD UNIVERSITY GUIDE 2018 — INSTITUTE OF TECHNOLOGY OF THE YEAR

AIT Research

Hot melt enteric targeted therapeutic delivery platform

Enhancing drug solubility through advanced polymer extruded drug delivery system

Student: Guangming Yan **Supervisor: Dr.** Noel Gately

Abstract

A novel oral controlled release matrix tablet based on Shellac resin will be designed and developed, using Fenofibrate as a poorly soluble model drug. The Shellac-based matrix tablets will be prepared by Holt Melt Extrusion using various amounts of Shellac and drug loading. The effect of processing, temperature profile and pH of medium on drug release from matrix tablets will be investigated. The in-situ polymerization plays a major role on the changes in Shellac properties during storage. Also a continuous downstream process to produce a finished, ready to package dosage form direct from the extruder will be developed.

Experimental Details

In this study, four different kinds of Shellac were chosen as the drug carrier. This includes two dewaxed Shellac's, the first sourced from A. F. Suter & Co Ltd named as HS700K, and another one, SSB 55 Pharma FL obtained from SSB Stroever Schellack, Bremen, Germany. Two wax containing Shellac's were acquired from A. F. Suter namely Shellac RTH and Shellac WL. Two more co-polymer material's from Eudragit, called S-100 and L-100 were also included in the study.

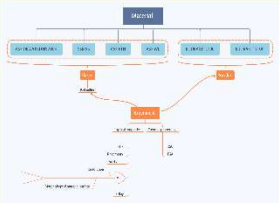

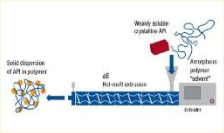

Fig. 1 Schematic representation of hot-melt extrusion using in pharmaceutical industry

Current Experiment Result

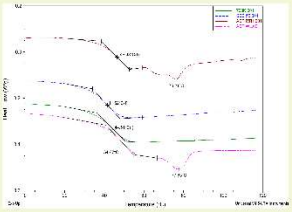

Fig. 2 Glass transition temperature (Tg) for each of the different Shellac's. The dewax Shellac have a lower Tg compare to the other two Shellac, and the Wax contain Shellac have an unexpected peak which may be the wax.

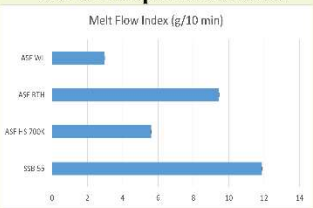

Fig. 3 Melt Flow Index of different Shellac (90°C, 1.2Kg), SSB 55 have the highest MFI value which indicate that at 90 °C the SSB 55 have a lower viscosity.

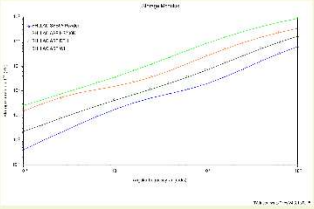

Fig. 4 Storage Modulus of the Shellac's at 90°C

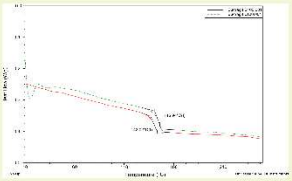

Fig. 5 Glass transition temperature (Tg) of Eudragit co-polymer, when compared to the Shellac Eudragit have a significant higher Tg.

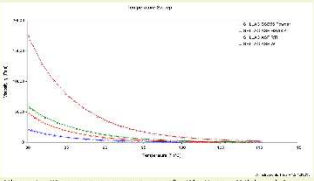

Fig. 6 Temperature sweep of Shellac. With rising temperature, the viscosity of Shellac decreases. In lower temperature range, SSB 55 have the lowest viscosity which correlates to the MFI result, but when at higher temperature range all Shellac's have the similar behavior, that being a very low viscosity value.

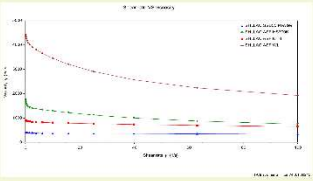

Fig. 7 Frequency sweep at 90 °C. With increasing shear rate, the viscosity of Shellac decreases. When compared to the others, SSB 55 have the lowest viscosity in all shear rate ranges.

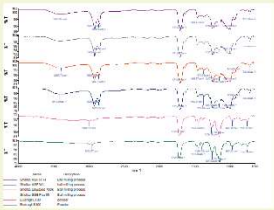

Fig. 8 FTIR Spectra for each of the Shellac resins and Eudragit co-polymer

Conclusion

Even though the investigated Shellac types all meet the pharmacopoeia specifications for physicochemical properties, differences between grades of Shellac resins are apparent such as Acid value, Tg , viscosity, pKa value, processability and dissolution profiles. This may be partly due to the different sources of Seedlac and the subsequent refining process (melting process, bleaching process, solvent extraction). Moreover, with long-term storage of the resin, self-esterification may become an issue for long-term stability..

Reference

Coelho, C., Nanabala, R., Ménager, M., Commereuc, S., & Verney, V. (2012). Molecular changes during natural biopolymer ageing - The case of Shellac. Polymer Degradation and Stability, 97(6), 936–940. https://doi.org/10.1016/j.polymdegradstab.2012.03.024

Farag, Y., & Leopold, C. S. (2009). Physicochemical properties of various Shellac types. Dissolution Technologies, 16(2), 33–39. https://doi.org/10.14227/DT160209P33

Pharma Solutions. (2018, April 21). Hot-melt extrusion for enhanced solubility and bioavailability. Retrieved from O-BASF: https://pharmaceutical.basf.com/en/Drug-Formulation/Hot-melt-extrusion.html

THE SUNDAY TIMES GOOD UNIVERSITY GUIDE 2018 — INSTITUTE OF TECHNOLOGY OF THE YEAR

AIT Research

AIT Research

Hot melt enteric targeted therapeutic delivery platform

Enhancing drug solubility through advanced polymer extruded drug delivery system

Student: Guangming Yan **Supervisor:** Dr. Noel Gately, Dr. Zhi Cao, Dr. Declan Devine

Abstract

The overall aim of this project is to produce a novel oral controlled release matrix tablet to increase the solubility of Fenofibrate based on shellac resin. This novel work currently characterises various types of shellac and investigates their physicochemical properties along with their processability in the hot melt extrusion process. Physicochemical and thermal properties of each material were characterized by various methods. The processability characterization was achieved using Melt flow index and rheology analysis. This initial study provides essential data to determine the processing conditions for each shellac material for subsequent hot melt extrusion processing.

Materials

In this study, four different commercially available pharmaceutical grade Shellac materials were chosen as potential drug carrier candidates. This includes two dewaxed Shellac's, the first sourced from A. F. Suter & Co Ltd named as 700K, and another one, SSB 55 Pha obtained from SSB Stroever Schellack, Bremen, Germany. Two wax containing Shellac's were acquired from A. F. Suter namely Shellac RTH and Shellac WL.

Experimental Details

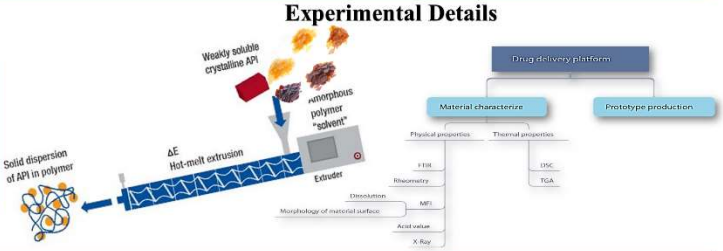

Current Experiment Result

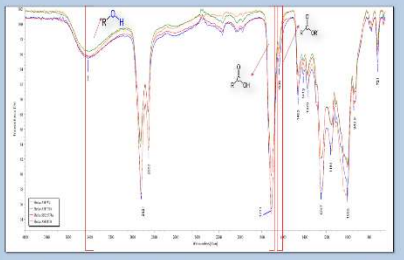

Fig.1 FTIR Spectra for each of the Shellac resins shows all the existing peaks of various shellac are almost the same, also it confined that shellac is a mixture contained ester, acid and hydroxyls groups.

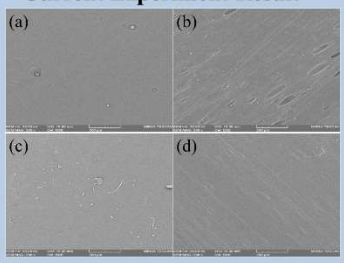

Fig.2 SEM image of four types of shellac at 200x for raw flake material, (a)Shellac ASF 700K, (b)Shellac ASF RTH, (c)Shellac SSB 55 Pha, (d)Shellac ASF WL.

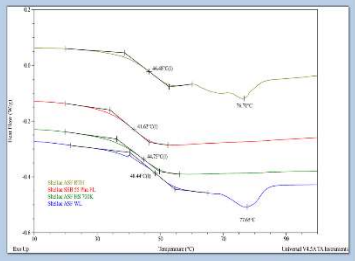

Fig.3 Glass transition temperature (T_g) for each Shellac material. The dewaxed Shellac have a lower T_g compare to the other two Shellac, and the Wax contain Shellac have an unexpected peak which is due to the wax.

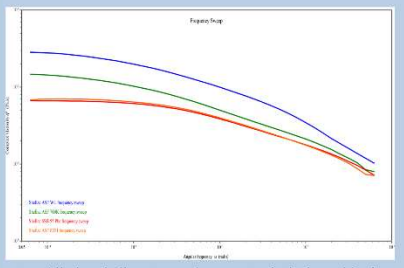

Fig.4 All the shellac types shows a typical shear-thinning behaviors, bleaching process and wax containing have greatly affected the properties of shellac.

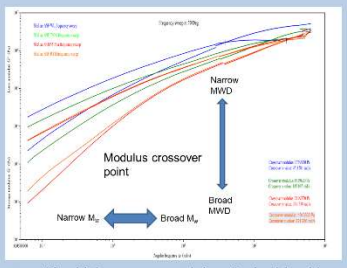

Fig.5 The higher wax containing & the bleaching process have an increasing viscosity effect and a shift modulus crossover point to the left.

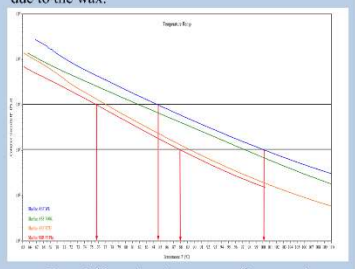

Fig.6 Extrudable viscosity range for a polymer material can be 1000 to 10000 Pa*s, which is low enough for the drug to dissolve in it and high enough for the extrusion process.

Conclusion

All shellac materials are amorphous with no melting peak visible by DSC and have little differences in chemical structure using FTIR. Based on the rheology, the wax containing versions & the bleaching process have an increasing viscosity effect and a shift modulus crossover point to the left suggesting an increase in the elasticity of the melt. Additionally, the extrudable temperature ranges of different types of shellac were determined and due to their shear-thinning behaviors, can be extruded in lower temperature. This initial study provides crucial data to determine the process conditions for the hot melt extrusion process for each shellac material.

Acknowledgments

This research was funded by Irish Research Council (GOIPG/2018/2067) and Athlone Institute of Technology, Presidents Seed Fund.

Reference

Pharma Solutions. (2018, April 21). Hot-melt extrusion for enhanced solubility and bioavailability. Retrieved from O-BASF: https://pharmaceutical.basf.com/en/Drug-Formulation/Hot-melt-extrusion.html

AIT Research

THE SUNDAY TIMES GOOD UNIVERSITY GUIDE 2020 INSTITUTE OF TECHNOLOGY OF THE YEAR

IRISH RESEARCH COUNCIL An Chomhairle um Thaighde in Éirinn

"My Heart, Your Heart"

Hot melt enteric targeted therapeutic delivery platform

Enhancing drug solubility through advanced polymer extruded drug delivery system

Guangming Yan, Dr Zhi Cao, Dr Declan Devine, Dr Noel Gately

Introduction

Cardiovascular diseases (CVDs) are the number 1 cause of death globally. Fenofibrate has been shown an excellent treating effect on CVDs. However, Fenofibrate is a neutral, lipophilic compound that is practically insoluble in water, making it challenging to achieve therapeutic levels consistently. As a result, this project was using shellac material as the polymeric matrix to enhance the solubility of Fenofibrate by producing solid dispersion by hot melt extrusion.

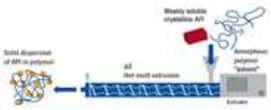

Aims

Enhance the solubility and bioavailability of Fenofibrate as an amorphous HME solid dispersion and develop a continuous downstream process to produce a finished, ready to package dosage form direct from the extruder.

Method

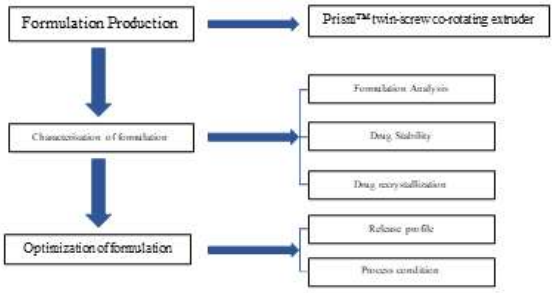

Result and discussion

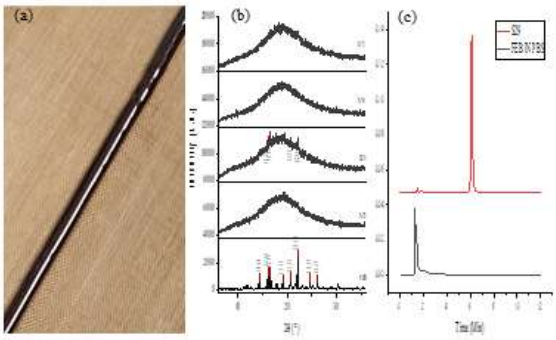

Fig. 1 (a) Formulation samples, (b) P-XRD result, (c) Overlay of HPLC response graph.

The extrudate can keep its shape well during processing, and the process condition has a noticeable impact on the extrudate and the state of the drug substance. Moreover, comparer to origin Fenofibrate substance, the drug in the shellac base solid dispersion formulation existing as amorphous state and have significant higher solubility in phosphate buffer solution.

Future Work

Formulation Optimise and downstream process study

- Formulation optimise and produce the formulation
- Characterization of the optimised formulation
- Downstream process review
- Downstream process development
- Downstream process simulation

Acknowledgment: This research was funded by Irish Research Council (GOIPG/2018/2067) and Athlone Institute of Technology, Presidents Seed Fund.

Reference

https://www.who.int/news-room/fact-sheets/detail/cardiovascular -diseases-(cvds)
https://www.drugbank.ca/drugs/DB01039

#Loveirish Research

THE SUNDAY TIMES GOOD UNIVERSITY GUIDE 2020 INSTITUTE OF TECHNOLOGY OF THE YEAR
AIT Research

THE SUNDAY TIMES GOOD UNIVERSITY GUIDE 2018 INSTITUTE OF TECHNOLOGY OF THE YEAR

AIT Research

Hot melt enteric targeted therapeutic delivery platform

Enhancing drug solubility through advanced polymer extruded drug delivery system

PHD Student: Guangming Yan **Supervisor:** Dr. Noel Gately, Dr. Zhi Cao, Dr. Declan Devine

#LoveIrish Research

Introduction

The solubility of the drug is a significant factor in achieving adequate absorption which correlates to poor bioavailability. However, literature states that about 70% of all drugs coming directly from synthesis are nowadays poorly soluble. If there is no way to improve drug solubility, it will not be able to be absorbed and reach the therapeutic concentration. However, hot melt extrusion (HME) has emerged as a powerful processing technology to produce pharmaceutical solid dosage forms that can provide improved bioavailability of poorly soluble drugs. Nonetheless, presently HME does not readily deliver a finished product that can be administered to the patient. Instead, HME provides molten material that needs to be further processed. In pharmaceutical applications, one of the significant challenges now is continuously shaping the final product. As a result, how to use HME consistently producing enhanced solubility drug formulation is a considerable challenge. In this context, this project funded by Irish government.

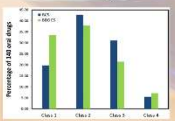

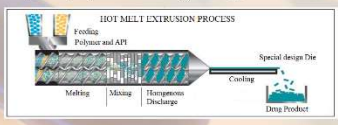

Therefore, the main aim of this study was to enhance the solubility and bioavailability of Fenofibrate as an amorphous HME solid dispersion and develop a continuous downstream process to produce a finished, ready to package dosage form direct from the extruder.

Methods

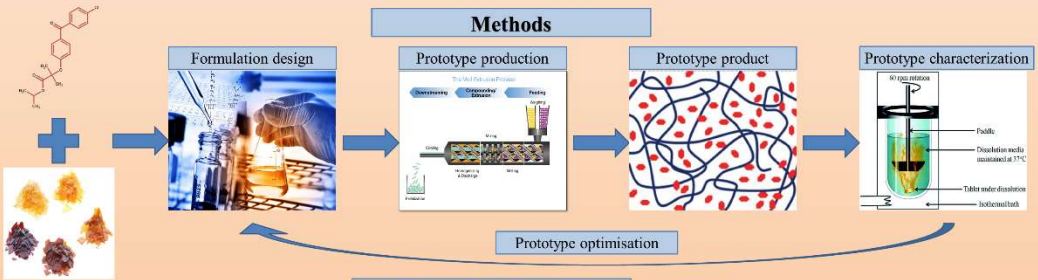

Current work result

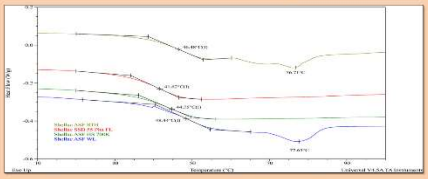

Fig.1 Glass transition temperature (T_g) for each Shellac material. It is advantageous that the glass transition temperature of the material well above storage or drug release temperature.

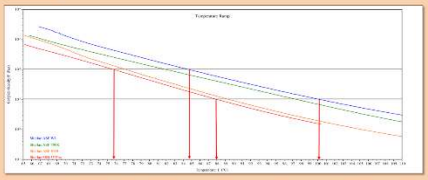

Fig. 2 Extrudable viscosity range for a polymer material can be 1000 to 10000 Pa*s, which is low enough for the drug to dissolve in it and high enough for the extrusion process.

Conclusion

Shellac material is a non-toxic and physiologically harmless material, FDA has listed shellac as GRAS material. Also because of its pH-sensitive properties, it can only be dissolved into a solution with a pH above 7.2. Our analysis showed that all shellac materials are amorphous with no melting peak visible by DSC and have an advantage that the glass transition temperature of the material well above storage and drug release temperature. Also, based on the rheology, the extrudable temperature ranges of different types of shellac were determined and due to their shear-thinning behaviors, can be extruded in lower temperature. This initial study provides crucial data to determine the process conditions for the hot melt extrusion process for each shellac material.

Acknowledgment

This research was funded by Irish Research Council (GOIPG/2018/2067) and Athlone Institute of Technology, Presidents Seed Fund.

Reference

Pharma Solutions. (2018, April 21). Hot-melt extrusion for enhanced solubility and bioavailability. Retrieved from O-BASF:https://pharm aceutical.basf.com/en/Drug-Formulation/Hot-melt-extrusion.html

Yanbin Huang, Wei-Guo Dai. 2014. Fundamental aspects of solid dispersion technology for poorly soluble drugs. Acta Pharmaceutica Sinica B, 2014; 4, (1): 18-25

https://medium.com/@jacob_barton/people-take-drugs-6ea5a762a0ce

https://kan.china.com/article/201729.html

http://www.yxxb.com.cn:8081/apsb/EN/abstract/html/20140105.htm

IRISH RESEARCH COUNCIL An Chomhairle um Thaighde in Éirinn

THE SUNDAY TIMES GOOD UNIVERSITY GUIDE 2018 INSTITUTE OF TECHNOLOGY OF THE YEAR

AIT Research

8.5 Appendix D Publication

polymers

MDPI

Article

Physical Properties of Shellac Material Used for Hot Melt Extrusion with Potential Application in the Pharmaceutical Industry

Guangming Yan [1], Zhi Cao [1], Declan Devine [1], Manfred Penning [2] and Noel M. Gately [1,*]

[1] Materials Research Institute, Technological University of the Shannon, Midlands Midwest, N37 HD68 Co. Westmeath, Ireland; g.yan@research.ait.ie (G.Y.); zhi.cao@tus.ie (Z.C.); declan.devine@tus.ie (D.D.)
[2] Shellac Consultant, Wormser Strasse 28, D-55277 Oppenheim, Germany; manfred.penning@t-online.de
* Correspondence: noel.gately@tus.ie; Tel.: +35-387-621-7186

Abstract: Hot melt extrusion offers an efficient way of increasing the solubility of a poorly soluble drug. Shellac has potential as a pharmaceutical matrix polymer that can be used in this extrusion process, with further advantages for use in enteric drug delivery systems. The rheological property of a material affects the extrusion process conditions. However, the literature does not refer to any published work that investigates the processability of various shellac materials. This work explores various types of shellac and explores their physicochemical and thermal properties along with their processability in the hot melt extrusion application. Physicochemical characterization of the materials was achieved using differential scanning calorimetry, Fourier transform infrared spectroscopy, scanning electron microscopy and energy-dispersive X-ray spectroscopy. Additional processability characterization was achieved using melt flow index and rheology analysis. The results indicated that there was no chemical difference between the various shellac types compared in this study. However, the extrudable temperature ranges and rheological properties of different shellac types varied; SSB 55 Pharma FL had the lowest processing temperature and glass transition temperatures. Due to the shear-thinning behaviours, shellac can be extruded at lower temperatures. This study provides necessary data to determine the processing conditions in hot melt extrusion applications for the range of shellac materials.

Keywords: shellac; hot melt extrusion; rheology; solubility enhancement; processability; DSC

check for updates

Citation: Yan, G.; Cao, Z.; Devine, D.; Penning, M.; Gately, N.M. Physical Properties of Shellac Material Used for Hot Melt Extrusion with Potential Application in the Pharmaceutical Industry. *Polymers* **2021**, *13*, 3723. https://doi.org/10.3390/polym13213723

Academic Editor: Beom Soo Kim

Received: 20 September 2021
Accepted: 26 October 2021
Published: 28 October 2021

Publisher's Note: MDPI stays neutral with regard to jurisdictional claims in published maps and institutional affiliations.

Copyright: © 2021 by the authors. Licensee MDPI, Basel, Switzerland. This article is an open access article distributed under the terms and conditions of the Creative Commons Attribution (CC BY) license (https://creativecommons.org/licenses/by/4.0/).

1. Introduction

Shellac is the refined form of the natural resin LAC produced by the female insect Kerria Lacca. India, Thailand and southwest China are the main production areas of LAC [1,2]. Shellac is a complex mixture consisting of aliphatic and alicyclic acid components. Different types of insect species and host trees determine the composition of shellac material. However, there are no chemical differences between various shellac material, only the contents of each component are different [3]. In various pharmacopoeias, shellac is classified by the refining process as well as the chemical properties and acid values. Besides the acid value, the shellac quality can be characterised by its glass transition temperature, pK_a value and intrinsic dissolution rate [4,5]. The use of shellac material can be traced back to ancient times; the best-known applications were as the binding material in music records and also used to prepare varnishes as the protective layer on artistic objects. However, it was replaced by synthetic polymer due to its brittleness [6–11]. Various types of shellac were developed to expand its application field by the addition of some additives or surfactants [10].

Because shellac is a non-toxic and physiologically harmless material, the US Food and Drug Administration (FDA) has listed shellac as Generally Recognized as Safe (GRAS)

material. With this fact, as well as its excellent film-forming and moisture-resistant properties, shellac has been widely used in the medicine and food industries as a coating material [12–15]. In the pharmaceutical industry, shellac was employed as an enteric coating material due to its pH-sensitive properties [16–19]. Pearnchob stated that shellac could provide the same water resistance and taste masking with a lower coating level [20]. Moreover, Ansari et al. (2013) made blends of shellac with novolac, which resulted in improved film properties. The new film showed improvement in gloss and impact resistance [21]. Silva et al. (2016) found that the encapsulated probiotic under simulated gastrointestinal conditions can be effectively protected by an alginate-shellac blend combined with coconut fat [22]. Additionally, Pearnchob et al. (2003) and Sontaya et al. (2008) investigated the feasibility of extended-release shellac-matrix tablets prepared by either compression of powder or wet granule methods [20,23]. In 2017, Gately et al. investigated targeted delivery of probiotics prepared by melt extrusion technology [24].

In modern industry, hot melt extrusion is a well-known, efficient industry processing technology. It forces raw materials through a die under controlled conditions to produce a product of uniform shape and density [25,26]. Over the last few years, hot melt extrusion has been inducted into the pharmaceutical industry [27]. It has long been known that twin-screw extrusion can increase the solubility of drugs by the formation of a solid dispersion [25,28]. Since Sekiguchi and Obi (1961) created the first solid dispersion, it has become the most successful method for enhancing the bioavailability of BCS class II compounds [29,30].

In the extrusion process, the material undergoes various temperatures and shear rates. Moreover, the melt behaviour of material in the extrusion process is significantly affected by the viscosity of the molten polymer. The processability of the material is appreciably affected by the way the polymer reacts with flow and deformation [31]. When determining the extrusion parameters before processing, for the polymers with high viscosity, they always require higher melt temperature profiles and higher shear rates in the barrel. Furthermore, discharge pressure and more power consumption are often required. This would help to reduce the number of trials needed to find the desired conditions for extrusion [32–35].

Following a review of the literature, it is clear that shellac is widely used in pharmaceutical and food industries as a coating material. However, the authors did not find a reference to any published work that investigates the processability of shellac material. As a result, this work will explore four different types of shellac (Dewaxed Shellac AFS HS 700K, AFS Shellac WL, AFS Shellac RTH and SSB 55 Pharma FL). From the material data sheet, all shellac materials used in this study were sourced from the same seedlac Kushmi type. However, refining processes are different, which results in different applications. Dewaxed shellac HS 700K and SSB 55 Pharma Fl are pharmaceutical grade and have a lower color index number because of the physical bleaching process. AFS shellac WL and AFS shellac RTH contain wax; they are refined from the same seedlac as the other two shellac types, but the hot melting process is used on a different date, which does not remove the naturally occurring wax contained in the Lac. In this study, the authors investigate the physicochemical properties and processability with the subsequent view of using shellac as a matrix polymer for enteric-targeted drug delivery systems [36,37].

2. Materials and Methods

2.1. Material

The shellac materials used in this study are shown in Table 1. Dewaxed Shellac AFS HS 700K, AFS Shellac WL and AFS Shellac RTH were received as gifts from A.F. Suter (Witham, UK). Shellac SSB 55 Pharma FL was received as a gift from SSB (Stroever Schellack, Bremen, Germany). All other reagents and solvents used were of analytical grade.

Table 1. Shellac materials used in this study.

Batch Name	Type	Seedlac	Refining Process	Bleaching Process	Wax Containing	Manufacture Date
Dewaxed Shellac AFS HS 700K	Dewaxed shellac	Kushmi	Solvent extraction	Activated carbon	Less than 0.2%	16 February 2017
SSB 55 Pharma FL	Dewaxed shellac	Kushmi	Solvent extraction	Activated carbon	Less than 0.2%	August 2017
AFS Shellac WL	Wax containing shellac	Kushmi	Melting process	N/A	4.5%	05 June 2017
AFS Shellac RTH	Wax containing shellac	Kushmi	Melting process	N/A	3.6%	13 December 2017

2.2. Grinding

Ground shellac was prepared by milling shellac flakes in a Planetary Mono Mill PULVERISETTE 6 (FRITSCH, Idar-Oberstein, Germany) classic line and sieving through a 500 µm mesh sieve. During the grinding process, a short grinding operation time of 30 s was employed to prevent the melting during milling. Ground shellac was used for the melt flow rate test; determination of thermal properties including glass transition temperatures (Tg), melt temperature and decomposition temperature (Td); Fourier transform Infrared spectroscopy (FT-IR) and rheology properties.

2.3. Differential Scanning Calorimetry (DSC)

A TA instrument DSC 2920 DSC (TA Instruments, New Castle, DE, USA) was used throughout the work. Samples of between 4 and 6 mg were weighed out using a Sartorius scale having a resolution of 1×10^{-5} g. Samples were then placed in non-perforated aluminium pans, which were crimped before testing, with an empty crimped aluminium pan being used as the reference cell. Volatiles were removed from the purging head with nitrogen at a rate of 30 mL/min. Calibration of the instrument was performed using indium as standard. Temperature ramp was from −30 to 120 °C at 10 °C/min. An isothermal step of 1 min at 120 °C was introduced to remove excessive water. The T_g and T_m were determined from the second heating run by TA Universal Analysis 2000 software version 4.5A (TA Instruments, New Castle, DE, USA) based on Standard ISO 11357-2 2020 [38]. The half-step-height method was used to determine the glass transition temperature.

2.4. Attenuated Total Reflectance Fourier Transform Infrared (ATR-FTIR) Spectroscopy

Attenuated total reflectance Fourier transform infrared spectroscopy (ATR-FTIR) Indexer (PerkinElmer, Waltham, MA, USA) was carried out on a Perkin Elmer Spectrum One fitted with a universal ATR sampling accessory. All data were recorded at room temperature, in the spectral range of 4000–650 cm^{-1}, utilizing a 16 scan per sample cycle and a fixed universal compression force of 70N. Subsequent analysis was carried out using OMNIC Spectrum software version 9.2.86 (Waltham, MA, USA).

2.5. Melt Flow Index (MFI)

Melt flow index values of the four different types of shellac were assessed using a fixed weight of 1.2 kg with a CEAST Melt Flow Quick Indexer (Instron Norwood, MA, USA) under ASTM D1238-10. The melted material flowed through an orifice of 2.095 mm diameter for 10 min, and the values were reported in g/10 min. All samples were tested at 90 °C.

2.6. Rheometer

Melt rheological experiments were carried out in an oscillatory mode, on a rotational rheometer TA Discovery HR-2 hybrid Rheometer (TA Instruments, New Castle, DE, USA) equipped with a parallel plate (25 mm diameter). All samples were measured at various

temperatures (70 °C, 80 °C, 90 °C) with 500 μm gap distance. Four types of experiments were carried out in this study. For the first experiment, oscillatory time sweeps were characterized at 90 °C and with constant angular frequency of 1 Hz and 1% strain. The second experiment was amplitude sweep performed with a strain range of 0.01% to 100% at an angular frequency of 1 Hz. The third experiment used oscillation frequency analysis with a constant strain of 1% and angular frequency performed with a range of 0.1 to 100 Hz. The final experiment was oscillation temperature sweep, where samples were heated from 65 to 110 °C with a heating ramp rate of 3 °C/min at a frequency of 1 Hz with a strain value of 1%. The instrument was calibrated before each test.

2.7. Dissolution Test

Dissolution testing was carried out using a Sotax AT7 smart dissolution system from Carl Stuart Ltd. (Sotax Corporation, Aesch, Switzerland). Tests were carried out using the Paddle method (USP XXV). The dissolution media used in these tests consisted of buffer solutions (pH 1.2, pH 7.4). All tests were carried out at 37 ± 0.5 °C. The stir rate was set to 100 rpm with 900 mL of dissolution media used per vessel. The wavelength and absorption of 100% shellac concentration were determined using a SHIMADZU UV-1280 UV–Vis Indexer (Shimadzu, Kyoto, Japan) spectrophotometer. In the case of melt flow index extruded samples, test specimens of constant size and surface area were produced by cutting the extrudate strands manually to give granules of length 1 cm and accurately weighed using a Sartorius scale having a resolution of 1×10^{-5} g. Samples were manually taken every 30 min, filtered with the glass microfiber filters (1.2 μm), recorded spectrophotometrically at 221 nm using a SHIMADZU UV-1280 UV spectrophotometer (Kyoto, Japan), and all the tested samples were returned to the dissolution vessel after reading. The dissolution profile was observed from a plot of time versus concentration in percentage.

3. Results and Discussion

3.1. IR Spectrum

FTIR spectroscopy was employed to investigate what chemical bonds were present in each material. Infrared spectroscopy is useful because the peak position in an infrared spectrum correlates with the molecular structure [39]. In this study, FTIR was used to compare each of the four shellac materials and search for visible differences in molecular structure.

Figure 1 shows the FTIR spectra of four different kinds of shellac. It can be seen that all the existing peaks of various shellac were almost identical and corresponded to those reported in the literature. There was a clear broad peak in the range of 3700–3200 cm^{-1} with a maximum at 3416 cm^{-1}, which was attributed to the –OH vibrations from acidic and hydroxylic functional groups [34,40], as well as a strong absorption band at 2928–2920 cm^{-1} and 2852 cm^{-1}, which represented –CH stretching [41]. The carbonyl band from the acid formation was visible at 1710 cm^{-1} with a slight shoulder at 1636 cm^{-1}, corresponding to the C=O band of an ester [13,42]. This region on the right-hand side of the diagram (from about 1500 to 600 cm^{-1}) is called the fingerprint region. It can be used to identify unknown or two different organic compounds by comparing their fingerprint spectroscopy graphs [43]. In Figure 1, the main absorption bands in the fingerprint region were at 1462 cm^{-1} (CH_2 bend), 1374 cm^{-1} (CH_3 bend), 1246 cm^{-1} ((C–O) stretch from ester), 1148 cm^{-1} (C–O stretch from acid), a broadband between 1010 and 1000 cm^{-1} (C–O stretch from alcohol), 943 cm^{-1} (C–H stretch/CH_2 from alkenes) and a weak peak visible at 720 cm^{-1}, which are the characteristic peaks of wax, representing CH_2 rocking from shellac wax [44,45]. Table 2 shows the absorbance of each shellac material at 720 cm^{-1}. The intensity difference of the samples is simply because AFS Shellac RTH and AFS Shellac WL have higher wax concentrations, which are around 4–5%. It is clear that even though SSB 55 Pharma FL and Dewaxed Shellac HS 700K are dewaxed shellac, there was still some traces of wax detectable in the sample.

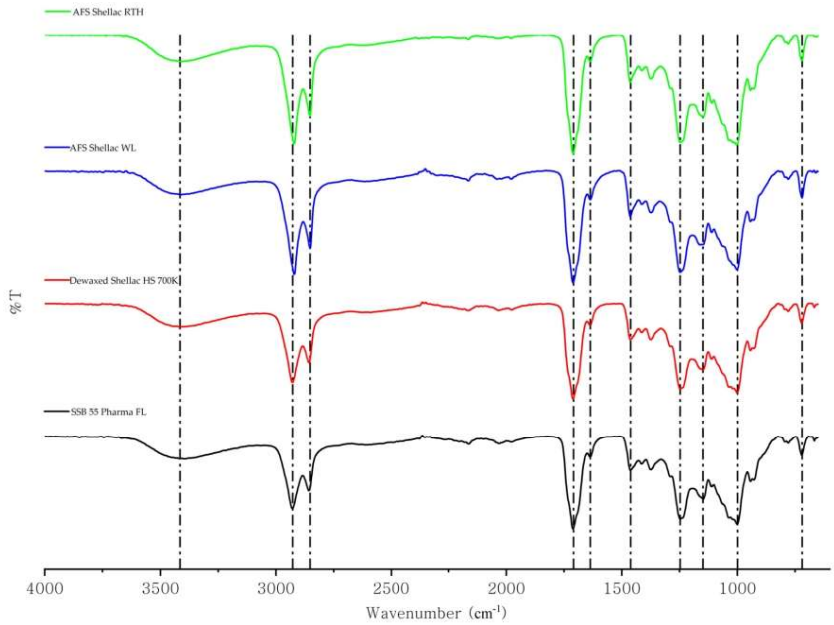

Figure 1. FTIR spectrum of different types of shellac.

Table 2. Shellac material used in this study.

Name	AFS Shellac RTH	AFS Shellac WL	Dewaxed Shellac HS 700K	SSB 55 Pharma FL
Absorbance at 720 cm^{-1}	0.026	0.03	0.021	0.02

The IR result showed that the received shellac is a mixture containing ester, acid and hydroxyls groups, which refer to the resin part of the composition [46]. Moreover, all the similar characteristic peaks observed showed there is no chemical difference between the four shellac types as all are Kushmi based. The main difference between each shellac sample was the content of each ingredient. As a result, it is not conceivable to identify each sample using its FTIR spectrum [24].

3.2. Melt Flow Index Analysis

Melt flow index (MFI) is a conventional and easy method used to measure the flow rate of a polymeric material through an orifice of specified length and diameter under the prescribed conditions of temperature and pressure [47,48]. MFI can determine the quality of a polymer, relate its flow properties to its application and measure the viscosity of the polymer in a molten state [49,50]. In modern industrial process technology, the shear stresses used during the production cycle are much higher than the applied shear stresses or resultant shear rates in this bench test, indicating that the data obtained from MFI analysis do not necessarily correlate with the processability of the polymer [51]. However, it does provide useful information about how each material flows when they are processed. Generally, a low molecular weight material is more amenable to flow than a high molecular weight material [34,52]. Thus, higher MFI values indicate the material flows better at the

tested temperature. Generally, if one material has a high MFI value, it may most often be chosen as the raw material when the industry process involves high rates of shear, such as in HME [47].

In this study, each type of shellac had a different MFI value. Shellac SSB 55 Pharma FL had the highest figure, 11.88 g/10 min, compared to other shellac batches. AFS Shellac RTH also had a high MFI value, 9.45 g/10 min. Nevertheless, AFS Shellac WL had the lowest MFI value (3.00 g/10 min), which means that compared to other shellac materials, AFS Shellac WL had the most resistance to flow in the test conditions. From the IR result, little to no chemical difference between various shellacs was observed; the only difference was the content of each ingredient was different owing to their origin from different types of seedlac and their refining processes [4]. According to the material certificate of analysis documents, AFS Shellac RTH and WL were refined by the same refining process and same raw materials, but with different processing parameters and different manufacturing dates, which resulted in their different flow viscosities and different grades of ageing. Moreover, Dewaxed Shellac HS 700K and SSB 55 Pharma FL were purified from the same type of seedlac (Kushmi seedlac) but by different company refining processes. Dewaxed shellac HS 700K was produced earlier, where the MFI value of dewaxed Shellac HS 700K was approximately half of the SSB 55 MFI value. This shows the ageing process will significantly affect the properties of shellac. Moreover, according to the material certificate of analysis documents, AFS Shellac WL had the highest wax content. The presence of wax will restrict the flow of the material, which resulted in the lower MFI value [53].

3.3. Rheology

Hot melt extrusion (HME) as a continuous manufacturing process is widely used in the plastic and rubber industries to manufacture a broad variety of products [54,55]. Compared to other methods, it has many benefits, such as no solvents are required during the process, and it may involve less process step. Recently, the pharmaceutical industry has demonstrated great interest in the HME process [50,56]. In this study, shellac was processed by HME technology. Therefore, a good understanding of rheological properties is very important. It not only investigates flow and deformation properties of a material at the specific settings and conditions, but also insight into the underlying molecular structure of the polymers is gained by comparing their viscoelastic properties [57]. Moreover, it allows us to determine the conditions of shellac processing [58]. In this study, steady-state rheometry was performed on all four shellac samples. The rheological behaviour of a polymer material may be affected by many factors [59].

The first set of rheology tests performed was oscillatory time sweeps. This test directly provides the necessary information about how material changes as a function of time. Before any subsequent rheological testing, it is important to identify that the material properties do not change during the test period at the constant test temperature of 90 °C. The result of oscillatory time sweep on shellac material shows that the material's storage modulus (G') remained at a steady value. This indicates that the material's structure was not altered during the 900 s testing period at 90 °C.

When the polymer material is under a critical stain, its rheological properties remain at a steady-state value. That range is called linear viscoelastic region (LVR) [60,61]. When the applied strain is higher than the linear viscoelastic region, the material structure would be destroyed, and its response would be non-linear. In addition, the storage modulus would begin to decrease [62]. As a result, determining the linear viscoelastic region of an unknown material would be the second necessary step in rheology analysis [61].

A strain sweep was used to determine the material's linear viscoelastic region (LVR). Figure 2 overlays the results of amplitude sweep of each shellac material at 90 °C. Additionally, Table 3 illustrates the linear viscoelastic region (LVR) of shellac materials at different temperatures. The test procedure could not be completed when the analysis is running at 60 °C, or even lower temperature, as the material was too viscous to flow, which exceeded

the test range of the machine. Except for AFS Shellac RTH, all other types of shellac had a narrow LVR at low temperatures.

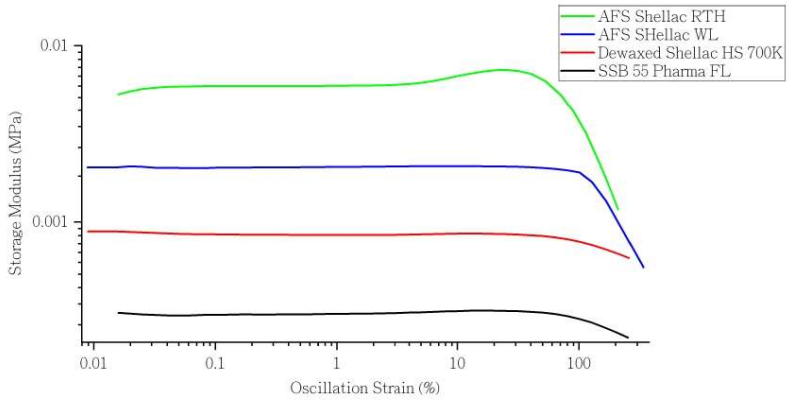

Figure 2. The storage modulus of various shellac materials versus oscillation strain (%) in amplitude sweep at 90 °C.

Table 3. The linear viscoelastic region of shellac at various temperatures.

Sample \ Temperature	60 °C	70 °C	80 °C	90 °C
AFS Shellac WL	N/A	0.2 ± 0.01	30.8 ± 0.8	78.9 ± 0.4
Dewaxed Shellac AFS HS 700K	N/A	0.1 ± 0.01	33.7 ± 0.6	82.6 ± 1.0
Shellac SSB 55 Pharma FL	N/A	0.1 ± 0.004	64.2 ± 1.6	85.5 ± 1.0
AFS Shellac RTH	N/A	15.3 ± 0.3	51.0 ± 0.2	68.4 ± 0.8

At a lower temperature, AFS Shellac RTH had a higher LVR range compared to the other three types of shellac, which is likely due to the existence of wax in the AFS Shellac RTH, acting as plasticiser when it is not in a molten state [63]. However, when the temperature increased to 80 °C, shellac SSB 55 Pharma had a wider LVR range, nearly twice that of Dewaxed Shellac AFS HS 700K and AFS Shellac WL.

During melt extrusion, the materials undergo vigorous mixing under pressure and shear rate, which accelerates dissolution of one component into the other in a drug/polymer mixed system. Therefore, it is necessary to ascertain the effect angular frequency would have on the viscosity of mixtures at a defined temperature [64]. As a result, oscillation frequency analysis is required to find out the effects of angular frequency on complex viscosities for each shellac at 70 °C. As shown in Figure 3, the viscosity was first determined at the given temperature at the angular frequency of 0.1 Hz, which was then increased gradually up to 100 Hz. The viscosity of shellac material in this study was found to follow a shear-thinning behaviour typical of many polymer responses, as shown in Figure 4. In all cases, with the increase in shear rate (indicative of processing speed) the viscosity of shellac decreased [34]. Moreover, AFS Shellac WL alone had the highest melt viscosity of all shellac types tested, which indicates the existence of wax, directly affecting the viscosity of the shellac at lower temperature. This result correlates well with results obtained using MFI analysis. Furthermore, in all cases, there was a much sharper decrease in viscosity with the increase in angular frequency. The profound drop in viscosity for AFS Shellac WL may attributed to the larger amount of wax initially present in the shellac. The viscosity reduction in Dewaxed Shellac HS 700K is much higher than Shellac SSB 55 Pharma FL, which may be because of the different processing parameters used by different supplier companies and the earlier manufacture date.

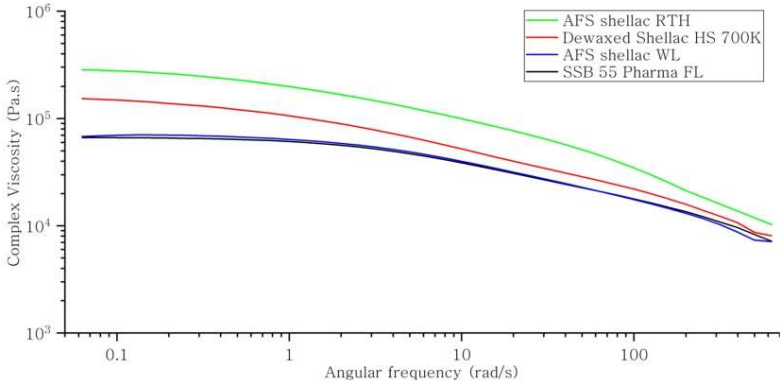

Figure 3. Complex viscosity versus frequency of various shellac in frequency sweep at 70 °C.

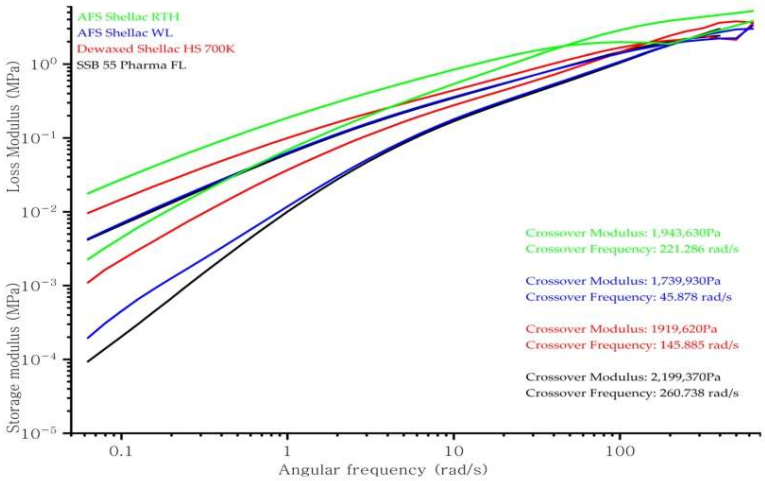

Figure 4. The storage modulus and loss modulus versus frequency of various shellac in frequency sweep at 70 °C.

Figure 4 illustrates the storage and loss modulus of the shellac in frequency sweep analysis at 70 °C. Typically, the molecular weight (Mw) and the molecular weight distribution (MWD) of the material would affect the crossover point of the modulus in frequency sweep analysis. When the polymer has a higher molecular weight (Mw), the crossover point will move to lower frequency compared to a low Mw. Alternatively, when the polymer has narrow MWD, the crossover point would shift to higher modulus values [65]. The result indicates that AFS Shellac WL had a lower Mw compared to other shellac materials assessed. Moreover, shellac SSB 55 Pharma FL had the narrowest MWD [31].

When using hot melt extrusion technology to process the polymer, the materials undergo a programmed temperature profile. As a result, it is necessary to determine what effect temperature has on the viscosity of mixtures across a range. Temperature ramp analysis investigates how increasing thermal energy affects the material's viscosity and also the materials melt strength [66,67]. The results of the temperature ramp of four types

of shellac at a constant strain and frequency are shown in Figure 5. The viscosity was first determined at the given strain at the temperature of 65 °C, which was then increased gradually up to 110 °C with a heating rate of 3 °C min^{-1}. Figure 5 illustrates that all the shellac materials were sloped almost identically as a function of temperature at an angular frequency of 1 Hz. With the temperature increasing the viscosity of shellac decreases. Moreover, the AFS Shellac WL alone had the highest melt viscosity when compared to all other shellacs, which suggests that the wax affects the viscosity of the shellac. Additionally, in all cases, there was a much sharper decrease in viscosity with an increase in temperature. The profound drop in viscosity for AFS Shellac WL may be attributed to the larger amount of wax initially present in the shellac, which melted gradually when the temperature increased. This experiment provided evidence that the viscosity of shellac SSB 55 pharma FL changed less as the temperature changed.

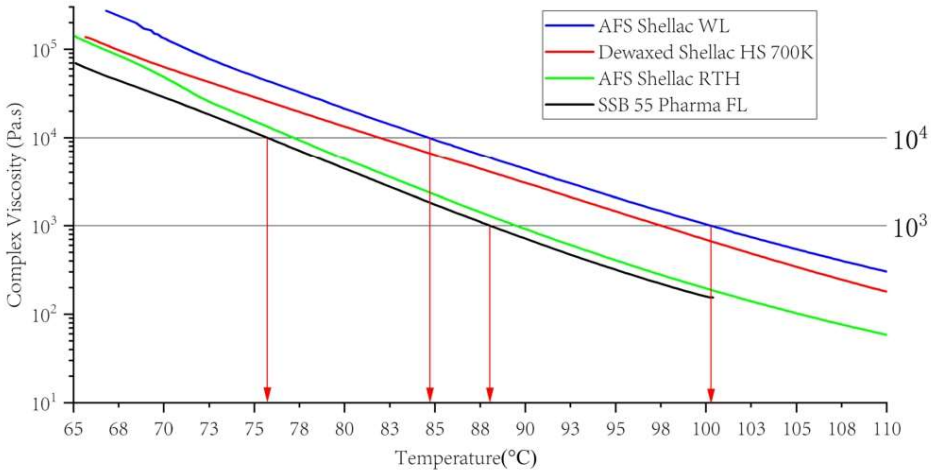

Figure 5. Viscosity versus temperature of various shellac.

From an earlier report by other researchers, the extrudable viscosity range for a polymer material was reported to be 1000 to 10,000 Pa s [66]. This range is determined by one simple rule: the viscosity of the polymer should be low enough for the drug to dissolve in it and high enough for the extrusion process to occur. For AFS Shellac WL, Dewaxed Shellac AFS HS 700K, AFS Shellac RTH and shellac SSB 55 Pharma FL, the temperatures corresponding to the viscosity of 1000 to 10,000 Pa s were 85 to 100 °C, 82 to 97 °C, 77 to 89 °C and 75 to 87 °C, respectively; therefore, the extrudable temperature range for various types of shellac was different [68]. However, due to the existence of shear-thinning behaviours, each shellac material may be extruded at lower temperatures.

3.4. Differential Scanning Calorimetry (DSC)

Glass transition temperature (T_g) is one of the fundamental properties of any material, and it is essential in material processing and design, especially for an amorphous polymer [69]. The glass transition is also known as glass–liquid transition, and it is the reversible process in an amorphous material or semi crystalline material where the polymer moves from the solid state into a rubbery state with increasing temperature, meaning the polymer molecular structure begins to become flexible [70]. The heat capacity of the various shellac resins changed during the glass transition process, and DSC is a useful method to determine the glass transition temperature [71,72]. However, the transition does

not occur at a specific temperature for a short time but somewhat over a temperature range, as shown in Figure 6. In this study, the half-step-height method was used to determine the T_g value. The shellac materials investigated in this study were proposed as potential matrix materials for drug delivery systems. As such, it is advantageous that the glass transition temperature of the selected material is well above the storage or drug release temperature [68].

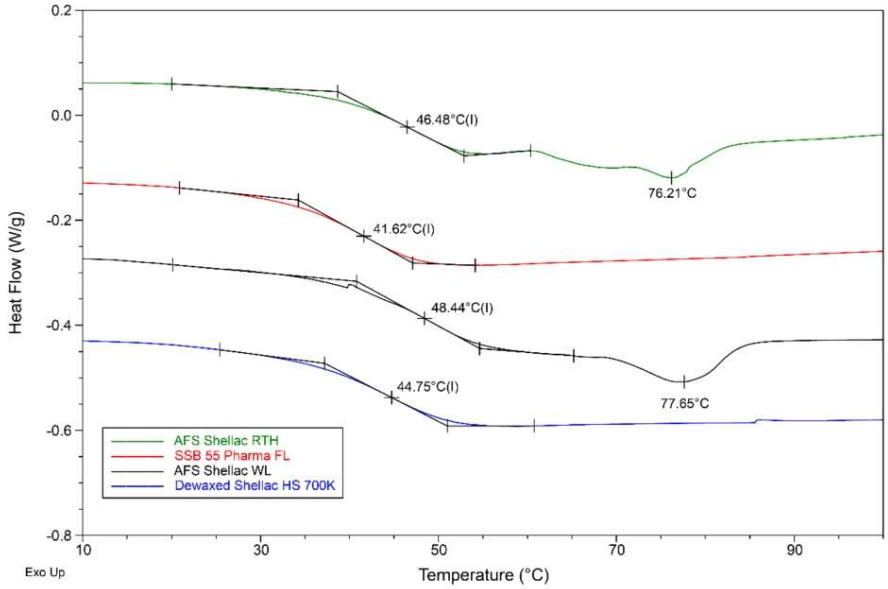

Figure 6. Overlaid DSC result of original shellac samples.

Differential scanning calorimetry can record data of the overall heat flow as a function of temperature. The study of the thermal behaviour of shellac was carried out using DSC analysis. In matrix-assisted laser desorption ionization mass spectroscopy (MALDI-MS) measurements, shellac consists mostly of monomeric and oligomeric compounds, though the glass transition still can be observed [73]. Below its T_g value shellac is a hard, brittle, amorphous substance, and above its T_g value shellac becomes a soft and flowable thermoplastic [4]. As it can be seen in Table 4, as well as Figure 6, all T_g values were in a range between 41 °C and 49 °C. All shellac grades showed relatively similar thermal behaviour, had a single glass transition temperature, and the onset temperature of glass transition process was perceptible. SSB 55 Pharma FL, based on Kushmi seedlac, had the lowest T_g (41.62 °C). The T_g value of Shellac HS 700K, refined by solvent extraction and based on Kushmi seedlac but with an early production date, was at 44.75 °C, which is higher than SSB 55 Pharma FL. Moreover, because of the existence of wax, the two wax-containing shellac grades AFS Shellac RTH and AFS Shellac WL, both refined by a melting process based on Kushmi seedlac, had T_g values much higher than the dewaxed shellac, which were 46.48 °C and 48.44 °C, respectively. This result corresponds well to the MFI test and rheology analysis where AFS Shellac WL had the lowest MFI value, but the highest viscosity and T_g value [5]. Nonetheless, the two wax-containing shellac batches had a noticeable small melting peak around 76 °C to 78 °C. This melting peak was the result of the shellac wax melting when the sample was heated [74].

Table 4. Glass-transition temperatures and melting temperatures of different shellac grades.

Material	T_g (°C)	T_m (°C)
Shellac SSB 55 Pharma F	41.7 ± 0.1	-
Dewaxed Shellac HS 700K	44.6 ± 0.1	-
AFS Shellac RTH	46.4 ± 0.1	76.5 ± 0.3
AFS shellac WL	48.2 ± 0.2	77.5 ± 0.2

3.5. Dissolution

In order to use a spectrophotometer to record the shellac dissolution profile, the wavelength and absorption of 100% shellac concentrations were determined first. As shown in Figure 7, all types of shellac showed similar spectrum curves, which is further confirmed with IR results. All types of shellac materials exhibited little chemical differences. The differences between shellac types were caused only by different amounts of their various constituent ingredients and not by their bulk structure. All of them had a maximum UV absorption at 221 nm independent of shellac type. The standard calibration line of each shellac types was determined depending on the investigated batch. In this study, the investigation was focused on the raw material without any drug loading; spectrophotometric detection was a suitable method for recording the dissolution profiles. From previous literature reviews, shellac is a weak acid. The dissolution profiles were expected to be pH dependent. Furthermore, because the nature of shellac is the same, the pH dependence was suitable for all samples. With increasing pH value, the dissolution rate and the amount of dissolved shellac increased.

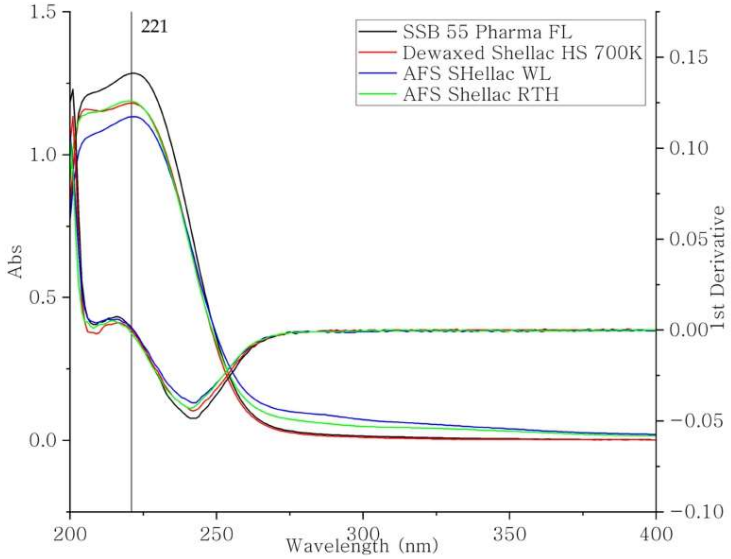

Figure 7. The UV spectrum and its 1st derivative curve of four different types of shellac.

The recorded dissolution profiles of shellac in different pH are shown in Figure 8. All types of shellac illustrated similar dissolution behaviours. At pH 1.2 no dissolution occurred. When the media changed to pH 7.4 PBS, the dissolution rate and the amount of dissolved shellac increased. From the result, shellac SSB 55 Pharma FL had the highest dissolution rate in any pH value compared to the others, which was expected, because of its lower T_g and acid value [5]. Moreover, as the dissolution process progressed, the

dissolution rate decreased. Compared to the two wax-containing shellac types, dewaxed shellac had a higher dissolution rate, which is attributed to the wax being hydrophobic and cannot be dissolved in aqueous media. At pH 7.4, shellac SSB 55 Pharma Fl showed complete dissolution after 3.5 h, and Dewaxed Shellac HS 700K completely dissolved after 5.5 h. AFS Shellac RTH had the longest dissolution time, being completely dissolved after 9.5 h. However, at pH 7.4, all shellac materials dissolved completely.

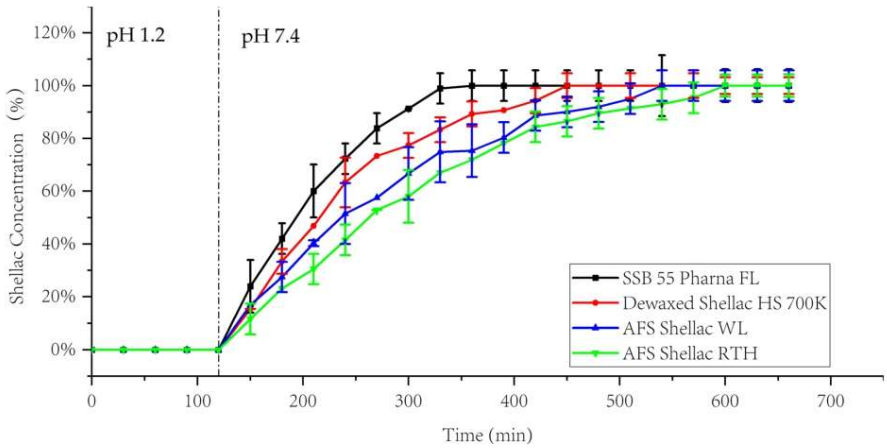

Figure 8. Dissolution profiles of the investigated shellac types at various pH.

3.6. Suggestion for Hot Melt Extrusion Process Conditions

From the DSC result, the glass transition temperature of the material was determined to be in the range of 41 °C and 49 °C. This means the temperature profile for the processing must be below 40 °C at the feeding zone and rise above the T_g of the material, along the extruder barrel to the die. Otherwise, the material would melt in the first conveying area, which is undesirable. Moreover, from the rheology analysis, all shellac materials exhibited shear thinning behaviour, which indicates that the processing temperature can be reduced at higher screw speed.

4. Conclusions

This work explores various types of shellac and investigates their physicochemical properties and processability as potential matrix materials for enteric-targeted drug delivery systems. Physical, thermal and rheology analyses of the shellac materials were conducted to support its application in hot melt extrusion as a potential drug delivery platform. All shellac materials were amorphous and had no difference in chemical structure by FTIR. During DSC analysis, the existence of a peak in two wax-containing shellac materials was due to the presence of the wax. The viscosity of the various shellac materials in this study was shown to follow shear-thinning behaviour, typical of many polymer responses, and correlated well with the melt flow index value. Moreover, based on the rheology results, the processing temperature ranges of different types of shellac for melt extrusion could be determined, and the extrudable temperature ranges were varied. Nevertheless, due to the shear-thinning behaviours, shellac can be extruded at lower temperature. Additionally, compared to the other shellac materials, shellac SSB 55 Pharma had the lowest process temperature, which indicates the highest processability. This study provides necessary data to determine the process conditions for the hot melt extrusion process involving shellac material. The content of wax and aging have significant effects on the physical properties

of shellac. However, the aging behaviour of shellac is based on the self-esterification of one compound of the natural resin: aleuritic acid. This difference can be observed by gas chromatography–mass spectrometry technology. As a result, future studies are recommended to use GC-MS or HPLC/MS technology to identify the chemical content differences of the various types of shellac.

Author Contributions: G.Y., Z.C. and N.M.G. conceived and designed the experiments; G.Y. performed the experiments; G.Y., Z.C. and N.M.G. analysed the data; G.Y. wrote the paper; D.D., Z.C., M.P. and N.M.G. reviewed the paper. All authors have read and agreed to the published version of the manuscript.

Funding: This research was funded by the Irish Research Council (GOIPG/2018/2067) and Technological University of the Shannon: Midlands Midwest, Presidents Seed Fund.

Institutional Review Board Statement: Not applicable.

Informed Consent Statement: Not applicable.

Data Availability Statement: Not applicable.

Acknowledgments: The authors are grateful to Centre for Industrial Services and Design (CISD) and Applied Polymer Technologies (APT) Enterprise Ireland Technology Gateway Centre (Athlone, Ireland) for administrative and technical support. Thanks to A.F. Suter (Witham, UK) and Stroever Schellack Bremen (Bremen, Germany) for donation materials used in this study.

Conflicts of Interest: The authors declare no conflict of interest. The funders had no role in the design of the study; in the collection, analyses, or interpretation of data; in the writing of the manuscript, or in the decision to publish the results.

References

1. Das, S.; Jacob, S.E. Shellac. *Dermatitis* **2011**, *22*, 220–222. [CrossRef]
2. Chauhan, V.S.; Ram, N.S.; Subramanian, G.B.V.; Singh, H. Chromatographic separation of the alkaline hydrolysis products of shellac. *J. Chromatogr. A* **1973**, *84*, 51–58. [CrossRef]
3. Wang, L.; Ishida, Y.; Ohtani, H.; Tsuge, S.; Nakayama, T. Characterization of natural resin shellac by reactive pyrolysis-gas chromatography in the presence of organic alkali. *Anal. Chem.* **1999**, *71*, 1316–1322. [CrossRef] [PubMed]
4. Buch, K.; Penning, M.; Wchtersbach, E.; Maskos, M.; Langguth, P. Investigation of various shellac grades: Additional analysis for identity. *Drug Dev. Ind. Pharm.* **2009**, *35*, 694–703. [CrossRef]
5. Farag, Y.; Leopold, C.S. Physicochemical properties of various shellac types. *Dissolution Technol.* **2009**, *16*, 33–39. [CrossRef]
6. Cornell, E.W.; Fadeyev, V.; Haber, C.; Jin, J.; Nordmeyer, R.; Golden, M. Using optical metrology to reconstruct sound recordings. *Nucl. Instrum. Methods Phys. Res. Sect. A Accel. Spectrometers Detect. Assoc. Equip.* **2007**, *579*, 901–904. [CrossRef]
7. Chiavari, G.; Fabbri, D.; Prati, S. Characterisation of Natural Resins by Pyrolysis—Silylation. *Chromatographia* **2002**, *55*, 611–616. [CrossRef]
8. Chiavari, G.; Fabbri, D.; Mazzeo, R.; Bocchini, P.; Galletti, G.C. Pyrolysis gas chromatography-mass spectrometry of natural resins used for artistic objects. *Chromatographia* **1995**, *41*, 273–281. [CrossRef]
9. Wang, X.; Li, J.; Fan, Y.; Jin, X. Present research on the composition and application of lac. *For. Stud. China* **2006**, *8*, 65–69. [CrossRef]
10. Pearnchob, N.; Dashevsky, A.; Bodmeier, R. Improvement in the disintegration of shellac-coated soft gelatin capsules in simulated intestinal fluid. *J. Control Release* **2004**, *94*, 313–321. [CrossRef]
11. Daher, C.; Paris, C.; Le Hô, A.S.; Bellot-Gurlet, L.; Échard, J.P. A joint use of Raman and infrared spectroscopies for the identification ofnatural organic media used in ancient varnishes. *J. Raman Spectrosc.* **2010**, *41*, 1494–1499. [CrossRef]
12. Cole, G.; Hogan, J.; Holton, M. *Pharmaceutical Coating Technology*; Taylor & Francis: Singapore, 1995; ISBN 978-0136628910.
13. Farag, Y.; Leopold, C.S. Development of shellac-coated sustained release pellet formulations. *Eur. J. Pharm. Sci.* **2011**, *42*, 400–405. [CrossRef]
14. Labuschagne, P.W.; Naicker, B.; Kalombo, L. Micronization, characterization and in-vitro dissolution of shellac from PGSS supercritical CO_2 technique. *Int. J. Pharm.* **2016**, *499*, 205–216. [CrossRef]
15. Krause, K.P.; Müller, R.H. Production of aqueous shellac dispersions by high pressure homogenisation. *Int. J. Pharm.* **2001**, *223*, 89–92. [CrossRef]
16. Alzahrani, H.; Bedir, Y.; Al-Hayani, A. Efficacy of shellac, a natural product, for the prevention of wet gangrene. *J. Int. Med. Res.* **2013**, *41*, 795–803. [CrossRef]
17. Panchapornpon, D.; Limmatvapirat, C.; Luangtana-Anan, M.; Nunthanid, J.; Sriamornsak, P.; Limmatvapirat, S. Fabrication of thermally stabilized shellac through solid state reaction with phthalic anhydride. *Mater. Lett.* **2011**, *65*, 1241–1244. [CrossRef]

18. Arnautov, A.; Korhov, V.; Faitelson, F. Physicomechanical Properties of Shellac Films. *Mech. Compos. Mater.* **2013**, *49*, 163–171. [CrossRef]
19. Soradech, S.; Limatvapirat, S.; Luangtana-anan, M. Stability enhancement of shellac by formation of composite film: Effect of gelatin and plasticizers. *J. Food Eng.* **2013**, *116*, 572–580. [CrossRef]
20. Pearnchob, N.; Siepmann, J.; Bodmeier, R. Pharmaceutical applications of shellac: Moisture-protective and taste-masking coatings and extended-release matrix tablets. *Drug Dev. Ind. Pharm.* **2003**, *29*, 925–938. [CrossRef] [PubMed]
21. Ansari, M.F.; Sarkhel, G.; Goswami, D.N.; Baboo, B. Effect of temperature on coating properties of shellac-novolac blends. *Pigment Resin Technol.* **2013**, *42*, 326–334. [CrossRef]
22. Silva, M.P.; Tulini, F.L.; Ribas, M.M.; Penning, M.; Fávaro-Trindade, C.S.; Poncelet, D. Microcapsules loaded with the probiotic Lactobacillus paracasei BGP-1 produced by co-extrusion technology using alginate/shellac as wall material: Characterization and evaluation of drying processes. *Food Res. Int.* **2016**, *89*, 582–590. [CrossRef] [PubMed]
23. Limmatvapirat, S.; Limmatvapirat, C.; Puttipipatkhachorn, S.; Nunthanid, J.; Luangtana-anan, M.; Sriamornsak, P. Modulation of drug release kinetics of shellac-based matrix tablets by in-situ polymerization through annealing process. *Eur. J. Pharm. Biopharm.* **2008**, *69*, 1004–1013. [CrossRef] [PubMed]
24. Gately, N.M.; Kennedy, J.E. The development of a melt-extruded shellac carrier for the targeted delivery of probiotics to the colon. *Pharmaceutics* **2017**, *9*, 38. [CrossRef] [PubMed]
25. Rauwendaal, C. *Polymer Extrusion*, 5th ed.; Hanser: Cincinnati, OH, USA, 2014; ISBN 9781569905166.
26. Chokshi, R.; Zia, H. Hot-Melt Extrusion technique: A Review. *Iran. J. Pharm. Res.* **2004**, *3*, 3–16.
27. Repka, M.A.; Battu, S.K.; Upadhye, S.B.; Thumma, S.; Crowley, M.M.; Zhang, F.; Martin, C.; McGinity, J.W. Pharmaceutical Applications of Hot-Melt Extrusion: Part II. *Drug Dev. Ind. Pharm.* **2007**, *33*, 1043–1057. [CrossRef]
28. Lu, M.; Guo, Z.; Li, Y.; Pang, H.; Lin, L.; Liu, X.; Pan, X.; Wu, C. Application of Hot Melt Extrusion for Poorly Water-Soluble Drugs: Limitations, Advances and Future Prospects. *Curr. Pharm. Des.* **2014**, *20*, 369–387. [CrossRef] [PubMed]
29. Sekiguchi, K.; Obi, N. Studies on Absorption of Eutectic Mixture. I. A Comparison of the Behavior of Eutectic Mixture of Sulfathiazole and that of Ordinary Sulfathiazole in Man. *Chem. Pharm. Bull.* **1961**, *9*, 866–872. [CrossRef]
30. Beneš, M.; Pekárek, T.; Beránek, J.; Havlíček, J.; Krejčík, L.; Šimek, M.; Tkadlecová, M.; Doležal, P. Methods for the preparation of amorphous solid dispersions—A comparative study. *J. Drug Deliv. Sci. Technol.* **2017**, *38*, 125–134. [CrossRef]
31. Aho, J.; Boetker, J.P.; Baldursdottir, S.; Rantanen, J. Rheology as a tool for evaluation of melt processability of innovative dosage forms. *Int. J. Pharm.* **2015**, *494*, 623–642. [CrossRef]
32. Bochmann, E.S.; Üstüner, E.E.; Gryczke, A.; Wagner, K.G. Predicting melt rheology for hot-melt extrusion by means of a simple Tg-measurement. *Eur. J. Pharm. Biopharm.* **2017**, *119*, 47–55. [CrossRef]
33. Gupta, S.S.; Parikh, T.; Meena, A.K.; Mahajan, N.; Vitez, I.; Serajuddin, A.T.M. Effect of carbamazepine on viscoelastic properties and hot melt extrudability of Soluplus®. *Int. J. Pharm.* **2015**, *478*, 232–239. [CrossRef]
34. Maru, S.M.; De Matas, M.; Kelly, A.; Paradkar, A. Characterization of thermal and rheological properties of zidovidine, lamivudine and plasticizer blends with ethyl cellulose to assess their suitability for hot melt extrusion. *Eur. J. Pharm. Sci.* **2011**, *44*, 471–478. [CrossRef]
35. Liu, H.; Zhang, X.; Suwardie, H.; Wang, P.; Gogos, C.G. Miscibility Studies of Indomethacin and Eudragit® E PO by Thermal, Rheological, and Spectroscopic Analysis. *J. Pharm. Sci.* **2012**, *101*, 2204–2212. [CrossRef]
36. Shellac-Wax-Containing Flakes. Available online: https://www.afsuter.com/product/wax-containing-shellac-flakes/ (accessed on 1 October 2021).
37. Shellac-Dewaxed Flakes—Food and Pharma Grade. Available online: https://www.afsuter.com/product/dewaxed-shellac-flakes-food-pharma/ (accessed on 1 October 2021).
38. Plastics—Differential Scanning Calorimetry (DSC)—Part 2: Determination of Glass Transition Temperature and Step Height. Available online: https://www.iso.org/standard/77310.html (accessed on 1 October 2021).
39. Brian, C.S. *Fundamentals of Fourier Transform Infrared Spectroscopy*, 2nd ed.; Taylor & Francis Group: Boca Raton, FL, USA, 2011; ISBN 9781420069303.
40. Wang, J.; Chen, L.; He, Y. Preparation of environmental friendly coatings based on natural shellac modified by diamine and its applications for copper protection. *Prog. Org. Coatings* **2008**, *62*, 307–312. [CrossRef]
41. Merlic, C.A.; Strouse, J. Problems in NMR and IR Spectroscopy NMR Links of Interest. Available online: https://webspectra.chem.ucla.edu// (accessed on 25 February 2019).
42. Tripathi, S.N.; Saini, P.; Gupta, D.; Choudhary, V. Electrical and mechanical properties of PMMA/reduced graphene oxide nanocomposites prepared via in situ polymerization. *J. Mater. Sci.* **2013**, *48*, 6223–6232. [CrossRef]
43. Stuart, B.H. *Infrared Spectroscopy: Fundamentals and Applications*; Ando, D.J., Ed.; John Wiley & Sons: Sydney, Australia, 2004; ISBN 0470854278.
44. Derry, J. *Investigating Shellac: Documenting the Process, Defining the Product*; University of Oslo: Oslo, Norway, 2012.
45. Pramono, E.; Utomo, S.B.; Wulandari, V.; Zahrotul, W.A.A.; Clegg, F. The effect of polyethylene glycol on shellac stability. *IOP Conf. Ser. Mater. Sci. Eng.* **2016**, *107*, 12066. [CrossRef]
46. Colombini, M.P.; Bonaduce, I.; Gautier, G. Molecular Pattern Recognition of Fresh and Aged Shellac. *Chromatographia* **2003**, *58*, 357–364. [CrossRef]

47. Kenny, E.K.; Gately, N.M.; Killion, J.A.; Devine, D.M.; Higginbotham, C.L.; Geever, L.M. Melt Extruded Bioresorbable Polymer Composites for Potential Regenerative Medicine Applications. *Polym. Plast. Technol. Eng.* **2016**, *55*, 432–446. [CrossRef]
48. ASTM D1238-10. *Standard Test Method for Melt Flow Rates of Thermoplastics by Extrusion Plastometer*; ASTM International: West Conshohocken, PA, USA, 2010. [CrossRef]
49. Guerreiro, S.D.C.; João, I.M.; Pimentel Real, L.E. Evaluation of the influence of testing parameters on the melt flow index of thermoplastics. *Polym. Test.* **2012**, *31*, 1026–1030. [CrossRef]
50. Rides, M.; Allen, C.; Omloo, H.; Nakayama, K.; Cancelli, G. Interlaboratory comparison of melt flow rate testing of moisture sensitive plastics. *Polym. Test.* **2009**, *28*, 572–591. [CrossRef]
51. Brown, R.P. Plastics materials. *Polym. Test.* **1988**, *8*, 370. [CrossRef]
52. TA Instruments Analytical Rheology. *Appl. Notes TA Instrum.* **2003**, 1–4. Available online: https://www.tainstruments.com/applications-library-search/ (accessed on 8 August 2021).
53. Cao, Z.; Daly, M.; Geever, L.M.; Major, I.; Higginbotham, C.L.; Devine, D.M. Synthesis and characterization of high density polyethylene/peat ash composites. *Compos. Part B Eng.* **2016**, *94*, 312–321. [CrossRef]
54. Srirangam, R.; Majumdar, S.; Upadhye, S.B.; Kumar Battu, S.; Repka, M.A.; Majumdar, S.; Kumar Battu, S.; Srirangam, R.; Upadhye, S.B. Applications of hot-melt extrusion for drug delivery. *Expert Opin. Drug Deliv.* **2008**, *5*, 1357–1376. [CrossRef]
55. Services, P.S.D.D. Technical Brief Volume 3: Hot-Melt Extrusion. *Tech. Br.* **2011**, *3*, 1–2.
56. Suwardie, H.; Wang, P.; Todd, D.B.; Panchal, V.; Yang, M.; Gogos, C.G. Rheological study of the mixture of acetaminophen and polyethylene oxide for hot-melt extrusion application. *Eur. J. Pharm. Biopharm.* **2011**, *78*, 506–512. [CrossRef] [PubMed]
57. D'Este, M.; Alini, M.; Eglin, D. Single step synthesis and characterization of thermoresponsive hyaluronan hydrogels. *Carbohydr. Polym.* **2012**, *90*, 1378–1385. [CrossRef]
58. Gupta, S.S.; Solanki, N.; Serajuddin, A.T.M. Investigation of Thermal and Viscoelastic Properties of Polymers Relevant to Hot Melt Extrusion, IV: Affinisol™ HPMC HME Polymers. *AAPS PharmSciTech* **2016**, *17*, 148–157. [CrossRef]
59. Kalyon, D.M.; Aktaş, S. Factors Affecting the Rheology and Processability of Highly Filled Suspensions. *Annu. Rev. Chem. Biomol. Eng.* **2014**, *5*, 229–254. [CrossRef] [PubMed]
60. Liptak, B.G. *Instrument Engineers' Handbook, Volume One: Process Measurement and Analysis*; Instrument Engineers' Handbook; CRC Press: Boca Raton, FL, USA, 2003; ISBN 9781420064025.
61. Kaboorani, A.; Blanchet, P. Determining the linear viscoelastic region of sugar maple wood by dynamic mechanical analysis. *BioResources* **2014**, *9*, 4392–4409. [CrossRef]
62. Menard, K.P. *Dynamic Mechanical Analysis: A Practical Introduction*; CRC Press: Boca Raton, FL, USA, 2008; ISBN 9781420049183.
63. Douroumis, D. *Hot-Melt Extrusion: Pharmaceutical Applications*; Douroumis, D., Ed.; John Wiley & Sons: Singapore, 2012; ISBN 9780470711187.
64. Solanki, N.; Gupta, S.S.; Serajuddin, A.T.M. Rheological analysis of itraconazole-polymer mixtures to determine optimal melt extrusion temperature for development of amorphous solid dispersion. *Eur. J. Pharm. Sci.* **2018**, *111*, 482–491. [CrossRef]
65. Coelho, C.; Nanabala, R.; Ménager, M.; Commereuc, S.; Verney, V. Molecular changes during natural biopolymer ageing—The case of shellac. *Polym. Degrad. Stab.* **2012**, *97*, 936–940. [CrossRef]
66. Gupta, S.S.; Meena, A.; Parikh, T.; Serajuddin, A. Investigation of thermal and viscoelastic properties of polymers relevant to hot melt extrusion-I: Polyvinylpyrrolidone and related polymers. Simerdeep. *J. Excip. Food Chem.* **2014**, *5*, 32–45. [CrossRef]
67. Monteyne, T.; Heeze, L.; Oldörp, K.; Vervaet, C.; Remon, J.P.; De Beer, T. Vibrational spectroscopy to support the link between rheology and continuous twin-screw melt granulation on molecular level: A case study. *Eur. J. Pharm. Biopharm.* **2016**, *103*, 127–135. [CrossRef] [PubMed]
68. Meena, A.; Parikh, T.; Gupta, S.S.; Serajuddin, A. Investigation of thermal and viscoelastic properties of polymers relevant to hot melt extrusion-II: Cellulosic polymers. *J. Excip. Food Chem.* **2014**, *5*, 46–55.
69. Austen Angell, C.; Sivarajan, S. Glass Transition. In *Reference Module in Materials Science and Materials Engineering*; Elsevier: Amsterdam, The Netherlands, 2017; ISBN 9780128035818.
70. Baghel, S.; Cathcart, H.; O'Reilly, N.J. Polymeric Amorphous Solid Dispersions: A Review of Amorphization, Crystallization, Stabilization, Solid-State Characterization, and Aqueous Solubilization of Biopharmaceutical Classification System Class II Drugs. *J. Pharm. Sci.* **2016**, *105*, 2527–2544. [CrossRef] [PubMed]
71. Thiry, J.; Lebrun, P.; Vinassa, C.; Adam, M.; Netchacovitch, L.; Ziemons, E.; Hubert, P.; Krier, F.; Evrard, B. Continuous production of itraconazole-based solid dispersions by hot melt extrusion: Preformulation, optimization and design space determination. *Int. J. Pharm.* **2016**, *515*, 114–124. [CrossRef] [PubMed]
72. Duflot, A.V.; Kitaeva, N.K.; Duflot, V.R. Radiation-chemical preparation of poly(vinyl alcohol) hydrogels. *Radiat. Phys. Chem.* **2015**, *107*, 1–6. [CrossRef]
73. Al-Gousous, J.; Penning, M.; Langguth, P. Molecular insights into shellac film coats from different aqueous shellac salt solutions and effect on disintegration of enteric-coated soft gelatin capsules. *Int. J. Pharm.* **2015**, *484*, 283–291. [CrossRef]
74. Zheng, H.; Zhang, R.; Zhang, H.; Feng, Y.; Li, K.; Zhang, W. Thermal analysis of four insect waxes based on differential scanning calorimetry (DSC). *Procedia Eng.* **2011**, *18*, 101–106. [CrossRef]